Antikaons in infinite nuclear matter and nuclei

Vom Fachbereich Physik
der Technischen Universität Darmstadt

zur Erlangung des Grades
eines Doktors der Naturwissenschaften
(Dr. rer. nat.)

genehmigte Dissertation von
Dipl.-Phys. Matthias Möller
aus Hanau

Darmstadt 2007
D17

Referent: PD Dr. Matthias F.M. Lutz
Korreferent: Prof. Dr. Jochen Wambach

Tag der Einreichung: 17. Juli 2007
Tag der Prüfung: 10. Dezember 2007

Zusammenfassung

In der vorliegenden Arbeit werden Antikaonen und Hyperonen in kalter Kernmaterie sowie endlichen Kernen behandelt.

Die Antikaonspektralfunktion und die $\bar{K}N$-Streuamplituden werden im Rahmen einer selbstkonsistenten und kovarianten Vielteilchentheorie berechnet, basierend auf einer relativistischen Meson-Nukleon Wechselwirkung und dem chiralen $SU(3)$ Lagrangian. Die $\bar{K}N$-Wechselwirkung bei niedrigen und mittleren Energien ist bemerkenswert komplex aufgrund der Hyperonresonanzen Λ und Σ im Bereich der Antikaon-Nukleon Schwellenenergie. Systematisch untersucht werden insbesondere die Auswirkungen von nuklearer Saturierung, implementiert in Form eines skalaren und vektoriellen Mean-Field des Nukleons. Dabei wird das Auftreten von Divergenzen und kinematischen Singularitäten durch Anwendung eines neuen Renormierungsschemas vermieden. Desweiteren wird ein Winkelmittelungsverfahren untersucht, das den numerischen Rechenaufwand deutlich verringert. Die Antikaonspektralfunktion sowie s-Wellen Streuamplituden werden mit Hilfe des Verfahrens zufriedenstellend reproduziert. Die Antikaonspektralfunktion zeigt unter Berücksichtigung des Nukleon Mean-Fields eine deutlich verringerte Breite, während die Auswirkung auf die Hyperonresonanzen und insbesondere das $\Lambda(1405)$ moderat ausfällt. Nur das $\Lambda(1520)$ wird in Kernmaterie bei Saturierungsdichte fast vollständig aufgelöst. Wir erzielen eine Attraktion von rund 30 MeV für das $\Lambda(1405)$ und 40 MeV für das $\Sigma(1385)$.

Die exotischen Kaonischen Atome bieten sich als Test der $\bar{K}N$-Wechselwirkung in Materie bei typischen Dichten bis zur Saturierungsdichte an, jedoch vermag bisher keine mikroskopische Theorie die vorhandenen Messungen zufriedenstellend zu reproduzieren. Im zweiten Teil der Arbeit wird ein nichtlokaler Ansatz entwickelt, der nichtlokale Beiträge zur Antikaonselbstenergie berücksichtigt. Letzere sind auf die Impuls- und Dichteabhängigkeit der $\bar{K}N$-Streuamplituden sowie die endliche Kernausdehnung zurückzuführen. Die atomaren Niveaus der Kaonischen Atome werden mit Hilfe der Klein-Gordon-Gleichung berechnet, in die ein nichtlokales optisches Potential basierend auf der nichtlokalen Antikaonselbstenergie eingeht. Eine erste nichtlokale Rechnung für Kohlenstoff wurde durchgeführt. Es zeigen sich signifikante Implikationen einer nichtlokalen Behandlung Kaonischer Atome, die eine weitergehende Untersuchung auf Grundlage einer verbesserten Vielteilchentheorie, wie sie im ersten Teil der Arbeit entwickelt wurde, erforderlich machen.

Contents

List of Figures

List of Tables

Chapter 1

Introduction

The present work deals with antikaons and hyperons in cold nuclear matter from two complementary points of view. The first subject is antikaons and hyperons in nuclear matter based on a self-consistent and covariant many-body approach. The effects of nucleon scalar and vector mean-fields are examined systematically. The second subject is a novel approach for the description of the various data on kaonic atoms using a non-local ansatz for the potential, calculated from microscopic in-medium $\bar{K}N$ scattering amplitudes.

The description of the properties of mesons and hyperons at low energies in infinite nuclear matter has been the subject of many theoretical investigations, some of which agree qualitatively but exhibit discrepancies in detail. These discrepancies suggest a further improvement of the theoretical models. In our analysis a self-consistent and covariant many-body approach is used to determine the antikaon spectral function and the in-medium $\bar{K}N$ scattering amplitudes. The microscopic description is based on a relativistic free-space meson-nucleon interaction [4], complying with chiral SU(3) symmetry. The $\bar{K}N$ interaction at low and intermediate energies is remarkably complex and rich due to different resonances in the vicinity of the antikaon-nucleon threshold energy. Furthermore, there are two baryons which are stable with respect to strong interactions, the Λ and Σ hyperons. At threshold energy the $\pi\Lambda$ and the $\pi\Sigma$ channels are open for a $\bar{K}N$ system. The $\Lambda(1405)$ resonance is widely interpreted as a $\bar{K}N$ bound state and thus cannot be addressed by simple perturbation theory.

It should be mentioned that there is further room for improvement of the free-space coupled-channel approach [4] because of the caveat arising from the recent measurement of the K^-p scattering length by the DEAR collaboration [6] and the older K^-p low energy scattering data [7]. Both measurements cannot be described simultaneously by the existing theoretical calculations. We will not go into detail concerning the free-space interaction and focus on the derivation of an effective in-medium interaction. The major aspects of the antikaon nucleon scattering in vacuum, that have to be considered from the point of view of an effective antikaon and hyperon in-medium interaction, will be summarized briefly later on.

We turn to the in-medium dynamics of antikaons and hyperons and summarize the major aspects that enter this work. When examining antikaons in cold nuclear matter the in-medium effects and in particular the density dependence of the $\bar{K}N$ interaction are dominated by the Pauli-blocking effect on the one hand and by the interaction of all baryons and mesons with the Fermi-sea of the nucleons on the other hand. The importance of Pauli-blocking was first pointed out in [8–10]. It prevents scattering into intermediate states that are already occupied by nucleons of the Fermi-sea. It leads to a broadening and repulsive mass shift of the $\Lambda(1405)$ resonance, that couples strongly to the $\bar{K}N$ channel. Self consistency proved to be another important aspect for the description of antikaons in nuclear matter, which means that the antikaon self-energy is calculated from an in-medium scattering amplitude that depends by itself on the self-energy. It was shown in [1] that a self-consistent approach is necessary, since a reduced antikaon mass has an effect on the $\Lambda(1405)$ resonance. While Pauli-blocking pushes the resonance to higher mass a self-consistent treatment counteracts and the resonance position stays almost unchanged. The aforementioned findings were qualitatively confirmed in [2], utilising a different approach. The next important point is the inclusion of p-wave interactions, see [11] and [12], which is of particular concern in connection with the p-wave $\Sigma(1385)$ resonance and kaonic atoms.

Our fully self-consistent and covariant many-body approach is based on [5], where s-, p- and d-waves are taken into account by means of an in-medium projector algebra. The applied on-shell reduction scheme is based on this algebra, which allows for a proper mixing of different partial waves in the medium. The inclusion of p-wave scattering leads to additional attraction for the $\Lambda(1405)$ resonance, and also for the $\Sigma(1385)$ p-wave and the $\Lambda(1520)$ d-wave resonances. Different results were obtained by [13] within a partially self-consistent scheme and a quasiparticle ansatz for the antikaon spectral function.

We will explore the effects of nuclear saturation on the antikaon and hyperon properties by means of scalar and vector mean-fields for the nucleons. For the implementation of the nucleon mean-fields the in-medium projector algebra approach of [5] has to be modified. First attempts to allow for a nucleon mean-field within a non-relativistic approach were made in [2, 9, 13–15] and the effects were found to be negligible. However, the latter results assume an attractive nucleon mean-field potential of about 50 MeV and the possibility of large scalar and vector mean-fields has never been studied. Our new approach is supplemented by a critical inspection of the angular average approximation applied in [2] and [14].

A realistic treatment of antikaon and hyperon in-medium dynamics requires a proper renormalization scheme in order to avoid medium-induced power-divergent structures. Especially as soon as p-wave interactions are considered the in-medium meson-baryon loop functions have to be renormalized in a systematic way. Furthermore, particularly for the case of large vector mean-fields our approach would be significantly affected by singular structures without a proper renormalization. We introduce a novel renormalization scheme that systematically avoids the occurrence of power-divergent terms as well as kinematical singularities. This renormalization scheme is a crucial issue of the improved many-body approach.

The subject of in-medium $\bar{K}N$ dynamics has recently gained new interest because of the prediction of exotic systems where the antikaon can be deeply bound by nuclei, see [16] and [17]. These analysis requires not only an antikaon-nucleon interaction that is reliable at high densities, but also sophisticated calculations for finite nuclei. We point out that only moderate attraction in the antikaon spectral function is found in the present analysis, which does not support the scenario of deeply bound states in heavy nuclei.

Parts of this work concerning the self-consistent and covariant many-body approach for the calculation of the antikaon and hyperon properties in cold nuclear matter are documented in the preprint [18].

The antikaon properties in nuclear matter between zero and saturation density can partially be extracted from the energy level shifts and widths of kaonic atoms. Since a long time the description of kaonic atoms data by a microscopic theory remains a challenge. In this work we apply the many-body approach of $\bar{K}N$ scattering in a novel way to describe kaonic atoms within a non-local framework. The energy eigenvalue of the atomic levels can be calculated from the Klein-Gordon equation. Besides the Coulomb potential for finite size nuclei leading order contributions from vacuum polarization have to be considered because of the smallness of the antikaon orbit. The vacuum polarization corrections are of the same size as the strong interaction effects, that is up to several keV compared to typical binding energies of about 1 MeV. The strong interaction of the antikaon with the nucleus is described by an optical potential. The eigenvalues of the atomic levels become complex because of the absorptive part of the optical potential. The actual form of the optical potential is widely controversial.

The large collection of experimental data on kaonic atoms indicates that the K^- feels an attractive potential, which appears to contradict the negative sign of the empirical K^-p scattering length a_{K^-p}, caused by the presence of the $\Lambda(1405)$ resonance below the threshold. The scattering length enters the optical potential derived from the low density theorem (LDT), which describes the $\bar{K}N$ interaction in a dilute nucleon gas. The LDT should be reproduced by any theoretical model for the antikaon optical potential in the low density limit. However, addressing bound state problems with the simple LDT is an unjustified approximation. Furthermore the empirical scattering length contradicts the leading order series expansion of the chiral Lagrangian, known as the Weinberg-Tomozawa term [19].

Experimentally it is difficult to draw any conclusion from the existing scattering data, as the antikaon self-energy probes the $\bar{K}N$ interaction below the kaon-nucleon threshold. The quoted shortcomings of a simple constant scattering length ansatz can be tackled promisingly within a microscopic approach by an effective nonlinear density dependent scattering length $a_{eff}(k_F)$ [1–3, 20]. The scattering length changes sign around $k_F = 100\,\text{MeV}$, which corresponds to nuclear densities at the nuclear surface. Consequently it complies both with the LDT and the attraction scenario from experiment. The density dependence of the scattering length in the microscopic approaches is mainly due to the propagation of the $\Lambda(1405)$ resonance in nuclear matter. The importance of the low density region for the antikaon-nucleus interaction is emphasized by the small overlap of the antikaon wave function with the nucleus density profile and suggested the consideration of gradient terms, acting on the density profile of the nucleus as well as on the antikaon wave function [3]. However, all the existing non-local approaches based on gradient terms are phenomenologic, the gradient ordering is not unique and a momentum expansion of the antikaon self-energy is not well justified. The presence of subthreshold resonances would require a partial resummation of gradient terms and a self-consistent approach for finite nuclear matter.

There are of course purely phenomenologic descriptions successfully reproducing the kaonic atom data [21], but a quantitative microscopic description is still lacking. Especially the measured level widths are significantly underestimated by the microscopic theories. Whereas the phenomenologic models favour a large attractive optical potential of about 200 MeV at saturation density, the microscopic theories suggest a rather shallow potential of about 40 MeV.

The analysis of kaonic atoms can be improved from the point of view of the underlying coupled channel dynamics and many-body theory. On the other hand the determination of the optical antikaon potential and the calculation of the atomic levels has to be improved. We will calculate a self-energy based on given $\bar{K}N$ in-medium scattering amplitudes, that covers non-local contributions due to the density dependence of the $\bar{K}N$ interaction and the finite size nucleus. The non-local potential can be determined straightforwardly by applying Feynman rules in coordinate space, but as already mentioned it is known from infinite nuclear matter calculations that a self-consistent approach is required. An analogous calculation for finite nuclear matter would be a horrendous task and we need an approximated, but well justified model, where the non-local self-energy and potential can be evaluated from existing $\bar{K}N$ scattering amplitudes for infinite nuclear matter.

Taking into account the momentum dependence of the $\bar{K}N$ interaction does not only result in an non-local potential. It also provides the opportunity to study the influence of higher partial waves on kaonic atoms explicitly, that is particularly the p-wave with the $\Sigma(1385)$ resonance. Higher partial waves enter the effective scattering length $a_{eff}(k_F)$ derived from s-wave $\bar{K}N$ scattering amplitudes only indirectly via its effect on the $\Lambda(1405)$ resonance. Additionally to the full non-local microscopic theory we present a semi-microscopic non-local model that allows to study the subtle cancellations between the different partial waves and the influence of the resonance properties – mass and width – on the energy level shifts and widths in an explicit and intuitive way.

In contrast to the scheme suggested in [22] we will treat the antikaon wave function exactly, because an expansion of the wave function proved to be a questionable approximation. Consequently we have to iterate the antikaon wave function until it converges.

The work is organized as follows: Chapter 2 starts with a brief introduction to the free-space meson-nucleon interaction [4]. The covariant projector algebra and the recoupling of the vacuum scattering amplitudes is introduced. The renormalization procedure of the loop functions is supplemented by a review of the angular average approximation. The technical part of the chapter is completed by the definition of the antikaon self-energy. Numerical results for the antikaon spectral function, self-energy and in-medium hyperon properties are shown for the various approximations without and including nucleon mean-fields at full, half and twice saturation density.

In Chapter 3 a review of the phenomenology of kaonic atoms is given. We comment on the solution of the Klein-Gordon equation and present the relevant electromagnetic potential contributions. Several existing theoretical models are compared for a variety of nuclei.

Our non-local framework for kaonic atoms is established in Chapter 4. The non-local self-energy, that can be calculated from $\bar{K}N$ scattering amplitudes, is linked to the non-local optical potential entering the Klein-Gordon equation. The approach is approved by comparison of calculations in the local limit within a simplified semi-microscopic model. The first full non-local calculation is done for carbon.

Chapter 2

Antikaons and hyperons in nuclear matter

2.1 Free-space antikaon-nucleon scattering

The self-consistent, covariant microscopic approach to antikaons and hyperons in cold nuclear matter, that will be developed in the present chapter, is based on a relativistic coupled-channel dynamics and a chiral SU(3) Lagrangian in [4]. We rewrite the Bethe-Salpeter equation, so that the free-space $\bar{K}N$ scattering amplitudes from [4] can be used as the interaction kernel for the in-medium scattering equation. The renormalization scheme of [4] will also be used and extended to the in-medium case. We will briefly describe the major aspects of [4] in the context of $\bar{K}N$ scattering.

The analysis of [4] includes s-, p- and d-waves with total angular momentum $J^P = \frac{1}{2}^\pm, \frac{3}{2}^\pm$ and parity P. Apart from the pseudo-scalar meson octet field with $J^P = 0^-$ and the baryon octet field with $J^P = \frac{1}{2}^+$ the relativistic chiral SU(3) Lagrangian from [4] covers explicitly the $J^P = \frac{3}{2}^+$ baryon decuplet field. The baryon nonet of d-wave resonances with $J^P = \frac{3}{2}^-$ is included phenomenologically. When applied to KN and especially $\bar{K}N$ systems the kaon-nucleon dynamics is non-perturbative due to the large kaon mass and a partial resummation by means of the Bethe-Salpeter equation is necessary. The Bethe-Salpeter equation in [4] contains interaction kernels up to chiral order Q^3. By using an appropriate on-shell reduction scheme these amplitudes are made independent of the choice of the interpolating fields. Renormalization is done with the help of of a minimal chiral subtraction scheme within dimensional regularization, compatible with the standard chiral counting rules. It is emphasized that no cutoffs are involved in [4]. The parameters in the chiral Lagrangian of [4] are adjusted to reproduce the empirical scattering cross sections of πN, KN and $\bar{K}N$.

Finally for antikaon-nucleon scattering a system of coupled channels $\bar{K}N$, $\pi\Sigma$, $\pi\Lambda$, $\eta\Lambda$, $\eta\Sigma$ and $K\Xi$ is obtained. It is particularly complex due to the open inelastic $\pi\Sigma$ and $\pi\Lambda$ channels. The $\Lambda(1405)$ resonance, which can be interpreted as a $K^- p$ bound state, is situated right below the antikaon-nucleon threshold and its dynamics strongly determines the antikaon-nucleon scattering amplitude. There is not only the s-wave $\Lambda(1405)$ resonance, but also the p-wave $\Sigma(1385)$ $J = \frac{3}{2}^+$ resonance below the $\bar{K}N$ threshold and the d-wave $\Lambda(1520)$ $J = \frac{3}{2}^-$ resonance not far above the threshold. Therefore the resonance structure is remarkably rich. The in-medium antikaon self-energy, which will be a key result of the subsequent chapter, is influenced strongly by these resonances.

The results of [4] for the antikaon-nucleon scattering are shown in Figures 2.1 and 2.2

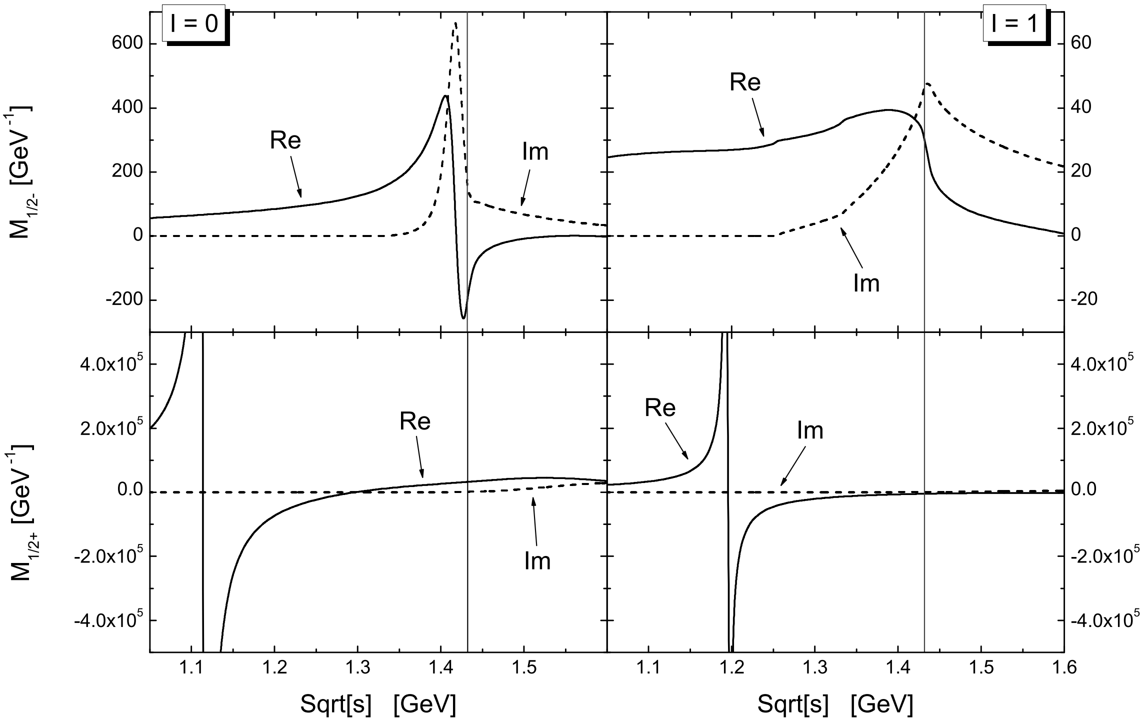

Figure 2.1: Reduced amplitudes $M_{\frac{1}{2}\pm}$ for $I = 0$ and $I = 1$ over $\sqrt{s}$ in GeV, real (solid) and imaginary (dotted) part. The vertical line marks the antikaon-nucleon threshold at $\sqrt{s} = m_K + m_N$.

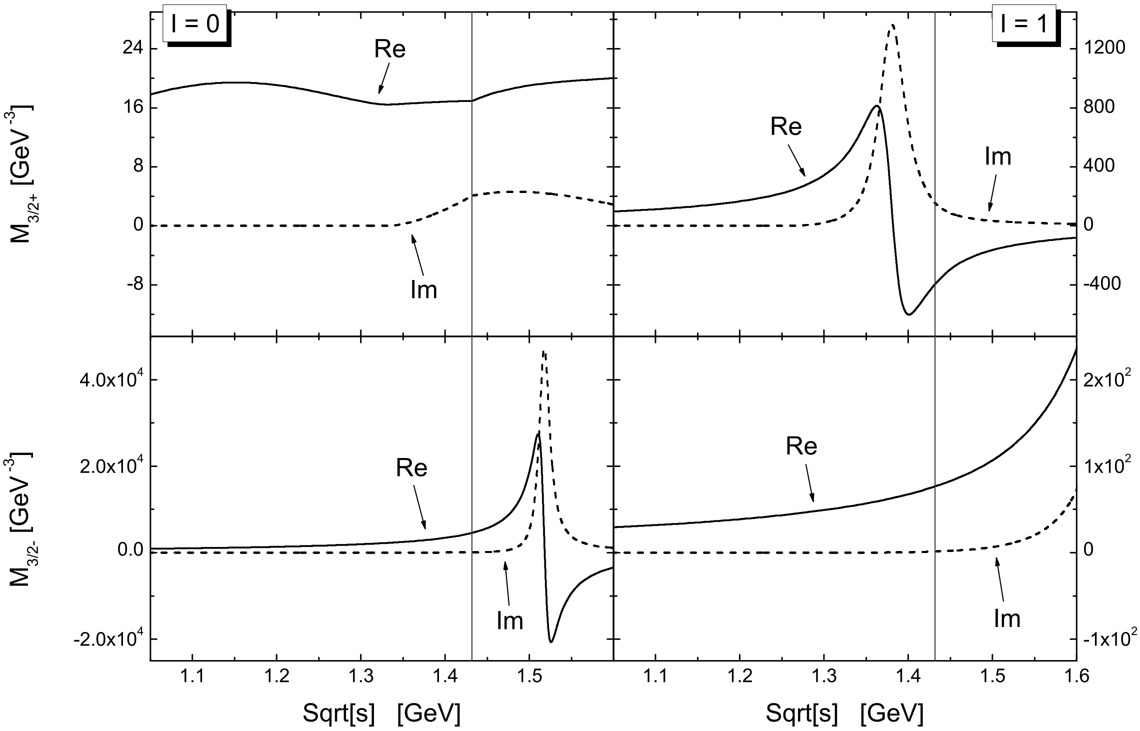

Figure 2.2: Reduced amplitudes $M_{\frac{1}{2}\pm}$ for $I = 0$ and $I = 1$ over $\sqrt{s}$ in GeV, real (solid) and imaginary (dotted) part. The vertical line marks the antikaon-nucleon threshold at $\sqrt{s} = m_K + m_N$.

in terms of the invariant free-space amplitudes $M^{(I)}_{JP}(\sqrt{s})$ for isospin $I = 0, 1$, total angular momentum J and parity P. The latter amplitudes provide a detailed picture especially of the higher partial waves because the phase-space factor is pulled out. We illustrate the convention by providing the total cross section for $K^- p \to K^- p$ scattering including s- and p-waves:

$$\begin{aligned}\sigma_{K^-p\to K^-p}(\sqrt{s}) &= 4\pi \Big[|f^{(0)}_{K^-p,J=\frac{1}{2}}(\sqrt{s})|^2 \\ &\quad + |f^{(1)}_{K^-p,J=\frac{1}{2}}(\sqrt{s})|^2 + 2|f^{(1)}_{K^-p,J=\frac{3}{2}}(\sqrt{s})|^2 \Big] \end{aligned} \tag{2.1}$$

with the reduced partial wave amplitudes $f^{(l)}_{K^-p,J=l\pm\frac{1}{2}}$ given by

$$\begin{aligned} f^{(0)}_{K^-p,J=\frac{1}{2}}(\sqrt{s}) &= \frac{1}{16\pi}(E_p + m_p)\left(M^{(I=0)}_{\frac{1}{2}^-} + M^{(I=1)}_{\frac{1}{2}^-}\right), \\ f^{(1)}_{K^-p,J=\frac{1}{2}}(\sqrt{s}) &= \frac{1}{16\pi}(E_p - m_p)\left(M^{(I=0)}_{\frac{1}{2}^+} + M^{(I=1)}_{\frac{1}{2}^+}\right), \\ f^{(1)}_{K^-p,J=\frac{3}{2}}(\sqrt{s}) &= \frac{p^2_{cm}}{16\pi}(E_p + m_p)\left(M^{(I=0)}_{\frac{3}{2}^-} + M^{(I=1)}_{\frac{3}{2}^-}\right) \end{aligned} \tag{2.2}$$

with the baryon mass m_p and E_p denotes the baryon energy and p_{cm} the relative momentum in the center of mass frame. For any other channel similar expressions in terms of the amplitudes $M^{(I)}_{JP}(\sqrt{s})$ can be obtained and for further details we refer to [4].

Figures 2.1 with $J = \frac{1}{2}$ and 2.2 with $J = \frac{3}{2}$ are separated for $I = 0$ on the left and $I = 1$ on the right hand side. In Figure 2.1 the $\Lambda(1405)$ resonance can clearly be seen in the upper left panel, the ground state $\Lambda(1115)$ is shown in the lower left panel. The antikaon-nucleon threshold is marked by a vertical line. In the lower right panel the $\Sigma(1195)$ ground state can be seen and the $\Sigma(1385)$ resonance in the upper right panel of Figure 2.2. The $\Lambda(1520)$ resonance is present in the lower left panel above the threshold. We want to call attention to the different scales of each panel in both figures when comparing the relative heights.

2.2 Self-consistent dynamics of antikaons in nuclear matter

The properties of antikaons and hyperons in nuclear matter will be described self-consistently within a relativistic many-body framework based on the Bethe-Salpeter equation. The formulation of the scattering process in terms of the Bethe-Salpeter equation guarantees Lorentz invariance and unitarity. This approach is based on [5] and will be extended developing a novel renormalization scheme. We also deal with the systematic application of nucleon mean-fields, from which we expect sizeable repercussion on the microscopic treatment of kaonic atoms.

The vacuum antikaon-nucleon scattering amplitude is defined by

$$\begin{aligned}\langle \bar{K}^j(\bar{q})N(\bar{p})|T|\bar{K}^i(q)N(p)\rangle &= (2\pi)^4\delta^4(q + p - \bar{q} - \bar{p}) \\ &\times\ \bar{u}(\bar{p})T^{ij}(\bar{q}, \bar{p}, q, p)u(p), \end{aligned} \tag{2.3}$$

with the Dirac isospin-doublet spinor $u(p)$ of the nucleon, initial and final four-momentum of antikaon q, $\bar{q}$ and nucleon p, $\bar{p}$ and $\delta^4(\ldots)$ assuring energy-momentum conservation. The antikaon isospin doublet is $\bar{K} = (K^-, \bar{K}^0)$. By the use of appropriate isospin projectors $P^{ij}_{I=0}$ and $P^{ij}_{I=1}$ the vacuum scattering amplitude is decomposed into its isospin channels

$$T^{ij}(\bar{q}, \bar{p}, q, p) = T^{(I=0)}(\bar{k}, k, w) P^{ij}_{(I=0)} + T^{(I=1)}(\bar{k}, k, w) P^{ij}_{(I=1)} \tag{2.4}$$

with

$$P^{ij}_{(I=0)} = \frac{1}{4}\left(\delta^{ij}\, 1 + (\tau)^{ij}\, \tau\right), \qquad P^{ij}_{(I=1)} = \frac{1}{4}\left(3\,\delta^{ij}\, 1 - (\tau)^{ij}\, \tau\right) \tag{2.5}$$

and

$$w = p + q = \bar{p} + \bar{q}, \qquad k = \frac{1}{2}(p - q), \qquad \bar{k} = \frac{1}{2}(\bar{p} - \bar{q}). \tag{2.6}$$

The scattering amplitudes $T^{(I)}_{\bar{K}N}$ follow as the solutions of the Bethe-Salpeter integral equation

$$T(\bar{k}, k, w) = K(\bar{k}, k, w) + \int \frac{d^4 l}{(2\pi)^4} K(\bar{k}, l, w) G(l, w) T(l, k, w) \tag{2.7}$$

with the two-particle propagator

$$G(l, w) = -i S_N\left(\frac{1}{2}w + l\right) D_{\bar{K}}\left(\frac{1}{2}w - l\right) \tag{2.8}$$

and the kernel of the Bethe-Salpeter equation $K(\bar{k}, l, w)$. The free-space nucleon and kaon propagator are given by

$$S_N(p) = \frac{1}{\not{p} - m_N + i\epsilon}, \qquad D_{\bar{K}}(q) = \frac{1}{q^2 - m_K^2 + i\epsilon}. \tag{2.9}$$

In order to calculate the antikaon self-energy we have to evaluate the in-medium modification of the $\bar{K}N$ scattering amplitude in nuclear matter. The scattering process can readily be generalized to the infinite nuclear matter case, where we will use a simplified notation with $\mathcal{T} = \mathcal{T}(k, \bar{k}, w, u)$ and $\mathcal{G} = \mathcal{G}(l, w, u)$. The in-medium scattering amplitude $\mathcal{T}$ and the in-medium two-particle propagator $\mathcal{G}$ now depend on the four-velocity u_μ of the nuclear matter. The Bethe-Salpeter equation in short notation now reads

$$\mathcal{T} = \mathcal{K} + \mathcal{K} \cdot \mathcal{G} \cdot \mathcal{T}. \tag{2.10}$$

Medium modifications of the interaction kernel will not be considered, hence we approximate $\mathcal{K} = K$. For nuclear matter moving with velocity $\mathbf{u}$ we have

$$u_\mu = \left(\frac{1}{\sqrt{1 - \frac{\mathbf{u}^2}{c^2}}}, \frac{\frac{\mathbf{u}}{c}}{\sqrt{1 - \frac{\mathbf{u}^2}{c^2}}}\right) \qquad \text{and} \qquad u^2 = 1. \tag{2.11}$$

The density dependence of the $\bar{K}N$ interaction is due to the interaction of all baryons and mesons with the Fermi sea of the nucleons, this manifests itself in a self-energy contribution to the in-medium propagators. However, in addition Pauli blocking prevents scattering into intermediate states already occupied by nucleons from the Fermi sea. Pauli blocking is realized by an in-medium nucleon propagator in the loop integral of the Bethe-Salpeter equation. In generalization to the previous work [5] the effect of nuclear saturation will be included by means of a general nucleon mean-field Σ_N. The nucleon mean-field can be a function of momentum and bulk matter velocity $\Sigma_N = \Sigma_N(p,u)$, here we choose a simple parameterization with a real scalar and vector contribution,

$$\Sigma_N = \Sigma_V \not{u} - \Sigma_S , \qquad \Sigma_V = \Sigma_V(\rho), \qquad \Sigma_S = \Sigma_S(\rho), \tag{2.12}$$

parameterized in terms of the nuclear density ρ. The mean-field strength is estimated from surveys [23–28] and chosen to be

$$\Sigma_V = 290\,\mathrm{MeV}\,\frac{\rho}{\rho_0}, \qquad \Sigma_S = 350\,\mathrm{MeV}\,\frac{\rho}{\rho_0}. \tag{2.13}$$

Neither the scalar nor the vector nucleon mean-field can directly be related to observable quantities. They are used as a phenomenological tool to address nuclear saturation effects in a manifestly covariant manner and they are inherently scheme dependent. The density dependence of the scalar mean-field Σ_S and vector mean-field Σ_V is model dependent, we use the mean-fields as given by (2.13) at saturation density ρ_0.

The in-medium modified two-particle propagator $\mathcal{G}$ can now be written as

$$\mathcal{G}(l,w,u) = -i\mathcal{S}_N\left(\frac{1}{2}w + l, u\right)\mathcal{D}_{\bar K}\left(\frac{1}{2}w - l, u\right). \tag{2.14}$$

The modified propagators for nucleon and antikaon are

$$\begin{aligned}
\mathcal{S}_N(p,u) &= \frac{1}{\not{p} - \Sigma_V\,\not{u} - m_N + \Sigma_S + i\varepsilon} + \Delta S_N(p,u), \\
\Delta S_N(p,u) &= 2\,\pi\,i\,\Theta\Big[(p\cdot u) - \Sigma_V\Big]\,\delta\Big[(p-\Sigma_V\,u)^2 - (m_N - \Sigma_S)^2\Big] \\
&\quad \times \Big(\not{p} - \Sigma_V\,\not{u} + m_N - \Sigma_S\Big)\,\Theta\Big[k_F^2 + p^2 - (p\cdot u)^2\Big]
\end{aligned} \tag{2.15}$$

and

$$\mathcal{D}_{\bar K}(q,u) = \frac{1}{q^2 - m_K^2 - \Pi(q,u)}. \tag{2.16}$$

The Fermi momentum k_F in (2.15) parameterizes the nucleon density ρ for isospin symmetric matter according to

$$\rho = -2\cdot \mathrm{Tr}\,\gamma_0 \int \frac{d^4p}{(2\pi)^4}\, i\,\Delta S(p,u) = \frac{2\,k_F^3}{3\,\pi^2\,\sqrt{1-\mathbf{u}^2/c^2}} \tag{2.17}$$

and in the rest frame of the bulk matter with $u_\mu = (1,\mathbf{0})$ from (2.17) one recovers the standard result

$$\rho = \frac{2k_F^3}{3\pi^2}. \tag{2.18}$$

The self consistency is accommodated by evaluating the self-energy $\Pi(q,u)$ in terms of the isospin averaged in-medium scattering amplitudes $\bar{\mathcal{T}}^{(I)}_{\bar K N}$ defined as

$$\bar{\mathcal{T}}_{\bar K N} = \frac{1}{4}\mathcal{T}^{(I=0)}_{\bar K N} + \frac{3}{4}\mathcal{T}^{(I=1)}_{\bar K N}, \tag{2.19}$$

which by itself implies propagators with self-energy contributions. The in-medium antikaon self-energy is

$$\Pi(q,u) = 2 \cdot \mathrm{Tr} \int \frac{d^4p}{(2\pi)^4} i\Delta S_N(p,u) \bar{\mathcal{T}}_{\bar{K}N} \left(\frac{1}{2}(p-q), \frac{1}{2}(p-q), p+q, u \right) . \tag{2.20}$$

For solving the self-consistent set of equations (2.10), (2.15), (2.16) and (2.20) we rewrite the Bethe-Salpeter equation as follows

$$\mathcal{T} = K + K \cdot \mathcal{G} \cdot \mathcal{T} = T + T \cdot \Delta\mathcal{G} \cdot \mathcal{T}, \qquad \Delta\mathcal{G} = \mathcal{G} - G, \tag{2.21}$$

where the vacuum scattering amplitude T and its corresponding self-energy Π are used as the input for the self-consistent problem. Basic aspects of the vacuum scattering amplitude were discussed in Section 2.1.

2.2.1 Covariant projector algebra

Prior to establishing the projector algebra for in-medium scattering amplitudes that will be used throughout this work we recall the definitions of the projectors introduced in [4] for kaon-nucleon vacuum scattering. The amplitudes are decomposed into their components with angular momentum $J = n + \frac{1}{2}$ and parity ± according to

$$\begin{aligned} T(\bar{k},k,w) &= \sum_{\pm} P^{\frac{1}{2}^{\pm}}(w) M_{\frac{1}{2}^{\pm}}(\sqrt{s}) \\ &+ \sum_{\pm} \bar{q}^{\mu} P^{\frac{3}{2}^{\pm}}_{\mu\nu}(w) q^{\nu} M_{\frac{3}{2}^{\pm}}(\sqrt{s}) + \ldots , \end{aligned} \tag{2.22}$$

$$w = p + q = \bar{p} + \bar{q}, \qquad k = \frac{1}{2}(p-q), \qquad \bar{k} = \frac{1}{2}(\bar{p} - \bar{q}),$$

with $s = w^2$ and the scalar on-shell amplitudes $M_{J^P}(\sqrt{s})$ that have been introduced in (2.2). In (2.22) we suppressed the isospin index I and restricted the algebra to $J = \frac{1}{2}, \frac{3}{2}$. Note that the notation in (2.22) differs slightly from the one used in [4]. The lowest order vacuum projectors are given by

$$\begin{aligned} P^{\frac{1}{2}^{\pm}}(w) &= \frac{1}{2}\left(\frac{\not{w}}{\sqrt{w^2}} \mp 1 \right) \\ P^{\frac{3}{2}^{\pm}}_{\mu\nu}(w) &= \frac{3}{2}\left(\frac{\not{w}}{\sqrt{w^2}} \pm 1 \right) \left\{ \frac{w_\mu \, w_\nu}{w^2} - g_{\mu\nu} + \frac{1}{3}\left(\gamma_\mu - \frac{\not{w}\, w_\mu}{w^2} \right) \left(\gamma_\nu - \frac{\not{w}\, w_\nu}{w^2} \right) \right\}, \end{aligned} \tag{2.23}$$

with $P^{\frac{1}{2}^{-}}$ projecting onto s-wave, $P^{\frac{1}{2}^{+}}$ and $P^{\frac{3}{2}^{+}}$ onto p-wave and $P^{\frac{3}{2}^{-}}$ onto d-wave.

In [5] a generalization of the projector algebra of (2.22) to the medium case, containing Dirac structures $\not{w}$, $\not{u}$ and $\not{w} \cdot \not{u}$ was developed. Taking the free-space scattering of [4], the in-medium scattering amplitude $\mathcal{T}$ has the form:

$$\begin{aligned}\mathcal{T} &= \sum_{i,j=1}^{2} T_{ij}^{(p)}(v,u)\, P_{ij}(v,u) \\ &+ \sum_{i=1}^{2}\sum_{j=3}^{8} \Big(T_{ij}^{(p)}(v,u)\, P_{ij}^{\mu}(v,u)\, q_\mu + T_{ji}^{(p)}(v,u)\, \bar{q}_\mu\, P_{ji}^{\mu}(v,u) \Big) \\ &+ \sum_{i,j=3}^{8} T_{ij}^{(p)}(v,u)\, \bar{q}_\mu\, P_{ij}^{\mu\nu}(v,u)\, q_\nu + \sum_{i,j=1}^{2} T_{ij}^{(q)}(v,u)\, \bar{q}_\mu\, Q_{ij}^{\mu\nu}(v,u)\, q_\nu , \end{aligned} \tag{2.24}$$

with

$$\begin{aligned} T_{ij}^{(p)}(v,u) &= M_{ij}^{(p)}(v,u) \Big[1 - \Delta J_{ij}^{(p)}(v,u)\, M_{ij}^{(p)}(v,u) \Big]^{-1} , \\ T_{ij}^{(q)}(v,u) &= M_{ij}^{(q)}(v,u) \Big[1 - \Delta J_{ij}^{(q)}(v,u)\, M_{ij}^{(q)}(v,u) \Big]^{-1} . \end{aligned} \tag{2.25}$$

The matrix of loop functions $\Delta J_{ij}^{(p,q)}$ will be discussed in Section 2.3 in detail and the matrix of free-space scattering amplitudes $M_{ij}^{(p,q)}$ will be specified in Section 2.2.2. The representation (2.24) is analogous to the one established in [5]. In (2.24) and (2.25) we introduced a new convenient four-momentum

$$v_\mu = w_\mu - \Sigma_V u_\mu \tag{2.26}$$

that accounts for a nonzero vector mean-field as defined in (2.12) and considerably simplifies the notation throughout this work. The index p and q in (2.24) and (2.25) refers to two different helicity states in so-called P- and Q-space. The generalized projectors P_{ij} and Q_{ij}, which do not mix among each other, form a complete algebra with the properties

$$\begin{aligned} & P_{ik} \cdot P_{lj} = \delta_{kl} P_{ij} , \quad P_{ik}^{\mu} \cdot \bar{P}_{lj}^{\nu} = \delta_{kl} P_{ij}^{\mu\nu} , \quad \bar{P}_{ik}^{\mu} g_{\mu\nu} P_{lj}^{\nu} = \delta_{kl} P_{ij} , \\ & Q_{ik}^{\mu\alpha} g_{\alpha\beta} P_{lj}^{\beta\nu} = P_{ik}^{\mu\alpha} g_{\alpha\beta} Q_{lj}^{\beta\nu} = 0 , \quad Q_{ik}^{\mu\alpha} g_{\alpha\beta} P_{lj}^{\beta} = \bar{P}_{ik}^{\alpha} g_{\alpha\beta} Q_{lj}^{\beta\nu} = 0 , \\ & Q_{ik}^{\mu\alpha} g_{\alpha\beta} Q_{lj}^{\beta\nu} = \delta_{kl} Q_{ij}^{\mu\nu} , \quad P_{ik}^{\mu\alpha} g_{\alpha\beta} P_{lj}^{\beta\nu} = \delta_{kl} P_{ij}^{\mu\nu} . \end{aligned} \tag{2.27}$$

The projectors P_{ij} and Q_{ij} are specified in Appendix A.1 in detail. As they cover the whole Dirac structure of the underlying theory the solution of the Bethe-Salpeter equation is simplified to the integration of loop functions $\Delta J_{ij}^{(p,q)}(v,u)$ and reconstruction of the amplitudes from a matrix equation. The form of the projector algebra given in (2.24) and (2.25) completely agrees with the one established in [5], except for the fact that we use the argument v_μ rather than w_μ. Due to the completeness of the projector algebra these representations are equivalent. In Section 2.2.2 we will address the problem of changing the representation, that is expressing quantities in terms of the 'physical' external momentum w_μ in the basis spanned by the v_μ dependent projectors and vice-versa.

2.2.2 Recoupling of the vacuum scattering amplitudes

Before we proceed with the definition and discussion of the matrix loop functions $\Delta J_{ij}^{(p,q)}(v,u)$ used in (2.25) we will focus on the interaction kernel given in terms of the $\bar{K}N$ vacuum scattering amplitude as defined in (2.21). Due to the use of the projectors with arguments v_μ and u_μ instead of w_μ this is slightly involved and we have to specify the recoupled free-space scattering amplitudes $M_{ij}^{(p,q)}(v,u)$ that will be linear combinations of the scalar on-shell amplitudes $M_{\frac{1}{2}^\pm}(\sqrt{s})$ and $M_{\frac{3}{2}^\pm}(\sqrt{s})$ as introduced in (2.22). The recoupled vacuum scattering amplitude T now reads

$$\begin{aligned} T(\bar{k},k,w) &= \sum_{i,j=1}^{2} M_{ij}^{(p)}(v,u)\, P_{ij}(v,u) \\ &+ \sum_{i=1}^{2}\sum_{j=3}^{8} \Big(M_{ij}^{(p)}(v,u)\, P_{ij}^{\mu}(v,u)\, q_\mu + M_{ji}^{(p)}(v,u)\, \bar{q}_\mu\, P_{ji}^{\mu}(v,u) \Big) \\ &+ \sum_{i,j=3}^{8} M_{ij}^{(p)}(v,u)\, \bar{q}_\mu\, P_{ij}^{\mu\nu}(v,u)\, q_\nu + \sum_{i,j=1}^{2} M_{ij}^{(q)}(v,u)\, \bar{q}_\mu\, Q_{ij}^{\mu\nu}(v,u)\, q_\nu \,, \end{aligned}$$

$$w = p+q = \bar{p}+\bar{q}, \qquad k = \frac{1}{2}(p-q), \qquad \bar{k} = \frac{1}{2}(\bar{p}-\bar{q}),$$

which is analogous to the representation of (2.24). The free-space amplitudes $M_{ij}^{(p,q)}(v,u)$ can be decomposed by using appropriate recoupling coefficients $C_{p,ij}^{\frac{1}{2}^\pm}(v,w,u)$ and $C_{q,ij}^{\frac{3}{2}^\pm}(v,w,u)$ according to

$$\begin{aligned} M_{ij}^{(p)}(v,u) &= \sum_{\pm} C_{p,ij}^{\frac{1}{2}^\pm}(v,w,u)\, M_{\frac{1}{2}^\pm}(\sqrt{s}\,) + \sum_{\pm} C_{p,ij}^{\frac{3}{2}^\pm}(v,w,u)\, M_{\frac{3}{2}^\pm}(\sqrt{s}\,)\,, \\ M_{ij}^{(q)}(v,u) &= \sum_{\pm} C_{q,ij}^{\frac{3}{2}^\pm}(v,w,u)\, M_{\frac{3}{2}^\pm}(\sqrt{s}\,)\,. \end{aligned} \tag{2.28}$$

Due to the orthogonality properties of the projectors the recoupling coefficients are determined by calculating traces over products of the vacuum and in-medium projectors. By comparison of the expressions (2.22) and (2.28) the recoupling can be formulated by writing relations between the vacuum (2.23) and in-medium projectors P_{ij} and Q_{ij}:

$$\begin{aligned} P^{\frac{1}{2}^\pm}(w) &= \sum_{i,j=1}^{2} C_{p,ij}^{\frac{1}{2}^\pm}(v,w,u) P_{ij}(v,u), \\ P_{\mu\nu}^{\frac{3}{2}^\pm}(w) &= \sum_{i,j=3}^{8} C_{p,ij}^{\frac{3}{2}^\pm}(v,w,u) P_{ij,\mu\nu}(v,u) \\ &\quad + \sum_{i,j=1}^{2} C_{q,ij}^{\frac{3}{2}^\pm}(v,w,u) Q_{ij,\mu\nu}(v,u). \end{aligned} \tag{2.29}$$

Finally we obtain three groups of recoupling coefficients,

$$\begin{aligned}
C^{\frac{1}{2}^\pm}_{p,ij}(v,w,u) &= \begin{cases} \frac{1}{2}\,\mathrm{Tr}\left[P_{ij}(v,u)P^{\frac{1}{2}^\pm}(w)\right] & \text{for} \quad i,j=1,2 \\ 0 & \text{else}, \end{cases} \\
C^{\frac{3}{2}^\pm}_{p,ij}(v,w,u) &= \begin{cases} \frac{1}{2}\,\mathrm{Tr}\left[P^{\mu\nu}_{ij}(v,u)P^{\frac{3}{2}^\pm}_{\nu\mu}(w)\right] & \text{for} \quad i,j=3,\ldots,8 \\ 0 & \text{else}, \end{cases} \\
C^{\frac{3}{2}^\pm}_{q,ij}(v,w,u) &= \begin{cases} \frac{1}{2}\,\mathrm{Tr}\left[Q^{\mu\nu}_{ij}(v,u)P^{\frac{3}{2}^\pm}_{\nu\mu}(w)\right] & \text{for} \quad i,j=1,2 \\ 0 & \text{else}. \end{cases}
\end{aligned} \tag{2.30}$$

When decomposing the vacuum projectors in terms of the in-medium projectors [5] according to

$$\begin{aligned}
P^{\frac{1}{2}^-}(v,u) &= P_{11}(v,u), \\
P^{\frac{1}{2}^+}(v,u) &= -P_{22}(v,u), \\
P^{\frac{3}{2}^+,\nu\mu}(v,u) &= -3\left[Q^{\mu\nu}_{11}(v,u)+P^{\mu\nu}_{77}(v,u)\right], \\
P^{\frac{3}{2}^-,\nu\mu}(v,u) &= 3\left[Q^{\mu\nu}_{22}(v,u)+P^{\mu\nu}_{88}(v,u)\right]
\end{aligned} \tag{2.31}$$

one observes a decoupling between P- and Q-space even for different arguments v and w, that is terms like $\mathrm{Tr}\left[P^{\mu\nu}_{ij}(v,u)Q^{kl}_{\nu\mu}(w,u)\right]$ and $\mathrm{Tr}\left[Q^{\mu\nu}_{ij}(v,u)P^{kl}_{\nu\mu}(w,u)\right]$ vanish. The normalization factor in (2.30) is obtained by calculating the traces

$$\mathrm{Tr}\left[P_{ij}(v,u)P^{\frac{1}{2}^\pm}(v)\right], \qquad \mathrm{Tr}\left[P^{\mu\nu}_{ij}(v,u)P^{\frac{3}{2}^\pm}_{\nu\mu}(v)\right] \tag{2.32}$$

for the same argument v of the vacuum and in-medium projectors, ensuring that

$$C^{\frac{1}{2}^-}_{p,11}(v,w,u) = C^{\frac{1}{2}^+}_{p,22}(v,w,u) = C^{\frac{3}{2}^+}_{p,77}(v,w,u) = C^{\frac{3}{2}^-}_{p,88}(v,w,u) = 1 \tag{2.33}$$

for the 'diagonal' elements in P-space and

$$C^{\frac{3}{2}^+}_{q,11}(v,w,u) = C^{\frac{3}{2}^-}_{q,22}(v,w,u) = 1 \tag{2.34}$$

in Q-space. The 'off-diagonal' elements have to vanish for $v = w$. The only normalization factor turns out to be $\frac{1}{2}$. A complete list of all the recoupling coefficients $C^{\frac{1}{2}^\pm}_{p,ij}(v,u)$ and $C^{\frac{3}{2}^\pm}_{q,ij}(v,u)$ is given in Appendix A.2.

2.3 Loop functions

The form of the reduced loop functions $\Delta J^{(p,q)}_{ij}(v,u)$ in (2.25) is determined by the two-particle propagator $\Delta\mathcal{G}$ in (2.21). The finite imaginary part can be taken from [5] except for a novel renormalization scheme eliminating power divergences and avoiding the occurrence of kinematical singularities, which is of special importance as soon as p-wave scattering and finite nucleon mean-fields are considered.

The two-particle propagator $\Delta\mathcal{G}$ is split into two parts, the in-medium $\mathcal{G}$ and the vacuum contribution G:

$$\Delta\mathcal{G} = -i\left(\mathcal{S}_N \mathcal{D}_{\bar{K}} - S_N D_{\bar{K}}\right). \tag{2.35}$$

Accordingly the reduced loop functions can be split into an in-medium and vacuum contribution,

$$\Delta J_{ij}^{(p,q)}(v,u) = J_{ij}^{(p,q)}(v,u) - J_{ij}^{(p,q),\mathrm{vac}}(v,u), \tag{2.36}$$

which will be reviewed separately further on.

The in-medium loop function matrix $J_{ij}^{(p,q)}(v,u)$ is explicitly defined by

$$\begin{aligned}
&-i\int \frac{d^4l}{(2\pi)^4}\frac{1}{\not{l}-m_N^*+i\varepsilon}\frac{1}{(v-l)^2-m_K^2-\Pi(v-l,u)} \\
&\quad = \sum_{i,j=1}^{2} J_{ij}^{(p)}(v,u)P_{ij}(v,u), \\
&-i\int \frac{d^4l}{(2\pi)^4}\left(v^\mu - l^\mu\right)\frac{1}{\not{l}-m_N^*+i\varepsilon}\frac{1}{(v-l)^2-m_K^2-\Pi(v-l,u)} \\
&\quad = \sum_{j=3}^{8}\left[J_{j1}^{(p)}(v,u)P_{j1}^{\mu}(v,u) + J_{j2}^{(p)}(v,u)P_{j2}^{\mu}(v,u)\right] \\
&\quad = \sum_{j=3}^{8}\left[J_{1j}^{(p)}(v,u)\bar{P}_{1j}^{\mu}(v,u) + J_{2j}^{(p)}(v,u)\bar{P}_{2j}^{\mu}(v,u)\right], \\
&-i\int \frac{d^4l}{(2\pi)^4}\left(v^\mu - l^\mu\right)\left(v^\nu - l^\nu\right)\frac{1}{\not{l}-m_N^*+i\varepsilon}\frac{1}{(v-l)^2-m_K^2-\Pi(v-l,u)} \\
&\quad = \sum_{i,j=3}^{8} J_{ij}^{(p)}(v,u)P_{ij}^{\mu\nu}(v,u) + \sum_{i,j=1}^{2} J_{ij}^{(q)}(v,u)Q_{ij}^{\mu\nu}(v,u).
\end{aligned} \tag{2.37}$$

Note that for simplicity of presentation in (2.37) we suppress the Pauli-blocking term from (2.15), later on it will be restored. We have $v_\mu = w_\mu - \Sigma_V u_\mu$ and we will use the short notation $m_N^* = m_N - \Sigma_S$. The loop functions $J_{ij}^{(p,q)}(v,u)$ are Lorentz scalar and can further be expressed in terms of the propagator part $g(l,v,u)$,

$$\begin{aligned}
g(l;v,u) \;=\;& -\frac{i}{l^2-{m_N^*}^2+i\varepsilon}\frac{1}{(v-l)^2-m_K^2-\Pi(v-l,u)} \\
&+2\,\pi\,\Theta\left(l\cdot u\right)\,\delta(l^2-{m_N^*}^2)\frac{\Theta\left(k_F^2+{m_N^*}^2-(l\cdot u)^2\right)}{(v-l)^2-m_K^2-\Pi(v-l,u)},
\end{aligned} \tag{2.38}$$

and scalar kernels $K_{ij}^{(p,q)}(l,v,u)$. These kernel functions contain powers of l^2, $l\cdot v$, $l\cdot u$, $v\cdot u$, v^2 and are implicitly defined via the loop functions $J_{ij}^{(p,q)}$. With the help of $g(l,v,u)$ and the kernel functions $K_{ij}^{(p,q)}$ the in-medium loop functions now read

$$J_{ij}^{(p,q)}(v,u) = \int \frac{d^4l}{(2\pi)^4}\, g(l,v,u)K_{ij}^{(p,q)}(l,v,u). \tag{2.39}$$

Detailed results will be derived in the subsequent section.

We turn to the second term in (2.36). In order to apply the same projector algebra in terms of v instead of w for the vacuum contribution of the two-particle propagator it has to be written in terms of $P_{ij}(v,u)$, etc. The vacuum contribution does not depend on the nucleon mean-fields. We shift the nucleon momentum according to $\breve{l}_\mu = l_\mu - \Sigma_V u_\mu$ and the vacuum loop functions $J_{ij}^{(p,q),\mathrm{vac}}(v,u)$ acquire the form

$$
\begin{aligned}
&-i\int \frac{d^4\breve{l}}{(2\pi)^4}\,\frac{1}{\not{\breve{l}} + \Sigma_V \not{u} - m_N + i\varepsilon}\,\frac{1}{(v-\breve{l})^2 - m_K^2 + i\varepsilon} \\
&\quad = \sum_{i,j=1}^{2} J_{ij}^{(p),\mathrm{vac}}(v,u)\,P_{ij}(v,u), \\
&-i\int \frac{d^4\breve{l}}{(2\pi)^4}\left(v^\mu - \breve{l}^\mu\right)\frac{1}{\not{\breve{l}} + \Sigma_V \not{u} - m_N + i\varepsilon}\,\frac{1}{(v-\breve{l})^2 - m_K^2 + i\varepsilon} \\
&\quad = \sum_{j=3}^{8}\left[J_{j1}^{(p),\mathrm{vac}}(v,u)\,P_{j1}^{\mu}(v,u) + J_{j2}^{(p),\mathrm{vac}}(v,u)\,P_{j2}^{\mu}(v,u)\right] \\
&\quad = \sum_{j=3}^{8}\left[J_{1j}^{(p),\mathrm{vac}}(v,u)\,\bar{P}_{1j}^{\mu}(v,u) + J_{2j}^{(p),\mathrm{vac}}(v,u)\,\bar{P}_{2j}^{\mu}(v,u)\right], \\
&-i\int \frac{d^4\breve{l}}{(2\pi)^4}\left(v^\mu - \breve{l}^\mu\right)\left(v^\nu - \breve{l}^\nu\right)\frac{1}{\not{\breve{l}} + \Sigma_V \not{u} - m_N + i\varepsilon}\,\frac{1}{(v-\breve{l})^2 - m_K^2 + i\varepsilon} \\
&\quad = \sum_{i,j=3}^{8} J_{ij}^{(p),\mathrm{vac}}(v,u)\,P_{ij}^{\mu\nu}(v,u) + \sum_{i,j=1}^{2} J_{ij}^{(q),\mathrm{vac}}(v,u)\,Q_{ij}^{\mu\nu}(v,u).
\end{aligned}
\tag{2.40}
$$

From the latter definition it is follows that the vacuum loop functions do not depend on the vector mean-field Σ_V, so that it can always be written as a linear combination of the tensor structures w_μ, γ_μ, $\not{w} w_\mu$, $\not{w}\gamma_\mu$ and scalar amplitudes depending on w^2. This implies that the free-space loop function matrix $J_{ij}^{(p,q),\mathrm{vac}}$ can be composed from non-vanishing master functions $J_i^V(w^2)$ that will be established in Section 2.3.1. The vacuum loop functions $J_{ij}^{(p,q),\mathrm{vac}}$ in (2.40) can be split into two contributions, the matrix structure of the first one is identical to the in-medium case (2.37) but with $\Sigma_V = 0$, $\Sigma_S = 0$ and $\Pi = 0$, denoted as $J_{ij,V}^{(p,q)}$. The second contribution $\Delta J_{ij,V}^{(p,q)}$ proportional to Σ_V arises from $\not{l} = \not{\breve{l}} + \Sigma_V \not{u}$ in the denominator of (2.40) and will add up to the vacuum loop functions:

$$
\begin{aligned}
J_{ij}^{(p,q),\mathrm{vac}}(v,u) &= J_{ij,V}^{(p,q)}(v,u) + \Sigma_V \Delta J_{ij,V}^{(p,q)}(v,u) \\
&= \int \frac{d^4 l}{(2\pi)^4}\, g_{\mathrm{vac}}(l,v,u)\left[K_{ij,V}^{(p,q)}(l,v,u) + \Sigma_V \Delta K_{ij,V}^{(p,q)}(l,v,u)\right].
\end{aligned}
\tag{2.41}
$$

The vacuum propagator part is given by

$$
g_{\mathrm{vac}}(l,v,u) = -i\,\frac{1}{l^2 - m_N^2 + i\varepsilon}\,\frac{1}{(v-l)^2 - m_K^2 + i\varepsilon}
\tag{2.42}
$$

and the kernel functions $K_{ij,V}^{(p,q)}(l,v,u)$ are identical to the in-medium ones $K_{ij}^{(p,q)}(l,v,u)$ from (2.39) in the free-space limit. The free-space loop functions $J_{ij}^{(p,q),\mathrm{vac}}(v,u)$ will be elaborated on in Appendix A.3. The Kernels $\Delta K^{(p,q)}_{ij,V}$ are implicitly given via the definition of the loop functions $\Delta J^{(p,q)}_{ij,V}$ in Appendix A.4.

Finally the loop functions with the subtracted vacuum contribution are

$$\begin{aligned}
\Delta J^{(p,q)}_{ij}(v,u) &= J^{(p,q)}_{ij}(v,u) - J^{(p,q),\mathrm{vac}}_{ij}(v,u) \\
&= \int \frac{d^4l}{(2\pi)^4}\Big[g(l,v,u)K^{(p,q)}_{ij}(l,v,u) - g_{\mathrm{vac}}(l,v,u)K^{(p,q),\mathrm{vac}}_{ij}(l,v,u)\Big]\,, \\
K^{(p,q),\mathrm{vac}}_{ij}(l,v,u) &= K^{(p,q)}_{ij,V}(l,v,u) + \Sigma_V \Delta K^{(p,q)}_{ij,V}(l,v,u). \qquad (2.43)
\end{aligned}$$

Up to now the expressions (2.43) are ultraviolet divergent. We will develop a new renormalization scheme that accounts for the vacuum limit proposed in [4].

2.3.1 Renormalization of the loop functions

Recall the in-medium loops function matrix

$$J^{(p,q)}_{ij}(v,u) = \int \frac{d^4l}{(2\pi)^4}\, g(l,v,u)K^{(p,q)}_{ij}(l,v,u). \qquad (2.44)$$

Causality requires that all diagonal loops of (2.44) have a positive imaginary part everywhere, which does not have be the case for the off-diagonal matrix elements. This issue can be used as an important consistency check of the projector algebra approach presented in the preceding sections and utilising the on-shell reduction scheme established in [5] and [4]. The matrix of loop functions in (2.44) can be composed out of thirteen independent scalar loop functions

$$J_i(v,u) = \int \frac{d^4l}{(2\pi)^4}\, g(l,v,u)K_i(l,v,u), \qquad (2.45)$$

this has been shown in [5]. We will stick to the transparent representation

$$\begin{aligned}
&K_0 = 1\,, \qquad\qquad K_1 = \frac{(l\cdot v)}{\sqrt{v^2}}\,, \\
&K_2 = -\frac{(v\cdot u)}{\sqrt{v^2}\,\sqrt{(v\cdot u)^2 - v^2}}\left[(l\cdot v) - \frac{v^2}{(v\cdot u)}\,(l\cdot u)\right]\,, \\
&K_5 = -\frac{2\,(v\cdot u)}{\sqrt{(v\cdot u)^2 - v^2}}\,K_1\,K_2 - \frac{(v\cdot u)^2}{(v\cdot u)^2 - v^2}\,K_1^2 + \frac{v^2\,(l\cdot u)^2}{(v\cdot u)^2 - v^2}\,, \\
&K_{11} = -\frac{(v\cdot u)^2}{(v\cdot u)^2 - v^2}\left[\frac{(v\cdot u)}{\sqrt{(v\cdot u^2) - v^2}}\,K_1 + 3\,K_2\right]K_1^2 \\
&\qquad - \frac{3\,(v\cdot u)}{\sqrt{(v\cdot u)^2 - v^2}}\,K_1\,K_5 + \frac{(v^2)^{3/2}\,(l\cdot u)^3}{\sqrt{(v\cdot u)^2 - v^2}^{\,3}}\,, \\
&K_3 = \tfrac{1}{2}\left[l^2 - K_1^2 + K_5\right]\,, \qquad K_4 = K_1^2\,, \\
&K_6 = K_1\,K_2\,, \qquad K_7 = K_1\,K_3\,, \qquad K_8 = \tfrac{1}{2}\left[(l^2 - K_1^2)\,K_2 + K_{11}\right]\,, \\
&K_9 = K_1^3\,, \qquad K_{10} = K_1^2\,K_2\,, \qquad K_{12} = K_1\,K_5\,. \qquad (2.46)
\end{aligned}$$

for the thirteen loop kernel functions $K_i(l,v,u)$ that are linearly combined to form the matrix of loop functions $J^{(p,q)}_{ij}(l,v,u)$ in conjunction with the propagator (2.38) according to (2.39) in

P- and Q-space. The matrix elements $J_{ij}^{(p,q)}$ are listed in Appendix A.5. The renormalization will be done with respect to these thirteen loop kernel functions.

The imaginary parts of the loop functions behave like v_0^n for large v_0 with n not always smaller than or equal to zero. Hence when calculating the real part of the loops by an (unsubtracted) dispersion integral, such as

$$\mathfrak{Re} J_i(v_0, \mathbf{w}) = \int\limits_{-\infty}^{+\infty} \frac{d\bar{v}_0}{\pi} \frac{\mathfrak{Im} J_i(\bar{v}_0, \mathbf{w})}{\bar{v}_0 - v_0}, \tag{2.47}$$

power divergencies will arise that have to be eliminated. The regularization of (2.45) could be done by a momentum cutoff λ in the imaginary part of the loops and λ has to be adjusted to match the $\bar{K}N$ scattering data. Nevertheless a three-momentum cutoff introduces a frame-dependent result and the Lorentz invariance of the scattering amplitude would be destroyed.

We continue with the subtraction scheme to render the real part of the loops finite and eliminate all power divergent terms. As the physical part of a consistent field theory has to be finite all such divergencies have to be absorbed into counter terms. Since we do not want to cope with such counter terms explicitly it is crucial to set up a proper renormalization. We require the in-medium loop functions $J_i(v, u)$ to approach the free-space form of the loops in the zero-density limit as introduced in [4]. It is imposed by

$$\begin{aligned} J_i(v,u) &\overset{\rho=0}{\longrightarrow} N_i(v) \int_{-\infty}^{+\infty} \frac{d\,\bar{v}^2}{\pi} \frac{v^2}{\bar{v}^2} \frac{\rho(\bar{v})}{\bar{v}^2 - v^2 - i\,\epsilon}\,, \\ \rho(v) &= \frac{\Theta\Big[v^2 - (m_N + m_K)^2\Big]}{16\,\pi\,\sqrt{v^2}} \sqrt{v^2 - 2\,(m_N^2 + m_K^2) + \frac{(m_N^2 - m_K^2)^2}{v^2}}\,, \end{aligned} \tag{2.48}$$

where the N_i are parts of the free-space loop functions and are given by [4]

$$\begin{aligned} N_0 &= 1, \qquad N_1 = \frac{v^2 + m_N^2 - m_K^2}{2\sqrt{v^2}}, \qquad N_2 = N_6 = N_8 = 0, \\ N_3 &= -N_5 = -\frac{\big[(m_N - m_K)^2 - v^2\big]\,\big[(m_N + m_K)^2 - v^2\big]}{12 v^2}, \qquad N_4 = N_1^2, \\ N_7 &= -N_{12} = N_1 N_3, \qquad N_9 = N_1^3, \qquad N_{10} = N_{11} = 0. \end{aligned} \tag{2.49}$$

With (2.48) the loop functions (2.45) are finite in the zero-density limit. We recall that the representation (2.48) was motivated by properties of the loop functions manifested within dimensional regularization [4]. Its form follows from the Passarino Veltman representation [29] supplemented by a subtraction of reduced tadpole contributions. The occurrence of power divergencies is avoided by the subtraction scheme defined by (2.48).

When changing to the in-medium case we cannot simply proceed with the aforementioned scheme, as we have to address the fact that the in-medium projectors exhibit singularities at $v^2 = 0$ and $v^2 = (v \cdot u)^2$. This behaviour imposes certain correlations on the loop functions (2.45) at the singular points that have to be considered. Ignoring such correlations of the loop functions would show up in artificial structures in the self-energy that contradict causality. This matters especially since the critical point at $v^2 = (w - \Sigma_V u)^2 = 0$ is within the scope of this work. Sufficient and necessary constraints on the loop functions which prevent kinematical singularities can be derived from the projector properties and lead to the requirements that

$$\begin{aligned}
J_1^R + \frac{(v\cdot u)}{\sqrt{(v\cdot u)^2}} J_2^R &= \mathcal{O}\left(\sqrt{v^2}\right) ,\\
J_7^R + \frac{(v\cdot u)}{\sqrt{(v\cdot u)^2}} J_8^R &= \mathcal{O}\left(\sqrt{v^2}\right) ,\\
J_7^R + J_5^R + 2\frac{(v\cdot u)}{\sqrt{(v\cdot u)^2}} J_6^R &= \mathcal{O}\left(\sqrt{v^2}\right) ,\\
J_{10}^R + J_{11}^R + 2\frac{(v\cdot u)}{\sqrt{(v\cdot u)^2}} J_{12}^R &= \mathcal{O}\left(\sqrt{v^2}\right) ,\\
\frac{(v\cdot u)}{\sqrt{(v\cdot u)^2}} J_9^R + 3J_{10}^R + J_{11}^R + 3\frac{(v\cdot u)}{\sqrt{(v\cdot u)^2}} J_{12}^R &= \mathcal{O}\left(\sqrt{v^2}\right) \qquad (2.50)
\end{aligned}$$

at $v^2 = 0$. Furthermore we need

$$J_2^R = J_3^R + J_5^R = J_6^R = J_8^R = J_7^R + J_{12}^R = 0 \qquad (2.51)$$

at $v^2 = (v\cdot u)^2$. Condition (2.51) leads to the decoupling of partial waves carrying different total angular momentum for $v^2 = (v\cdot u)^2$, which is in general no longer true for $v^2 \neq (v\cdot u)^2$ in the nuclear medium [5] because total angular momentum is not conserved. The free-space limit (2.48) proves to be incompatible with the requirements (2.50) and (2.51) and we have to generalize expression (2.48) to

$$\begin{aligned}
J_i^R(v,u) \quad &\overset{\rho=0}{\longrightarrow} \quad J_i^V(v) \equiv N_i(v) \int_{-\infty}^{+\infty} \frac{d\bar{v}^2}{\pi}\, \frac{v^2}{\bar{v}^2}\, \frac{\rho(\bar{v})}{\bar{v}^2 - v^2 - i\varepsilon} \\
&+ \quad \Delta_i^{(4)}(v) \int_{-\infty}^{+\infty} \frac{d\bar{v}^2}{\pi} \left(\frac{v^2}{\bar{v}^2}\right)^2 \rho(\bar{v}) + \Delta_i^{(6)}(v) \int_{-\infty}^{+\infty} \frac{d\bar{v}^2}{\pi} \left(\frac{v^2}{\bar{v}^3}\right)^2 \rho(\bar{v}) \qquad (2.52)
\end{aligned}$$

in order to fulfill constraints (2.50) and (2.51). The additional minimal subtraction terms $\Delta_i^{(4)}$ and $\Delta_i^{(6)}$ are

$$\begin{aligned}
\Delta_3^{(4)} &= -\Delta_5^{(4)} = \frac{(m_N^2 - m_K^2)^2}{3(v^2)^2} ,\\
\Delta_9^{(4)} &= \frac{1}{8}\frac{(m_N^2 - m_K^2)^3}{\sqrt{v^2}(v^2)^2} ,\\
\Delta_7^{(4)} &= -\Delta_{12}^{(4)} = -\left(\frac{N_1}{12} - \frac{N_1 N_5}{v^2} - \frac{(m_N^2 - m_K^2)^2}{8\sqrt{v^2}^3} \right) ,\\
\Delta_7^{(6)} &= -\Delta_{12}^{(6)} = \left(\frac{(m_N^2 - m_K^2)^2 N_1}{12\,(v^2)^2} + \frac{(m_N^2 - m_K^2)^2}{8\sqrt{v^2}^3} + \frac{(m_N^2 - m_K^2)^3}{24\sqrt{v^2}^5} \right) . \qquad (2.53)
\end{aligned}$$

All remaining ones are zero. With the additional subtractions we now fulfill conditions (2.50) and (2.51). The generalization of (2.52) from vacuum to in-medium is hindered by the fact that some loops vanishing in the vacuum take finite values in the medium.

We proceed with the dispersion integral representation of the renormalized in-medium loop functions in terms of spectral weight functions $\mathfrak{Im} J_i^R(v_0, \bar{v}_0, \mathbf{w})$ relying on the definition of external energies $v_0 = w_0 - \Sigma_V$ and internal ones $\bar{v}_0$. The renormalized in-medium loop functions in the nuclear matter rest frame with $\mathbf{u} = 0$ denoted by $J_i^R(v_0, \mathbf{w})$ are introduced as

$$J_i^R(v_0, \mathbf{w}) = \int_{-\infty}^{+\infty} \frac{d\bar{v}_0}{\pi} \frac{\text{sign}(\bar{v}_0 - \mu)\, \mathfrak{Im} J_i^R(v_0, \bar{v}_0, \mathbf{w})}{\bar{v}_0 - v_0 - i\varepsilon(\bar{v}_0 - \mu)} + J_i^C(v_0, \mathbf{w}) \tag{2.54}$$

with the chemical potential $\mu = \sqrt{{m_N^*}^2 + k_F^2}$. The imaginary part of the loop functions is

$$\begin{aligned} \mathfrak{Im} J_i^R(v_0, \bar{v}_0, \mathbf{w}) &= \int \frac{d^3 l}{2(2\pi)^3} \frac{1}{E_N^*} \\ &\times \Big\{ K_i^R(l_+, v_0, \bar{v}_0, \mathbf{w}) \rho_K(\bar{v}_+, \mathbf{w} - \mathbf{l}) \left[\Theta(+\bar{v}_+) - \Theta(k_F - |\mathbf{l}|) \right] \\ &\quad + K_i^R(l_-, v_0, \bar{v}_0, \mathbf{w}) \rho_K(\bar{v}_-, \mathbf{w} - \mathbf{l}) \Theta(-\bar{v}_-) \Big\}, \\ l_\pm^\mu &= (\pm E_N^*, \mathbf{l}), \\ \bar{v}_\pm &= \bar{v}_0 \mp E_N^* \end{aligned} \tag{2.55}$$

with $E_N^* = \sqrt{{m_N^*}^2 + \mathbf{l}^2}$. The antikaon spectral function is given by

$$\rho_K(\omega, \mathbf{q}) = -\frac{1}{\pi} \mathfrak{Im} \frac{1}{\omega^2 - \mathbf{q}^2 - m_K^2 - \Pi(\omega, \mathbf{q})}. \tag{2.56}$$

The scalar functions $K_i^R(l_\pm, v_0, \bar{v}_0, \mathbf{w})$ that comply with the vacuum limit (2.52) and constraints (2.50) and (2.51) are listed in Appendix A.6. The loop function kernels (A.21) depend on 'external' and 'internal' variables $v_\mu = (v_0, \mathbf{w})$ and $\bar{v}_\mu = (\bar{v}_0, \mathbf{w})$ and in the limit $\bar{v}_0 = v_0$ the functions $K_i(l, v, u)$ (2.46) are reproduced. By construction the dispersion integral (2.54) is finite, as for large energies $\bar{v}_0$ the spectral weight functions $\mathfrak{Im} J_i^R$ are bounded. We assume that the antikaon in-medium self-energy approaches zero at large energies.

The subtraction terms $J_i^C(v_0, \mathbf{w})$ in (2.54), necessary for compliance with the free-space limit (2.52) and the decoupling of all partial waves at $\mathbf{w} = 0$ as dictated by (2.51), are given in Appendix A.7 in terms of the integrals

$$\begin{aligned} \bar{C}_{a,n}^{ijk}(\mathbf{w}) &= \int_{-\infty}^{+\infty} \frac{d\bar{v}_0}{\pi} \int \frac{d^3 l}{2(2\pi)^3} \frac{1}{E_N^*} \\ &\times \Bigg\{ (\bar{v} \cdot u)^a \frac{(\bar{l}_+ \cdot \bar{v})^i (\bar{l}_+ \cdot u)^j (\bar{l}_+^2)^k}{(\bar{v}^2)^n} \rho_K(\bar{v}_+, \mathbf{w} - \mathbf{l}) \left[\Theta(+\bar{v}_+) - \Theta(k_F - |\mathbf{l}|) \right] \\ &\quad + (\bar{v} \cdot u)^a \frac{(\bar{l}_- \cdot \bar{v})^i (\bar{l}_- \cdot u)^j (\bar{l}_-^2)^k}{(\bar{v}^2)^n} \rho_K(\bar{v}_-, \mathbf{w} - \mathbf{l}) \Theta(-\bar{v}_-) \Bigg\} \end{aligned} \tag{2.57}$$

and

$$\bar{l}_\pm^\mu = l_\pm^\mu - \frac{1}{2} \bar{v}^\mu, \qquad u^\mu = (1, \mathbf{0}). \tag{2.58}$$

By inspecting the asymptotic behaviour of the integrand (2.57) for large $\bar{v}_0$ we observe that all coefficients $\bar{C}^{ijk}_{a,n}$ that are needed in $J^C_i(v_0, \mathbf{w})$ are finite. In the limit $\mathbf{w} = \mathbf{u} = 0$ we have

$$(\bar{l}_\pm \cdot \bar{v}) \to \frac{m_N^2 - m_K^2}{2}, \quad (\bar{l}_\pm \cdot u) \to \frac{m_N^2 - m_K^2}{2\bar{v}_0}, \quad \bar{l}_\pm^2 \to \frac{m_N^2 + m_K^2}{2} - \frac{\bar{v}_0^2}{4} \tag{2.59}$$

and consequently the integrals in (2.57) prove to be finite for

$$\begin{aligned} a - j + 2k - 2n &\leq -2 \quad \text{if} \quad a + j = \text{odd}, \\ a - j + 2k - 2n &\leq -1 \quad \text{if} \quad a + j = \text{even}. \end{aligned} \tag{2.60}$$

Indeed, all the coefficients $\bar{C}^{ijk}_{a,n}$ that contribute to the subtraction terms J^C_i in Appendix A.7 are compatible with conditions (2.60).

The interpretation of J^C_i in (2.54) as counter terms requires that the underlying coefficients $\bar{C}^{ijk}_{a,n}$ exhibit polynomial behaviour as functions of the three-momentum $\mathbf{w}$. However, this is not necessarily the case for $n > 1$. In this case the coefficients are proportional to $(\bar{v}^2)^{-n}$ may be ill behaved at $\bar{v}_0 = \pm|\mathbf{w}|$. Considering that in the vacuum limit all $\bar{C}^{ijk}_{a,n}$ become constants independent of momentum, which is a direct consequence of covariance, would suggest using a polynomial ansatz for the coefficients $\bar{C}^{ijk}_{a,n}$. The antikaon spectral function (2.56) is non-zero for $\omega < -m_K$ and $\omega > m_\Lambda - \sqrt{{m_N^*}^2 + k_F^2} - \Sigma_V$ with the Λ ground state mass m_Λ. Therefore at sufficiently low momenta $\mathbf{w}$ the integral (2.57) is well behaved, because the troublesome region around $\bar{v}_0 = \pm|\mathbf{w}|$ is excluded. Thus we define well behaved coefficients $C^{ijk}_{a,n}$ by means of a Taylor expansion in momentum according to

$$C^{ijk}_{a,n}(\mathbf{w}) = \bar{C}^{ijk}_{a,n}(0) + \frac{1}{2}\mathbf{w}^2 \left(\nabla_\mathbf{w} \cdot \nabla_\mathbf{w}\right) \bar{C}^{ijk}_{a,n}(0). \tag{2.61}$$

It has already been pointed out that the subtraction terms J^C_i are predominantly needed to cancel kinematical singularities at vanishing three-momentum and to obtain the proper vacuum limit, hence we have to keep the minimal order in (2.61) to be consistent with (2.51) and (2.52). It can be shown by further investigation that higher orders than in expression (2.61) are not necessary to fulfill the constraints.

We remark that for sufficiently small three-momenta $\mathbf{w}$ both contributions to (2.54) can be summarized to the loop functions $J^M_i(v_0, \mathbf{w})$, which are detailed in Appendix A.8. By inspecting expressions (A.26) it is obvious that the latter comprise higher subtraction terms $\propto \frac{1}{(\bar{v}^2)^2}$ and $\propto \frac{1}{(\bar{v}^2)^3}$ that are not properly defined using a dispersion integral ansatz. The higher subtraction terms were shifted to the $J^C_i(v_0, \mathbf{w})$ in (2.54). Nevertheless, in a numerical calculation at sufficiently low three-momenta $\mathbf{w}$ the higher order subtractions do not contribute and representation (A.24) is used. It is favourable due to the more closed expressions, whereas the decomposition (2.54) involves subtle cancellation effects.

2.3.2 Loop functions in the center of mass frame and angular average approximation

We close this section by describing an angular average approximation for the calculation of the loop functions, which in a different manner is also applied in [2] and [14]. Nevertheless, we cannot directly compare our angular average procedure with the cited calculations as the treatment of the $J = \frac{3}{2}$ partial waves is different. The most striking advantage of the angular average approximation is the simple angular dependence which can be integrated analytically and for the in-medium loops it is about 100 times faster in computing time.

The description of self-consistent $\bar{K}N$ in-medium scattering and the loop functions as introduced in this work are manifestly covariant and we may evaluate the loops in any frame. They depend on the scalars v^2 and $v \cdot u$, for the angular average approximation we have to calculate the imaginary part of the loops in the center of mass frame. The latter frame will be denoted as 'cm-frame' in the following, whereas 'lab-frame' refers to the nuclear matter rest frame used so far. The external momentum v in the cm-frame is given by

$$v_\mu^{\mathrm{cm}} = \left(\frac{v_0}{|v_0|}\sqrt{s}, \mathbf{0}\right) \qquad \text{with} \qquad s = v_0^2 - \mathbf{w}^2, \tag{2.62}$$

but the bulk matter three-velocity $\mathbf{u}$ will be nonzero. Note the sign change of $\sqrt{s}$ for negative energies in (2.62). Recall in the lab-frame we have

$$v_\mu^{\mathrm{lab}} = (v_0, \mathbf{w}) \qquad \text{and} \qquad u_\mu^{\mathrm{lab}} = (1, \mathbf{0}). \tag{2.63}$$

Hence the angular dependence of the loop functions is now contained in terms like $l \cdot u$ instead of $l \cdot v$. The covariant variables in the cm-frame that the loop functions depend on are u^2 and $v \cdot u$, which read

$$u^2 = 1 = u_{0,\mathrm{cm}}^2 - \mathbf{u}_{\mathrm{cm}}^2, \quad \Rightarrow \quad u_{0,\mathrm{cm}} = \sqrt{1 + \mathbf{u}_{\mathrm{cm}}^2} = \sqrt{\frac{s + \mathbf{w}_{\mathrm{lab}}^2}{s}} = \frac{v_{0,\mathrm{lab}}}{\sqrt{v_{\mathrm{lab}}}} \tag{2.64}$$

and

$$v \cdot u = \sqrt{s}\, u_{0,\mathrm{cm}} = \sqrt{s}\sqrt{1 + \mathbf{u}_{\mathrm{cm}}^2} = v_{0,\mathrm{lab}} \tag{2.65}$$

with

$$\mathbf{u}_{\mathrm{cm}}^2 = \frac{s + \mathbf{w}_{\mathrm{lab}}^2}{s} - 1 = \frac{\mathbf{w}_{\mathrm{lab}}^2}{s}. \tag{2.66}$$

The antikaon self-energy can be formulated in terms of the two invariants

$$(v - l)^2 = (\sqrt{s} - l_0)^2 - \mathbf{l}^2 = (v_{0,\mathrm{lab}}^2 - l_0^2)^2 - (\mathbf{w}_{\mathrm{lab}}^2 - \mathbf{l}^2)^2 \tag{2.67}$$

and

$$(v - l) \cdot u = (\sqrt{s} - l_0) u_{0,\mathrm{cm}} + \mathbf{l} \cdot \mathbf{u}_{\mathrm{cm}} = v_{0,\mathrm{lab}} - l_0. \tag{2.68}$$

Thus the arguments of the self-energy in the cm-frame are

$$\omega = q \cdot u = (v - l) \cdot u = (\sqrt{s} - l_0)\sqrt{1 + \mathbf{u}_{\mathrm{cm}}^2} + \mathbf{l} \cdot \mathbf{u}_{\mathrm{cm}} \tag{2.69}$$

and

$$\begin{aligned} \mathbf{q}^2 &= (q \cdot u)^2 - q^2 = [(v - l) \cdot u]^2 - (v - l)^2 \\ &= \left[(\sqrt{s} - l_0)\sqrt{1 + \mathbf{u}_{\mathrm{cm}}^2} + \mathbf{l} \cdot \mathbf{u}_{\mathrm{cm}}\right]^2 - (\sqrt{s} - l_0)^2 + \mathbf{l}^2. \end{aligned} \tag{2.70}$$

Both the upper momentum cutoff as well as the Pauli-blocking realized with appropriate Θ-functions have to be formulated in the cm-frame. Numerically we have to use a cutoff $l_{\max}$ in (2.55) and (2.57). Once the momentum cutoff is chosen high enough we can apply the same cutoff in the lab- and cm-frame which proved to be well justified. Otherwise we would have to calculate a new cutoff constrained by $\frac{(l\cdot v)^2}{v^2} - l^2 < {l_{\rm max}^{\rm cm}}^2$ if we require the momentum cutoff to be independent of the angle in the cm-frame. On the other hand according to $(l\cdot u)^2 - l^2 < {l_{\rm max}^{\rm lab}}^2$ a cutoff independent of the angle in the lab-frame would imply an angular dependence in the cm-frame.

Pauli blocking is implemented by means of a modified Heaviside function in the cm-frame,

$$\Theta\left(k_F^2 + {m_N^*}^2 - \left(l_0\sqrt{1+\mathbf{u}_{\rm cm}^2} - \mathbf{l}\cdot\mathbf{u}_{\rm cm}\right)^2\right), \tag{2.71}$$

as compared to

$$\Theta\left(k_F^2 - \mathbf{l}^2\right) \tag{2.72}$$

in the lab-frame. Pauli blocking now acquires an angular dependence $z = \cos\theta(\mathbf{l},\mathbf{w})$ that is also implemented by [2] and [14].

In analogy to (2.55) the representation of the in-medium loops in the cm-frame is derived:

$$\begin{aligned}
\Im\mathfrak{m} J_i^R(v_0,\bar v_0,\mathbf{w}) &= \int \frac{d^3l}{2(2\pi)^3}\frac{1}{E_N^*} \\
&\quad \times\Big\{K_i^R(l_+,v_0,\bar v_0,\mathbf{w})\rho_K(\bar v_+,\mathbf{k}_+)\left[\Theta(+\bar v_+) - \Theta(k_F^{\rm cut})\right] \\
&\qquad + K_i(l_-,v_0,\bar v_0,\mathbf{w})\rho_K(\bar v_-,\mathbf{k}_-)\Theta(-\bar v_-)\Big\}, \\
l_\pm^\mu &= (\pm E_N^*, \mathbf{l}), \\
\bar v_\pm &= \left(\pm\sqrt{s} - l_0^\pm\right)\sqrt{1+\mathbf{u}_{\rm cm}^2} + \mathbf{l}\cdot\mathbf{u}_{\rm cm}, \\
\mathbf{k}_\pm^2 &= \mathbf{l}^2 + (\mathbf{l}\cdot\mathbf{u}_{\rm cm})^2 + \mathbf{u}_{\rm cm}^2\left(\pm\sqrt{s} - l_0^\pm\right)^2 \\
&\quad + 2(\mathbf{l}\cdot\mathbf{u}_{\rm cm})\left(\pm\sqrt{s} - l_0^\pm\right)\sqrt{1+\mathbf{u}_{\rm cm}^2}, \\
k_F^{\rm cut} &= k_F^2 + {m_N^*}^2 - \left(l_0^+\sqrt{1+\mathbf{u}_{\rm cm}^2} - \mathbf{l}\cdot\mathbf{u}_{\rm cm}\right)^2,
\end{aligned} \tag{2.73}$$

see (2.71) for $\Theta(k_F^{\rm cut})$. The derivation of the coefficients $\bar C_{a,n}^{ijk}$ (2.57) of the subtraction terms J_i^C in the cm-frame is straightforward, the form of the antikaon spectral function and its arguments $l_\pm^\mu$, $\bar v_\pm$ and $\mathbf{k}_\pm^2$ can be taken over from (2.73). To be more explicit we state the building blocks

$$(\bar l\cdot v) = E_N^* v_{0,\rm lab} - \frac{v_{0,\rm lab}^2 - \mathbf{w}_{\rm lab}^2}{2} - \mathbf{l}\cdot\mathbf{w}_{\rm lab}, \qquad (\bar l\cdot u) = E_N^* - \frac{v_{0,\rm lab}}{2} \tag{2.74}$$

in the lab-frame and

$$(\bar l\cdot v) = \left(E_N^* - \frac{\sqrt{s}}{2}\right)\sqrt{s}, \qquad (\bar l\cdot u) = \left(E_N^* - \frac{\sqrt{s}}{2}\right)\sqrt{1+\mathbf{u}_{\rm cm}^2} - \mathbf{l}\cdot\mathbf{u}_{\rm cm} \tag{2.75}$$

in the cm-frame for the first contribution in (2.73) $\propto [\Theta(+\bar v_+) - \Theta(k_F^{\rm cut})]$. By explicit numerical simulations we confirm that (2.55) and (2.73) agree identically. Consequently also the real part of the loop function matrix coincides.

Our angular average approximation consists of omitting all terms linear in $(\mathbf{l}\cdot\mathbf{u}_{\rm cm})$ and averaging $(\mathbf{l}\cdot\mathbf{u}_{\rm cm})^2$ by $\frac{2}{3}(|\mathbf{l}|\cdot|\mathbf{u}_{\rm cm}|)^2$ due to the integration $\int\limits_{-1}^{1} dz\ (|\mathbf{l}|\cdot|\mathbf{u}_{\rm cm}|z)$. The full angular dependence of the Pauli-blocking (2.71) is kept. Additionally we assume the factorization of the Pauli-blocking Θ-function and the loop kernel part when performing the angular integration:

$$\int \frac{dz}{4\pi} K_i^R \rho_K \Theta(k_F^{\rm cut}) \longrightarrow \left(\int \frac{dz}{4\pi} K_i^R \rho_K\right) \left(\int \frac{dz}{4\pi} \Theta(k_F^{\rm cut})\right). \tag{2.76}$$

The same approximation is also applied when calculating the coefficients $C_{a,n}^{ijk}$ in (2.57) for the subtraction terms J_i^C. The vacuum loop matrix (2.41) is unchanged. Note that in [14] all terms $(\mathbf{l}\cdot\mathbf{u}_{\rm cm})^2$ are also omitted and in addition the correction term $\sqrt{1+\mathbf{u}_{\rm cm}^2}$ for ω is neglected. The simplest scalar loop function J_0 in the cm-frame with an angular average approximation after energy integration reads

$$\begin{aligned} J_0(\sqrt{s},\mathbf{u}_{\rm cm}) &= \int \frac{d^3l}{16\pi^3} \frac{1}{E_N^*} \frac{1}{(\sqrt{s}-E_N)^2 - \mathbf{l}^2 - \frac{1}{3}\left(|\mathbf{l}|\cdot|\mathbf{u}_{\rm cm}|\right)^2 - m_K^2 - \Pi(\omega,|\mathbf{q}|)} \\ &\quad \Theta\left(k_F^2 + {m_N^*}^2 - \left(E_N^*\sqrt{1+\mathbf{u}_{\rm cm}^2} - \mathbf{l}\cdot\mathbf{u}_{\rm cm}\right)^2\right). \end{aligned} \tag{2.77}$$

for the first contribution in (2.73) $\propto [\Theta(+\bar{v}_+) - \Theta(k_F^{\rm cut})]$. The arguments ω and $|\mathbf{q}|$ of the self-energy Π in the cm-frame are determined by (2.69) and (2.70). In order to examine the effect of the angular average approximation it is sufficient to calculate the thirteen loop functions in the cm-frame, tabulated as functions of v_0. The matrix of loop functions (2.43) involves just factors containing powers of $\sqrt{v^2}$, $v\cdot u$ and $(v\cdot u)^2 - v^2$, which are identically the same in both reference frames by construction.

One of the reasons why the angular average approximation is widely used in nuclear many-body theory is the prevention of the coupling of different partial waves. Indeed we checked analytically and observe also numerically that for the in-medium loops

$$J_2 = J_6 = J_8 = J_{10} = J_{11} = 0 \tag{2.78}$$

for each external momentum $\mathbf{w}$ and not just for $\mathbf{w}=0$. Additionally we fulfill

$$J_3 + J_5 = J_7 + J_{12} = 0 \tag{2.79}$$

for each $\mathbf{w}$.

2.3.3 Analytic angular integration for the angular average approximation

The major benefit of the angular average approximation that has been described in the previous sections is that the angle $z=\cos\theta(\mathbf{l},\mathbf{w})$ appears nowhere else but in the Θ-function from Pauli-blocking (2.71). Hence the angular integration can be evaluated analytically and what remains is a one-dimensional momentum integral that has to be computed numerically. As the angular integration just involves the propagator part of the in-medium loop functions we will state as an example the result from the analytic angular integration in terms of J_0, the simplest loop function. The superscript J_0^R is omitted, because we refer to the imaginary part of the loop and the renormalization procedure stays identically the same in lab- and cm-frame. The additional phase space factors $(\bar{l}\cdot v)$ and $(\bar{l}\cdot u)$ do not depend on z in the angular average approximation. All the following expressions just apply for the first contribution in (2.73) $\propto [\Theta(+\bar{v}_+) - \Theta(k_F^{\rm cut})]$. For the second contribution $\propto \Theta(-\bar{v}_-)$ Pauli-blocking is inactive and the angular integration is trivial and evaluates to a factor of two from the angular integration. For the analytic solution we have to define J_0 in sections. We recall

$$k_F^{\rm cut} = k_F^2 + m_N^2 - \left(E_N^*\sqrt{1+\mathbf{u}_{\rm cm}^2} - |\mathbf{l}|\cdot|\mathbf{u}_{\rm cm}|\cdot z\right)^2. \tag{2.80}$$

and

$$\omega = (\sqrt{s} - E_N^*)\sqrt{1 + \mathbf{u}_{\mathrm{cm}}^2}, \quad \mathbf{q}^2 = \omega^2 - (\sqrt{s} - E_N^*)^2 + \mathbf{l}^2 + \frac{1}{3}\left(|\mathbf{l}| \cdot |\mathbf{u}_{\mathrm{cm}}|\right)^2. \tag{2.81}$$

We present the result of the analytic angular integration exemplary for the simplest scalar loop function $J_0(\sqrt{s}, \mathbf{u}_{\mathrm{cm}})$ in terms of the angular independent integral kernel $J_0(\sqrt{s}, \mathbf{u}_{\mathrm{cm}}, \mathbf{l})$:

$$J_0(\sqrt{s}, \mathbf{u}_{\mathrm{cm}}) = \int_0^{l_{\mathrm{max}}} dl\, J_0(\sqrt{s}, \mathbf{u}_{\mathrm{cm}}, \mathbf{l}). \tag{2.82}$$

Taking into account (2.80) we have $J_0(\sqrt{s}, \mathbf{u}_{\mathrm{cm}}) = 0$ for $\omega > 0 \wedge k_F^{\mathrm{cut}} \geq 0$ or $\omega \leq 0 \wedge k_F^{\mathrm{cut}} < 0$. For the analytic integration we have to distinguish several cases both for $\omega > 0$ and $\omega < 0$ and we will give the resulting expressions separately. We define three new objects

$$\begin{aligned}
&\mathcal{A} = \sqrt{k_F^2 + {m_N^*}^2}, && \mathcal{A} > 0, \\
&\mathcal{B} = E_N^* \sqrt{1 + \mathbf{u}_{\mathrm{cm}}^2}, && \mathcal{B} > 0, \\
&\mathcal{C} = |\mathbf{l}| \cdot |\mathbf{u}_{\mathrm{cm}}|, && \mathcal{C} \geq 0.
\end{aligned} \tag{2.83}$$

With (2.83) the angular integrated loop function $J_0(\sqrt{s}, \mathbf{u}_{\mathrm{cm}}, \mathbf{l})$ for $\omega \geq 0$ reads

$$J_0(\sqrt{s}, \mathbf{u}_{\mathrm{cm}}, \mathbf{l}) = \begin{cases}
\breve{J}_0(\sqrt{s}, \mathbf{u}_{\mathrm{cm}}, \mathbf{l}), & \mathcal{A} - \mathcal{B} = 0 \ \wedge \ \mathcal{A} - \mathcal{B} - \mathcal{C} < 0 \\
& \wedge\ \mathcal{A} + \mathcal{B} - \mathcal{C} \geq 0 \\
2\,\breve{J}_0(\sqrt{s}, \mathbf{u}_{\mathrm{cm}}, \mathbf{l}), & \left[\mathcal{A} - \mathcal{B} = 0 \ \wedge \ \mathcal{A} - \mathcal{B} - \mathcal{C} = 0\right] \\
& \vee \left[\mathcal{A} - \mathcal{B} < 0 \ \wedge \ \mathcal{A} - \mathcal{B} + \mathcal{C} \leq 0\right] \\
2\,\breve{J}_0(\sqrt{s}, \mathbf{u}_{\mathrm{cm}}, \mathbf{l})\frac{\mathcal{C} - \mathcal{A}}{\mathcal{C}}, & \left[\mathcal{A} - \mathcal{B} \leq 0 \ \wedge \ \mathcal{A} + \mathcal{B} - \mathcal{C} < 0\right] \\
& \vee \left[\mathcal{A} + \mathcal{B} - \mathcal{C} < 0\right] \\
\breve{J}_0(\sqrt{s}, \mathbf{u}_{\mathrm{cm}}, \mathbf{l})\frac{\mathcal{C} + \mathcal{B} - \mathcal{A}}{\mathcal{C}}, & \left[\mathcal{A} - \mathcal{B} < 0 \ \wedge \ \mathcal{A} - \mathcal{B} + \mathcal{C} > 0\right. \\
& \left.\wedge\ \mathcal{A} + \mathcal{B} - \mathcal{C} \geq 0\right] \ \vee \ \left[\mathcal{A} - \mathcal{B} > 0\right. \\
& \left.\wedge\ \mathcal{A} + \mathcal{B} - \mathcal{C} \geq 0 \ \wedge \ \mathcal{A} - \mathcal{B} - \mathcal{C} < 0\right] \\
0, & \text{else}
\end{cases} \tag{2.84}$$

and for $\omega < 0$ analogously

$$J_0(\sqrt{s}, \mathbf{u}_{\mathrm{cm}}, \mathbf{l}) = \begin{cases}
2\,\breve{J}_0(\sqrt{s}, \mathbf{u}_{\mathrm{cm}}, \mathbf{l}), & \left[\mathcal{A} - \mathcal{B} = 0 \ \wedge \ \mathcal{C} = 0\right] \\
& \vee \left[\mathcal{A} - \mathcal{B} > 0 \ \wedge \ \mathcal{A} - \mathcal{B} - \mathcal{C} \geq 0\right] \\
2\,\breve{J}_0(\sqrt{s}, \mathbf{u}_{\mathrm{cm}}, \mathbf{l})\frac{\mathcal{A}}{\mathcal{C}}, & \left[\mathcal{A} - \mathcal{B} \leq 0 \ \wedge \ \mathcal{A} + \mathcal{B} - \mathcal{C} < 0\right] \\
& \vee \left[\mathcal{A} + \mathcal{B} - \mathcal{C} < 0\right] \\
\breve{J}_0(\sqrt{s}, \mathbf{u}_{\mathrm{cm}}, \mathbf{l})\frac{\mathcal{A} - \mathcal{B} + \mathcal{C}}{\mathcal{C}}, & \left[\mathcal{A} - \mathcal{B} = 0 \ \wedge \ \mathcal{C} > 0 \ \wedge \ \mathcal{A} + \mathcal{B} - \mathcal{C} \geq 0\right] \\
& \vee \left[\mathcal{A} - \mathcal{B} < 0 \ \wedge \ \mathcal{A} + \mathcal{B} - \mathcal{C} \geq 0\right. \\
& \left.\wedge\ \mathcal{A} - \mathcal{B} + \mathcal{C} > 0\right] \ \vee \ \left[\mathcal{A} - \mathcal{B} > 0\right. \\
& \left.\wedge\ \mathcal{A} + \mathcal{B} - \mathcal{C} \geq 0 \ \wedge \ \mathcal{A} - \mathcal{B} - \mathcal{C} < 0\right] \\
0, & \text{else.}
\end{cases} \tag{2.85}$$

In (2.84) and (2.85) the angular dependence is eliminated and a one-dimensional integral remains. The kernel $\breve{J}_0(\sqrt{s},\mathbf{u}_{\rm cm},\mathbf{l})$ is given by

$$\breve{J}_0(\sqrt{s},\mathbf{u}_{\rm cm},\mathbf{l}) = \frac{1}{8\pi^2}\frac{1}{E_N^*}\frac{\mathbf{l}^2}{(\sqrt{s}-E_N^*)^2-\mathbf{l}^2-\frac{1}{3}(|\mathbf{l}|\cdot|\mathbf{u}_{\rm cm}|)^2-m_K^2-\Pi(\omega,|\mathbf{q}|)} \tag{2.86}$$

with ω and $\mathbf{q}^2$ from (2.81).

2.4 Antikaon self-energy

The in-medium self-energy is evaluated in terms of the properly isospin averaged in-medium scattering amplitudes $\bar{\mathcal{T}}(\bar{k},k,w,u)$,

$$\bar{\mathcal{T}} = \frac{1}{4}\mathcal{T}^{(I=0)} + \frac{3}{4}\mathcal{T}^{(I=1)}, \tag{2.87}$$

as

$$\Pi(q,u) = 2\cdot\mathrm{Tr}\int\frac{d^4p}{(2\pi)^4}\,i\,\Delta S(p,u)\bar{\mathcal{T}}\left(\frac{1}{2}(p-q),\frac{1}{2}(p-q),p+q,u\right). \tag{2.88}$$

The in-medium scattering amplitude is decomposed with the help of the projector formalism and thus the trace in (2.88) comprises the Dirac contribution of the nucleon propagator and the projectors. The trace results in coefficients $c_{ij}^{(p,q)}(q,w,u)$ of the invariant amplitudes $\bar{T}_{ij}^{(p,q)}(v,u)$ and the integrand of the self-energy can be written as

$$\begin{aligned}&\frac{1}{2}\mathrm{Tr}\left[(\not{p}+m_N^*)\bar{\mathcal{T}}\left(\frac{1}{2}(p-q),\frac{1}{2}(p-q),p+q,u\right)\right]\\ &\quad=\sum_{i,j=1}^{8}c_{ij}^{(p)}(q,w,u)\bar{T}_{ij}^{(p)}(w,u)+\sum_{i,j=1}^{2}c_{ij}^{(q)}(q,w,u)\bar{T}_{ij}^{(q)}(w,u).\end{aligned} \tag{2.89}$$

In the nuclear matter rest frame it holds that

$$\begin{aligned}\Pi(q,u) = &-\sum_{i,j=1}^{8}\int_0^{k_F}\frac{d^3p}{(2\pi)^3}\frac{2}{E_N^*}c_{ij}^{(p)}(q,w,u)\bar{T}_{ij}^{(p)}(w,u)\\ &-\sum_{i,j=1}^{2}\int_0^{k_F}\frac{d^3p}{(2\pi)^3}\frac{2}{E_N^*}c_{ij}^{(q)}(q,w,u)\bar{T}_{ij}^{(q)}(w,u).\end{aligned} \tag{2.90}$$

The scalar coefficients $c_{ij}^{(p,q)}(q,w,u)$ are listed in Appendix A.9 and exactly coincide with the ones published in [5] even for a non-vanishing nucleon mean-field. Evaluating the trace in (2.89) over the Dirac part of propagator and the projector algebra in terms of v instead of w is identical to taking the coefficients $c_{ij}^{(p,q)}(q,w,u)$ as functions of w and substitute $p_\mu \to \breve{p}_\mu + \Sigma_V u_\mu$. Therefore we can write the coefficients in terms of w and shift the scalar amplitudes entering the self-energy calculation by Σ_V.

Expression (2.90) together with (2.38), (2.39), (2.42), (2.43) and (2.24), (2.25) form a self-consistent set of equations defining the antikaon self-energy. Given the free-space partial wave scattering amplitudes $M_{J^P}(\sqrt{s})$ along with a renormalization scheme for the in-medium loop functions the antikaon self-energy can be calculated by iteration. The Bethe-Salpeter equation (2.21) reduces to a simple matrix equation

$$\begin{aligned}
T^{(p)}_{ij}(v,u) &= M^{(p)}_{ij}(v,u) + \sum_{l,k=1}^{8} M^{(p)}_{ik}(v,u)\Delta J^{(p)}_{kl}(v,u)T^{(p)}_{lj}(v,u), \\
T^{(q)}_{ij}(v,u) &= M^{(q)}_{ij}(v,u) + \sum_{l,k=1}^{2} M^{(q)}_{ik}(v,u)\Delta J^{(q)}_{kl}(v,u)T^{(q)}_{lj}(v,u). \qquad (2.91)
\end{aligned}$$

We emphasize that the kaon self-energy $\Pi(\omega,\mathbf{q})$ given by (2.90) is only trustworthy for positive energies. In this case the self-energy describes the propagation of antikaons. The properties of kaons are determined for negative energy arguments $\omega < 0$ according to our convention. In this region – covered by the second term in (2.55) with $\Theta(-\bar{v}_-)$ – the self-energy could be approximated by an energy and momentum independent term linear in the nuclear matter density ρ. The self-energy has to be adjusted so as to reproduce the well established kaon mass shift of about 20 MeV at saturation density. In our calculations the effect of this contribution is of minor importance and the loop functions are largely dominated by the first term in (2.55) for negative energies. Furthermore we have to take care of the imaginary part of the loop functions at $\bar{v}_0 < \mu$, when the in-medium mass of the antinucleon is probed.

2.5 Numerical results

The previously discussed renormalization scheme in principle renders the in-medium dynamics independent of a momentum cutoff. However, since the input vacuum amplitudes are not available at all energies and the computation of the in-medium amplitudes in practice will also be restricted to a certain range, the antikaon self-energy can only be evaluated on a finite grid in energy ω and momentum $\mathbf{q}$. This grid has to be chosen carefully [5] both in antikaon energy ω and momentum $\mathbf{q}$. The self-energy is calculated in $T\rho$ approximation according to (2.90) and the free-space scattering amplitude is taken from [4]. The self-energy grid is restricted by $0 \leq \omega \leq 1.2\,\mathrm{GeV}$ and $0 \leq |\mathbf{q}| \leq 1.0\,\mathrm{GeV}$. The finite grid of the self-energy enters into the calculation of the loop functions. It is well justified to substitute the in-medium propagator with the free one outside the region of the self-energy grid, as for high energies the $\bar{K}N$ interaction will be very weak. However, one has to take care that the numerically inevitable momentum cutoff for the imaginary part of the in-medium loops is high enough not to generate further peculiarities. We choose $|\mathbf{l}_{\max}| = 1.5\,\mathrm{GeV}$, guaranteeing convergence of the loops.

In the iterative process the in-medium modification of the loops $\Delta J^R_{ij}(v_0,\mathbf{w})$ is calculated, whereas the real part is subjected to the reviewed renormalization scheme from Section 2.3.1. The loops are also evaluated in the angular-average approximation from Section 2.3.2 and we will compare to the results obtained with the full calculation. Afterwards the antikaon self-energy is calculated again from the in-medium modified loops and from experience the iteration converges rapidly after 4 to 5 iterations.

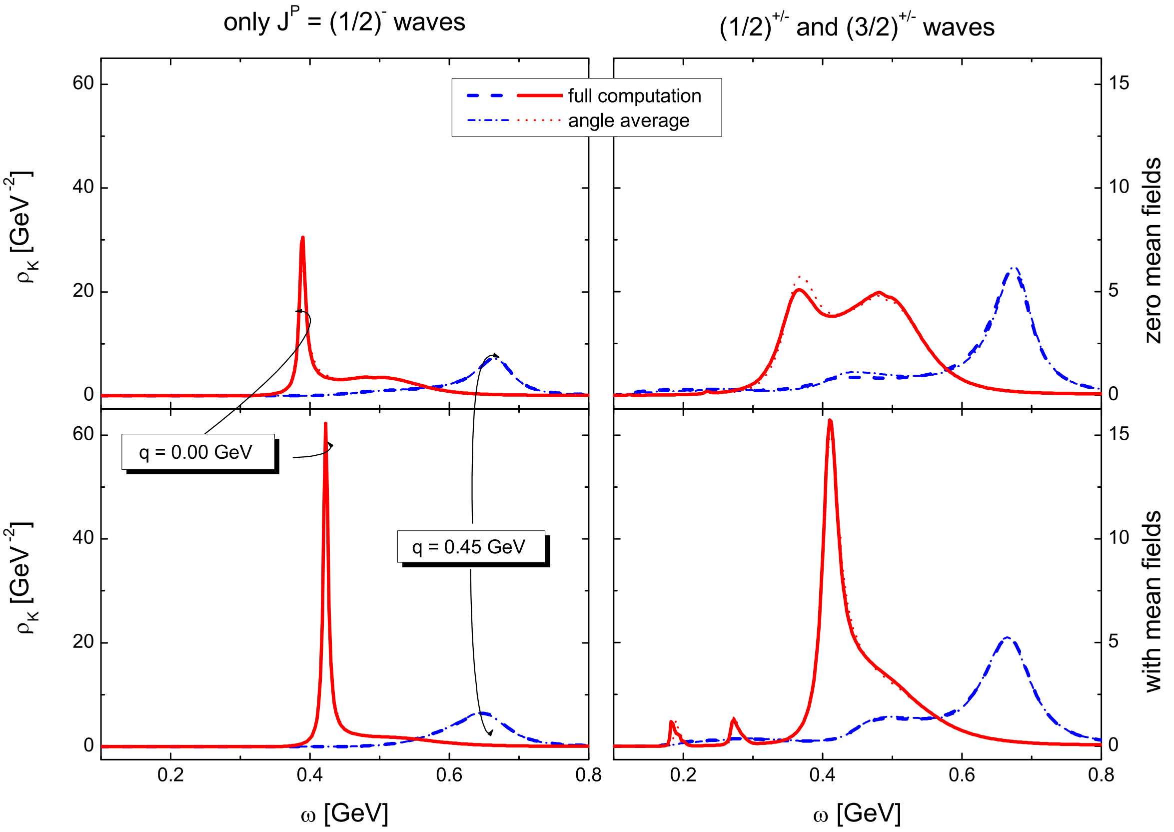

Figure 2.3: Antikaon spectral function at nuclear saturation density ρ_0 as a function of energy ω and momentum $\mathbf{q}$. The upper (lower) panels show calculations with switched off (on) mean-fields. On the left hand side only s-wave interactions are considered, on the right hand side s-, p- and d-waves are included.

2.5.1 Spectral function and self-energy

The plots shown for the antikaon spectral function $\rho_K(\omega, \mathbf{q})$ (Figure 2.3) and the self-energy $\Pi(\omega, \mathbf{q})$ (Figures 2.4, 2.5) at nuclear saturation density $\rho_0 = 0.17\,\text{fm}^{-3}$ comprise four panels. In the upper row for the case without nucleon mean-fields $\Sigma_S = \Sigma_V = 0$ and in the lower row including the nucleon mean-fields (2.13). On the left hand side the results were obtained with exclusively taking into account s-wave interactions, on the right hand side also the $J = \frac{1}{2}$ and $J = \frac{3}{2}$ p-waves and the $J = \frac{3}{2}$ d-wave were included. For the spectral function we joined two plots in each panel, one at antikaon momentum $|\mathbf{q}| = 0\,\text{GeV}$ and one at $|\mathbf{q}| = 0.45\,\text{GeV}$. Note that there is a different scale plotted in the left and right row.

Figure 2.3 shows a quite broad spectral function with a distinct two-peak structure at $|\mathbf{q}| = 0\,\text{GeV}$ without mean-fields in the upper panels. Switching on p- and d-waves moves strength from the lower peak to the higher one. The spectral function we obtain is quite different compared to the latest results from [14]. Especially the effect of the p-waves is much more pronounced in our calculation. To our experience the obvious differences cannot be traced back solely to the angular average approximation applied in [14]. The dashed lines in Figure 2.3 correspond to the angular average approximation described in Section 2.3.2 and the repercussion on the spectral function compared to the full calculation proves to be small. Also for finite $|\mathbf{q}|$ there is no appreciable effect of the approximation that could explain the difference to [14]. Nevertheless, we have to object that our angular approximation is different to the one used in [14], in particular for p- and d-waves. The results in Figure 2.3 for the spectral function do not rule out the angular average approximation as an improper tool at all. Notable differences for the approximation are only seen for switched off mean-fields including p- and d-waves.

Switching on scalar and vector mean-fields has a dramatic implication on the spectral function. At zero momentum the pronounced lower mode is significantly pushed upwards, also for the pure s-wave interaction. We predict significant strength in the soft modes for $\mathbf{q} = 0$ at energies around $0.2 - 0.3\,\mathrm{GeV}$. The latter modes are due to the presence of hyperon nucleon-hole states. For finite antikaon momenta the effect on the soft modes is less pronounced.

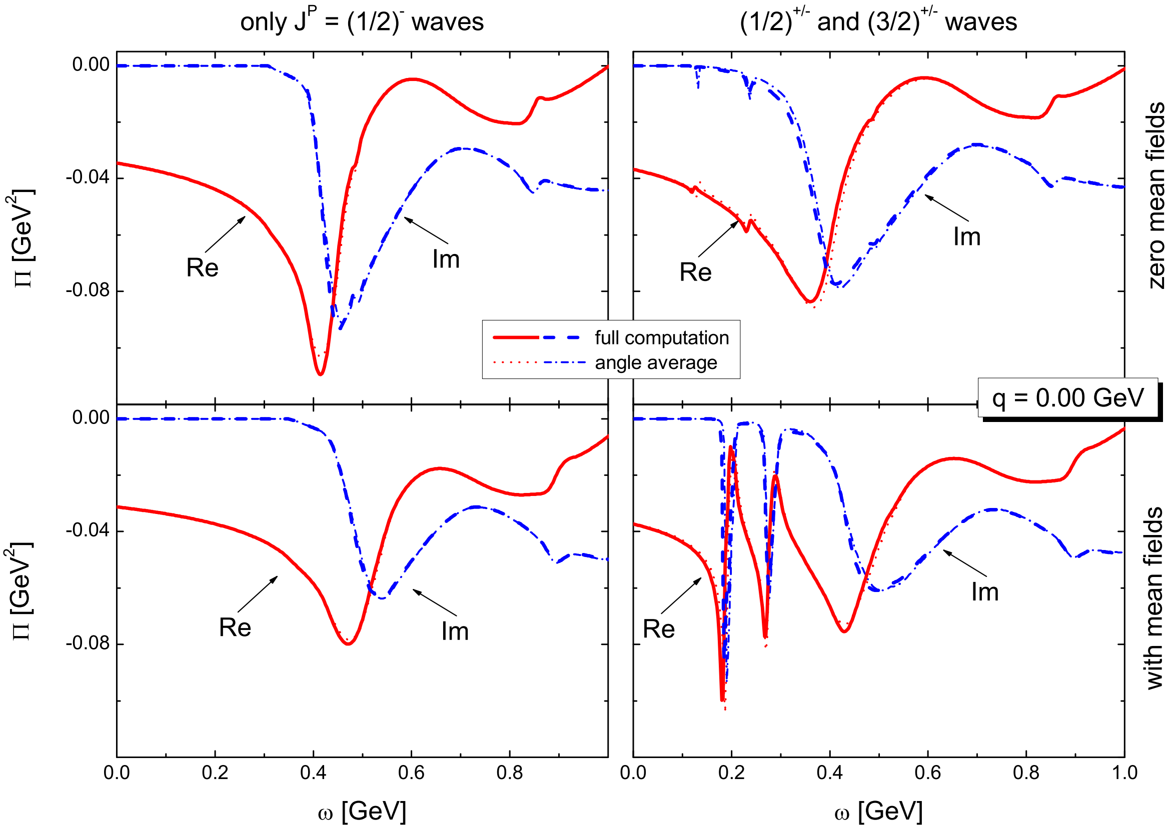

Figure 2.4: Antikaon self-energy at nuclear saturation density ρ_0 as a function of energy ω at momentum $|\mathbf{q}| = 0\,\mathrm{GeV}$. The upper (lower) panels show calculations with switched off (on) mean-fields. On the left hand side only s-wave interactions are considered, on the right hand side s-, p- and d-waves are included.

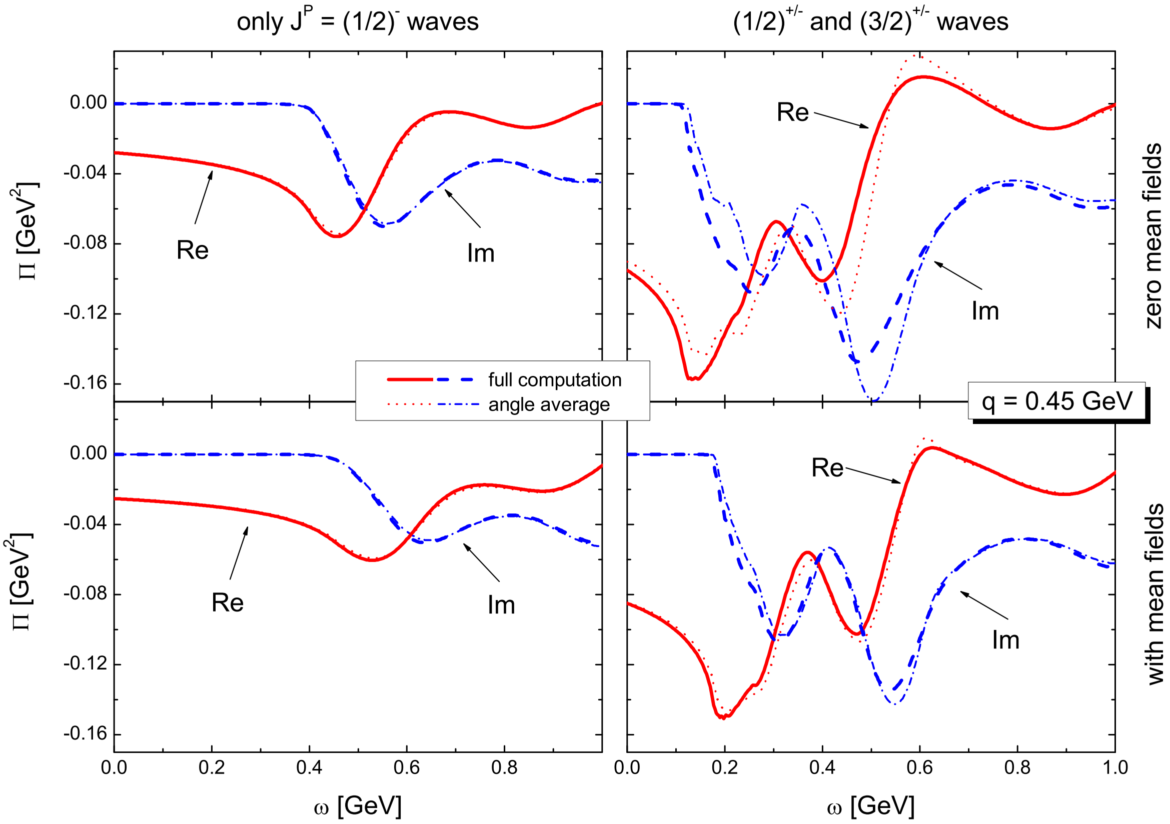

Figure 2.5: Antikaon self-energy $\Pi(\omega, \mathbf{q})$ at nuclear saturation density ρ_0 as a function of energy ω at momentum $|\mathbf{q}| = 0.45\,\mathrm{GeV}$. The upper (lower) panels show calculations with switched off (on) mean-fields. On the left hand side only s-wave interactions are considered, on the right hand side s-, p- and d-waves are included.

The Figures 2.4 and 2.5 for the self-energy $\Pi(\omega, \mathbf{q})$ as a function of energy and momentum permit a more quantitative comparison of the full and angular averaged calculation. Figure 2.4 is showing results for zero antikaon momentum, Figure 2.5 for $|\mathbf{q}| = 0.45\,\text{MeV}$. Still the angular averaging coincides quite well with un-approximated self-energy, except for the case including p- and d-waves at finite antikaon momentum, depicted in Figure 2.5. Especially for switched off mean-fields the approximation significantly deviates from the full computation. The influence of the nucleon mean-fields is less important for the self-energy at higher antikaon momenta, but at zero momentum there is a strong enhancement of the two modes around $\omega = 0.2\,\text{GeV}$. It is in compliance with the findings stated for the spectral function. This effect is not observable with the s-wave interaction only but finite mean-fields. For finite antikaon momentum the inclusion of p- and d-waves leads to a drastic enhancement of the self-energy by a factor of two.

A comparison of the self-energy with [14] confirms the important and obvious differences also found for the spectral function. Particularly the effect of p-waves in our case manifests itself in an significantly enriched structure. However, the differences of our results compared to [14] may to a large extent presumably not be due to the angular average approximation. The use of different interactions and a possibly strong cutoff dependence in [14] could also give reason to the deviations in the spectral function and self-energy.

2.5.2 In-medium properties of the $J = \frac{1}{2}^{\pm}$ hyperons

The in-medium properties of the $J^P = \frac{1}{2}^{\pm}$ hyperons, that are the ground states $\Lambda(1115)$, $\Sigma(1195)$ and the $\Lambda(1405)$ resonance, will be discussed in a different way than the $J^P = \frac{3}{2}$ hyperons. The latter ones are presented in two different helicity states corresponding to the P- and Q-space (2.25). In P-space there is a mixing of the $J^P = \frac{1}{2}^{\pm}$ and $J^P = \frac{3}{2}^{\pm}$ states as can be seen from (2.25) and (2.91), which is by construction not present in Q-space. However, the influence of the $J^P = \frac{3}{2}^{\pm}$ amplitudes on the $J^P = \frac{1}{2}^{\pm}$ amplitudes is found to be negligible.

In a given isospin channel the scattering amplitude is given by (2.24) and (2.25), which is in the basis of $v_0 = w_0 - \Sigma_V$. In this basis the off-diagonal matrix elements of $T_{ij}^{(p,q)}(v, u)$ gain sizeable contributions due to the recoupling of the free-space amplitudes in Section 2.2.2 for finite $\mathbf{w}$. The physical interpretation of the resonance structures in this basis is not straightforward and misleading. Hence, the amplitudes will be presented in the basis of w_0 analogous to [5]. This can be accomplished by expanding the in-medium scattering amplitudes (2.24) with the help of the recoupling scheme established in Section 2.2.2. The associated scalar amplitudes $M_{J^P}(w_0, \mathbf{w})$ reflect the structure of the free-space amplitudes introduced in (2.22) and have well defined angular momentum and parity. They are used for illustration of the hyperon in-medium properties. For the $J^P = \frac{1}{2}^{\pm}$ amplitudes we have to sum four contributions in P-space:

$$\begin{aligned} M_{\frac{1}{2}^{\pm}}(w_0, \mathbf{w}) &= \frac{1}{2}\left(\frac{v_0 w_0 - \mathbf{w}^2}{\sqrt{v_0^2 - \mathbf{w}^2}\sqrt{w_0^2 - \mathbf{w}^2}} \mp 1\right) T_{11}^{(p)}(v_0, \mathbf{w}) \\ &\quad -\frac{1}{2}\left(\frac{v_0 w_0 - \mathbf{w}^2}{\sqrt{v_0^2 - \mathbf{w}^2}\sqrt{w_0^2 - \mathbf{w}^2}} \pm 1\right) T_{22}^{(p)}(v_0, \mathbf{w}) \\ &\quad -\frac{1}{2}\frac{i|\mathbf{w}|(v_0 - w_0)}{\sqrt{v_0^2 - \mathbf{w}^2}\sqrt{w_0^2 - \mathbf{w}^2}}\Big(T_{12}^{(p)}(v_0, \mathbf{w}) + T_{21}^{(p)}(v_0, \mathbf{w})\Big) \end{aligned} \qquad (2.92)$$

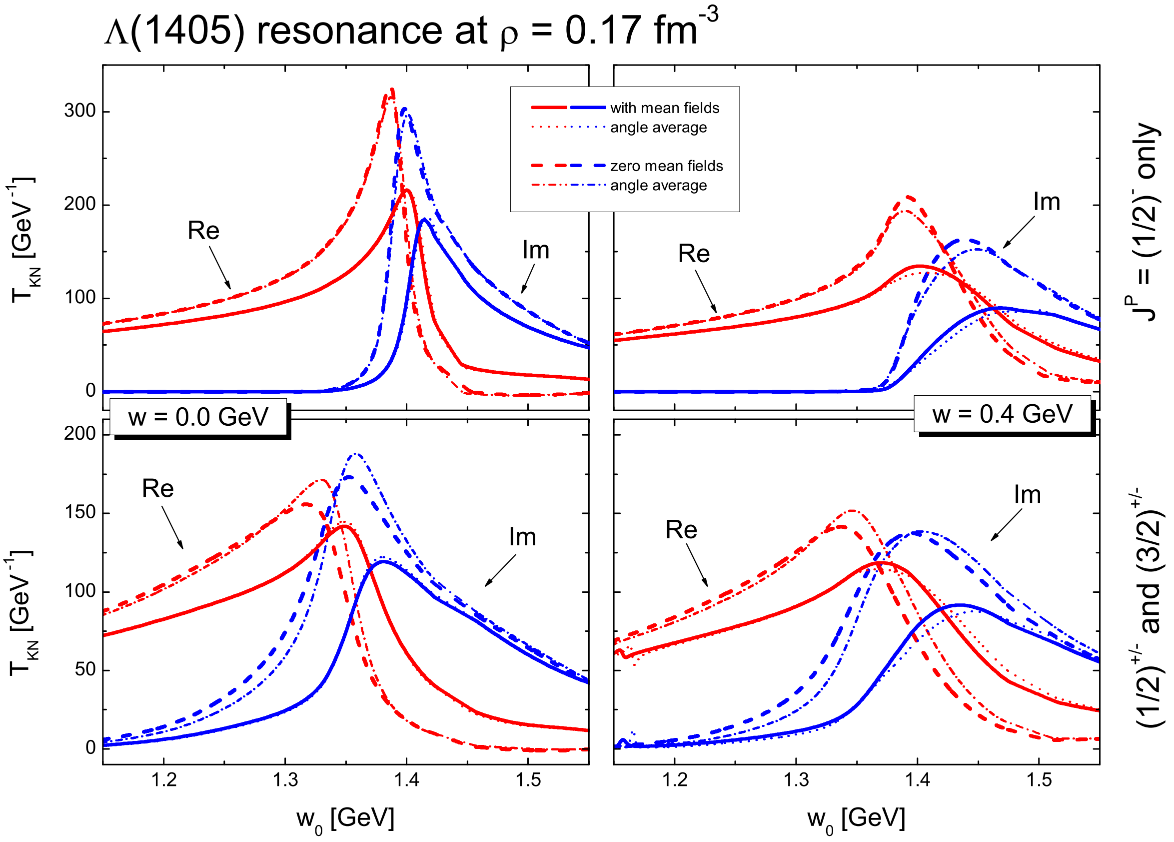

Figure 2.6: $\Lambda(1405)$ mass distribution as a function of energy w_0 and momentum $\mathbf{w}$ at nuclear saturation density ρ_0. The results are given for full calculation and for angular average approximation. For the upper panels only s-wave interactions are considered, the lower panels include s- ,p- and d-waves.

in a given isospin channel.

The isospin zero s-wave $\bar{K}N$ amplitude $M_{\frac{1}{2}^-}$ at saturation density is shown in Figure 2.6. The results plotted in the upper part are obtained by considering s-wave interactions only, in the lower part also p- and d-waves are taken into account. For s-wave interactions only the $\Lambda(1405)$ resonance gets substantially broadened by switching on nucleon mean-fields and the central mass is basically unchanged. For vanishing external momentum $\mathbf{w}$ the effect on the resonance mass is less pronounced. The angular average approximation works quite well for the s-wave only case. Including p- and d-wave interactions in the lower part of Figure 2.6 the resonance mass is shifted downwards by about 30 MeV and a further broadening is observed. Note the different scales of the upper and lower panels in Figure 2.6, which differ by a factor of two. The angular average approximation is still doing well for switched on nucleon mean-fields and p- and d-waves, but without mean-fields there is some sizeable deviation from the full calculation.

The mixing effects between the $J^P = \frac{1}{2}\pm$ amplitudes can be seen at finite external momentum $\mathbf{w}$ in Figure 2.6, because for vanishing $|\mathbf{w}| = 0$ the contribution from the $J^P = \frac{1}{2}^+$ is phase-space suppressed. The mixing effects are significantly enhanced once nucleon mean-fields are included, but were already present in [5]. On the left hand side in the lower right panel there are is a distinct contribution from the $\Lambda(1115)$ ground state for the full and angular averaged computation.

The mixing of the partial waves is much more pronounced in the basis of v due to the recoupling of the vacuum amplitudes. In Figure 2.7 we illustrate the recoupling by showing the matrix elements T_{11}, T_{12} and T_{22} as functions of energy v_0 with switched on nucleon mean-fields. One can clearly see the contribution of $\Lambda(1115)$ in T_{11} and T_{12}. Note that T_{12} has an additional factor i. The expansion (2.92) introduces a summation over the diagonal and off-diagonal matrix elements T_{ij} and thus causes a partial cancellation of the strong mixing effects once nucleon mean-fields are included. The mixing also explains the striking structure at low antikaon energies in the self-energy, see Figure 2.4 in the lower right panel. The structure almost disappears for the case without mean-fields.

Additionally to the $\Lambda(1405)$ resonance we plot the isospin $I = 1$ s-wave amplitudes in Figure 2.8. This may be important to estimate the change of a $\bar{K}N$ density dependent scattering length for the use with kaonic atoms.

The hyperon ground states with $J^P = \frac{1}{2}^+$ are the $\Lambda(1115)$ in the isospin $I = 0$ and the $\Sigma(1195)$ in the isospin $I = 1$ channel. The full and angular average approximated calculations with and without nucleon mean-fields are given in Figures 2.9 and 2.10. For the calculation with switched on mean-fields we add a repulsive mass shift of 16 MeV to the $\Lambda(1115)$ in order to reproduce the attractive shift of $25 - 30$ MeV at nuclear saturation density demanded by hyper-nuclear spectroscopic data [30]. The same shift is applied for the angular average approximation including mean-fields. Without mean-fields the $\Lambda(1115)$ ground state is shifted about 50 MeV downwards, the angular average approximation leads to a somewhat smaller shift of 40 MeV. Including mean-fields the attractive mass shift of the $\Lambda(1115)$ for the approximation is also reduced. Again we observe that the results without mean-fields are more affected by the approximation.

The $\Sigma(1195)$ ground state in Figure 2.10 experiences a relatively small attractive mass shift of 15 MeV in the medium, the deviation of the various calculations is relatively small. The attraction for the angular averaged results is lowered by a few MeV both with and without mean-fields.

2.5.3 In-medium properties of the $J = \frac{3}{2}^{\pm}$ hyperons

In analogy to the representation (2.92) for the $J = \frac{1}{2}$ partial waves the higher partial waves with $J = \frac{3}{2}$ are presented with respect to the tensor structure present in vacuum. In P-space we have to sum a large number of contributions and the amplitudes at finite momenta $\mathbf{w}$ are given separately in P- and Q-space. We identify the amplitudes

$$\begin{aligned} M^{(p)}_{\frac{3}{2}^{\pm}}(w_0, \mathbf{w}) &= \frac{1}{9}\sum_{i,j=3}^{8} C^{\frac{3}{2}^{\pm}}_{p,ij}(v_0, \mathbf{w}) T^{(p)}_{ij}(v_0, \mathbf{w}), \\ M^{(q)}_{\frac{3}{2}^{\pm}}(w_0, \mathbf{w}) &= \frac{1}{9}\sum_{i,j=1}^{2} C^{\frac{3}{2}^{\pm}}_{q,ij}(v_0, \mathbf{w}) T^{(q)}_{ij}(v_0, \mathbf{w}) \end{aligned} \qquad (2.93)$$

with the coefficients $C^{\frac{3}{2}^{\pm}}_{p,ij}$ and $C^{\frac{3}{2}^{\pm}}_{q,ij}$ tabulated in Appendix A.2. In the free-space limit of the latter expression (2.93) the vacuum amplitudes $M_{\frac{3}{2}^{\pm}}(\sqrt{s})$ of (2.28) are recovered.

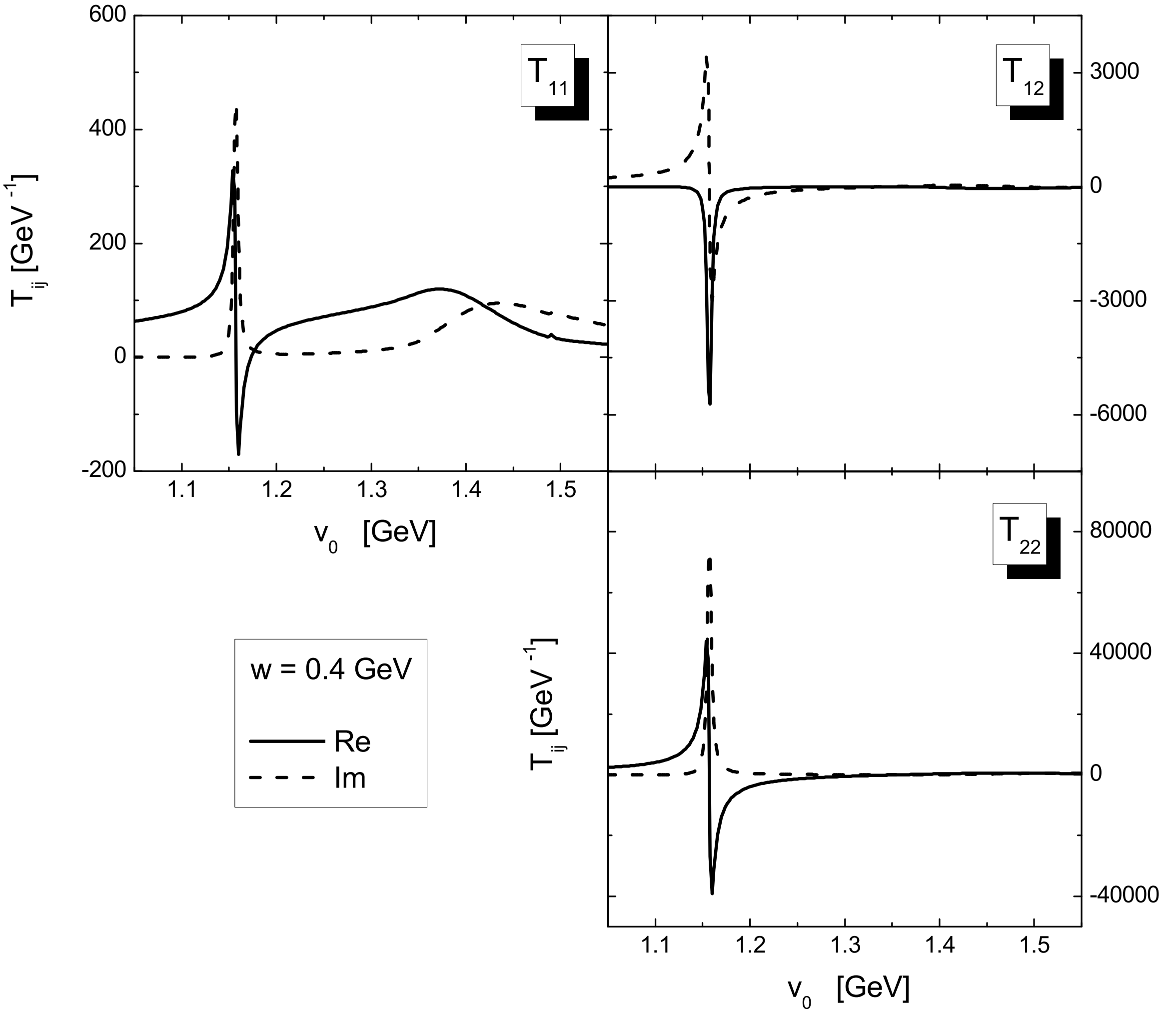

Figure 2.7: Matrix elements $T_{11}^{(I=0)}$, $T_{12}^{(I=0)}$ and $T_{22}^{(I=0)}$ in the basis of $P_{ij}(v,u)$ as functions of v_0, including nucleon mean-fields at finite momentum $|\mathbf{w}| = 0.4\,\mathrm{GeV}$. Due to the recoupling of the vacuum scattering amplitudes from Section 2.2.2 contributions of the $\Lambda(1115)$ ground state can seen below the $\lambda(1405)$ in T_{11} and the off-diagonal T_{12}.

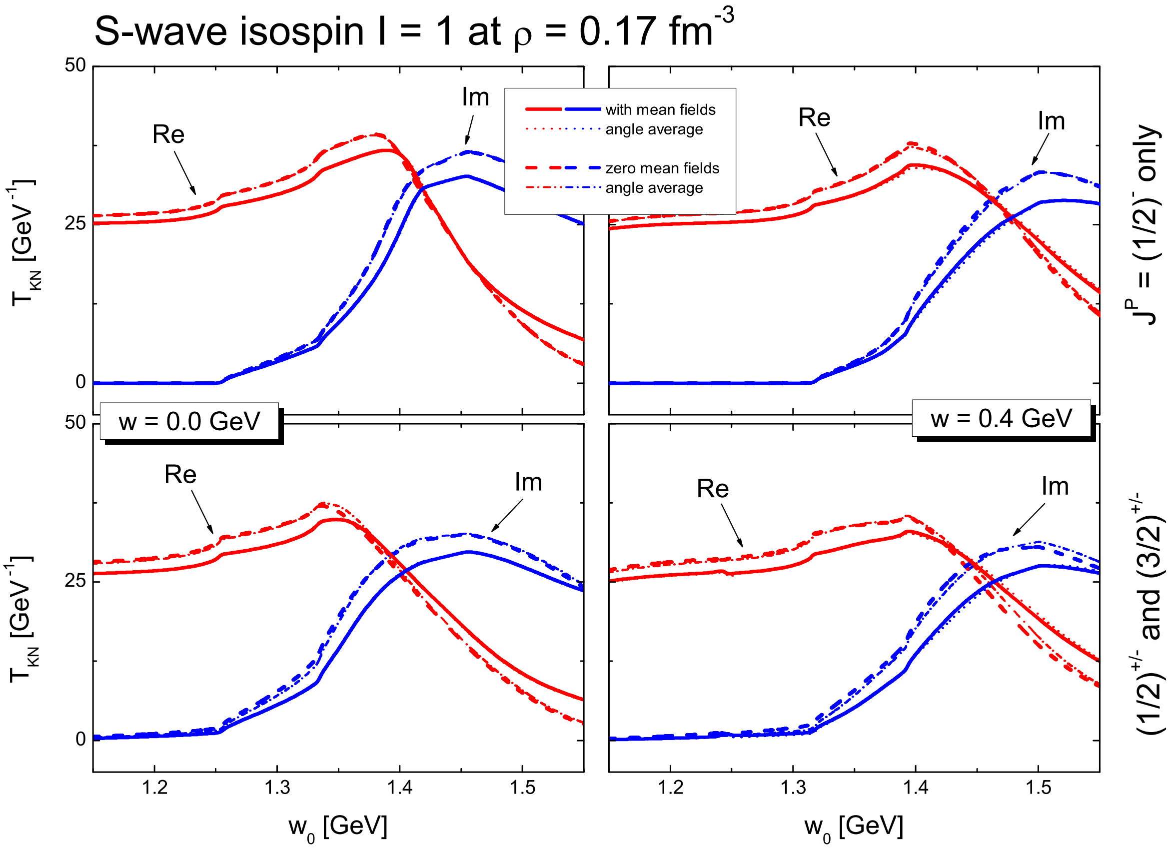

Figure 2.8: S-wave isospin $I = 1$ amplitudes as a function of energy w_0 and momentum $\mathbf{w}$ at nuclear saturation density ρ_0. The results are given for full calculation and for angular average approximation. For the upper panels only s-wave interactions are considered, the lower panels include s- ,p- and d-waves.

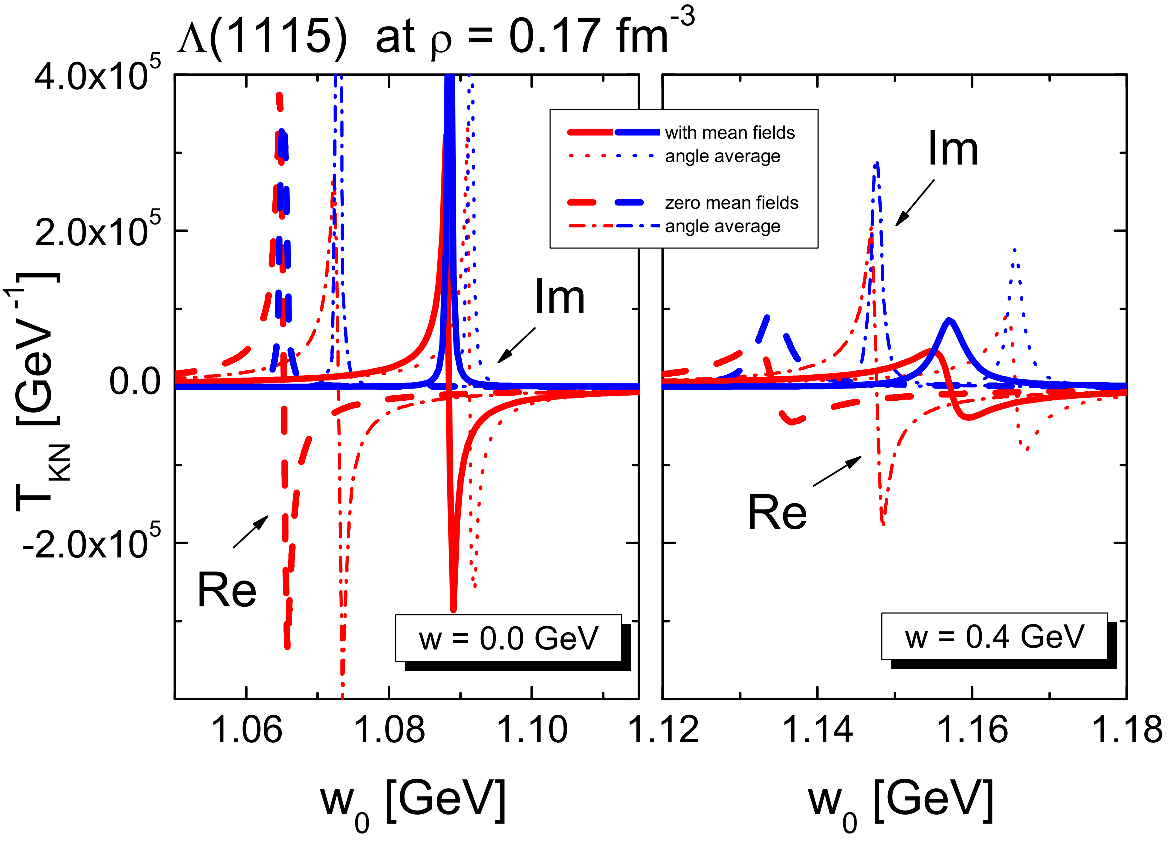

Figure 2.9: $\Lambda(1115)$ mass distribution as a function of energy w_0 and momentum $\mathbf{w}$ at nuclear saturation density ρ_0. The results are given for full calculation and for angular average approximation. The results are given for full calculation and for angular average approximation.

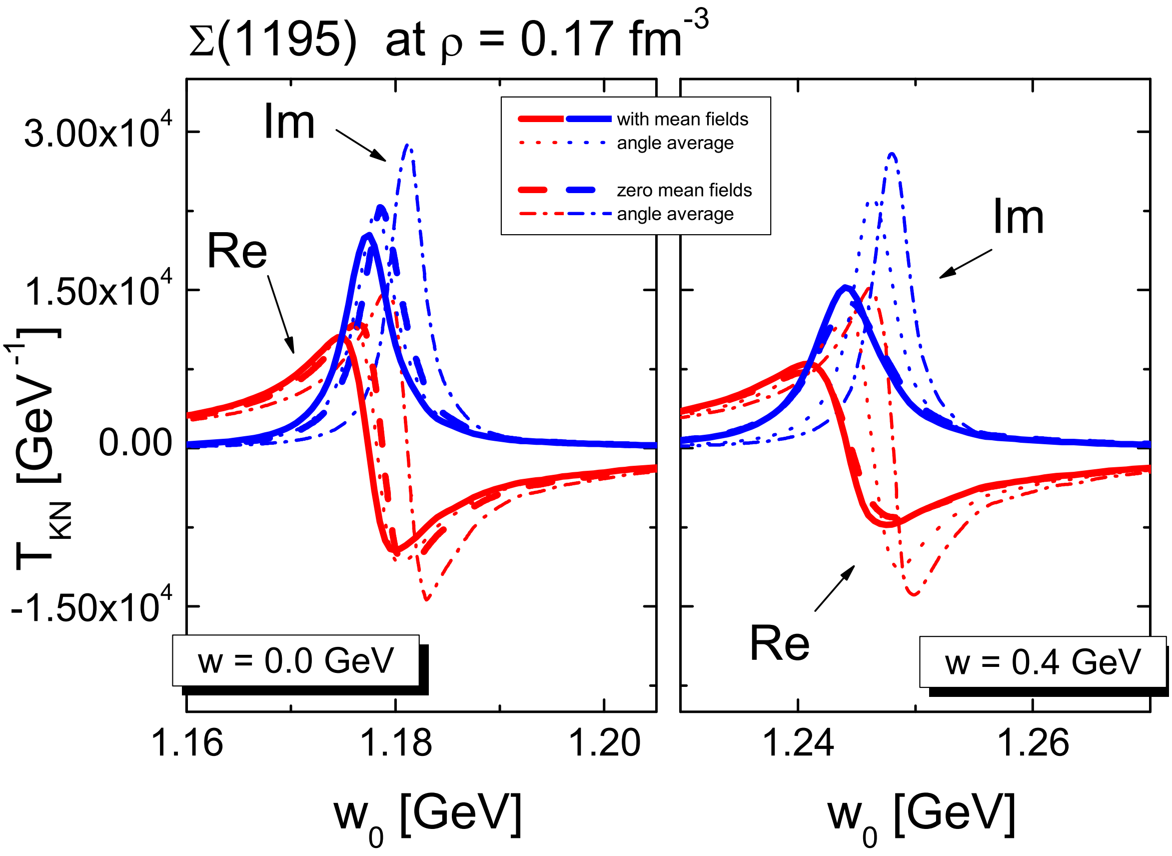

Figure 2.10: Σ(1195) mass distribution as a function of energy w_0 and momentum $\mathbf{w}$ at nuclear saturation density ρ_0. The results are given for full calculation and for angular average approximation. The results are given for full calculation and for angular average approximation.

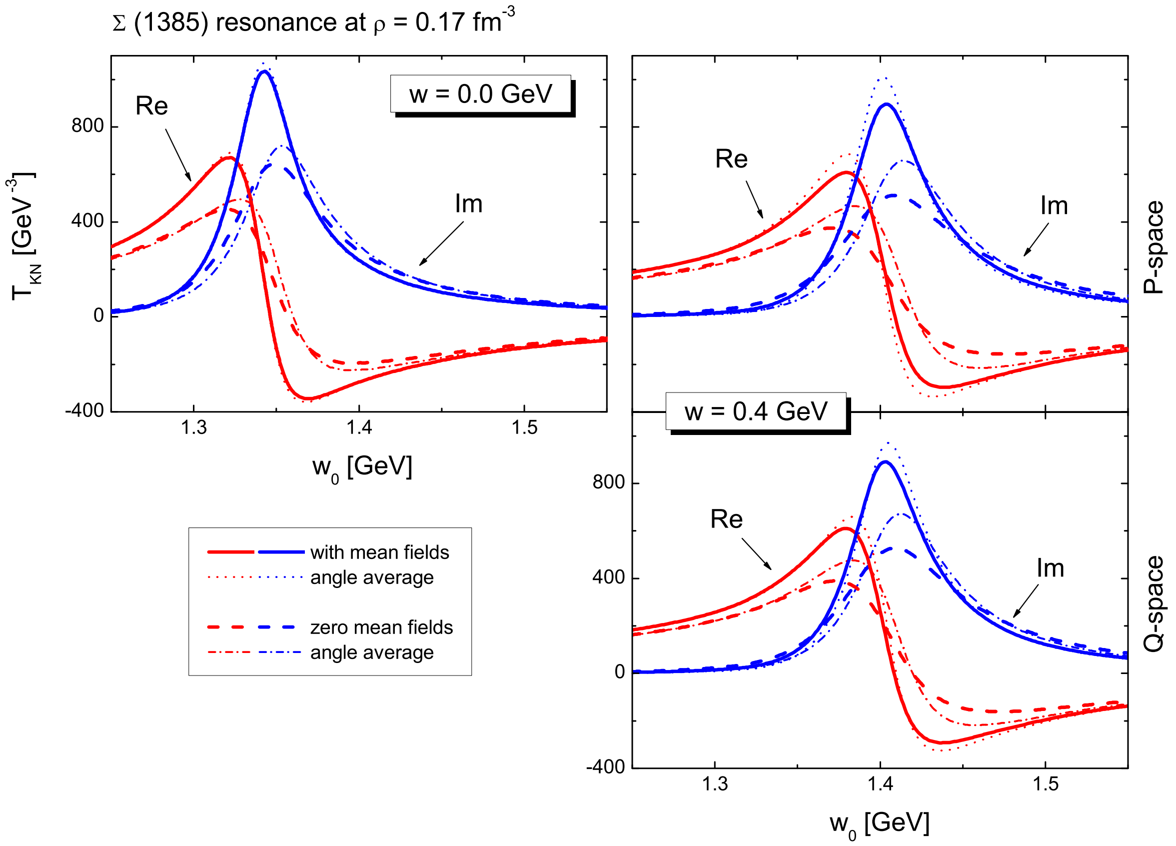

Figure 2.11: $\Sigma(1385)$ mass distribution as a function of energy w_0 and momentum $\mathbf{w}$ at nuclear saturation density ρ_0. The results are given for full calculation and for angular average approximation. The results are given for full calculation and for angular average approximation. For vanishing momentum $\mathbf{w} = 0$ the P- and Q-space amplitudes are degenerate and for finite $\mathbf{w}$ the results are given separately on the right hand side.

The $\Sigma(1385)$ p-wave resonance in Figure 2.11 receives an attractive mass shift of 40 MeV in the medium for the full calculation including nucleon mean-fields and almost 10 MeV less without mean-fields. In contrast to the $\Lambda(1405)$ and $\Lambda(1520)$ resonances the $\Sigma(1385)$ gets broader when the mean-fields are switched off. There is sizeable deviation of the angular average approximation from the full computation without mean-fields. At finite external momenta $\mathbf{w}$ the degeneracy between the two helicity states in P- and Q-space is rather low, but the difference of the angular average results increases. The attractive mass shift and width of the $\Sigma(1385)$ resonance is found to be considerably larger than in [14]. With switched on mean-fields our results agree with [5], whereas in [14] a much smaller mass shift of only 7 MeV is found.

The most striking impact of the nucleon mean-fields and the angular average approximation can be seen in Figure 2.12 for the $\Lambda(1520)$ d-wave resonance. While without mean-fields the $\Lambda(1520)$ is attracted by almost 150 MeV by doing the angular approximation for switched off mean-fields the shift by is reduced by about 50 MeV. We conclude that for higher partial wave amplitudes the angular average approximation fails. The approximation is less reliable

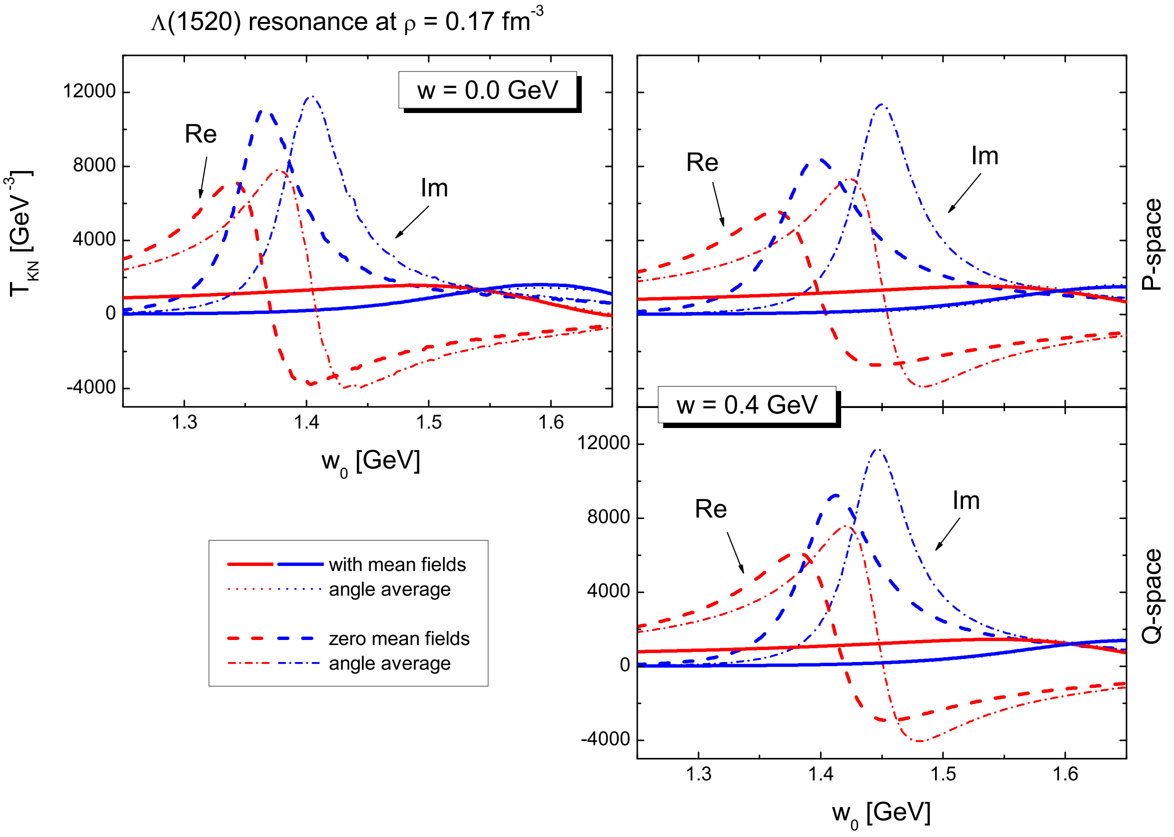

Figure 2.12: $\Lambda(1520)$ mass distribution as a function of energy w_0 and momentum $\mathbf{w}$ at nuclear saturation density ρ_0. The results are given for full calculation and for angular average approximation. The results are given for full calculation and for angular average approximation. For vanishing momentum $\mathbf{w} = 0$ the P- and Q-space amplitudes are degenerate and for finite $\mathbf{w}$ the results are given separately on the right hand side.

the higher the partial waves are. Switching on the mean-fields the resonance gets very broad and almost dissolves in the medium.

2.5.4 Comparison of different mean-field strengths at saturation density

We estimate the effect of different mean-field strengths by comparing the already presented calculation based on (2.13), denoted as 'medium mean-fields', with two different mean-field strengths. The 'weak mean-fields' are

$$\Sigma_V = 220\,\mathrm{MeV}\,\frac{\rho}{\rho_0}, \qquad \Sigma_S = 280\,\mathrm{MeV}\,\frac{\rho}{\rho_0} \tag{2.94}$$

and the 'strong mean-fields'

$$\Sigma_V = 350\,\mathrm{MeV}\,\frac{\rho}{\rho_0}, \qquad \Sigma_S = 400\,\mathrm{MeV}\,\frac{\rho}{\rho_0}. \tag{2.95}$$

The results shown are all computed at saturation density ρ_0 and no angular average approximation is used.

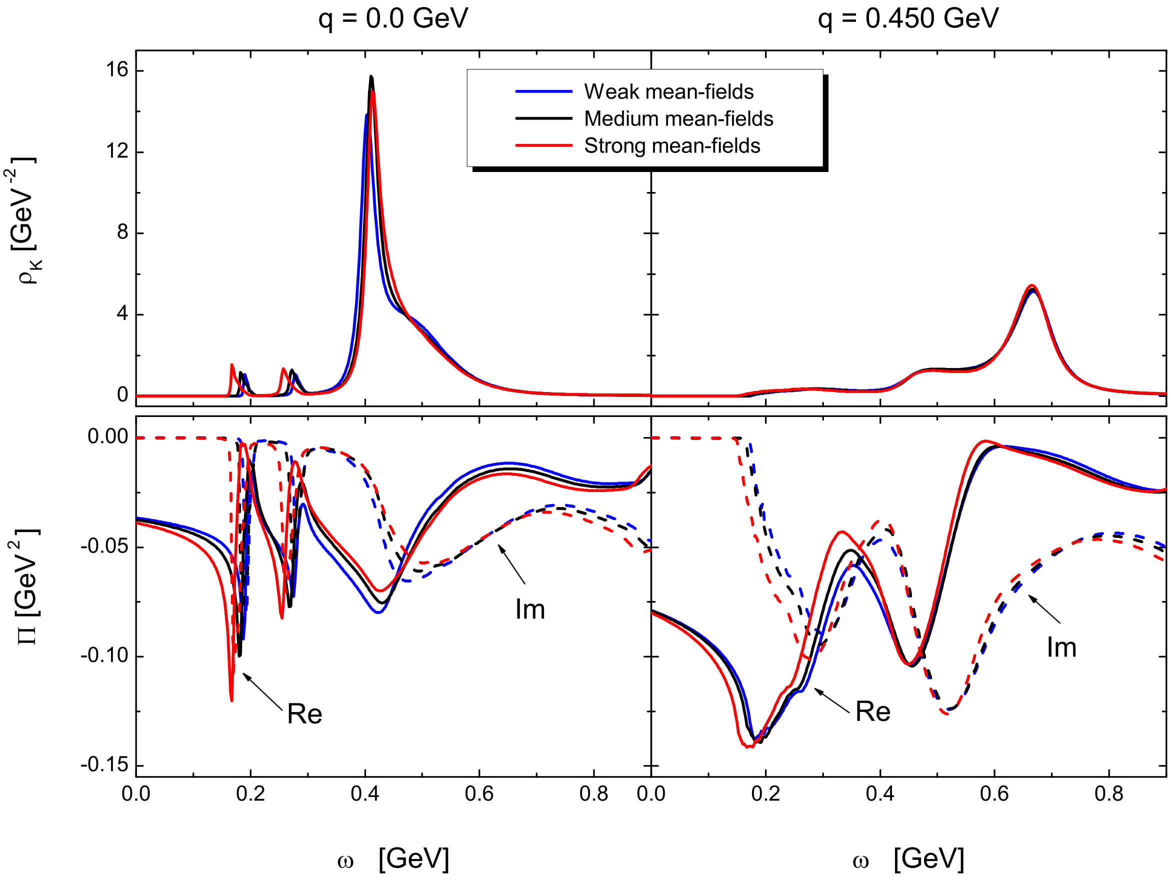

Figure 2.13: Antikaon spectral function (upper panels) and self-energy (lower panels) as a function of energy ω and momentum $\mathbf{q}$. Comparison of three different mean-field strengths at nuclear saturation density ρ_0.

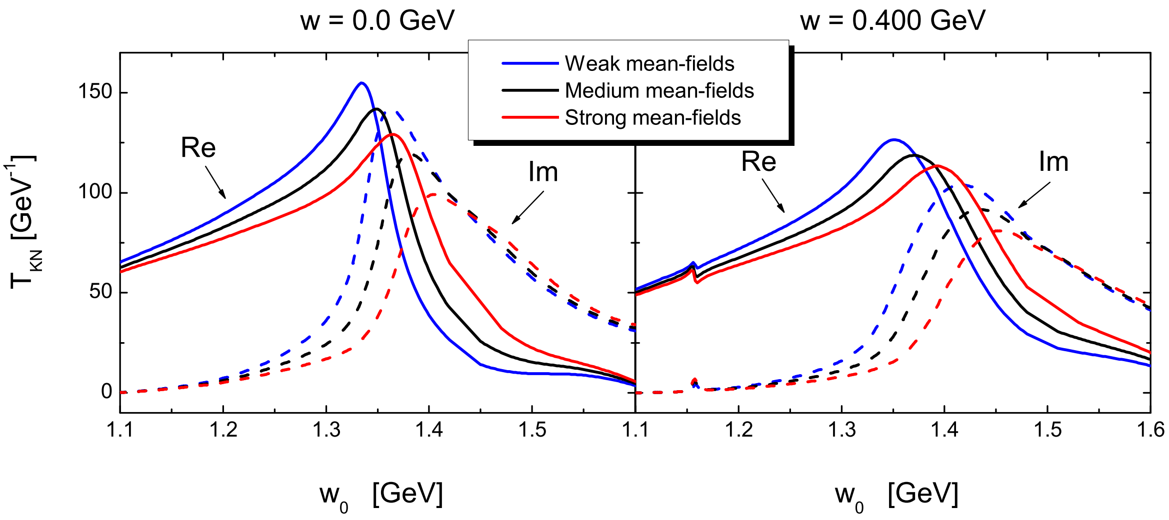

Figure 2.14: Mass distribution of $\Lambda(1405)$ as function of energy w_0 and momentum $\mathbf{w}$. Comparison of three different mean-field strengths at nuclear saturation density ρ_0.

Figure 2.13 summarizes the spectral function in the upper part and the self-energy in the lower part as a function of antikaon energy ω and momentum $\mathbf{q}$. The spectral function is affected only slightly by the variation of the mean-field strengths, especially at finite momenta $\mathbf{q}$ basically the same spectral function is obtained. The self-energy shows some notable differences, but the qualitative behaviour stays the same.

The hyperon properties are compared in Figure 2.14 for the $\Lambda(1405)$ s-wave and in Figures 2.15 and 2.16 for the $J = \frac{3}{2}$ $\Sigma(1385)$ p-wave and $\Lambda(1520)$ d-wave. We omit to show the $\Lambda(1115)$ and $\Sigma(1195)$ ground states, as the $\Lambda(1115)$ is shifted in each calculation and appears at exactly the same position according to the experimental data. Also the $\Sigma(1195)$ is basically located at the same mass position. The central mass of the ground states proves to be rather independent of the chosen mean-field strengths.

By increasing the mean-field strengths the attractive shift of the $\Lambda(1405)$ is reduced and the resonance is broadened significantly, as can be seen in Figure 2.14. Within the chosen mean-fields range the effect on the $\Lambda(1405)$ scales almost linearly. Similarly the $\Sigma(1385)$ and $\Lambda(1520)$ move upwards with a larger mean-field strengths, but while the Λ gets broader the $\Sigma(1385)$ width is reduced. Also the central mass shift of the $\Sigma(1385)$ is smaller. The $\Lambda(1520)$ dissolves very rapidly when mean-fields are switched on. The effect seems to be less pronounced when the mean-fields strengths is further increased.

2.5.5 Comparison of large scalar and vector mean-fields to a weak scalar mean-field only

The work of [14] assumes an attractive mean-field of 50 MeV, but does not take into account large scalar and vector mean-fields. However, we expect sizeable implications from our approach considering both scalar and vector mean-fields explicitly. The latter ansatz with (2.13) can be compared to a more simple model just allowing for a weak scalar mean-field with

$$\Sigma_V = 0\,\mathrm{MeV}\,\frac{\rho}{\rho_0}, \qquad \Sigma_S = 60\,\mathrm{MeV}\,\frac{\rho}{\rho_0}. \tag{2.96}$$

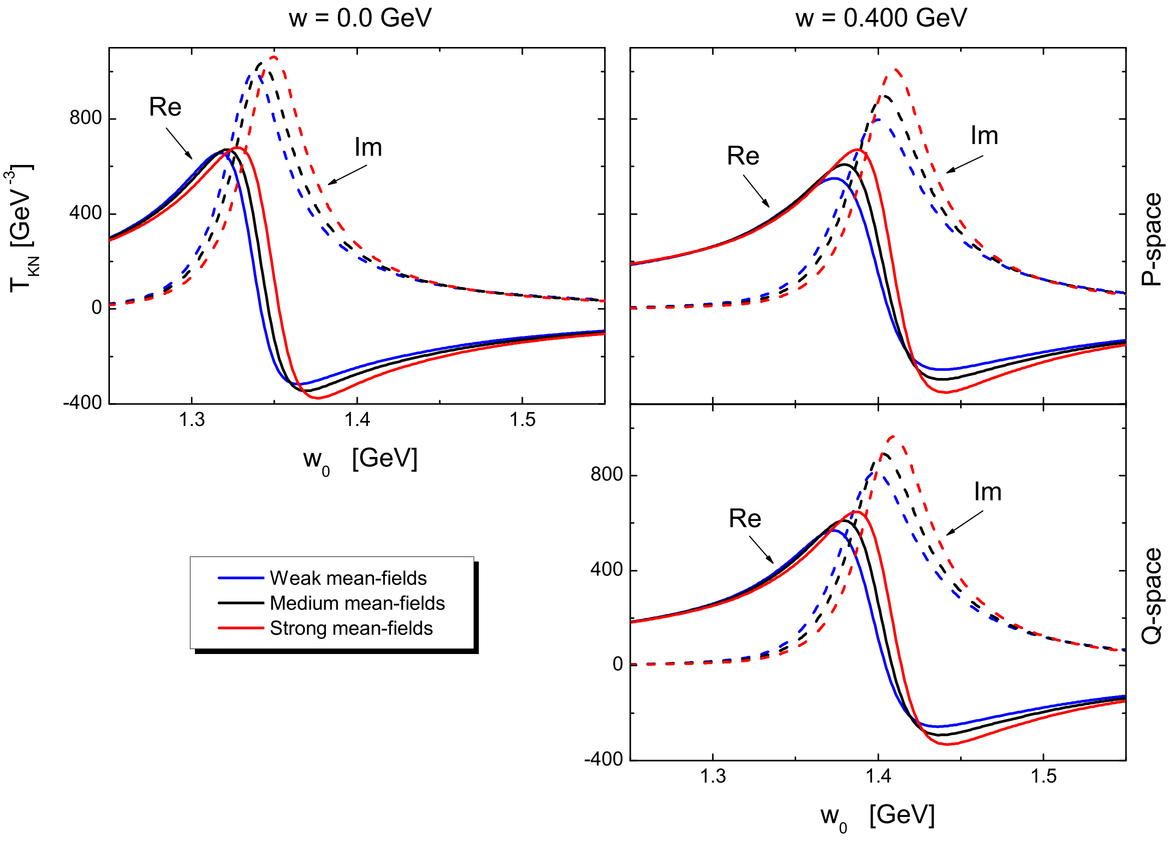

Figure 2.15: Mass distribution of $\Sigma(1385)$ as function of energy w_0 and momentum $\mathbf{w}$. Comparison of three different mean-field strengths at nuclear saturation density ρ_0.

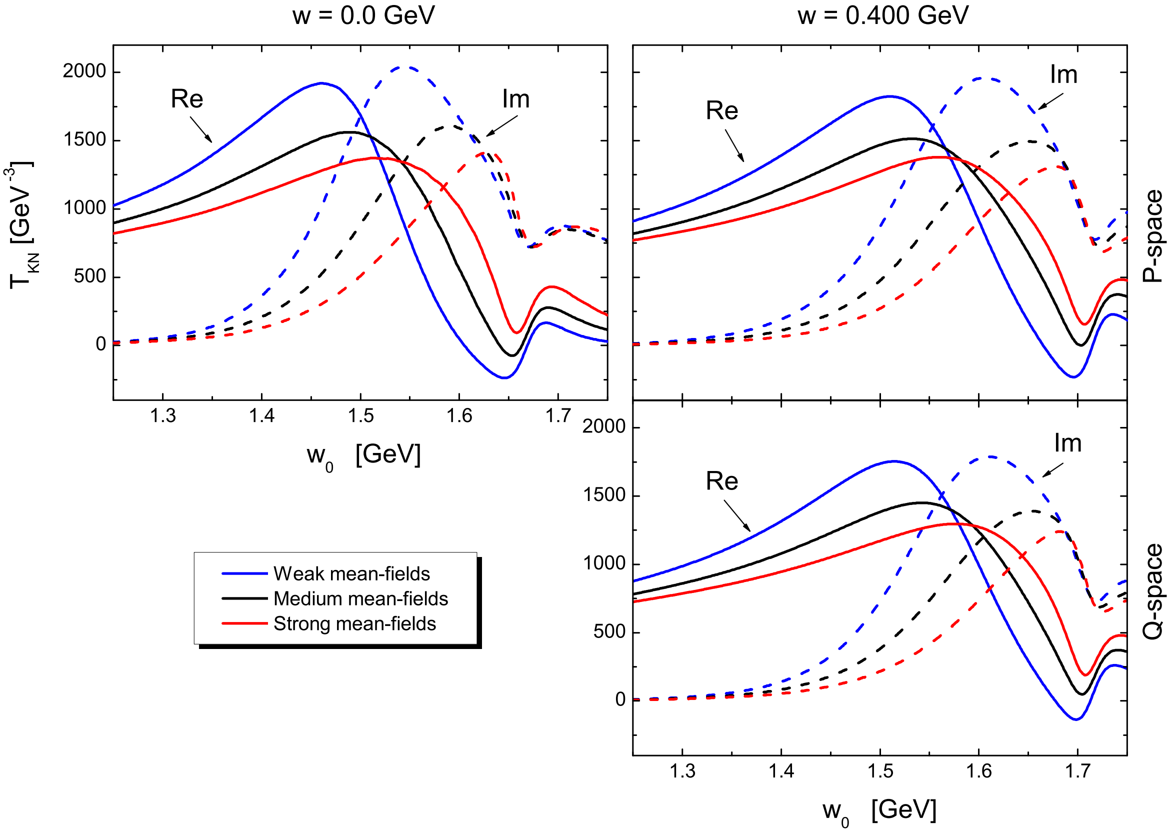

Figure 2.16: Mass distribution of $\Lambda(1520)$ as function of energy w_0 and momentum $\mathbf{w}$. Comparison of three different mean-field strengths at nuclear saturation density ρ_0.

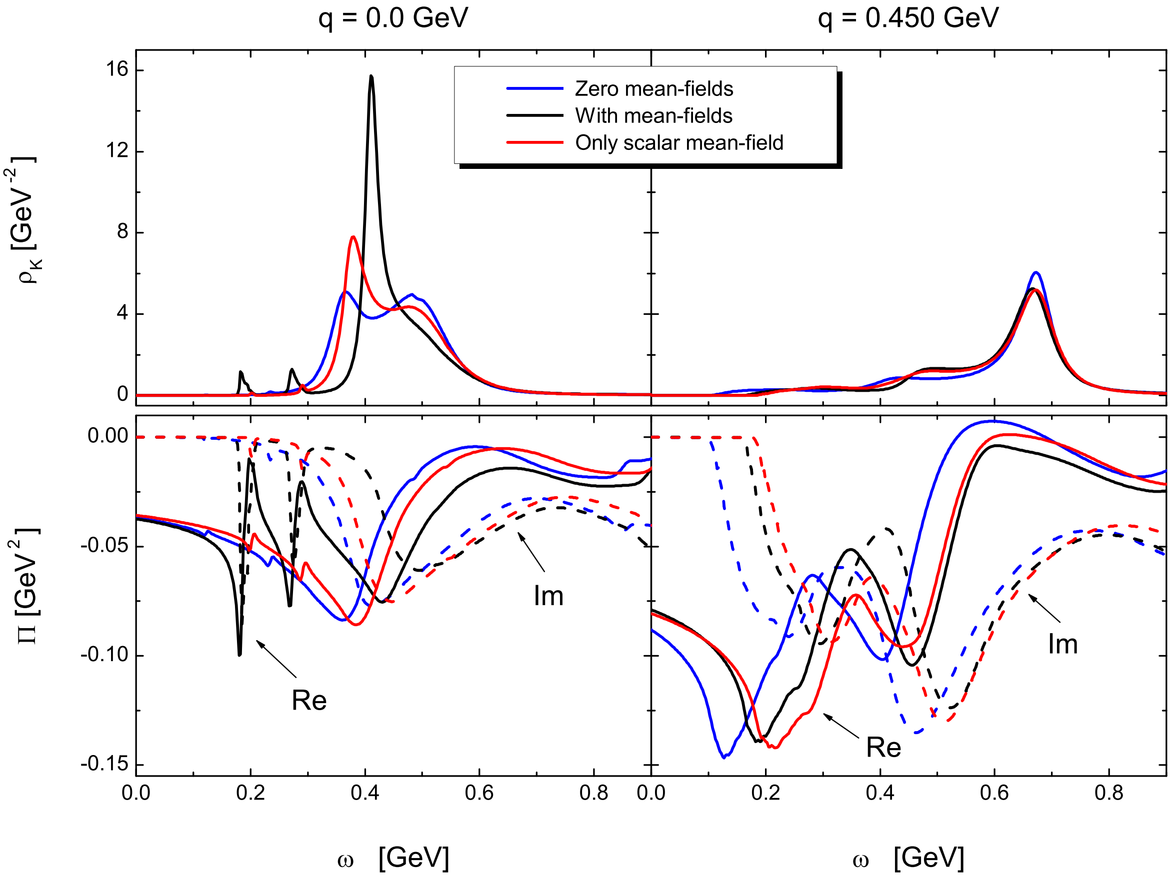

Figure 2.17: Antikaon spectral function (upper panels) and self-energy (lower panels) as a function of energy ω and momentum $\mathbf{q}$. Comparison at nuclear saturation density ρ_0 of calculations with mean-fields, zero mean-fields and scalar mean-field of $\Sigma_S = 60\,\mathrm{MeV}$ only.

The scalar Σ_S corresponds to the difference of scalar and vector contribution in (2.13). The results for scalar mean-field only are compared to the results with switched off and also switched on (2.13) mean-fields. Significant deviations between the two runs with mean-fields can already be observed in the spectral function and self-energy in Figure 2.17. With large scalar and vector mean-fields for zero antikaon momentum considerably more strength is moved to the lower peak and the soft modes. The strong enhancement of the two lower modes in the self-energy at $\mathbf{q} = 0$ can only be seen in the case of large scalar and vector mean-fields. For finite antikaon momenta the spectral function is less sensitive to the mean-field strengths, but the self-energy still shows significant deviations, which will also be present in the hyperons.

The $\Lambda(1405)$ is plotted in Figure 2.18, the $\Sigma(1385)$ in Figure 2.19 and the $\Lambda(1520)$ in Figure 2.20. With weak scalar mean-field only the $\Lambda(1405)$ is attracted by almost 50 MeV with respect to the zero mean-fields case, whereas with both mean-field contributions the central mass shift is reduced. For scalar mean-field only further attractive shift can also be observed for the $\Sigma(1385)$ in Figure 2.19. Contrary the $\Lambda(1520)$ feels an attractive mass shift of roughly 130 MeV for scalar mean-field only, which is 20 MeV less than without mean-

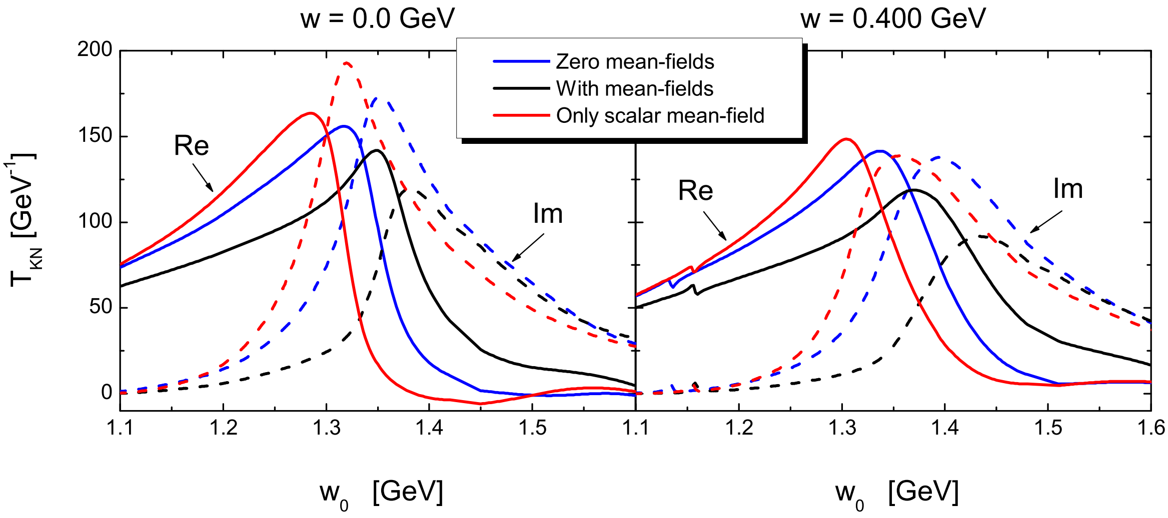

Figure 2.18: Mass distribution of $\Lambda(1405)$ as function of energy w_0 and momentum $\mathbf{w}$. Comparison at nuclear saturation density ρ_0 of calculations with mean-fields, zero mean-fields and scalar mean-field of $\Sigma_S = 60\,\text{MeV}$ only.

fields. The huge difference to the $\Lambda(1520)$ in Figure 2.20 with switched on scalar and vector mean-fields is obvious.

We conclude that the effects of large scalar and vector mean-fields cannot be modeled by a more simple ansatz with a weak scalar mean-field only, as has been done in [14]. Huge deviations are already observed for the spectral function and self-energy and manifest itself in the hyperon properties. In order to study the implications of nuclear saturation one has to take into account both scalar and vector mean-fields.

2.5.6 Spectral function, self-energy and hyperons with nucleon mean-fields at half and twice saturation density

Spectral function, self-energy and scattering amplitudes are computed at half and twice nuclear saturation density including nucleon mean-fields, in each case compared to the results with zero mean-fields. At half saturation density we scaled the mean-field strengths linearly with density according to (2.13) and choose

$$\Sigma_V = 145\,\text{MeV}, \qquad \Sigma_S = 175\,\text{MeV}, \qquad \rho = \frac{\rho_0}{2}. \tag{2.97}$$

The results for twice saturation density were calculated with

$$\Sigma_V = 600\,\text{MeV}, \qquad \Sigma_S = 600\,\text{MeV}, \qquad \rho = 2\,\rho_0, \tag{2.98}$$

where the choice of Σ_S accounts for saturation of the scalar mean-field with increasing density [31]. For comparison the results at saturation density are also shown.

The spectral function and self-energy are given as a function of antikaon energy ω and momentum $\mathbf{q}$ in Figures 2.21 and 2.22. At half saturation density the lower soft modes are strongly suppressed, while at twice saturation density they become very broad and feel

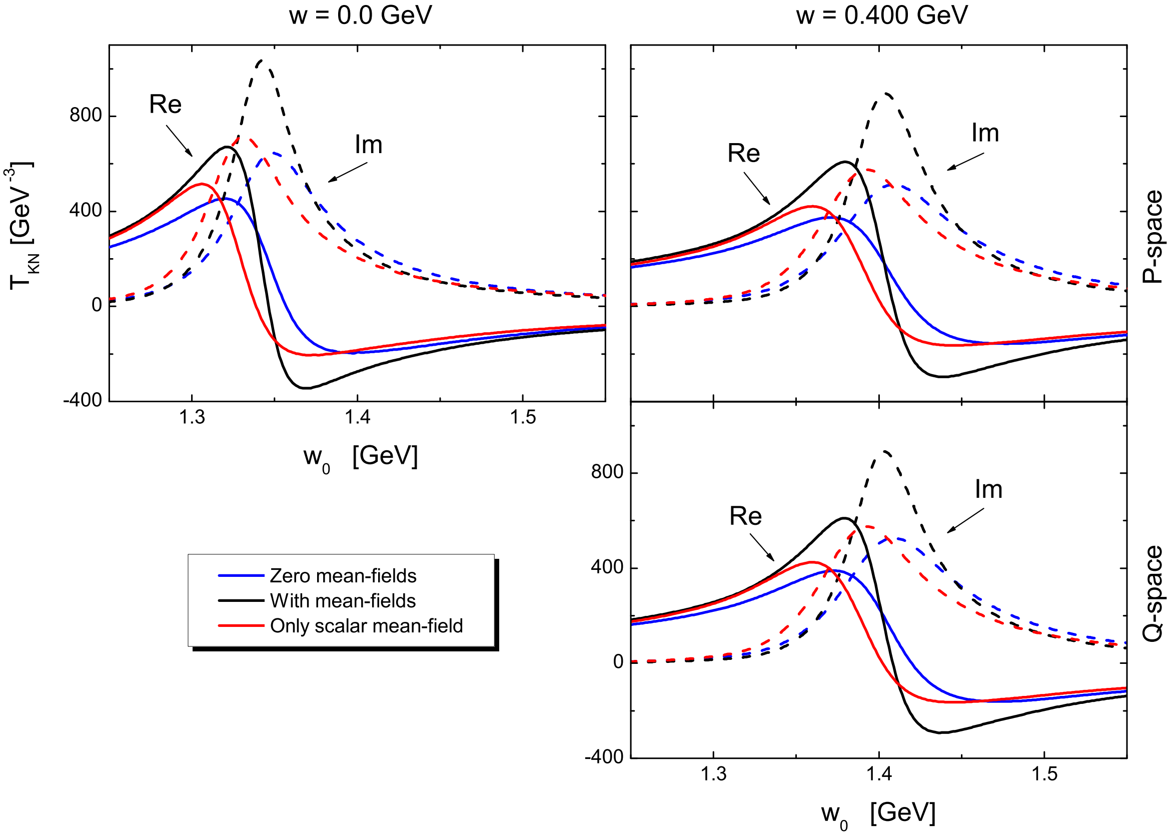

Figure 2.19: Mass distribution of $\Sigma(1385)$ as function of energy w_0 and momentum $\mathbf{w}$. Comparison at nuclear saturation density ρ_0 of calculations with mean-fields, zero mean-fields and scalar mean-field of $\Sigma_S = 60\,\mathrm{MeV}$ only.

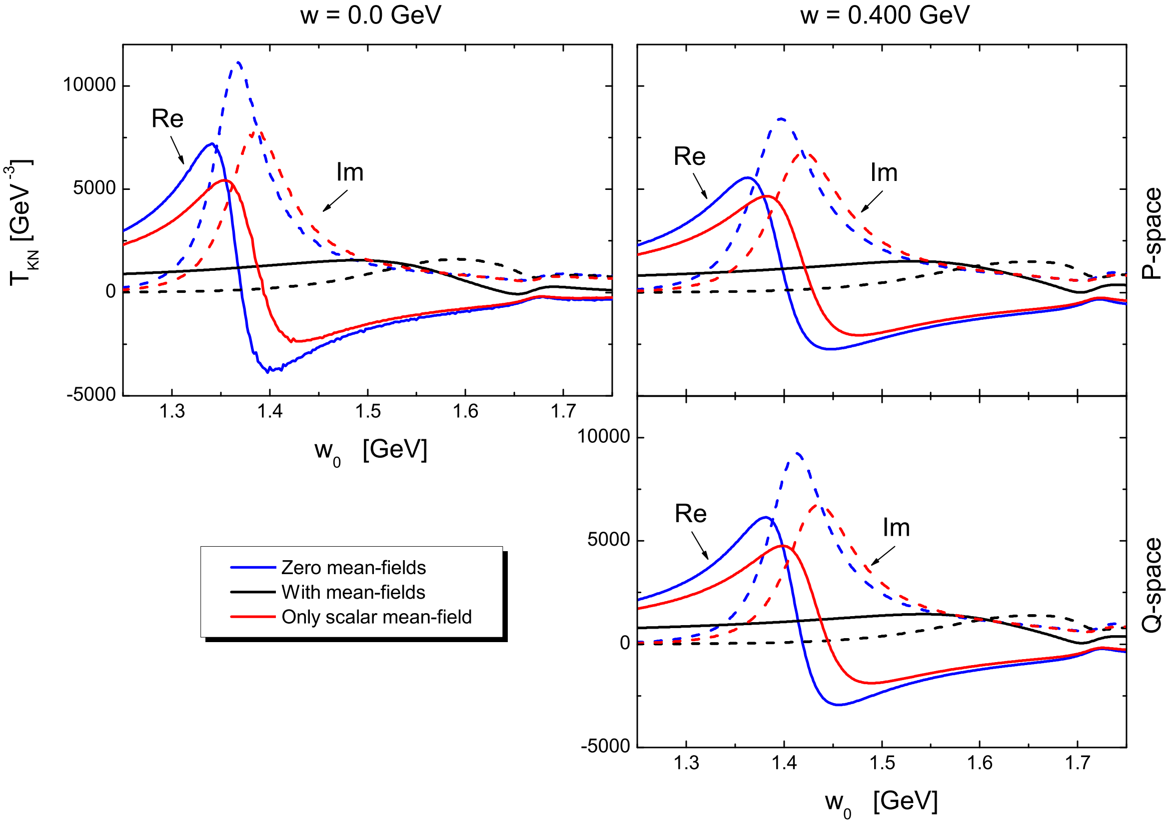

Figure 2.20: Mass distribution of $\Lambda(1520)$ as function of energy w_0 and momentum $\mathbf{w}$. Comparison at nuclear saturation density ρ_0 of calculations with mean-fields, zero mean-fields and scalar mean-field of $\Sigma_S = 60\,\mathrm{MeV}$ only.

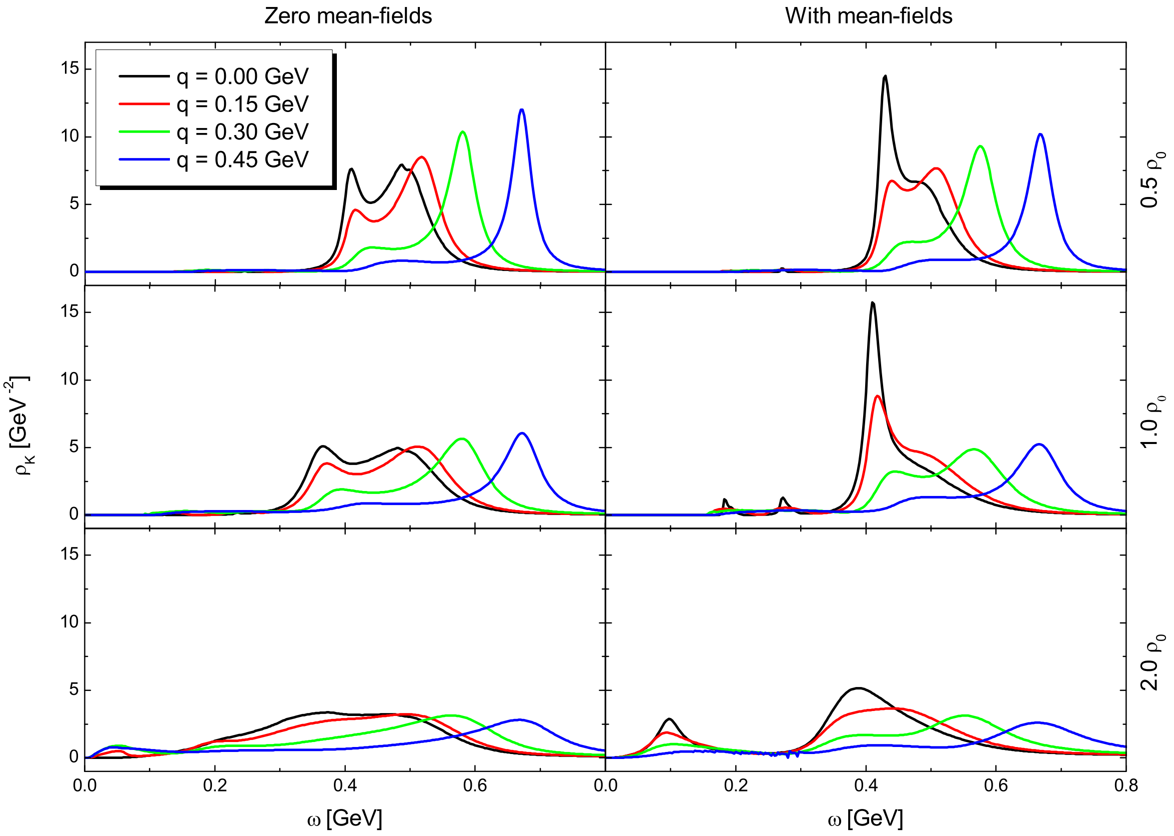

Figure 2.21: Antikaon spectral function as a function of energy ω and momentum $\mathbf{q}$ at half (upper panels), full (middle panels) and twice (lower panels) nuclear saturation density. Each calculation includes s-, p- and d-waves for the full computation (no angular average).

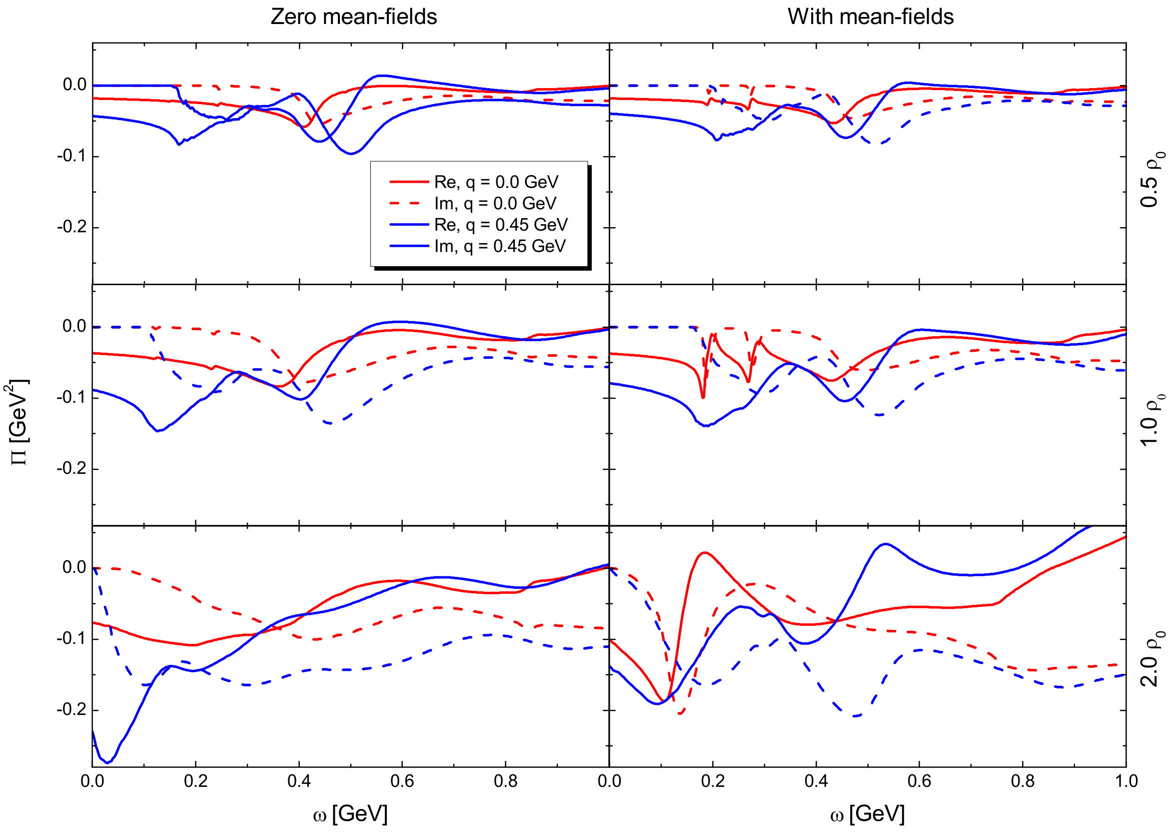

Figure 2.22: Antikaon self-energy as a function of energy ω and momentum $\mathbf{q}$ at half (upper panels), full (middle panels) and twice (lower panels) nuclear saturation density. Each calculation includes s-, p- and d-waves for the full computation (no angular average).

sizeable attraction. Note that there is only one peak of two left. This may be a numerical artefact of a $\Lambda(1115)$ ground state with zero width at twice saturation density, see Figure 2.24. It is caused by a vanishing imaginary part of the in-medium loop functions in the corresponding energy region. Both in spectral function and self-energy there is considerably more structure with switched on mean-fields than for zero mean-fields.

At half saturation density the $\Lambda(1405)$ in Figure 2.23 is only slightly affected by switching on mean-fields, which can be seen by comparing the upper and lower panels. In contrast the large mean-fields at twice saturation density have a dramatic effect. Whereas for switched off mean-fields the $\Lambda(1405)$ is attracted by about 100 MeV, including mean-fields it is pushed upwards by several hundred MeV and diminishes drastically.

The $\Lambda(1115)$ and $\Sigma(1195)$ ground states are shown inn Figures 2.24 and 2.25. The 16 MeV repulsive mass shift of the $\Lambda(1115)$ including mean-fields at saturation density has been scaled linearly with density. For twice saturation density the self consistency causes a huge attractive mass shift. The same can be observed for the $\Sigma(1195)$ ground state, which is significantly broadened at twice saturation density and almost dissolves. Again we see that the central mass position of the ground states is quite insensitive to the nucleon mean-fields.

For ease of demonstration the $J = \frac{3}{2}$ hyperons are splitted into separate figures for zero and with nucleon mean-fields. At half saturation density the mass shift of the $\Sigma(1385)$ is

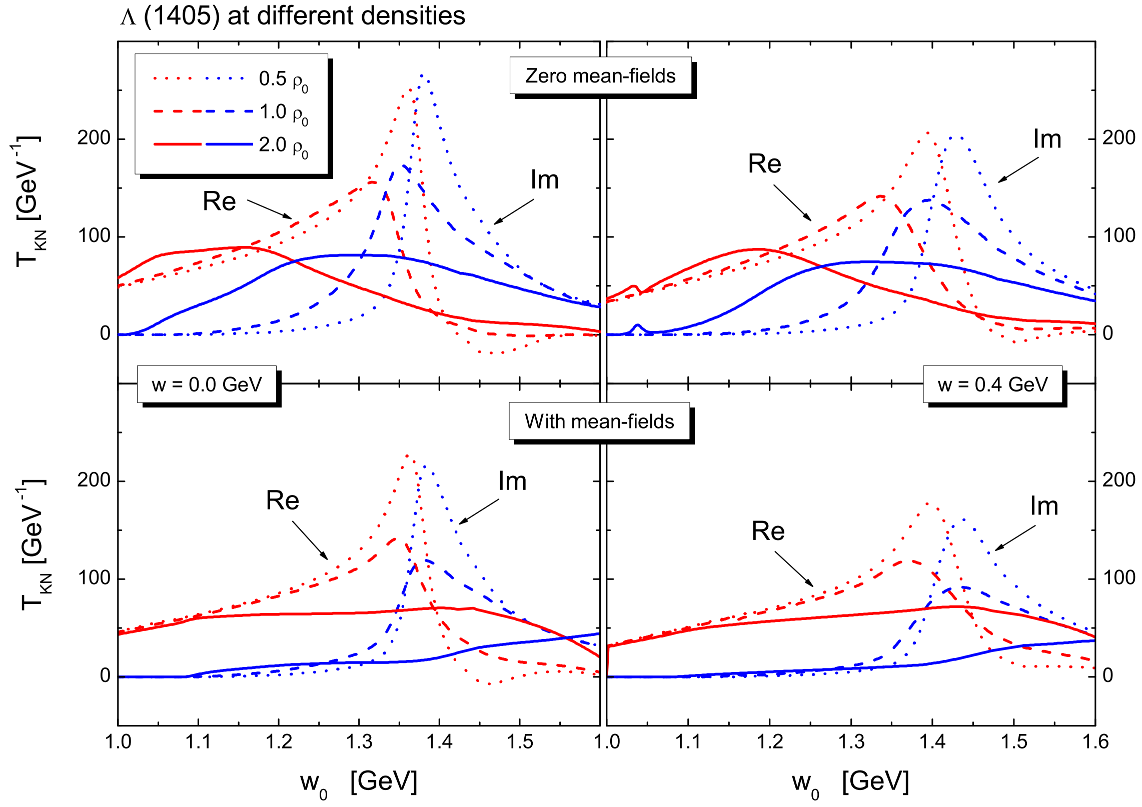

Figure 2.23: Mass distribution of $\Lambda(1405)$ as function of energy w_0 and momentum $\mathbf{w}$ at half (dotted), full (dashed) and twice (solid) nuclear saturation density. Each calculation includes s-, p- and d-waves for the full computation (no angular average).

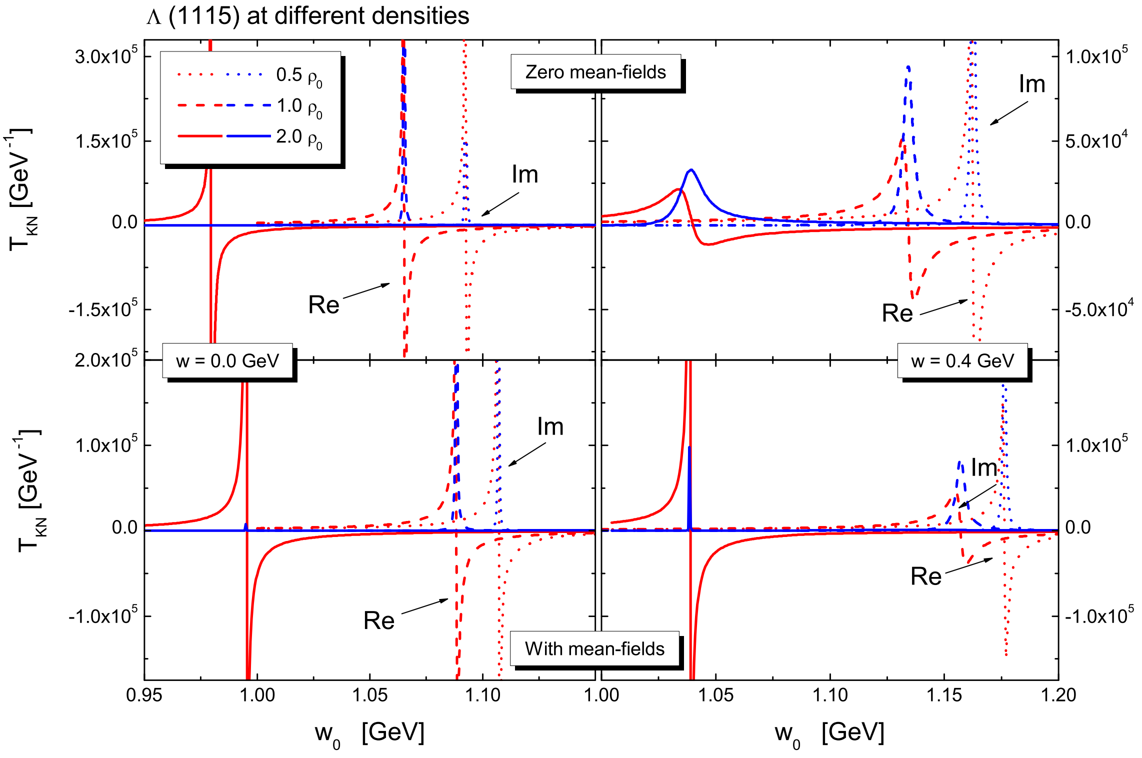

Figure 2.24: Mass distribution of $\Lambda(1115)$ as function of energy w_0 and momentum $\mathbf{w}$ at half (dotted), full (dashed) and twice (solid) nuclear saturation density. Each calculation includes s-, p- and d-waves for the full computation (no angular average).

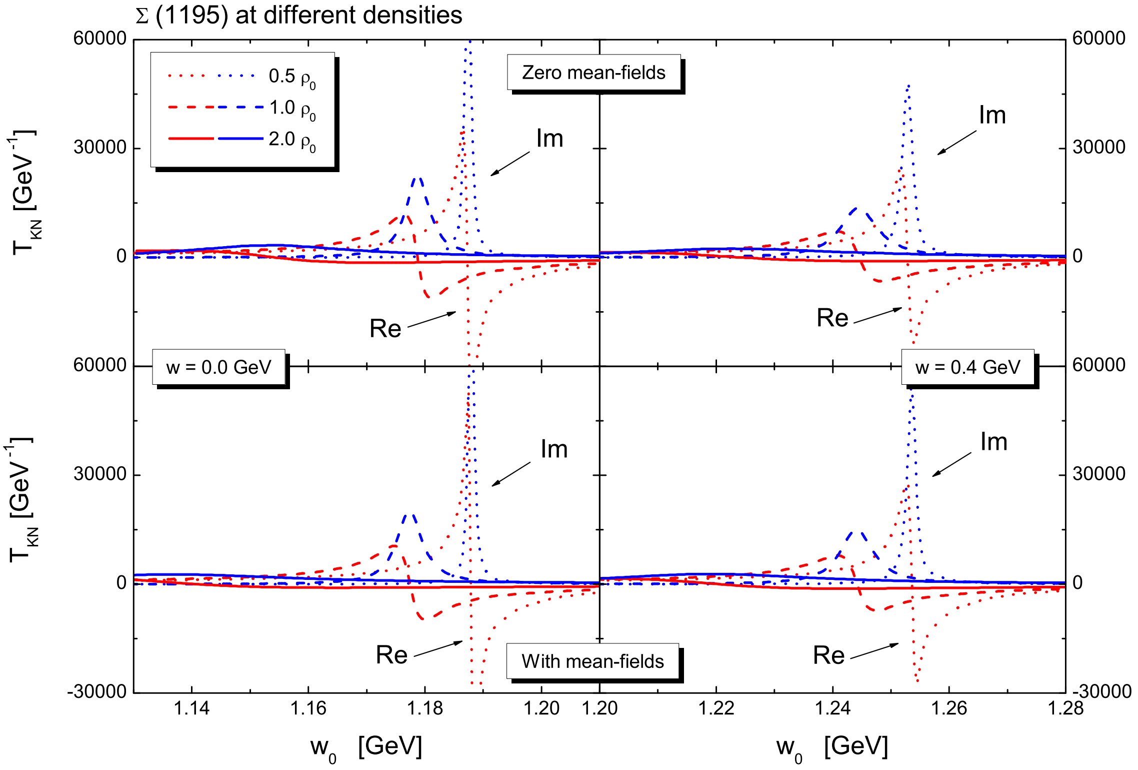

Figure 2.25: Mass distribution of $\Sigma(1195)$ as function of energy w_0 and momentum $\mathbf{w}$ at half (dotted), full (dashed) and twice (solid) nuclear saturation density. Each calculation includes s-, p- and d-waves for the full computation (no angular average).

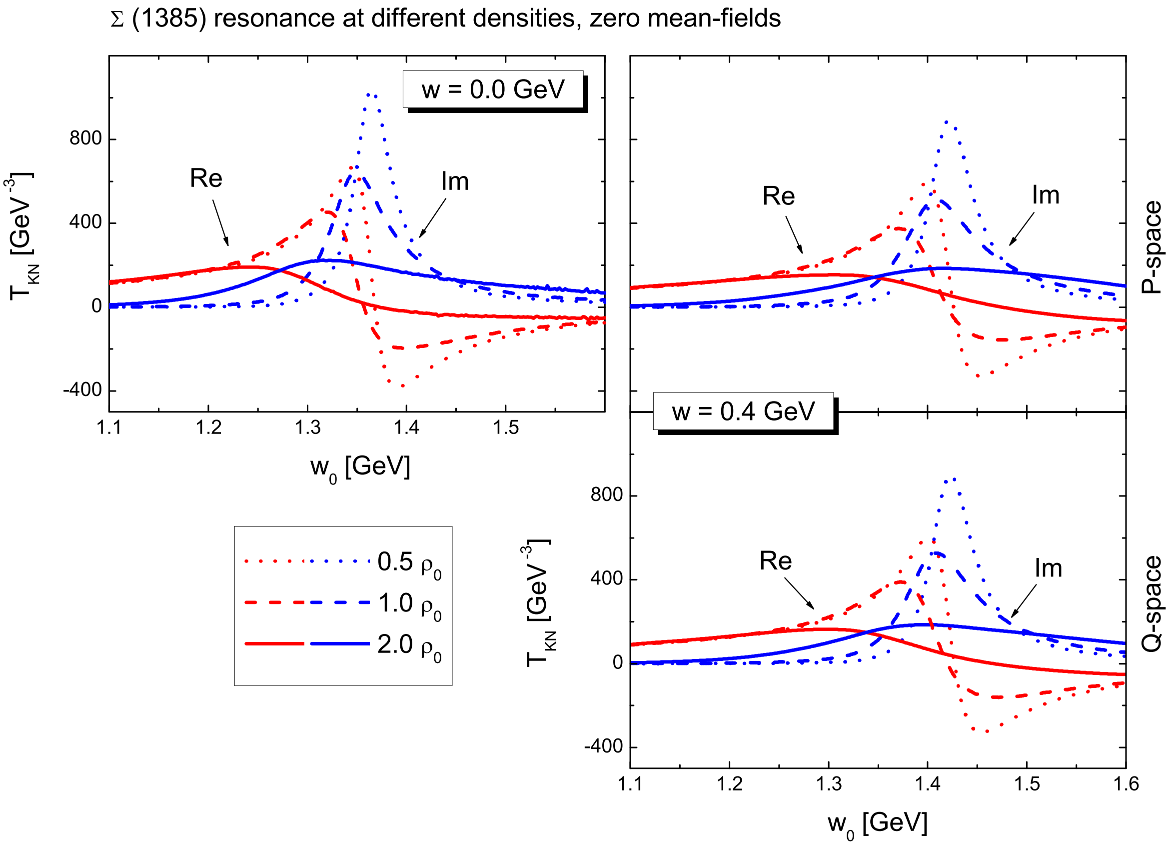

Figure 2.26: Mass distribution of $\Sigma(1385)$ as function of energy w_0 and momentum $\mathbf{w}$ at half (dotted), full (dashed) and twice (solid) nuclear saturation density. Each calculation includes s-, p- and d-waves for the full computation (no angular average). Zero nucleon mean-fields.

30 MeV without and 25 MeV including mean-fields, see Figures 2.26 and 2.27. Switching on mean-fields at twice saturation density the $\Sigma(1385)$ is back at its free-space position. The opposite effect is observed for zero mean-fields, where the resonance is broadened and receives an attractive shift of almost 80 MeV.

Inspecting Figures 2.28 with zero mean-fields and 2.29 with mean-fields for the $\Lambda(1520)$ the resonance mass shift increases with the density if mean-fields are switched off. Contrary is it shifted upwards with increasing density including mean-fields. The $\Lambda(1520)$ gets broader in both cases, but with mean-fields the resonance strength is reduced by a factor of 5 and even more at twice saturation density.

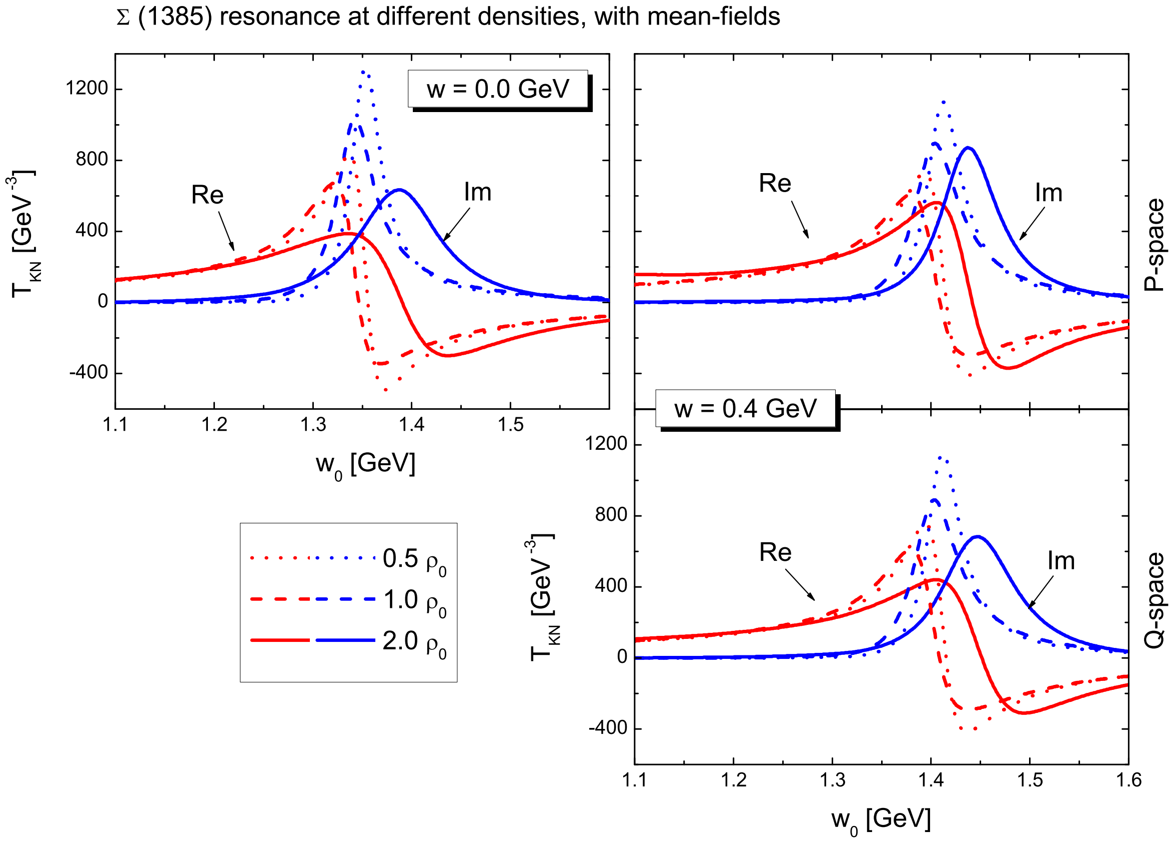

Figure 2.27: Mass distribution of $\Sigma(1385)$ as function of energy w_0 and momentum $\mathbf{w}$ at half (dotted), full (dashed) and twice (solid) nuclear saturation density. Each calculation includes s-, p- and d-waves for the full computation (no angular average). With nucleon mean-fields.

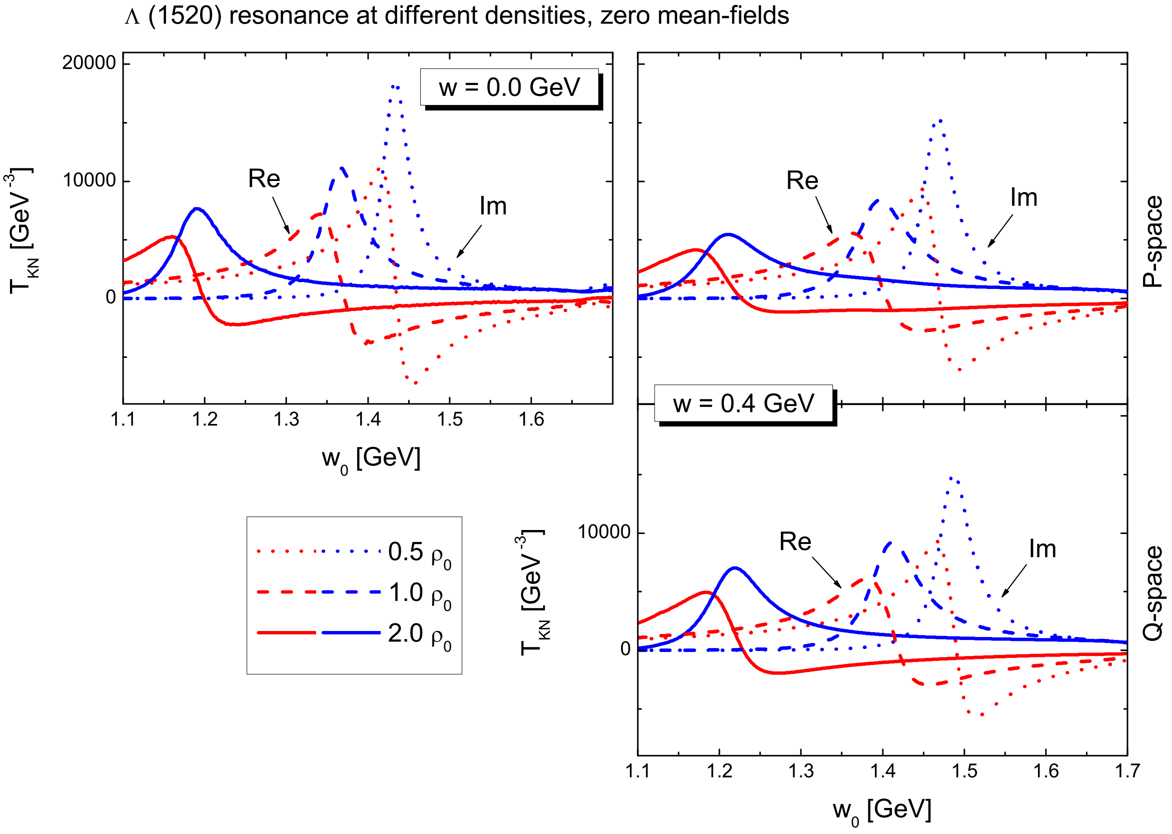

Figure 2.28: Mass distribution of $\Lambda(1520)$ as function of energy w_0 and momentum $\mathbf{w}$ at half (dotted), full (dashed) and twice (solid) nuclear saturation density. Each calculation includes s-, p- and d-waves for the full computation (no angular average). Zero nucleon mean-fields.

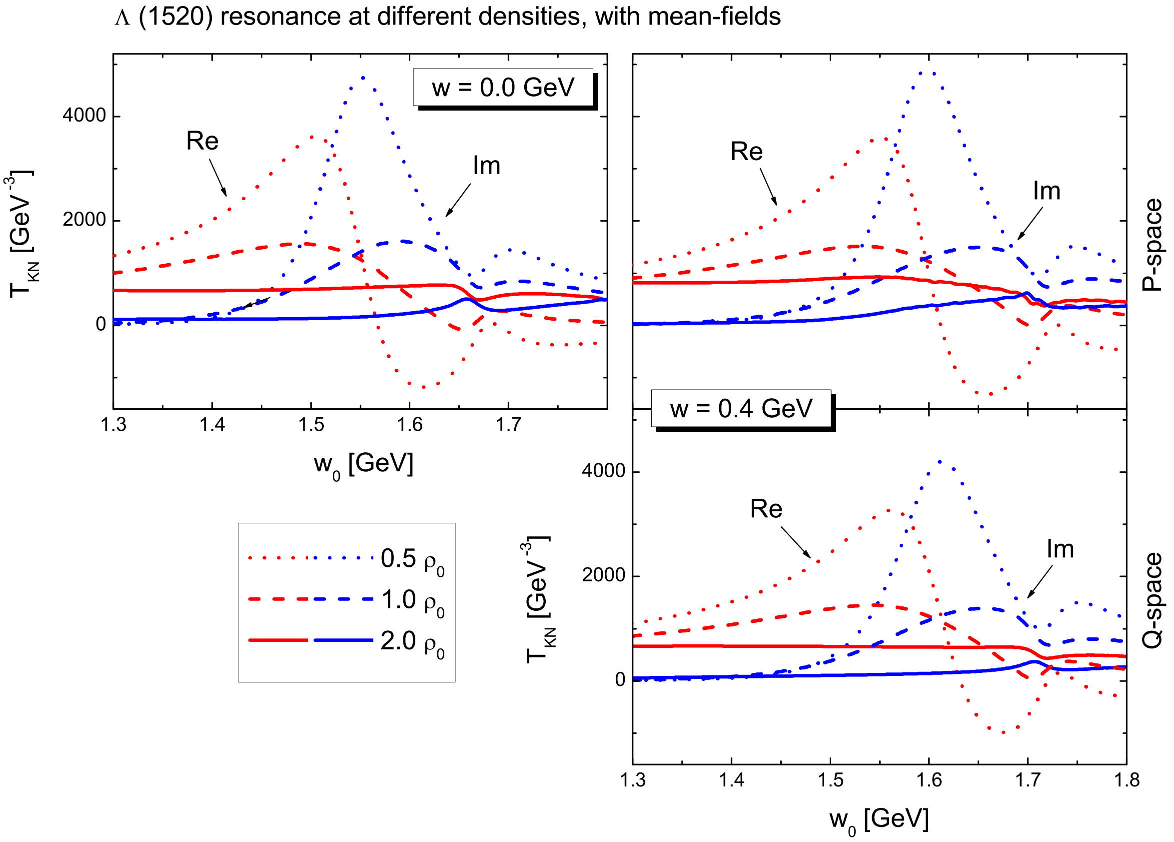

Figure 2.29: Mass distribution of $\Lambda(1520)$ as function of energy w_0 and momentum $\mathbf{w}$ at half (dotted), full (dashed) and twice (solid) nuclear saturation density. Each calculation includes s-, p- and d-waves for the full computation (no angular average). With nucleon mean-fields.

Chapter 3

Present status of kaonic atoms – Phenomenology

In [22] various phenomenological and microscopic approaches for the description of kaonic atom data were compared. None of the models has the ability to sufficiently describe the measured level shifts and widths. This motivates us to try an alternative non-local treatment of kaonic atoms based on microscopic $\bar{K}N$ in-medium scattering amplitudes [5]. Some of the microscopic models even introduce non-local aspects utilising gradient terms acting on the wave function and density distribution. Still these approaches are not yet unique and call for a more systematic treatment of non-local effects. In this section we summarize the comparison of the different models and comment on their advantages and disadvantages. The experimental data on kaonic atoms can be found in [32–42], covering the range from lithium up to uranium.

The parameters for the density distributions of the nuclei are based on [43], the nuclear binding energies E_{nuc} necessary for calculating the nuclear masses $m_{\text{nuc}} = Zm_P + (A - Z)m_N - E_{\text{nuc}}$ are taken from [44], where A and Z denote the number of nucleons and protons respectively. The proton and neutron masses are $m_P = 938.271998\,\text{MeV}$ and $m_N = 939.565330\,\text{MeV}$. For $A \leq 16$ the density distributions are parameterized by a modified harmonic-oscillator distribution (MHO),

$$\rho_{\text{MHO}}(r) = \rho_0 \left[1 + a\left(\frac{r}{R}\right)^2\right] e^{-\left(\frac{r}{R}\right)^2} \tag{3.1}$$

with a mean radius R. Note that in the MHO case the 'border width' a is a dimensionless quantity. For nuclei with $A > 16$ a two-point Fermi distribution is used:

$$\rho_{\text{2pF}}(r) = \rho_0 \left[1 + e^{\left(\frac{r-R}{a}\right)}\right]^{-1}. \tag{3.2}$$

The normalization constant ρ_0 is fixed by the condition

$$A = 4\pi \int\limits_0^\infty \rho(r) r^2 dr. \tag{3.3}$$

The neutron and proton density distributions – $\rho_N(r)$ and $\rho_P(r)$ – add up to the total density distribution $\rho(r) = \rho_N(r) + \rho_P(r)$. For heavier neutron-rich nuclei we do not correct the neutron density distribution and have $\rho_N(r) = \rho_P(r)$ as these corrections prove to be negligible.

	$\rho(r)$	Transition	Nuclear mass [MeV]	R [fm]	A [fm]
$^{12}_{6}$C	MHO	3d → 2p	11174.862215	1.516	2.234
$^{32}_{16}$S	2pF	4f → 3d	29773.616592	3.218	0.502
$^{35}_{17}$Cl	2pF	4f → 3d	32564.590103	3.451	0.497

Table 3.1: Measured transition, nuclear mass and parameters of the density distribution.

The relevant parameters for the discussed nuclei carbon, sulphur and chlorine are given in Table 3.1.

The third column of Table 3.1 refers to the measured transition between the antikaon orbits in standard atomic physics notation. For all the relevant levels we have $n - l = 1$. As the upper levels are practically unaffected by the strong antikaon-nuclei interaction the hadronic energy shifts $\Delta E = \Delta E_{\rm exp} - \Delta E_{\rm em}$ can be determined by comparing the measured energy levels $\Delta E_{\rm exp}$ to those solely determined by the electromagnetic contributions $\Delta E_{\rm em}$.

3.1 Solution of the Klein-Gordon equation

We will briefly summarize the methods used for solving the Klein-Gordon equation. Special issues arising in connection with non-local potentials will be addressed later on. There are two possibilities for solving operator equations of the type $D\,y(x) = \lambda\,y(x)$ with an operator D containing derivative operators and an eigenvalue λ. Firstly the operator equation can be regarded either as an eigenvalue problem or a differential equation. Secondly the operators will be uniquely defined by applying appropriate boundary conditions to $y(x)$. The Klein-Gordon equation is formulated as a boundary condition problem with one parameter, the (complex) energy eigenvalue λ, reflecting the correlation between eigenvalue problems and the solution of differential equations subjected to boundary conditions. The task is to determine the eigenvalues λ corresponding to nontrivial solutions $y(x) \neq 0$.

In general the Klein-Gordon equation for a spin-0 particle bound by an energy dependent local optical potential $U_{opt}(\omega - V_{em}, \mathbf{r})$ takes the form

$$\left(\nabla^2 - \mu^2 + (\omega - V_{em}(r))^2\right)\phi(\mathbf{r}) = 2\mu\, U_{opt}(\omega - V_{em}, \mathbf{r})\phi(\mathbf{r}). \tag{3.4}$$

Here μ is the reduced mass of the antikaon-nucleus system, the energy $\omega = \mu + E - \frac{i}{2}\Gamma$ gives the binding energy E and the level width Γ, while $\phi(\mathbf{r})$ denotes the wave function of the antikaon. Both determine the electromagnetic potential $V_{em}(r)$ which is radially symmetric. Besides from the Coulomb potential for a finite size nucleus there are also vacuum polarization corrections which have to be considered due to the high kaon mass. Details will be described in Section 3.2.

In Appendix B.1 we summarize the asymptotic and analytic solutions of the Klein-Gordon equation (3.4) for vanishing optical potential and restricting the electromagnetic potential to the Coloumb contribution for a point-like charge. These solutions have to be applied as boundary conditions for the numerical solution of the Klein-Gordon equation when taking into account optical potentials. The numerical solution of the Klein-Gordon equation in coordinate space will be determined by using two different methods, for bound states with $l < 4$ and lower mass nuclei ($A \leq 35$) the scheme [45] and for $l \geq 4$ bound states a shooting method based on a two point boundary condition problem. The latter schemes are suitable for solving bound state problems with real and complex eigenvalues. We briefly describe the main features and the implementation of both methods in Appendix B.2.

3.2 Electromagnetic potential

The electromagnetic potential $V_{em}(r)$ entering the Klein-Gordon equation (3.4) is made up of the Coulomb potential for a finite size nucleus and three leading vacuum polarization corrections, the leading order $\alpha Z\alpha$ [46], order $\alpha(Z\alpha)^3$ [47] and order $\alpha^2(Z\alpha)$ [48]. For the vacuum polarization contributions analytic expressions based on a series expansion are used. As the finite size effects for the vacuum polarization involve highly divergent terms [49] that are difficult to handle numerically and their contributions are just significant for heavy nuclei, they will be neglected.

3.2.1 Coulomb potential for finite size nuclei

The radially symmetric Coulomb potential $V_C(r) = -\frac{Z\alpha}{r}$ for a point-like particle with charge Z has to be folded with the charge distribution $\rho(r)$,

$$V_C^{FS}(\mathbf{r}) = -\int d^3r' \frac{\rho(\mathbf{r}')}{|\mathbf{r}-\mathbf{r}'|}, \tag{3.5}$$

which is specified by the normalization condition

$$4\pi \int_0^\infty r^2 \rho(r) dr = Z\alpha \tag{3.6}$$

for a radially symmetric potential. Analogously $V_C^{FS}(r)$ can be derived from the solution $\psi(\mathbf{r})$ of the Poisson equation

$$\nabla^2 V_C^{FS}(\mathbf{r}) = -4\pi\rho(\mathbf{r}) \tag{3.7}$$

which avoids the singular integrand in (3.5). For the radial component of $V_C^{FS}(r)$ with the radial Laplace operator in spherical coordinates $\triangle_{rad}\psi = \frac{1}{r^2}\frac{\partial}{\partial r}\left(r^2\frac{\partial\psi}{\partial r}\right)$ we have

$$\frac{d^2}{dr^2}(r \cdot V_C^{FS}(r)) \equiv \frac{d^2}{dr^2}\psi(r) = -4\pi\rho(r). \tag{3.8}$$

The boundary conditions of the differential equation (3.8) are $\psi(r) = 0$ at $r = 0$ and $\psi(r) = Z\alpha$ for $r \to \infty$. The charge distribution $\rho(r)$ is parameterized in the same way as the density distribution according to (3.1) and (3.2), but the normalization is given by (3.6).

3.2.2 Vacuum polarization

The strong overlap of the antikaon wave function and the Coulomb field near the nucleus requires the consideration of vacuum polarization corrections when dealing with kaonic atoms. The contribution from vacuum polarization can reach up to several keV which is of the same order as the strong interaction shift. In Table 3.2 we summarized the different vacuum polarization contributions as well as the Coulomb energy (B.21) from the Klein-Gordon equation

	KG [MeV]	FC	$\alpha Z\alpha$ [eV]	$\alpha^2(Z\alpha)$ [eV]	$\alpha(Z\alpha)^3$ [eV]	$\sum_{em}$ [MeV]
${}^{12}_{6}$C	0.113327	-6	441	3	0	0.113765
${}^{32}_{16}$S	0.368040	-15	1566	11	-1	0.369601
${}^{35}_{17}$Cl	0.416101	-27	1837	13	-2	0.417923
${}^{58}_{28}$Ni	0.638895	-6	2663	19	-6	0.641565
${}^{238}_{92}$U	2.272314	-10	9778	69	-223	2.281928

Table 3.2: Electromagnetic potential contributions for different nuclei, Coulomb potential for a point-like charge (KG), finite size Coulomb potential (FC) and leading order vacuum polarization corrections.

(KG) and the finite size correction (FC) for our sample of nuclei. For comparison we also included nickel and uranium. The energies correspond to the lower levels given in Table 3.1.

The classification of vacuum polarization corrections is done perturbatively in terms of the effective coupling $Z\alpha$ and α respectively, at which for heavy elements $Z\alpha$ can no longer be considered as $\ll 1$. In principle vacuum polarization could also involve exotic particle/antiparticle pairs apart from e^+/e^-, but these effects are usually not considered because of the high energies necessary for exotic pair creation. Also polarization of the nucleus and electron screening is neglected, as the heavy antikaon is effectively subjected to a charge $Z\alpha$. A summary of the relevant vacuum polarization corrections and their convenient series expansions in the context of exotic atoms can also be found in [50].

The leading so-called Uehling potential [46] is derived from a one loop correction where the e^+/e^- pair is propagating freely, unaffected by the Coulomb field of the nucleus in contrast to the $\alpha(Z\alpha)^3$ correction. It is widely used for the Rutherford scattering cross section near the Coulomb barrier and fusion cross sections at energies below the Coulomb barrier. Note that for the following easy to handle series expansions, $m_e = 1$ for the electron mass is used, hence $\hat{r} = m_e r$. The Uehling potential is given by

$$\begin{aligned} V_{\text{Ueh}}(r) =& \frac{\alpha Z\alpha}{\pi r}\left[\frac{5}{9} + \frac{2}{3}(\log\hat{r} + C) - \frac{\pi}{2}\hat{r} + \hat{r}^2 - \frac{2}{9}\pi\hat{r}^3\right. \\ &\left. + \frac{7}{18}\hat{r}^4 + \frac{1}{6}(\log\hat{r} + C)\hat{r}^4 + \frac{127}{8100}\hat{r}^6 - \frac{1}{135}(\log\hat{r} + C)\hat{r}^6 + \mathcal{O}(\hat{r}^7)\right] \end{aligned} \tag{3.9}$$

with the Euler constant

$$C = -\int_0^\infty dt\, e^{-t}\ln t = 0.577215665. \tag{3.10}$$

The expressions for all the vacuum polarization potentials are expansions in $\frac{2r}{\lambda_e}$, which means that the approximations are valid for $r < \lambda_e = \frac{\hbar}{m_e c} \approx 386\,\text{fm}$ with λ_e the electron Compton wave length. For the Uehling potential in [49] an approximation applicable in the region $0 \leq r \leq \infty$ is derived. The asymptotic Uehling potential for $r \gg \frac{\hbar}{m_e c}$ reads

$$V_{\text{Ueh}}(r) = -\frac{\alpha}{4\sqrt{\pi}}Z\alpha\frac{e^{-m_e r}}{r(m_e r)^{\frac{3}{2}}} \tag{3.11}$$

with its characteristic exponential decrease.

The correction of order $\alpha(Z\alpha)^3$ [47] – denoted by 'Wichmann-Kroll' – takes into account the interaction of the e^+/e^- pair with the nucleus Coulomb field to all orders in the effective coupling constant $Z\alpha$. In lowest order the Uehling correction $\alpha Z\alpha$ reappears, further contributions of order $\alpha(Z\alpha)^n$ with $n \geq 3$ were calculated in [47]. For even power n there is no contribution according to the Furry theorem [51]. For kaonic atoms the term $\propto \alpha(Z\alpha)^3$ is of relevance with its series expansion

$$\begin{aligned}V_{\mathrm{WK}}(r) =& \frac{\alpha(Z\alpha)^3}{\pi r}\left[\left(-\frac{2}{3}\zeta(3)+\frac{1}{6}\pi^2-\frac{7}{9}\right)+2\pi\zeta(3)\hat{r}-\frac{1}{4}\pi^3\hat{r}\right.\\ &+\left(-6\zeta(3)+\frac{1}{16}\pi^4+\frac{1}{6}\pi^2\right)\hat{r}^2+\frac{2}{9}\pi(\ln\hat{r}+C)\hat{r}^3\\ &+\left(\frac{2}{3}\pi\zeta(3)+\frac{4}{9}\pi\ln 2-\frac{31}{27}\pi\right)\hat{r}^3+\frac{1}{12}(\ln\hat{r}+C)^2\hat{r}^4\\ &+\left(\frac{5}{54}\pi^2-\frac{19}{36}\right)(\ln\hat{r}+C)\hat{r}^4+\left(\frac{13}{18}\zeta(3)-\frac{109}{432}\pi^2+\frac{859}{864}\right)\hat{r}^4\\ &\left.+\mathcal{O}(\hat{r}^5\ln\hat{r})\right]. \end{aligned} \tag{3.12}$$

and $\zeta(x)$ is the Riemann zeta function defined as

$$\zeta(x)=\sum_{k=1}^{\infty}k^{-x} \tag{3.13}$$

with $\zeta(3)\approx 1.20206$. Note that $V_{\mathrm{WK}}(r)$ is repulsive $\forall\, r$ and the energy shift ΔE_{WK} is negative in contrast to the other electromagnetic corrections. For large distances the asymptotic behaviour is given by

$$V_{\mathrm{WK}}(r)=-\frac{\alpha(Z\alpha)^3}{\pi r}\frac{32}{225}\frac{1}{(2m_e r)^4}+\ldots \tag{3.14}$$

and shows a power law behaviour. The aforementioned asymptotic Uehling potential (3.11) decreases exponentially, for this reason the order $\alpha(Z\alpha)^3$ correction dominates at distances of several λ_e, that is for highly bound levels. It reflects a somewhat peculiar phenomenon in QED, as effects of higher order in perturbation expansion are expected to be suppressed. The first exact calculation was done in [52], nevertheless based on [47], whereas [53] consideres finite size effects.

The polarization correction of order α^2 can be split into a reducible two-loop diagram and an irreducible one-loop vacuum polarization with self-energy insertion of the fermion loop. The two-loop polarization can be ascribed to the one-loop Uehling correction. In [48] the remaining self-energy insertions linear in $(Z\alpha)$ for point-like nuclei are derived and the series expansion – denoted by 'Källen-Sabry' –

$$\begin{aligned} V_{\mathrm{KS}}(r) =& \frac{\alpha^2(Z\alpha)}{\pi^2 r}\left[-\frac{4}{9}(\ln\hat{r}+C)^2-\frac{13}{54}(\ln\hat{r}+C)+\left(\zeta(3)+\frac{1}{27}\pi^2+\frac{65}{648}\right)\right. \\ &+\frac{13}{9}\pi^2\hat{r}+\frac{32}{9}(\pi\ln 2)\hat{r}-\frac{766}{135}\pi\hat{r}+\frac{5}{3}(\ln\hat{r}+C)\hat{r}^2-\frac{65}{18}\hat{r}^2 \\ &+\left(\frac{14}{27}\pi^2-\frac{80}{81}\pi\right)\hat{r}^3-\frac{5}{18}(\ln\hat{r}+C)^2\hat{r}^4+\frac{323}{216}(\ln\hat{r}+C)\hat{r}^4 \\ &\left.+\left(\frac{1}{6}\zeta(3)-\frac{5}{216}\pi^2-\frac{6509}{2592}\right)\hat{r}^4+\mathcal{O}(\hat{r}^5)\right] \end{aligned} \tag{3.15}$$

can be found in [50]. The derivation was extended to the case of finite radially symmetric charge distributions in [49].

3.3 Phenomenologic and microscopic models

We will give a brief review of the results obtained in [22] and summarize the different representative models, their benefits and shortcomings. The most simple ansatz is based on the low density theorem (LDT), where the optical potential $U_{opt}(\omega, r)$ of the Klein-Gordon equation (3.4) is parameterized in terms of the isospin-averaged s-wave scattering length,

$$2\mu\, U_{opt}(\omega, r) = -4\pi\left(1+\frac{m_K}{m_N}\right)\frac{1}{4}\left(a_{\bar{K}N}^{(I=0)}+3a_{\bar{K}N}^{(I=1)}\right)\rho(r)+\mathcal{O}(\rho^{4/3}). \tag{3.16}$$

The LDT describes the $\bar{K}N$ interaction in a dilute nucleon gas and thus represents the low density limit of other theoretical models. It connects the leading in-medium modification of the antikaon self-energy to the antikaon-nucleon scattering length and can be derived from non-relativistic many-body theory [54] as well as from quantum field theory [55]. The empirical scattering lengths in the isospin channels are $a_{\bar{K}N}^{(I=0)} = (-1.70 + i\,0.68)\,\mathrm{fm}$ and $a_{\bar{K}N}^{(I=1)} = (0.37 + i\,0.60)\,\mathrm{fm}$ respectively. The isospin averaged

$$a_{\bar{K}N} = \frac{1}{4}\left(a_{\bar{K}N}^{(I=0)}+3a_{\bar{K}N}^{(I=1)}\right) \approx (-0.18 + i\,0.67)\mathrm{fm}, \tag{3.17}$$

leads to a repulsive mass shift. On the other hand data of kaonic atoms demand a sizeable attraction at typical nuclear densities. Furthermore (3.17) is in conflict with the leading order term of the chiral Lagrangian, known as the Weinberg-Tomozawa term [19]. As an attractive antikaon self-energy probes the $\bar{K}N$ interaction below the threshold there is no straight experimental access to this problem. Compliance with the LDT at low densities and a changeover from repulsion to attraction in the vicinity of the nuclear surface can be accomplished by a nonlinear effective density dependent scattering length $a_{eff}(k_F)$. The density dependence is mainly due to the propagation of the $\Lambda(1405)$ resonance in nuclear matter, see for example [1–3, 20]. Because of the mentioned deficiencies of the LDT it is not considered in [22].

Despite the manifold efforts of the latter microscopic theories a simple χ^2-fit of the optical potential

$$2\mu\, U_{opt}(r) = -4\pi\left(1+\frac{m_K}{m_N}\right)a_{eff}\rho(r) \tag{3.18}$$

was done in [21] and the strongly attractive scattering length – denoted by 'Gal' –

$$a_{eff} = (0.63 + i\,0.89)\mathrm{fm} \tag{3.19}$$

leads to a fairly good agreement with the experimental data, thus violating (3.17). The overlap of the antikaon wave function and the nucleus covers a large range of densities and the existence of the $\Lambda(1405)$ just 27 MeV below the K^-p threshold also suggests a density dependent scattering length $a_{eff}(\rho(r))$. First attempts to address this question were made in [56] and [21] and the latter phenomenologic ansatz – denoted as 'Gal DD-term' – gives

$$a_{eff} \to b_0 + B_0 \left[\frac{\rho(r)}{\rho(0)}\right]^{\alpha} \tag{3.20}$$

with α positive so that the second term vanishes for $\rho(r) \to 0$ and the LDT is reproduced if $b_0 \approx (-0.15 + i\,0.62)\mathrm{fm}$. A fit to the data gives $B_0 \approx (1.66 - i\,0.04)\mathrm{fm}$ and $\alpha \approx 0.24$, but there is no physical interpretation of the purely phenomenologic parameters entering (3.20). Ansatz (3.20) leads to a deep attractive potential of about $\mathfrak{Re}[U_{\mathrm{opt}}] \equiv 200\,\mathrm{MeV}$ in the nuclear interior. Microscopic theories favour a shallow potential of about $\mathfrak{Re}[U_{\mathrm{opt}}] \equiv 40\,\mathrm{MeV}$.

Non-Local terms with gradients acting on the density distribution $\rho(r)$ of the nucleus and the antikaon wave function $\phi(\mathbf{r})$ were considered in [57] for the first time. In [58] the potential – denoted by '∇ Mizoguchi' –

$$2\mu\, U_{opt}(\mathbf{r}, \nabla) = -4\pi \left(1 + \frac{m_K}{m_N}\right) \left(a_{\bar{K}N}\rho(r) - b\nabla\rho(r)\nabla\right), \tag{3.21}$$

is used, using $b \approx (0.47 + i0.30)\mathrm{fm}^3$ by fitting to the data. For $a_{\bar{K}N}$ the empirical scattering length (3.17) is used.

Microscopic theories of the antikaon self-energy in nuclear matter $\Pi(\omega, \mathbf{q}, k_F)$ imply a density dependent effective scattering length $a_{eff}(k_F)$ via

$$2\mu\, U_{opt}(\omega, r) = \Pi(\omega = m_K, \mathbf{q} = \mathbf{0}, k_F(r)), \tag{3.22}$$

where the density is parameterized by the Fermi momentum k_F. The first approach is based on the publication [1]. The antikaon self-energy is derived from a self-consistent many-body theory with microscopic $\bar{K}N$ interaction. The Lagrangian density includes not only the isospin doublet $K^\dagger = (K^-, \bar{K}^0)$ and $N = (p, n)$ but also pions and the hyperon ground states $\Lambda(1115)$ and $\Sigma(1195)$. The channels $\pi\Sigma$ and $\pi\Lambda$ couple strongly to the $\bar{K}N$ system and the resummation of the ladder diagrams is done by means of the Bethe-Salpeter equation. The free parameters were fitted to the empirical scattering data. The resulting scattering length $a_{eff}(k_F)$ is shown in figure (3.1) on the left side. The rather shallow optical potential of 40 MeV at ρ_0 is counter-balanced by a large absorptive imaginary part of 80 MeV. The complex energy dependence of the $\Lambda(1405)$ resonance near the threshold is reproduced, as self consistency leads to a compensation of the attractive K^- mass shift with the repulsive Pauli-blocking. The resonance stays just below the threshold near the vacuum position. The obtained scattering length was applied to kaonic atoms via

$$2\mu\, U_{opt}(\omega, r) = -4\pi \left(1 + \frac{m_K}{m_N}\right) a_{eff}(k_F(r))\rho(r) \tag{3.23}$$

in [3] – denoted by 'Lutz' – for the first time.

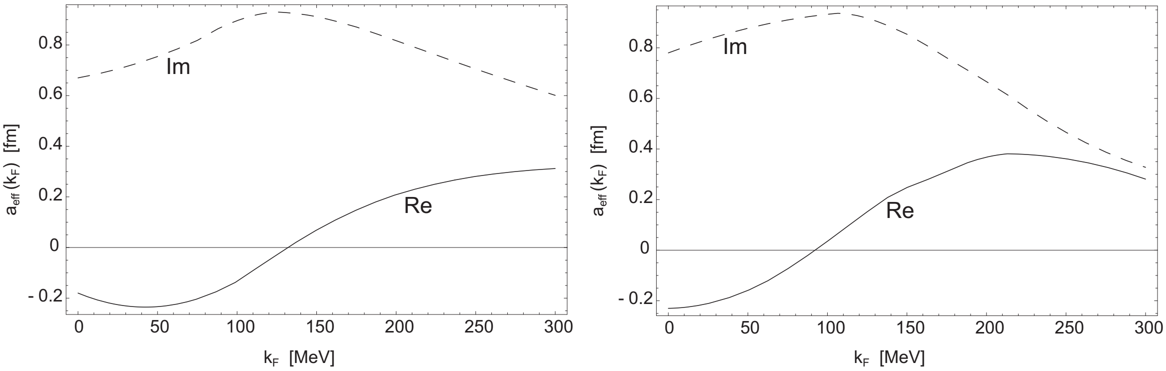

Figure 3.1: Effective scattering lengths $a_{eff}(k_F)$ of [1] on the left and of [2] on the right hand side.

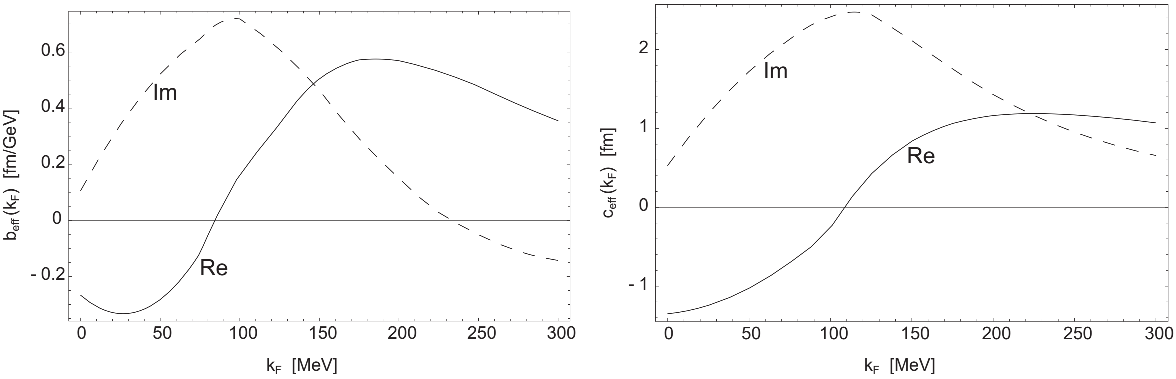

Figure 3.2: Slope parameter $b_{eff}(k_F)$ on the left and $c_{eff}(k_F)$ on the right hand side, see [3].

The second microscopic model [59] – denoted by 'Oset' – is based on a s-wave meson-nucleon interaction with strangeness -1 and a Lippmann-Schwinger coupled channel formalism. The interaction comprises the leading order terms of the chiral Lagrangian. The latter interaction [59] is used for the self-consistent microscopic calculation of the K^- self-energy in nuclear matter [2]. Resummation is done by means of a Lippmann-Schwinger equation and the nucleon propagator involves Pauli-blocking and a linearly density dependent mean-field potential. The in-medium modification of π and $\bar{K}$ mesons is taken into account via their self-energies and as in [1] the dynamics of the $\Lambda(1405)$ resonance is reproduced qualitatively.

The effective scattering lengths from [1] and [2] are depicted in Figure 3.1. The real part of the scattering length from [2] changes from repulsion to attraction at about 100 MeV, corresponding to a density of $\rho \equiv 0.04\,\rho_0$. The impact of a dressed pion propagator on the scattering length was found to be small, but the change of sign 25 MeV below the corresponding Fermi momentum in the scattering length of Lutz is expected to lead to larger level widths.

The third and last microscopic model compared in [22] was published in [3] and is an extension of the density dependent scattering length (3.23) by gradient terms. An expansion of the self-energy in momentum $\mathbf{q}$ and energy ω induces additional terms with gradients acting on the density distribution ρ and the wave function $\phi(\mathbf{r})$. The ansatz of handling non localities in [3] is more systematic than the purely phenomenologic ones, because the expansion of the self-energy $\Pi(\omega, \mathbf{q}, k_F)$ for small $\mathbf{q}$ and ω around m_K leads to a replacement $\mathbf{q} \to -i\nabla$ in the self-energy and the optical potential

$$2\mu\, U_{opt}(\omega, r) = \Pi(\omega = m_K, \mathbf{q} = \mathbf{0}, k_F(r)). \tag{3.24}$$

Note that the the antikaon momentum for a typical binding energy of 0.5 MeV is $|\mathbf{q}| \equiv 20\,\mathrm{MeV} < k_F$ for densities where the optical potential is of relevant order. The expansion of the self-energy up to second order is given by

$$\begin{aligned}\Pi(\omega, \mathbf{q}, k_F) = &-\frac{8}{3\pi}\left(1+\frac{m_K}{m_N}\right)\left(a_{eff}(k_F)k_F^3 + b_{eff}(k_F)k_F^2\mathbf{q}^2\right)\\ &+\frac{8}{3\pi}\left(1+\frac{m_K}{m_N}\right)c_{eff}(k_F)k_F^2(\omega - m_K)\\ &+\mathcal{O}\left(\mathbf{q}^4, (\omega-m_K)^2, \mathbf{q}^2(\omega - m_K)\right),\end{aligned} \tag{3.25}$$

where the slope parameter $b_{eff}(k_F)$ and $c_{eff}(k_F)$ are corrections to the scattering length $a_{\bar{K}N}$ and can be stated analytically, see [20]. The numerical results for the slope parameters related to the effective scattering length (3.24) are shown in Figure 3.2. Based on the expansion (3.25) there are several combinations for non-local terms in the Klein-Gordon equation (3.4) induced by a heuristic replacement $\mathbf{q} \to -i\nabla$. We emphasize that the gradient arrangement of ∇ and ∇^2 acting on ρ and the wave function is not unique and an expansion of the self-energy for small momenta is not valid anymore in the border region of the density profile. Apart from this the self-energy is obtained self-consistently, thus the meaning of an expansion of the very same seems to be questionable. In [3] consequently only linear gradients were considered, affecting the density distribution, the wave function as well as $b_{eff}(k_F)$. As the gradients act on the full wave function $\phi(\mathbf{r})$ the radial part $u_l(r)$ has to be renormalized and finally we end up with the Klein-Gordon equation

$$\begin{aligned}Z(r)\left(\frac{d^2}{dr^2} - \frac{l(l+1)}{r^2}\right)u_l(r) \;=\;& \bar{Z}(r)\left\{\mu^2 - \left(\mu - E - i\frac{\Gamma}{2} - V_{em}(r)\right)^2\right\}u_l(r)\\ &+\; U_1(r)u_l(r) + U_2(r)\left(\frac{d}{dr}u_l(r)\right)\end{aligned} \tag{3.26}$$

with the potentials

$$\begin{aligned}U_1(r) &= -\frac{8}{3\pi}\left(1+\frac{m_K}{m_N}\right)\left\{a_{eff}(k_F(r))k_F^3(r) + \frac{d}{rdr}b_{eff}(k_f(r))k_F^2(r)\right\},\\ U_2(r) &= \frac{8}{3\pi}\left(1+\frac{m_K}{m_N}\right)\frac{d}{dr}b_{eff}(k_F(r))k_F^2(r)\end{aligned} \tag{3.27}$$

and the renormalization functions

$$\begin{aligned}Z(r) &= 1 - \frac{8}{3\pi}\left(1+\frac{m_K}{m_N}\right)b_{eff}(k_F(r))k_F^2(r),\\ \bar{Z}(r) &= 1 - \frac{8}{3\pi}\left(1+\frac{m_K}{m_N}\right)\frac{k_F^2(r)}{2m_K}c_{eff}(k_F(r)).\end{aligned} \tag{3.28}$$

	$^{12}_{6}$C	$^{32}_{16}$S	$^{35}_{17}$Cl
a_{eff} Gal	598	462	897
DD-term Gal	487	549	1057
∇ Mizoguchi	451	440	813
$a_{eff}(k_F)$ Oset	639	629	1140
$a_{eff}(k_F)$ Lutz	607	618	1101
a_{eff}, b_{eff}, c_{eff} Lutz	565	555	995
Experiment	590 ± 80	494 ± 38	1000 ± 170

Table 3.3: Level shifts ΔE [eV] for different phenomenologic and microscopic approaches, compared with experimental value.

3.3.1 Comparison of phenomenologic and microscopic models

The phenomenologic and microscopic models briefly reviewed in the preceeding section were compared in [22] based on $N = 24$ measurements with different nuclei over the whole mass region from Lithium to Uranium. For the nuclei from Table 3.1 we give the detailed results for the level shift ΔE in Table 3.3 and the level width Γ in Table 3.4. The spreading for different isotopes of one nuclei was found to be small. If more than one measurement exists for one nuclei the experimental value given corresponds to a mean value identical with [60]. We emphasize that the tendencies for the different models stay basically the same over the whole range of nuclei and the predictable power does not change with the nuclear mass and the parameters of the density distribution. For the whole range of nuclei we state the χ^2/N in Table 3.5 separately for the level shift and width, because the largest deviation is manifestly due to a significant underestimation of the level width.

Still the best agreement with the experimental values can be achieved with the simple phenomenologic ansatz (3.18) and (3.20). A remarkable feature is the good reproduction of the level width, which is an effect of the deep potential compared to the shallow microscopic ones. Even though the model (3.21) is fitted to the experimental data it systematically underestimates the level width. Of special interest is a comparison of the two microscopic density dependent scattering lengths, see Figure 3.1. As already mentioned the change from repulsion to attraction appears at lower Fermi momentum for the scattering length from [2], which indeed leads to a better agreement for the level width compared to $a_{eff}(k_F)$ from [1]. Nevertheless it is still below the values of the phenomenologic models by Gal. The energy shift is overestimated by both effective scattering lengths. Taking into account the gradient terms and wave function renormalization of (3.26) does not only improve the level width, but still reproduces the energy shift quite well. Hence a further understanding of the non-local nature of kaonic atoms is demanded.

Concerning the survey especially of heavy nuclei it is questionable if such rudimentary descriptions of the nuclei properties based on a Thomas-Fermi theory density distribution is still applicable. As soon as deformations and low lying nuclear excitations come into play one should think about a more sophisticated theoretical description. This objection in particular applies as soon as deeply bound states and hyper-nuclei are considered.

	${}^{12}_{6}$C	${}^{32}_{16}$S	${}^{35}_{17}$Cl
a_{eff} Gal	1360	1968	3181
DD-term Gal	1501	2053	3276
∇ Mizoguchi	1187	1615	2622
$a_{eff}(k_F)$ Oset	1314	1636	2621
$a_{eff}(k_F)$ Lutz	1024	1328	2149
a_{eff}, b_{eff}, c_{eff} Lutz	1093	1439	2332
Experiment	1730 ± 150	2187 ± 103	2910 ± 240

Table 3.4: Level widths Γ [eV] for different phenomenologic and microscopic approaches, compared with experimental value.

	a_{eff} Gal	DD-term	Mizoguchi	$a(k_F)$ Oset	$a(k_F)$ Lutz	a, b, c
χ^2/N Shift ΔE	1.41	1.06	1.61	3.74	3.96	1.84
χ^2/N Width Γ	2.07	1.73	6.31	5.70	14.75	11.11
χ^2/N Mean value	1.74	1.40	3.96	4.72	9.36	6.47

Table 3.5: χ^2-test of level shifts ΔE and widths Γ for $N = 24$ nuclei.

Chapter 4

Non-Local approach for kaonic atoms

Due to the presence of subthreshold resonances in the $\bar{K}N$ system a conventional gradient expansion for the calculation of kaonic atom levels is inappropriate. The following ansatz for a non-local optical potential rests on the developments of [22]. It accounts for the momentum dependence of the underlying scattering amplitudes and exhibits an approximation-free treatment of the non-local wave function. For brevity we will use the notation 'non-local wave function' for any wave function that has been calculated from a Klein-Gordon equation including a non-local optical potential as introduced below. We will also include nucleon mean-field potentials as discussed in Chapter 2.

We start from the Klein-Gordon equation

$$\left(\nabla^2 - \mu^2 + (\omega - V_{em}(r))^2\right) \phi(\mathbf{r}) = 2\mu \int d^3r'\, U(\omega - V_{em}(r), \mathbf{r}, \mathbf{r}')\phi(\mathbf{r}') \tag{4.1}$$

for the antikaon wave function $\phi(\mathbf{r})$. It includes a non-local optical potential $U(\omega - V_{em}(r), \mathbf{r}', \mathbf{r})$. One may introduce an effective local potential satisfying

$$U_{\mathrm{opt}}(\omega - V_{em}(r), \mathbf{r}) = \int d^3r'\, U(\omega - V_{em}(r), \mathbf{r}', \mathbf{r}) \frac{\phi(\mathbf{r}')}{\phi(\mathbf{r})}, \tag{4.2}$$

referred to as 'Trivially Equivalent Local Potential' (TELP) in the literature. We will also make use of (4.2) for a descriptive discussion and comparison of the potentials. However, we will not solve the integro-differential equation (4.1) in terms of an TELP, as it does not allow for roots of the wave function $\phi(\mathbf{r})$ and therefore restricts the behaviour of its solution.

The non-local potential in (4.1) is linked to the non-local antikaon self-energy $\Pi(\omega, \mathbf{r}', \mathbf{r})$ via

$$2\mu\, U(\omega, \mathbf{r}', \mathbf{r}) = \Pi(\omega, \mathbf{r}', \mathbf{r}). \tag{4.3}$$

Our aim is to establish an approximate expression for $\Pi(\omega, \mathbf{r}', \mathbf{r})$ in terms of the in-medium $\bar{K}N$ scattering amplitudes $\mathcal{T}_{\bar{K}N}$ that have been calculated in Chapter 2. We proceed with the inverse Wigner-transform of the self-energy in Wigner-representation, $\Pi_W(\omega, \mathbf{q}, \mathbf{R})$ defined as

$$\Pi(\omega, \mathbf{r}', \mathbf{r}) = \int \frac{d^3q}{(2\pi)^3} e^{-i\mathbf{q}(\mathbf{r}'-\mathbf{r})} \Pi_W\left(\omega, \mathbf{q}, \mathbf{R}\right), \quad \mathbf{R} = \frac{\mathbf{r} + \mathbf{r}'}{2}. \tag{4.4}$$

In the course of this chapter we will use the Wigner representation $A(\mathbf{q},\mathbf{R})$ of any two-point function $A(\mathbf{r}',\mathbf{r})$ as follows:

$$A(\mathbf{r}',\mathbf{r}) = \int \frac{d^3q}{(2\pi)^3} e^{-i\mathbf{q}\cdot(\mathbf{r}-\mathbf{r}')} A\left(\mathbf{q},\mathbf{R}\right). \tag{4.5}$$

The actual form of the correlator $\Pi_W(\omega,\mathbf{q},\mathbf{R})$ which may attain also negative values is yet unknown. One may raise the question whether a local-density identification with the antikaon self-energy

$$\Pi_W(\omega,\mathbf{q},\mathbf{R}) \overset{?}{=} \Pi(\omega,\mathbf{q},k_F(\mathbf{R})) \tag{4.6}$$

is justified and sufficient. Here $k_F(\mathbf{R})$ is the local Fermi momentum of the nucleons.

4.1 Non-Local antikaon self-energy

The computation of the non-local optical potential (4.3) from a given self-energy is straightforward once we have defined a systematic way of how a self-consistent $\bar{K}N$ scattering amplitude relates to a non-local antikaon self-energy. The nucleon propagator is

$$\begin{aligned} i\,S_N(p,R) &= \int d^4x \langle N|T\,\Psi(R+\frac{x}{2})\bar{\Psi}(R-\frac{x}{2})|N\rangle e^{-ix\cdot p} \\ &= \frac{i}{\not{p} - m_N - \Sigma_N(p,R)} \end{aligned} \tag{4.7}$$

with a nucleon field Ψ and the energy eigenstate $|N\rangle$ describing a (ground state) nucleus localized around the origin. We assume the nucleon self-energy Σ_N in (4.7) to be of the form

$$\begin{aligned} \Sigma_N(p,\mathbf{R}) &= -\Sigma_S(\mathbf{R}) + \Sigma_V(\mathbf{R})\gamma_0 \\ &\quad + i\varepsilon\left[\Theta(|\mathbf{p}| - k_F(\mathbf{R})) - \Theta(k_F(\mathbf{R}) - |\mathbf{p}|)\right]\Theta(p_0) \end{aligned} \tag{4.8}$$

with scalar and vector mean fields that do not depend on time. Since the antikaon in our case is not probing details of the nuclear structure the rough approximation (4.8) should be sufficient. Furthermore the nucleon self-energy modeled by scalar and vector mean fields proved to be well suited for modeling the ground state of finite nuclei with good accuracy [23]. We have to require that the choice of (4.7) and the energy and momentum independent self-energy (4.8) reproduces the nuclear density distribution ρ of the nucleus, that is

$$\rho(\mathbf{R}) = -i\mathrm{Tr}\int \frac{d^4p}{(2\pi)^4} \Delta S_N(p_0,\mathbf{p},\mathbf{R}) = \frac{2k_F^3(\mathbf{R})}{3\pi^2}. \tag{4.9}$$

The in-medium nucleon propagator ΔS_N in (4.9) is given by

$$\begin{aligned} \Delta S_N(p_0,\mathbf{p},\mathbf{R}) &= \frac{2\pi i}{2E_N^*}\left(\not{p} + m_N - \Sigma_S(\mathbf{R}) - \Sigma_V(\mathbf{R})\gamma_0\right)\Theta\left(k_F(\mathbf{R}) - |\mathbf{p}|\right) \\ &\times\ \delta\left(p_0 - \Sigma_V(\mathbf{R}) - E_N^*\right) \end{aligned} \tag{4.10}$$

with $E_N^* = \sqrt{(m_N - \Sigma_S(\mathbf{R}))^2 + \mathbf{p}^2}$.

From previous studies it is known that a self-consistent treatment of the antikaon self-energy is essential. The numerical evaluation of an in-medium antikaon self-energy for finite nuclei is a formidable task. Therefore we have to propose and prove certain simplifications that allow to use a self-energy determined for infinite nuclear matter as established in Chapter 2 or [5].

Let us start with a generic, properly isospin averaged vacuum scattering amplitude in coordinate space $\bar{T}(p_0, \mathbf{y}, \mathbf{y}', \omega, \mathbf{r}, \mathbf{r}')$. It depends on the two nucleon coordinates $\mathbf{y}'$ and $\mathbf{y}$ and the antikaon coordinates $\mathbf{r}'$ and $\mathbf{r}$, and the corresponding energies p_0 and ω, respectively. The non-local antikaon self-energy in coordinate space is then given by

$$\Pi(\omega, \mathbf{r}', \mathbf{r}) = i\mathrm{Tr} \int d^3y' \int d^3y \int \frac{dp_0}{2\pi} \bar{T}(p_0, \mathbf{y}, \mathbf{y}'; \omega, \mathbf{r}', \mathbf{r}) \Delta S_N(p_0, \mathbf{y}', \mathbf{y}) \tag{4.11}$$

and does not depend on the time component $t - t'$ for a stationary, bound $\bar{K}N$ system. Hence ω and p_0 are the only energy components. The in-medium nucleon propagator $\Delta S_N(p_0, \mathbf{y}', \mathbf{y})$ is given by the inverse Wigner transform of (4.10),

$$\Delta S_N(p_0, \mathbf{y}', \mathbf{y}) = \int \frac{d^3p}{(2\pi)^3} \Delta S_N \left(p_0, \mathbf{p}, \frac{\mathbf{y} + \mathbf{y}'}{2} \right) e^{-i\mathbf{p}(\mathbf{y}' - \mathbf{y})}. \tag{4.12}$$

The free-space scattering amplitude $\bar{T}(p_0, \mathbf{y}, \mathbf{y}', \omega, \mathbf{r}, \mathbf{r}')$ is translational invariant. By performing a Fourier transformation it can be connected to a momentum dependent amplitude $\bar{T}(\bar{q}, q, w)$ with the antikaon initial and final four-momenta $q^\mu = (\omega, \mathbf{q})$ and $\bar{q}^\mu = (\omega, \mathbf{q}')$:

$$\bar{T}(p_0, \mathbf{y}, \mathbf{y}'; \omega, \mathbf{r}', \mathbf{r}) = \int \frac{d^3q'}{(2\pi)^3} \int \frac{d^3q}{(2\pi)^3} \int \frac{d^3w}{(2\pi)^3} \bar{T}(\omega, \mathbf{q}', \mathbf{q}; \omega + p_0, \mathbf{w}) e^{-i\mathbf{q}\cdot\mathbf{r}} e^{i\mathbf{q}'\cdot\mathbf{r}'} e^{i\mathbf{w}(\mathbf{y}' - \mathbf{y})}. \tag{4.13}$$

The external momentum $w = p + q = \bar{p} + \bar{q}$ assures momentum conservation, with the nucleon four-momenta $p^\mu = (p_0, \mathbf{p})$ and $\bar{p}^\mu = (p_0, \mathbf{p}')$. We proceed with the Wigner transform $\Pi(\omega, \mathbf{q}, \mathbf{R})$ of the self-energy $\Pi(\omega, \mathbf{r}', \mathbf{r})$ (4.11) analogous to (4.4),

$$\Pi(\omega, \mathbf{q}, \mathbf{R}) = i\, \mathrm{Tr} \int d^3z\, \Pi \left(\omega, \mathbf{R} + \frac{\mathbf{z}}{2}, \mathbf{R} - \frac{\mathbf{z}}{2} \right) e^{-i\mathbf{q}\cdot\mathbf{z}} \tag{4.14}$$

with $\mathbf{r}' = \mathbf{R} + \frac{\mathbf{z}}{2}$ and $\mathbf{r} = \mathbf{R} - \frac{\mathbf{z}}{2}$. After combining (4.11), (4.12), (4.13) and (4.14) we can carry out the integration in $\mathbf{y}$ and $\mathbf{y}'$ by using the identity

$$\Delta S_N \left(p_0, \mathbf{p}, \frac{\mathbf{y} + \mathbf{y}'}{2} \right) = e^{\frac{\mathbf{y}+\mathbf{y}'}{2} \frac{\partial}{\partial \mathbf{R}}} \Delta S_N(p_0, \mathbf{p}, \mathbf{R}). \tag{4.15}$$

Here the differentiation with respect to $\mathbf{R}$ in (4.15) acts excusively on $\Delta S_N(p_0, \mathbf{p}, \mathbf{R})$. Combining all remaining exponents we can perform all momentum integrations besides d^4p and arrive at the expression

$$\Pi(\omega, \mathbf{q}, \mathbf{R}) = i\, \mathrm{Tr} \int \frac{d^4p}{(2\pi)^4} \bar{T} \left(\omega, \mathbf{q} - \frac{i}{2} \frac{\partial}{\partial \mathbf{R}}, \mathbf{q} + \frac{i}{2} \frac{\partial}{\partial \mathbf{R}}; \omega + p_0, \mathbf{w}, k_F(\mathbf{R}) \right) \Delta S_N(p_0, \mathbf{p}, \mathbf{R}), \tag{4.16}$$

at which $\mathbf{w} = \mathbf{p} + \mathbf{q}$ does not contain any derivative in $\mathbf{R}$. Equation (4.16) for the antikaon self-energy is valid without approximation for a free-space amplitude. The differential operator $\frac{\partial}{\partial \mathbf{R}}$ probes the R-dependence of the nucleon propagator (4.12) due to the finite size of the nucleus.

Up to now in (4.16) we were considering a vacuum scattering amplitude $\bar{T}$ but matters turn more complicated once in-medium modifications are taken into account. We have to analyze to what extent expression (4.16) is still valid.

First let us have a look at a toy interaction in leading order g of some coupling strength. For simplicity we suppress the energy argument ω of the self-energy. The exact expression for the self-energy in coordinate space is

$$\Pi(\mathbf{r}', \mathbf{r}) = i\, g \,\mathrm{Tr}\left[\Delta S_N(\mathbf{r}', \mathbf{r})\delta^3(\mathbf{r}' - \mathbf{r})\right] + \mathcal{O}(g^2). \tag{4.17}$$

With (4.8) and (4.9) the Wigner transform of the self-energy (4.17) is given by

$$\Pi(\mathbf{q}, \mathbf{R}) = g\, \rho(\mathbf{R}) + \mathcal{O}(g^2, k_F^5). \tag{4.18}$$

The second order contribution in the coupling constant g in coordinate space looks like

$$\Pi(r', r) = g^2 \mathcal{D}_{\bar{K}}(r', r) \mathrm{Tr}\left[S_N(r', r)\Delta S_N(r, r')\right] \tag{4.19}$$

with the Wigner-transform of $S_N(r', r)$ and $\Delta S_N(r, r')$ of (4.7) and (4.10) respectively. For the antikaon propagator we allow for an effective antikaon self-energy $\Pi_{eff}(q, \mathbf{R})$. After defining the loop function

$$J(w, \mathbf{R}) = -i \int \frac{d^4 l}{(2\pi)^4} \mathcal{D}_{\bar{K}}(l, \mathbf{R}) S_N(w - l, \mathbf{R}) \tag{4.20}$$

with

$$\mathcal{D}_{\bar{K}}(q, \mathbf{R}) = \frac{1}{q^2 - m_K^2 - \Pi_{eff}(q, \mathbf{R})} \tag{4.21}$$

we can state the self-energy in Wigner representation up to second order:

$$\Pi(q, \mathbf{R}) = i\, \mathrm{Tr} \int \frac{d^4 p}{(2\pi)^4} \left[g + g^2 J(p + q, \mathbf{R}) + \mathcal{O}(g^3)\right] \Delta S_N(p, \mathbf{R}). \tag{4.22}$$

Result (4.22) is even valid at order g^2 if used with the in-medium scattering amplitude

$$T(w, \mathbf{R}) = \frac{g}{1 - g\, J(w, \mathbf{R})} = g + g^2\, J(w, \mathbf{R}) + \mathcal{O}(g^3), \tag{4.23}$$

where $T(w, \mathbf{R})$ corresponds to an amplitude calculated for infinite nuclear matter, thus $T(w, \mathbf{R}) = T(w, k_F(\mathbf{R}))$. This also holds if an antikaon self-energy $\Pi_{eff} = \Pi(q, k_F(\mathbf{R}))$ is used in (4.21).

A continuation of the derivation to higher orders in the coupling g turns out to be more and more complex and for a further investigation we refer to [61]. The evaluation of the non-local higher order corrections – given an in-medium scattering amplitude – turns out to be a tedious task and we will restrict our analysis to the form given by (4.16), which is exact up to second order also for (effective) in-medium scattering amplitudes.

4.2 Non-Local optical potential

We parameterize the full wave function $\phi(\mathbf{r})$ in terms of the radial wave function $u_l(r)$ with $r = |\mathbf{r}|$ given as solution of the radial Klein-Gordon equation. The subscript l denotes the angular dependence of the radial wave function and the non-local potential. The angular behaviour of the full wave function is determined by $Y_{lm}(\vartheta,\varphi)$:

$$\phi_{lm}(\mathbf{r}) = \frac{u_l(r)}{r} Y_{lm}(\vartheta,\varphi) \tag{4.24}$$

with

$$u_l(r) = r^{l+1} \quad \text{for} \quad r \to 0 \tag{4.25}$$

from phase-space considerations. The angular behaviour of the potential $U_l(\omega - V_{em}(r), \mathbf{r}', \mathbf{r})$ is yet unknown, but because of the intrinsic radial symmetry it should depend only on l, which is indicated by the subscript l. From applying a Taylor expansion to the wave function $\phi(\mathbf{r}')$ around $\mathbf{r}' = \mathbf{r}$ it is obvious that the right hand side of the Klein-Gordon equation

$$2\mu\, U_l(\omega, \mathbf{r}')\phi_{lm}(\mathbf{r}') \propto Y_{lm}(\vartheta', \varphi') \tag{4.26}$$

with

$$2\mu\, U_l(\omega, \mathbf{r})\phi_{lm}(\mathbf{r}) = 2\mu \int d^3r'\, U_l(\omega, \mathbf{r}, \mathbf{r}')\phi_{lm}(\mathbf{r}') \tag{4.27}$$

holds. Thus we can project on the proper angular dependence by acting with

$$\sum_{m=-l}^{l} \frac{1}{2l+1} \int d\vartheta' d\varphi' Y_{lm}^*(\vartheta', \varphi') \tag{4.28}$$

on

$$2\mu\, U_l(\omega, \mathbf{r}) = \int d^3r' \int \frac{d^3q}{(2\pi)^3} e^{-i\mathbf{q}(\mathbf{r}-\mathbf{r}')} \Pi\left(\omega, \mathbf{q}, \frac{\mathbf{r}+\mathbf{r}'}{2}\right) \phi_{lm}(\mathbf{r}'). \tag{4.29}$$

The product of $Y_{lm}(\vartheta,\varphi)$ and $Y_{lm}^*(\vartheta',\varphi')$ can be reduced to a Legendre polynomial by the use of the addition theorem

$$\frac{1}{2l+1} \sum_{m=-l}^{l} Y_{lm}^*(\vartheta', \varphi') Y_{lm}(\vartheta, \varphi) = \frac{1}{4\pi} P_l(\cos\theta), \tag{4.30}$$

whereas the argument of the Legendre polynomial denotes the cosine of the angle between $\mathbf{r}$ and $\mathbf{r}'$:

$$\cos\theta = \frac{\mathbf{r}\cdot\mathbf{r}'}{|\mathbf{r}|\cdot|\mathbf{r}'|}. \tag{4.31}$$

Finally we arrive at

$$2\mu\, U_l(\omega, \mathbf{r}) = \int d^3r' \int \frac{d^3q}{(2\pi)^3} e^{-i\mathbf{q}(\mathbf{r}-\mathbf{r}')} \Pi\left(\omega, \mathbf{q}, \frac{\mathbf{r}+\mathbf{r}'}{2}\right) P_l(\cos\theta) \frac{u_l(|\mathbf{r}'|)}{|\mathbf{r}'|} \tag{4.32}$$

for the right-hand-side of the Klein-Gordon equation.

After the non-local potential (4.32) has been specified in terms of the non-local self-energy (4.16) relying on the approximation scheme described in the previous section we have to calculate the optical potential from a given in-medium isospin averaged scattering amplitude

$\bar{T}(\bar{q},q,w,\mathbf{R})$. For a detailed review of the self-consistent treatment of $\bar{K}N$ in-medium scattering we refer to Chapter 2, here we recall the generic structure of the amplitude decomposed in terms of the projector algebra P_{ij} and Q_{ij} specified in Section 2.2.1:

$$\begin{aligned}\bar{T}(\bar{q},q,w,k_F) = \sum_{i,j=1}^{2} &\bar{T}^{(p)}_{ij}(v_0,\mathbf{w},k_F)\,P_{ij}(v_0,\mathbf{w})\\ +\sum_{i=1}^{2}\sum_{j=3}^{8}&\Big(\bar{T}^{(p)}_{ij}(v_0,\mathbf{w},k_F)\,P^{\mu}_{ij}(v_0,\mathbf{w})\,q_\mu+\bar{T}^{(p)}_{ji}(v_0,\mathbf{w},k_F)\,\bar{q}_\mu\,P^{\mu}_{ji}(v_0,\mathbf{w})\Big)\\ +\sum_{i,j=3}^{8}&\bar{T}^{(p)}_{ij}(v_0,\mathbf{w},k_F)\,\bar{q}_\mu\,P^{\mu\nu}_{ij}(v_0,\mathbf{w})\,q_\nu\\ +\sum_{i,j=1}^{2}&\bar{T}^{(q)}_{ij}(v_0,\mathbf{w},k_F)\,\bar{q}_\mu\,Q^{\mu\nu}_{ij}(v_0,\mathbf{w})\,q_\nu \end{aligned} \tag{4.33}$$

where the density dependence via k_F is also contained in

$$v_0 = w_0 - \Sigma_V(k_F). \tag{4.34}$$

Given the amplitude (4.33) we can calculate the antikaon self-energy $\Pi(\omega,\mathbf{q},\mathbf{R})$ according (4.16). It holds

$$\begin{aligned}\Pi(\omega,\mathbf{q},\mathbf{R}) &= i\,\mathrm{Tr}\int\frac{d^4p}{(2\pi)^4}\bar{T}\left(\omega,\mathbf{q}-\frac{i}{2}\frac{\partial}{\partial\mathbf{R}},\mathbf{q}+\frac{i}{2}\frac{\partial}{\partial\mathbf{R}};\omega+p_0,\mathbf{w},k_F(\mathbf{R})\right)\Delta S_N(p_0,\mathbf{p},\mathbf{R})\\ &= -2\sum_{i,j=1}^{8}\int\frac{d^3p}{(2\pi)^3}\frac{1}{E^*_N}C^{(p)}_{ij}(\nabla_\mathbf{R},\omega,\mathbf{q},w_0,\mathbf{w})\bar{T}^{(p)}_{ij}(v_0,\mathbf{w},k_F(\mathbf{R}))\Theta(k_F(\mathbf{R})-|\mathbf{p}|)\\ &\quad -2\sum_{i,j=1}^{2}\int\frac{d^3p}{(2\pi)^3}\frac{1}{E^*_N}C^{(q)}_{ij}(\nabla_\mathbf{R},\omega,\mathbf{q},w_0,\mathbf{w})\bar{T}^{(q)}_{ij}(v_0,\mathbf{w},k_F(\mathbf{R}))\Theta(k_F(\mathbf{R})-|\mathbf{p}|)\end{aligned} \tag{4.35}$$

with $w_0 = \omega + E^*_N$, $\mathbf{w} = \mathbf{p}+\mathbf{q}$ and $E^*_N = \sqrt{{m^*_N}^2+\mathbf{p}^2}$. The coefficient functions $C^{(p,q)}_{ij}$ generalize the corresponding functions $c^{(p,q)}_{ij}$ derived in [5] for the case of infinite nuclear matter to the case of finite nuclei and can be decomposed into four contributions,

$$\begin{aligned}C^{(p,q)}_{ij}(\nabla_\mathbf{R},q,w) &= c^{(p,q)}_{ij,0}(q,w)+\frac{1}{4}\nabla^2_\mathbf{R}c^{(p,q)}_{ij,1}(q,w)\\ &\quad+\frac{1}{4}\left(\mathbf{w}\cdot\nabla_\mathbf{R}\right)^2c^{(p,q)}_{ij,2}(q,w)\\ &\quad+\frac{1}{4}\left(\mathbf{w}\cdot\nabla_\mathbf{R}\right)\left(\mathbf{p}\cdot\nabla_\mathbf{R}\right)c^{(p,q)}_{ij,3}(q,w),\end{aligned} \tag{4.36}$$

in which the first term exactly coincides with the coefficients given in [5], $c^{(p,q)}_{ij,0}(q,w) = c^{(p,q)}_{ij}(q,w)$. The remaining three contributions account for the non-local nature of the self-energy (4.35) and are inherently frame-dependent. They can be derived by simple substitutions from general covariant frame-independent coefficient functions $c^{(p,q)}_{ij}(q,v,u)$. The latter coefficients $c_{ij}^{(p,q)}(q,v,u)$ are defined by:

$$\begin{aligned}
c_{ij}^{(p)}(q,v,u) &= \frac{1}{2}\mathrm{Tr}\left[(\not{p}-\Sigma_V\not{u}+m_N^*)P_{ij}(v,u)\right] \quad \text{for} \quad i,j<3, \\
c_{ij}^{(p)}(q,v,u) &= \frac{1}{2}\mathrm{Tr}\left[(\not{p}-\Sigma_V\not{u}+m_N^*)P_{ij}^{\mu}(v,u)q_\mu\right] \quad \text{and} \\
&\quad \frac{1}{2}\mathrm{Tr}\left[(\not{p}-\Sigma_V\not{u}+m_N^*)\bar{q}_\mu P_{ij}^{\mu}(v,u)\right] \quad \text{for} \quad i<3, \\
c_{ij}^{(p)}(q,v,u) &= \frac{1}{2}\mathrm{Tr}\left[(\not{p}-\Sigma_V\not{u}+m_N^*)\bar{q}_{mu}P_{ij}^{\mu\nu}(v,u)q_\nu\right] \quad \text{for} \quad i,j>2, \\
c_{ij}^{(q)}(q,v,u) &= \frac{1}{2}\mathrm{Tr}\left[(\not{p}-\Sigma_V\not{u}+m_N^*)\bar{q}_\mu Q_{ij}^{\mu\nu}(v,u)q_\nu\right]. \qquad (4.37)
\end{aligned}$$

Note that the aforementioned expressions correspond to the old coefficients [5] in terms of w^μ by substituting $p_\mu \to p_\mu + \Sigma_V u_\mu$, therefore we will state the coefficients in terms of w^μ and shift the scalar amplitudes $\bar{T}_{ij}^{(p,q)}$ entering the self-energy calculation (4.35) and (4.33). The covariant coefficient functions $c_{ij}^{(p,q)}(q,w,u)$ are given in Appendix B.3. The frame dependent coefficient functions for finite nuclear matter are defined via

$$\begin{aligned}
&\frac{1}{2}\mathrm{Tr}\left[(\not{p}+m_N^*)\bar{T}\left(\omega,\mathbf{q}-\frac{i}{2}\nabla_{\mathbf{R}},\mathbf{q}+\frac{i}{2}\nabla_{\mathbf{R}};\omega+p_0,\mathbf{q}+\mathbf{p},k_F(R)\right)\right] \\
&= \sum_{i,j=1}^{8} c_{ij;1}^{(p)}(\omega,\mathbf{q},\mathbf{p})\bar{T}_{ij}^{(p)}(w_0,\mathbf{w},k_F(R)) + \sum_{i,j=1}^{2} c_{ij;1}^{(q)}(\omega,\mathbf{q},\mathbf{p})\bar{T}_{ij}^{(q)}(w_0,\mathbf{w},k_F(R)) \\
&\quad + \frac{1}{4}\nabla_{\mathbf{R}}^2\left(\sum_{i,j=1}^{8} c_{ij;2}^{(p)}(\omega,\mathbf{q},\mathbf{p})\bar{T}_{ij}^{(p)}(w_0,\mathbf{w},k_F(R))\right. \\
&\qquad \left. + \sum_{i,j=1}^{2} c_{ij;2}^{(q)}(\omega,\mathbf{q},\mathbf{p})\bar{T}_{ij}^{(q)}(w_0,\mathbf{w},k_F(R))\right) \\
&\quad + \frac{1}{4}\left(\mathbf{w}\cdot\nabla_{\mathbf{R}}\right)^2\left(\sum_{i,j=1}^{8} c_{ij;3}^{(p)}(\omega,\mathbf{q},\mathbf{p})\bar{T}_{ij}^{(p)}(w_0,\mathbf{w},k_F(R))\right. \\
&\qquad \left. + \sum_{i,j=1}^{2} c_{ij;3}^{(q)}(\omega,\mathbf{q},\mathbf{p})\bar{T}_{ij}^{(q)}(w_0,\mathbf{w},k_F(R))\right) \\
&\quad + \frac{1}{4}\left(\mathbf{w}\cdot\nabla_{\mathbf{R}}\right)\left(\mathbf{p}\cdot\nabla_{\mathbf{R}}\right)\left(\sum_{i,j=1}^{8} c_{ij;4}^{(p)}(\omega,\mathbf{q},\mathbf{p})\bar{T}_{ij}^{(p)}(w_0,\mathbf{w},k_F(R))\right. \\
&\qquad \left. + \sum_{i,j=1}^{2} c_{ij;4}^{(q)}(\omega,\mathbf{q},\mathbf{p})\bar{T}_{ij}^{(q)}(w_0,\mathbf{w},k_F(R))\right) \qquad (4.38)
\end{aligned}$$

in terms of w^μ. The coefficients $c_{ij,0}^{(p,q)}(q,w) = c_{ij}^{(p,q)}(q,w)$ are detailed in Appendix A.9. They can be derived from (4.37) with

$$\bar{q}\cdot q \to q\cdot q, \quad \bar{q}\cdot\hat{w} \to q\cdot\hat{w}, \quad \bar{q}\cdot u \to q\cdot u, \quad p\cdot\bar{q} \to p\cdot q \qquad (4.39)$$

and

$$\hat{w}_\mu = w_\mu/\sqrt{w^2}, \quad w = p+q, \quad u = (1,\mathbf{0}), \quad p = (E_N, \mathbf{p}), \quad q = (\omega, \mathbf{q}). \tag{4.40}$$

The 'non-local' coefficients $c^{(p,q)}_{ij,a}(q,w)$ with $a = 1,2,3$ follow by $\bar{q} \equiv q'$, $q \equiv q$ and

$$\mathbf{q}' \to \mathbf{q} - \frac{i}{2}\nabla_{\mathbf{R}}, \qquad \mathbf{q} \to \mathbf{q} + \frac{i}{2}\nabla_{\mathbf{R}}. \tag{4.41}$$

It is observed that the gradient $\nabla_{\mathbf{R}}$ appears only quadratically in $(\mathbf{q}\cdot\mathbf{q}')$, $(\mathbf{q}\cdot\mathbf{w})(\mathbf{q}'\cdot\mathbf{w})$ and $(\mathbf{q}\cdot\mathbf{p})(\mathbf{q}'\cdot\mathbf{w})$. The 'non-local' coefficients are listed in Appendix B.4 and enjoy the symmetry relation $c^{(p,q)}_{[ij],a} = c^{(p,q)}_{[ji],a}$. In P-space we have $c^{(p)}_{[1j],a} = 0$, $c^{(p)}_{[2j],a} = 0$ and $c^{(p)}_{[i1],a} = 0$, $c^{(p)}_{[i2],a} = 0$ respectively for $a = 1,2,3$. All the coefficients which are not given explicitly or by symmetry relation are identically zero. For the complete matrix structure also coefficients linear in $\nabla_{\mathbf{R}}$ will arise, $\propto (\mathbf{p}\cdot\nabla_{\mathbf{R}})$ and $\propto (\mathbf{w}\cdot\nabla_{\mathbf{R}})$. Still there are no such contributions in Q-space and in P-space for terms involving P_{ij} and $\bar{q}_\mu P^{\mu\nu}_{ij} q_\nu$. We don't have to take into account these terms, as the corresponding coefficient matrix turns out to be antisymmetric, $c^{(p)}_{ij} = -c^{(p)}_{ji}$. Hence all such contributions vanish as the amplitude matrix $\bar{T}^{(p)}_{ij}$ is symmetric and the summation for the self-energy over all matrix elements will not contribute. From (4.35) and (4.36) we derive

$$\begin{aligned}\Pi(\omega,\mathbf{q},\mathbf{R}) &= \int \frac{d^3p}{(2\pi)^3}\Bigg[\Pi_0(q,p,\mathbf{R}) + \frac{1}{4}\nabla^2_{\mathbf{R}}\Pi_1(q,p,\mathbf{R}) + \frac{1}{4}(\mathbf{w}\cdot\nabla_{\mathbf{R}})^2\Pi_2(q,p,\mathbf{R}) \\ &\quad + \frac{1}{4}(\mathbf{w}\cdot\nabla_{\mathbf{R}})(\mathbf{p}\cdot\nabla_{\mathbf{R}})\Pi_3(q,p,\mathbf{R})\Bigg]\Theta(k_F(\mathbf{R}) - |\mathbf{p}|)\end{aligned} \tag{4.42}$$

where we defined the integral kernels

$$\begin{aligned}\Pi_a(q,p,\mathbf{R}) &= -\sum_{i,j=1}^{8}\frac{2}{E^*_N}c^{(p)}_{ij,a}(q,w)\bar{T}_{ij}(p)(w,k_F(\mathbf{R})) \\ &\quad -\sum_{i,j=1}^{2}\frac{2}{E^*_N}c^{(q)}_{ij,a}(q,w)\bar{T}_{ij}(q)(w,k_F(\mathbf{R})),\end{aligned} \tag{4.43}$$

with $a = 0,\ldots,3$. Now with (4.9), (4.32), (4.42) and (4.43) we have a rule on how to calculate the non-local optical potential $U_l(\omega,\mathbf{r},\mathbf{r}')$, given an in-medium $\bar{K}N$ scattering amplitude $\bar{T}^{(p,q)}_{ij}$.

Rather than performing the fault-prone derivatives on the scattering amplitudes in (4.42) numerically we apply a partial integration with respect to $\mathbf{R}$. All terms that are of the form $[u(R)v(R)]^{R\to\infty}_{R=0}$, $R = |\mathbf{R}|$ and that are not included in the integral do not contribute, as for $R = 0$ because of the phase-space element R^2 in spherical coordinates it gives zero. For $R \to \infty$ we impose the optical potential to vanish. Hence after partial integration the self-energy for a rotationally symmetric system ($R = |\mathbf{R}|$) reads

$$\begin{aligned}\Pi(\omega,\mathbf{q},\mathbf{R}) &= \int_0^{k_F(R)} \frac{d^3p}{(2\pi)^3}\Bigg[\Pi_0(q,p,R) - \mathbf{q}^2\Pi_1(q,p,R) - (\mathbf{w}\cdot\mathbf{q})^2\Pi_2(q,p,R) \\ &\quad -(\mathbf{w}\cdot\mathbf{q})(\mathbf{p}\cdot\mathbf{q})\Pi_3(q,p,R)\Bigg]\Theta(k_F(R) - |\mathbf{p}|)\end{aligned} \tag{4.44}$$

and it is evident that (4.44) depends on R only via $k_F(R)$.

The one-dimensional radial Klein-Gordon equation is given by

$$\begin{aligned}\left(\frac{d^2}{dr^2}-\frac{l(l+1)}{r^2}\right)u_l(r) \quad &- \quad \left[\mu^2-(\omega-V_{em}(r))^2\right]u_l(r)\\ &= \int\limits_0^\infty dr'\,r'\,U_l(\omega-V_{em}(r),r,r')u_l(r')\end{aligned} \tag{4.45}$$

with the optical potential

$$U_l(\omega,r,r')=\int\limits_0^\infty dq\,q\int\limits_{-1}^{+1}d\cos\theta\frac{\sin(q|\mathbf{r}-\mathbf{r}'|)}{\pi|\mathbf{r}-\mathbf{r}'|}P_l(\cos\theta)\Pi(\omega,q,R) \tag{4.46}$$

after the angular integration has been carried out. Note that the potential (4.46) depends on l via $P_l(\cos\theta)$ and thus has to be calculated for each atomic level separately.

4.3 Non-Local semi-microscopic approximation and numerical results

We continue our investigation of non-local effects in kaonic atoms with a simplified semi-microscopic model. Writing the non-local potential in terms of some isospin-averaged scattering amplitudes $\bar{T}_{\bar{K}N}$ rather than in terms of a self-energy Π allows a more transparent and amenable survey. Recalling that expression (4.16) is exact as long as only vacuum scattering amplitudes are considered we can test out non-local ansatz by just taking into account free-space scattering [4]. It will provide a first impression of the requirements for a full non-local calculation.

4.3.1 Non-Local optical potential in the $\Pi = -\rho t$ approximation

Our approximation for the semi-microscopic model relies on the assumption that we can neglect the momentum dependence $\mathbf{p} = 0$ of the nucleon in (4.35). Furthermore we set the antikaon energy ω to be constant, $\omega = m_K$. The non-local self-energy $\Pi \equiv \Pi(\omega = m_K, \mathbf{q}, k_F(\mathbf{R}))$ that enters the right hand side of the Klein-Gordon equation (4.1)

$$2\mu\int d^3r'U_l(\omega,\mathbf{r},\mathbf{r}')\phi(\mathbf{r}')=\int d^3r'\int\frac{d^3q}{(2\pi)^3}e^{-i\mathbf{q}\cdot(\mathbf{r}-\mathbf{r}')}\Pi(\omega,\mathbf{q},k_F(\mathbf{R}))\phi(\mathbf{r}') \tag{4.47}$$

follows from (4.42) and (4.43). For simplicity in the following we will write $r = |\mathbf{r}|$, $r' = |\mathbf{r}'|$, $q = |\mathbf{q}|$. Projection on proper angular momentum will be carried out by applying (4.28) and (4.30) to (4.47) as has been done before in Section 4.2.

With the former assumptions the self-energy in our semi-microscopic model is given by

$$\Pi(\omega = m_K, q) = -\rho\,\bar{T}(q) \tag{4.48}$$

and

$$
\begin{aligned}
\bar{T}(q) \;&=\; \frac{1}{2}\left(1+\frac{m_K+m_N}{\sqrt{s}}\right)\bar{M}_{\frac{1}{2}^-}(q)+\frac{1}{2}\left(-1+\frac{m_K+m_N}{\sqrt{s}}\right)\bar{M}_{\frac{1}{2}^+}(q)\\
&+\mathbf{q}^2\left[\frac{m_N^2\left((m_K+m_N+\sqrt{s})\right)}{\sqrt{s}^3}+\left(1+\frac{m_K+m_N}{\sqrt{s}}\right)\left(\frac{\mathbf{q}^2}{s}-1\right)\right]\bar{M}_{\frac{3}{2}^+}(q).
\end{aligned}
\tag{4.49}
$$

The density dependence $k_F(\mathbf{R})$ of the self-energy in (4.47) is suppressed, because we are dealing with free-space scattering amplitudes exclusively. The projector decomposition of the vacuum scattering amplitude $\bar{T}(q)$ follows (2.22) and (2.23). A more precise derivation of (4.48) and (4.49) is deferred to Appendix B.6. The isospin index I is suppressed, as all the expressions will be of the same type for $I = 0$ and $I = 1$ and we are dealing with isospin averaged objects $\bar{T} = \frac{1}{4}\left(T^{(I=0)} + 3T^{(I=1)}\right)$. For brevity the scalar amplitudes $\bar{M}_{J\pm}$ are given in terms of antikaon momentum q instead of $\sqrt{s}$ as we approximate $s = (m_K + m_N)^2 - \mathbf{q}^2$. Also the argument k_F of the self-energy (4.47) can be suppressed, because at the moment we are considering free-space amplitudes exclusively. In (4.49) the $J = \frac{1}{2}$ s- and p-wave as well as the $J = \frac{3}{2}$ p-wave contributions are taken into account. Because the $\Lambda(1520)$ resonance is located above the antikaon-nucleon threshold the $J = \frac{3}{2}$ d-wave is neglected.

The reduced vacuum amplitudes $M^{(I)}_{JP}$ for s-wave, $J = \frac{1}{2}$ p-wave and $J = \frac{3}{2}$ p-wave and d-wave were shown in Figures 2.1 and 2.2 as functions of $\sqrt{s}$ for isospin $I = 0$ and $I = 1$, respectively. The $J = \frac{1}{2}$ p-wave reduced vacuum amplitude contains the $\Lambda(1115)$ and $\Sigma(1195)$ ground states. The structure of the real part given on a finite grid cannot be resolved sufficiently, furthermore the imaginary contribution to the self-energy integral (4.48) has to be evaluated analytically. On the other hand we expect the contribution of the poles to the self-energy integral (4.50) to be negligible. In the Appendix B.5 we describe how to handle the pole structure of the $J = \frac{1}{2}$ p-wave vacuum amplitude analytically in order to examine its effect on the non-local self-energy. For the determination of the $C^{J^\pm}(q)$ we refer to Appendix B.6.

With the substitution $\Pi = -\rho\bar{T}(q)$ we obtain from (4.47) and (4.48)

$$
\begin{aligned}
&2\mu\int d^3r' U_l(\mathbf{r},\mathbf{r}')\phi(\mathbf{r}') =\\
&\quad= -\int d^3r'\int\frac{d^3q}{(2\pi)^3}e^{-i\mathbf{q}(\mathbf{r}-\mathbf{r}')}\bar{T}(q)\rho\left(\left|\frac{\mathbf{r}+\mathbf{r}'}{2}\right|\right)P_l(\cos\theta)\frac{u(r')}{r'}\\
&\quad= -\int_0^{r'_{max}}dr'\int_{-1}^{1}d\cos\theta\int_0^{q_{max}}\frac{dq}{\pi}\,q\,r'\,\frac{\sin\left(q|\mathbf{r}-\mathbf{r}'|\right)}{|\mathbf{r}-\mathbf{r}'|}\bar{T}(q)\rho\left(\left|\frac{\mathbf{r}+\mathbf{r}'}{2}\right|\right)P_l(\cos\theta)u(r').
\end{aligned}
\tag{4.50}
$$

In the latter expression the angular integration for $\cos\theta' = \frac{\mathbf{q}\cdot\mathbf{a}}{q\cdot a}$, $\mathbf{a} = \mathbf{r} - \mathbf{r}'$ has been done analytically by using

$$\int_{-1}^{1} dz' e^{-iqaz'} = 2\frac{\sin qa}{qa}. \tag{4.51}$$

The integration in $\cos\theta$ and q has to be done numerically.

4.3.2 Implementation notes, local limit benchmark and iteration procedure

For our studies a momentum cutoff of $q_{max} = 700\,\mathrm{MeV}$ is used in (4.50). The optical potential $U_l(r, r')$ is highly oscillatory, whereas the oscillation frequency is determined by the momentum cutoff q_{max} and thus the momentum cutoff has to be chosen carefully. We checked the momentum cutoff and the necessary grid size and spacing of $U_l(r, r')$ by examining the local limit

$$\bar{T}(q) \overset{loc}{\to} \bar{T}(q = 0). \tag{4.52}$$

The latter condition should reproduce the level shifts and widths from a scattering length calculation. In the local limit the integration in dr' can be done analytically and should coincide with the full numerical solution from the non-local model. For the right hand side of the Klein Gordon equation (4.47) it follows

$$\begin{aligned}
2\mu \int d^3r' U_l(\mathbf{r}, \mathbf{r}')\phi(\mathbf{r}') = \\
&= -\bar{T}(0) \int d^3r' \int \frac{d^3q}{(2\pi)^3} e^{-i\mathbf{q}(\mathbf{r}'-\mathbf{r})} \rho\left(\left|\frac{\mathbf{r}+\mathbf{r}'}{2}\right|\right) P_l(\cos\theta)\frac{u(r')}{r'} \\
&= -\bar{T}(0) \int d^3r'\, \delta^3\left(\mathbf{r}' - \mathbf{r}\right) \rho\left(\left|\frac{\mathbf{r}+\mathbf{r}'}{2}\right|\right) P_l(\cos\theta)\frac{u(r')}{r'} \\
&= -\bar{T}(0)\rho(r)\frac{u(r)}{r}
\end{aligned} \tag{4.53}$$

with proper normalization $\delta(x) = \frac{1}{2\pi}\int dq e^{ixq}$. The latter expression can be compared to the effective potential from the local density theorem:

$$2\mu\, U(r)\varphi(r) \quad \to \quad 2\mu\, U(r) = -\bar{T}(0)\rho(r) \quad \Leftrightarrow \quad 2\mu\, U(r) = -4\pi\left(1 + \frac{m_K}{m_N}\right)\rho(r)a. \tag{4.54}$$

Recall that the s-wave scattering amplitude determines the scattering length a via

$$a = \bar{T}(0)\left(4\pi\left(1 + \frac{m_K}{m_N}\right)\right)^{-1}. \tag{4.55}$$

For $q = 0$ only the s-wave contributes to $\bar{T}(q)$ due to phase-space arguments. The local benchmark calculations can easily be done using conventional methods for local wave equations, see the previous Chapter 3.

For illustration of the non-local wave functions we will show the reduced wave function u_l^{red},

$$u_l^{red}(r) = \frac{u_l(r)}{r^{l+1}}, \tag{4.56}$$

where the dominating phase space factor has been divided out. The complex wave function is given in terms of the modulus $|u_l^{red}(r)|$ and the phase $\varphi(r)$ with $u_l^{red}(r) = |u_l^{red}(r)|e^{i\varphi(r)}$, which is between $-\pi$ and $+\pi$ and should converge to a constant for large radii. For non-local potentials we show the TELP potential $U_l(r)^{TELP}$ already introduced in (4.2) and for a radially symmetric potential it is given by

$$U_l(r)^{TELP} = \frac{1}{u_l(r)} \int U_l(r, r')u_l(r')dr'. \tag{4.57}$$

Note that the latter expression fails as soon as the non-local wave function exhibits any roots. An equidistant grid with a spacing of 0.1 fm and a range between $r, r' = 20\,\mathrm{fm}$ for carbon and up to $r, r' = 40\,\mathrm{fm}$ for nickel ensures a stable local potential (4.57) within the typical range of about 10 fm. Due to the finite grid size in r' the optical potential starts oscillating further out. The integral in (4.45) is approximated by a Riemann sum.

In Figure 4.1 we compare the wave function based on a local LDT calculation with a constant scattering length (3.16) obtained from [5],

$$a_{\bar{K}N} = (-0.25 + i\,0.71)\,\mathrm{fm}, \tag{4.58}$$

and the non-local wave function iterated from the corresponding non-local potential in the local limit (4.52), thus corresponding to the constant scattering length (4.58). The results were obtained for sulfur. In the lower left panel the local optical potential (3.16) and the TELP potential from the iterated solution are shown. The density distribution in terms of the nucleon Fermi momentum $k_F(r)$ of sulfur is plotted in the lower right panel. The agreement of the local and non-local wave function is excellent, also the local and iterated TELP potential agree very well. The deviation below 1 fm is due to the numerical error of the wave function, by which the non-local potential has been divided. The TELP potential is just used for illustration and does not enter further calculations. Both calculations agree on the same energy level shift $\Delta E = 496\,\mathrm{eV}$ and width $\Gamma = 1025\,\mathrm{eV}$ and the numerical techniques of our non-local calculations are approved.

Performing the iteration procedure of non-local potentials appeared to be a tedious task in some cases and requires a modifications of the straightforward ansatz (4.45) for the Klein-Gordon equation. Recall the non-local Klein-Gordon equation with the non-local optical potential (4.62)

$$\left[\frac{d^2}{dr^2} - \frac{l(l+1)}{r^2} - \mu^2 + (\omega - V_{em}(r))^2\right] u_l(r) = \int_0^{r'_{max}} dr'\, U_l^{\mathrm{int}}(r', r) u_l(r'). \tag{4.59}$$

Equation (4.59) is solved by iteration, starting with an initial wave function $u_l^{(0)}(r')$. The potential kernel potential kernel $U_l^{\mathrm{int}}(r', r)$ is calculated once and the remaining spacial integration dr' is performed after each iterative step to obtain the right-hand-side of the Klein-Gordon equation. The iteration should converge to a wave function $\phi(\mathbf{r})$ and eigenvalue ω. If no initial wave function is given explicitly we require $u_l^{(0)}(r') = 0$ and the first iterative step will yield the pure electromagnetic solution. It turned out that we have to modify (4.59) in order to guarantee the convergence of the iteration procedure. We rewrite the integro-differential equation (4.59) according to

$$\left[\frac{d^2}{dr^2} - \frac{l(l+1)}{r^2} - \mu^2 + (\omega - V_{em}(r))^2\right] u_l^{(n+1)}(r) = \int_0^{r'_{max}} dr'\, k_a U_{l,a}^{\mathrm{int}}(r', r) \tilde{u}_l^{(n)}(r'). \tag{4.60}$$

with the n-th wave function $\tilde{u}_l^{(n)}(r')$ being the average over K former wave functions with weights w_k:

$$\tilde{u}_l^{(n)}(r') = \sum_{k=1}^{K} w_k u_l^{(n-1-k)}(r') \tag{4.61}$$

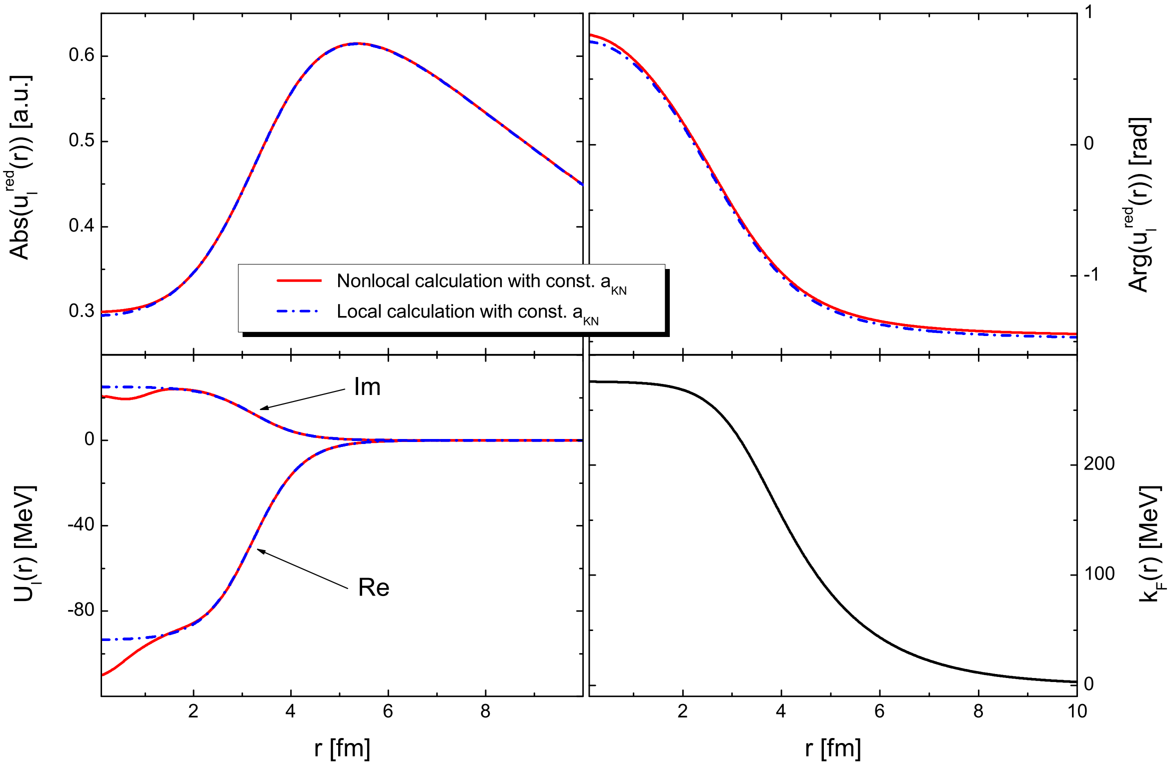

Figure 4.1: Comparison of the reduced wave function $u_l^{red}(r)$ and potential $U_l(r)$ from a local potential with a constant scattering length and the iterated non-local wave function and TELP potential utilising a corresponding non-local potential in the local limit. The results are shown for sulfur.

	${}^{12}_{6}$C		${}^{32}_{16}$S		${}^{35}_{17}$Cl	
	ΔE [eV]	Γ [eV]	ΔE [eV]	Γ [eV]	ΔE [eV]	Γ [eV]
S-wave only	211	112	232	186	381	417
S-wave and $J = \frac{3}{2}$ p-wave	197	77	218	152	364	350
Experiment	590 ± 80	1730 ± 150	494 ± 38	2187 ± 103	1000 ± 170	2910 ± 240

Table 4.1: Level energy shifts and widths from non-local calculations with the free-space scattering amplitude [4].

and $\sum_{k=1}^{K} w_k = 1$. Note that averaging over a number K of previous wave functions significantly slows down the convergence of the iteration. On the other hand it turned out to be suitable for stabilizing especially the early stage of the iteration. It also helps to stick to an given initial wave function. The prefactor $k_a = 0, \ldots, 1$ in (4.60) in conjunction with the index a for the potential $U^{\text{int}}_{l,a}(r', r)$ is introduced for switching on the potential adiabatically. The solution wave function for a certain potential strength k_a will be the initial wave function for the next iterative step with increased k_a.

Exemplary, four typical iterations for carbon are shown in Figure 4.2. The calculations are based on different non-local optical potentials from the preceeding results sections. The negative level width $-\Gamma$ and binding energy E is plotted versus the number of iterative steps. The upper left an lower right example describes the ideal case, it is converging within a few iterations and does not oscillate at all. On the upper right side the convergence is poor, even after a large number of steps. On the lower left hand side the iteration in unstable at the beginning, but finally converges sufficiently.

4.3.3 Numerical results for the semi-microscopic model with free-space scattering amplitude

The free-space scattering case described in Section 4.3.1 will be the first test and benchmark of our non-local approach to kaonic atoms. All the following tabulated results for carbon, sulfur and chlorine are calculated with s-wave contribution (4.49) only and in combination with the $J = \frac{3}{2}$ p-wave. The $J = \frac{1}{2}$ p-wave was included using the scheme described in Appendix B.5 and its contribution is less than 5 eV for each calculation. The results confirm our conjecture that the $J = \frac{1}{2}$ p-wave can be neglected within our simplified semi-microscopic ansatz.

Table 4.1 summarizes the energy level shifts and widths for the different nuclei with non-local optical potentials calculated from the free-space scattering amplitudes of [4]. Remarkable is the huge underestimation of the energy level shift and especially the width. It is a strong hint for the importance of the in-medium dynamics of the $\Lambda(1405)$ resonance. The contribution from the $J = \frac{3}{2}$ p-wave is relatively small, nevertheless in a full microscopic calculation the structure is more complex and there could be strong nonlinear cancellation effects from the non-local treatment. Obviously taking only the vacuum scattering amplitudes does not reproduce empirical kaonic atom spectra in the non-local approach.

To get an idea of the results changing due to in-medium modified amplitudes we redo

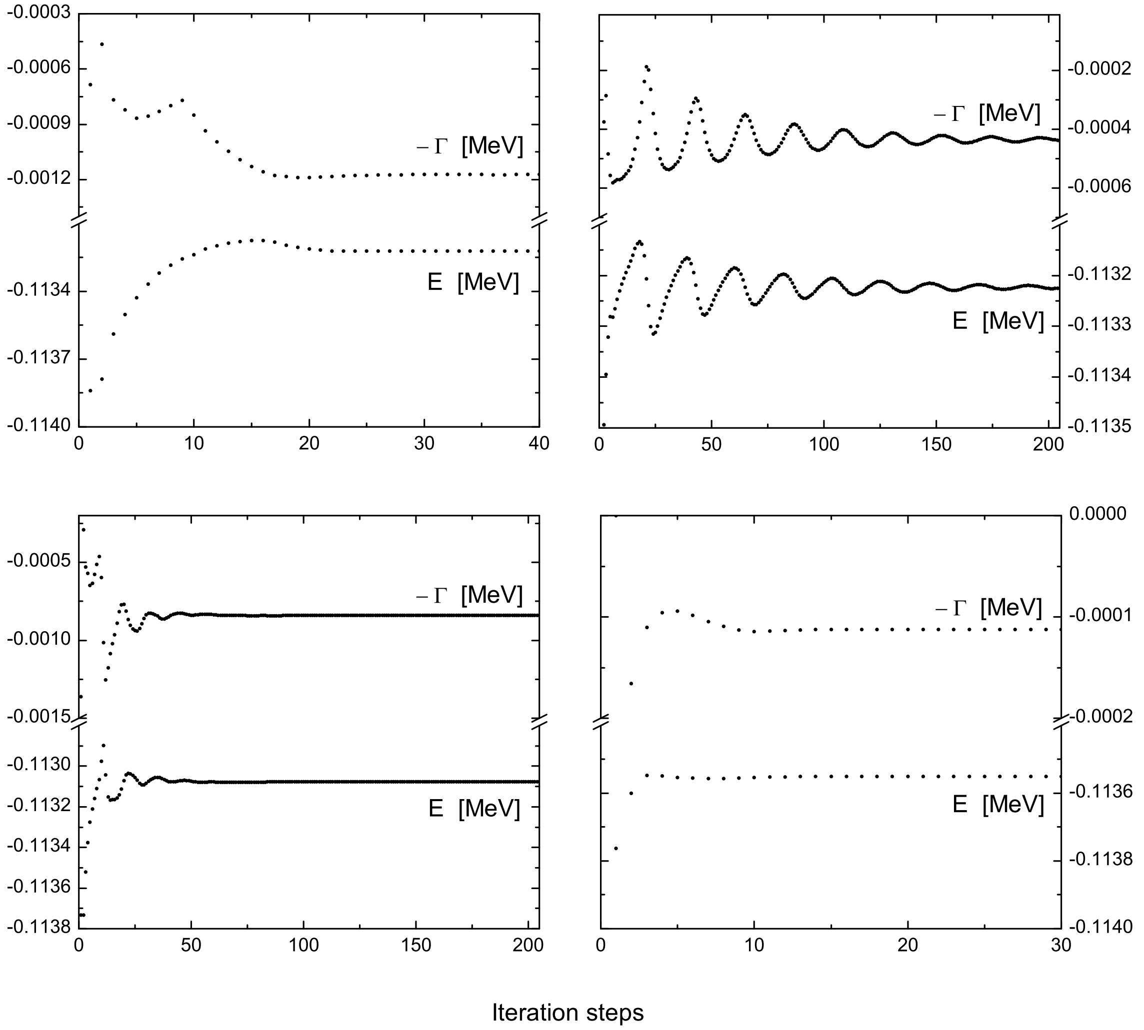

Figure 4.2: Iteration of binding energy E and level width Γ for carbon versus the number of iterative steps for different non-local potentials $U_l^{int}(r', r)$.

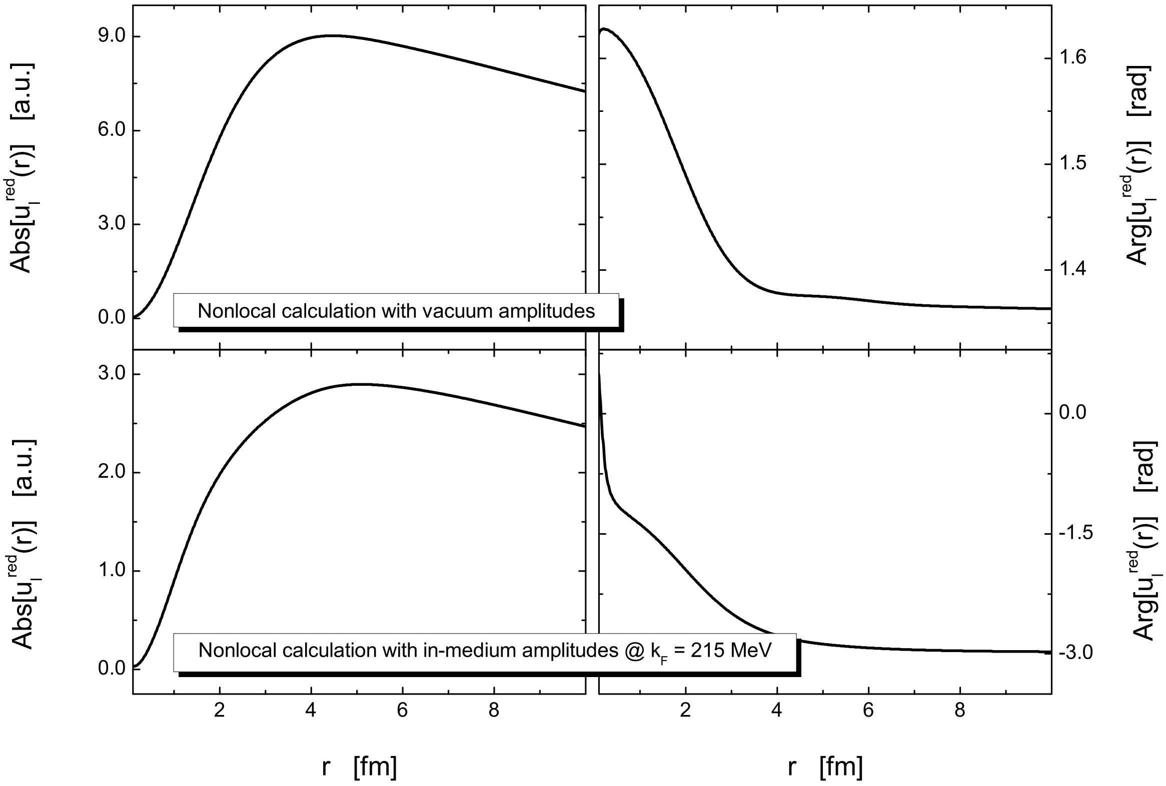

Figure 4.3: Modulus and phase of the reduced wave functions $u_l^{red}(r)$ from non-local calculations with free-space scattering amplitude (upper panels) and in-medium scattering amplitude (lower panels) at half saturation density, s-wave only for carbon.

	${}^{12}_{6}\mathrm{C}$		${}^{32}_{16}\mathrm{S}$		${}^{35}_{17}\mathrm{Cl}$	
	ΔE [eV]	Γ [eV]	ΔE [eV]	Γ [eV]	ΔE [eV]	Γ [eV]
S-wave only	539	435	251	1579	389	2691
S-wave and $J = \frac{3}{2}$ p-wave	369	166	362	976	593	1610
Experiment	590 ± 80	1730 ± 150	494 ± 38	2187 ± 103	1000 ± 170	2910 ± 240

Table 4.2: Level energy shifts and widths from non-local calculations with the in-medium scattering amplitude [5] at half saturation density.

the latter calculations, with the in-medium scattering amplitudes calculated in [5]. We take the amplitudes at a nucleon Fermi momentum of $k_F = 215\,\mathrm{MeV}$, which roughly corresponds to a nuclear matter density of $\rho = \frac{\rho_0}{2}$. The increase of the energy level shifts and widths in Table 4.2 for the s-wave contribution is quite remarkable. The influence of the $J = \frac{3}{2}$ p-wave in conjunction with the s-wave increases significantly, but the level width is consistently smaller than for the s-wave only calculations. One has to keep in mind that the results in Table 4.2 are based on a rather crude modification, as the average nuclear density probed by the antikaon is presumably lower than $\rho = \frac{\rho_0}{2}$. For carrying out a detailed analysis of the density dependence of the $\bar{K}$-nucleus interaction a model covering the whole range from zero to saturation density is required.

Figure 4.3 shows the modulus and phase of the reduced wave functions $u_l^{red}(r)$ of the latter calculations with free-space and in-medium scattering amplitude for carbon and s-wave only.

4.3.4 Semi-microscopic model with interpolated in-medium scattering amplitude

In order to get an intuitive impression how the outcome of a non-local optical potential calculation is influenced by the in-medium modifications of the underlying scattering amplitudes we can utilise the semi-microscopic model from Section 4.3.1. Instead of the vacuum scattering amplitudes any k_F-dependent in-medium scattering amplitudes can be used as input. We substitute the vacuum amplitude $\bar{T}(q)$ in (4.50) by an adequate interpolation, utilising the vacuum M_{J^P} and in-medium $M_{ij}^{(p,q)}$ amplitudes [4] and [5] at different Fermi momenta k_F. Any reasonable interpolation of the scattering amplitudes should satisfactorily match the effective density dependent scattering length (3.23) at $q = 0$. Due to the little overlap of the antikaon wave function with the nucleus density distribution one may naively expect the contribution from the high-density ($\rho > \frac{\rho_0}{2}$) region of the density-dependent scattering length to be rather low. From the first point of view the low density behaviour of the scattering length is dominating for kaonic atoms, particularly the change-over from repulsion to attraction of $\mathfrak{Re}[a_{eff}(k_F)]$, that typically happens around $k_F = 100 - 125\,\mathrm{MeV}$. In general a crossing from repulsion to attraction at lower k_F leads to a larger level width.

The interpolated density dependent amplitude $T_{\mathrm{int}}^{\frac{1}{2}^-,\frac{3}{2}^+}(k_F, q)$ is given in Appendix B.7 and comprises contributions from $J^P = \frac{1}{2}^-$ s-wave and $J^P = \frac{3}{2}^+$ p-wave, which can be switched on

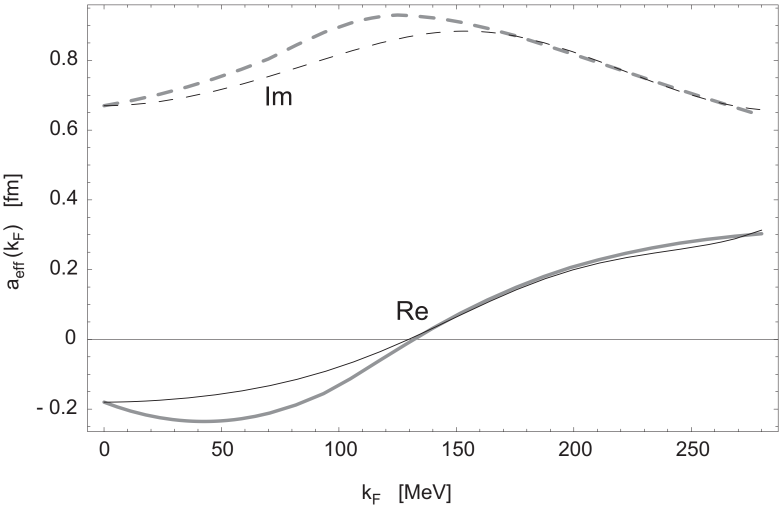

Figure 4.4: Interpolated scattering length $a_{eff}^{\rm int}(k_F)$ from (B.56) in [fm] (thin lines), compared to the effective scattering length of [3] (thick lines).

separately. The corresponding effective scattering length based on (B.56) is shown in Figure 4.4, compared to the effective scattering length of [3] that has already been shown in Figure 3.1. The crossing from repulsion to attraction happens around the same Fermi momentum.

The isospin-averaged interpolated scattering amplitude (B.58) for s-wave only is shown in Figure 4.5 as a function of Fermi momentum k_F and antikaon momentum q. The smoothness of the interpolating function $T_{\rm int}^{J^\pm}$ is well enhanced by doing the interpolation in terms of the inverse reduced amplitudes according to (B.56). One can clearly see density dependence of the $\Lambda(1405)$ resonance structure. The non-local optical potential with interpolated density dependence $U_l^{\rm int}$ reads

$$\begin{aligned} U_l^{\rm int}(r',r) &= \int_{-1}^{1} d\cos\theta \int_0^{q_{max}} \frac{dq}{\pi}\, q\, r' \,\frac{\sin\left(q\sqrt{r^2+r'^2-2rr'\cos\theta}\right)}{\sqrt{r^2+r'^2-2rr'\cos\theta})} \\ &\quad \times T_{\rm int}^{\frac{1}{2}^-,\frac{3}{2}^+}(k_F(\mathbf{R}),q)\rho\,(\mathbf{R})\,P_l(\cos\theta) \end{aligned} \tag{4.62}$$

in the framework of our semi-microscopic model. For illustration we show the s-wave only optical potential (4.62) in Figure 4.6 for carbon. For reasons of convergence the non-local potential for carbon is calculated up to 20 fm in r and r', here we plot a smaller region near the origin.

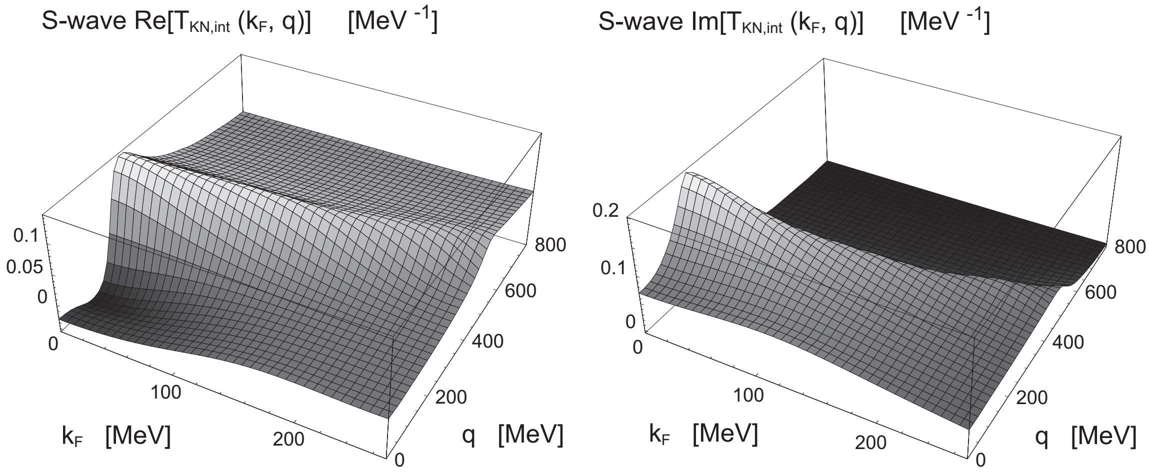

Figure 4.5: S-wave $T^{\frac{1}{2}^-}_{\bar{K}N,\text{int}}(k_F, q)$ inverse interpolation, real and imaginary part.

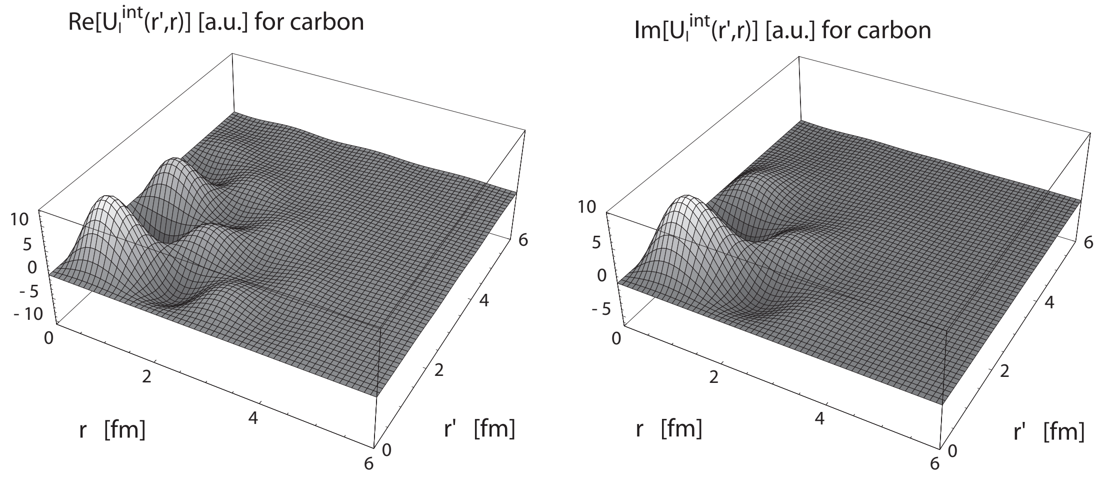

Figure 4.6: Real and imaginary part of the non-local optical potential $U_l^{\text{int}}(r', r)$ (4.62) for carbon, including both s- and p-wave contributions.

	${}^{12}_{6}$C		${}^{32}_{16}$S		${}^{35}_{17}$Cl	
	ΔE [eV]	Γ [eV]	ΔE [eV]	Γ [eV]	ΔE [eV]	Γ [eV]
Local calculation $a^{\text{int}}_{eff}(k_F)$	541	1173	553	1480	980	2211
Non-Local s-wave only calculation	683	836	281	560	483	1120
Non-Local s-wave and $J = \frac{3}{2}$ p-wave	687	791	321	283	270	801

Table 4.3: Local calculations with the effective scattering length $a^{\text{int}}_{eff}(k_F)$ and non-local calculations with the interpolated scattering amplitude $T^{\frac{1}{2}^-,\frac{3}{2}^+}_{\text{int}}$ for carbon, sulfur and chlorine.

4.3.5 Numerical results of the semi-microscopic model with interpolated in-medium scattering amplitude

We applied our semi-microscopic non-local approach with the interpolated density dependence of the scattering amplitudes to the nuclei carbon, sulfur and chlorine. The non-local calculations are compared to corresponding local ones by taking the local limit $q = 0$ in $T^{\frac{1}{2}^-}_{\text{int}}(k_F, q = 0)$ and we obtain an effective scattering length $a^{\text{int}}_{eff}(k_F)$.

In Table 4.3 the numerical results for energy level shifts ΔE and widths Γ are given for our set of three nuclei, the non-local potential comprises the s-wave $T^{\frac{1}{2}^-}_{\text{int}}$ contribution only as well as the s-wave and p-wave $T^{\frac{3}{2}^+}_{\text{int}}$ contributions. In addition the results for a calculation in the local limit of $T^{\frac{1}{2}^-}_{\text{int}}$ are given, corresponding to the effective scattering length $a^{\text{int}}_{eff}(k_F)$ shown in Figure 4.4. The results for the effective scattering length $a^{\text{int}}_{eff}(k_F)$ agree quite well with the calculations based on the microscopic effective scattering length $a_{eff}(k_F)$ from [3], see Tables 3.3 and 3.4. The measured energy level shifts can be reproduced satisfactorily, whereas the level widths are significantly underestimated. Nevertheless, the results confirm our interpolation scheme on the level of a density dependent scattering length. As we will see later on the values for carbon agree quite well with the results of a full non-local calculation and thus approve the approximations of our semi-microscopic model from Section 4.3.1 and the interpolation scheme of $T^{\frac{1}{2}^-,\frac{3}{2}^+}_{\text{int}}$. By comparing the non-local calculations in Table 4.3 with the effective scattering length results we observe that especially the level widths are considerably smaller. This tendency is continued by switching on p-wave contributions, but the effect from the p-wave is less pronounced than for the density independent results of Table 4.2.

The modulus and phase of the reduced wave functions for the calculations of Tables 4.1 and 4.1 are plotted in Figure 4.7 for carbon. Compared to the density-independent calculations in Figure 4.3 the qualitative behaviour of the wave functions changes significantly.

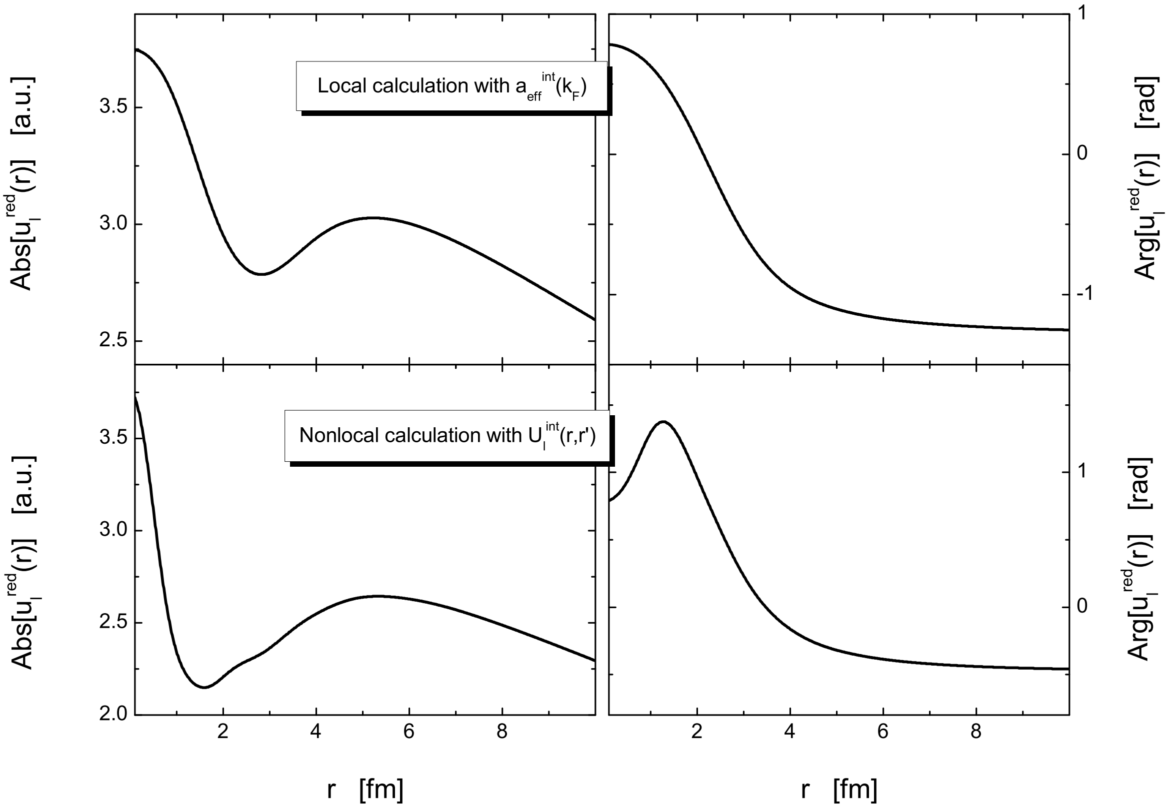

Figure 4.7: Modulus and phase of the reduced wave functions $u_l^{red}(r)$ from non-local calculations with interpolated density-dependent scattering amplitude $T_{\text{int}}^{\frac{1}{2}^-}$ (lower panels) compared to the corresponding effective scattering length $a_{eff}^{\text{int}}(k_F)$ in the local limit (upper panels).

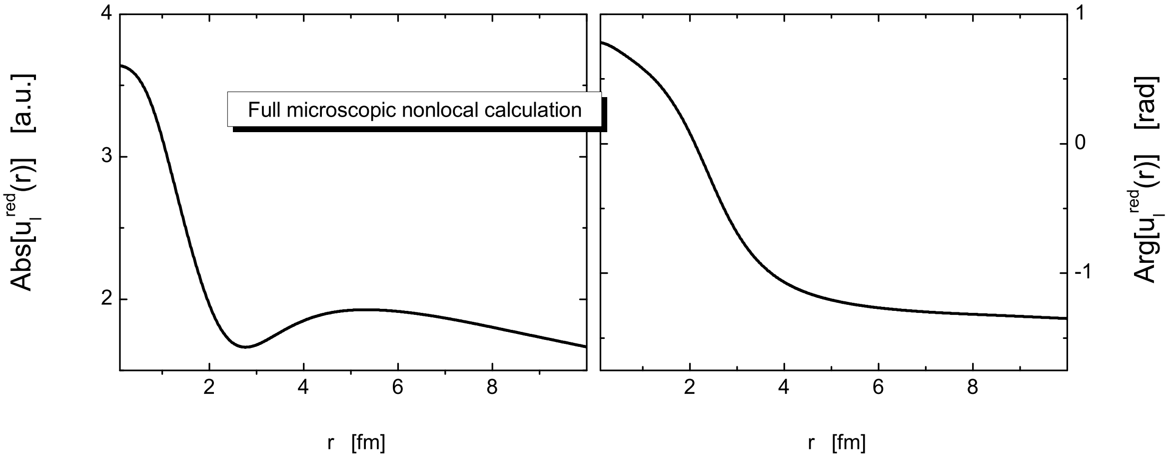

Figure 4.8: Modulus and phase of non-local reduced wave function for carbon, full non-local calculation.

	$^{12}_{6}$C	
	ΔE [eV]	Γ [eV]
$U_l(\omega, r, r')$	545	1030
$U_l(\omega = m_K, r, r')$	566	1047
Experiment	590 ± 80	1730 ± 150

Table 4.4: Level shift ΔE and width Γ [eV] for carbon, full non-local calculation.

4.3.6 Full non-local calculation

After testing our non-local approach for the optical potential with a simplified, semi-microscopic model based on the vacuum scattering amplitudes of [4] and a suitable density dependent interpolation we perform a full non-local calculation according to (4.44), (4.45) and (4.46). Based on the self-consistent in-medium hyperon and antikaon framework of [5] we calculate the non-local optical potential $U_l(\omega, r, r')$ at first instance for carbon. The local wave function based on an effective scattering length was likewise taken as the starting point for the iteration of the non-local solution.

Figure 4.8 shows the modulus and phase of the non-local reduced wave function (4.56). Qualitatively the wave function is similar to the one obtained within our semi-microscopic model in Figure 4.7. In Table 4.4 the results and the experimental values are listed. The numbers suggest a further survey of non-local effects for a larger set of nuclei. The systematically underestimated level widths indicate the need for an improved in-medium dynamics. For comparison we state a calculation where the energy-dependence of the optical potential has been neglected, that is $U_l(\omega = m_K, r, r')$.

The full non-local calculation for carbon does still not improve the agreement with the experimental data, which may be due to shortcomings of the underlying in-medium antikaon and hyperon dynamics [5]. We observe significant effects from a non-local treatment of kaonic atoms. We deduce that a non-local treatment of kaonic atoms is much more sensitive to the hyperon in-medium dynamics than a local effective scattering length framework and the non-local ansatz for the optical potential is capable to distinguish even small variations of the complex hyperon in-medium dynamics. We expect further improvement on the description of kaonic atoms data by utilising our non-local potential approach, with self-consistent in-medium amplitudes developed in Chapter 2.

Chapter 5

Summary and outlook

In this work we studied the properties of antikaons and hyperons in infinite cold nuclear matter. The in-medium antikaon-nucleon scattering amplitude and self-energy has been calculated within a covariant many-body framework in the first part. Nuclear saturation effects have been taken into account in terms of scalar and vector nucleon mean-fields. In the second part of the work we introduced a non-local method for the description of kaonic atoms. The many-body approach of $\bar{K}N$ scattering can be tested by the application to kaonic atoms, as a satisfactory microscopic investigation of kaonic atoms is still missing in literature.

A self-consistent and covariant many-body approach has been used for the determination of the antikaon spectral function and $\bar{K}N$ scattering amplitudes. It considers s-, p- and d-waves and the application of an in-medium projector algebra accounts for proper mixing of partial waves in the medium. The on-shell reduction scheme is also implemented by means of the projector algebra. The Bethe-Salpeter equation has been rewritten, so that the free-space $\bar{K}N$ scattering of [4] can be used as the interaction kernel for the in-medium scattering equation. The latter free-space scattering is based on a realistic coupled-channel dynamics and chiral $SU(3)$ Lagrangian. Our many-body approach is generalized from [5] for the presence of large scalar and vector nucleon mean-fields. It is supplemented by an improved renormalization scheme, that systematically avoids the occurrence of medium-induced power-divergent structures and kinematical singularities. A proper renormalization scheme is a matter of particular interest especially when p- and higher partial waves are included. A modified projector basis has been introduced, that allows for a convenient inclusion of nucleon mean-fields. The description of the results in terms of the 'physical' basis is done with the help of a recoupling scheme based on the projector algebra properties.

We found relevant effects by considering scalar and vector nucleon mean-fields. The antikaon spectral function becomes significantly more narrow and strength is moved to the lower soft modes due to hyperon nucleon-hole states. The enhanced soft modes are also present in the self-energy at vanishing antikaon momentum, whereas at finite antikaon momenta the effects of the nucleon mean-fields are less pronounced. The structure of both spectral function and self-energy is enriched by including p-wave interactions. The hyperon properties are affected moderately by the mean-fields, with the exception of the $\Lambda(1520)$ d-wave resonance, that almost completely dissolves already at nuclear saturation density. The p-wave ground states $\Lambda(1115)$ and $\Sigma(1195)$ central mass positions are basically unaffected by the nucleon mean-fields. For the $\Lambda(1405)$ s-wave resonance we obtain an attractive shift of about 30 MeV, which is in agreement with the results of [5]. Without mean-fields the attractive shift increases, but the resonance is considerably broadened by including mean-fields. The opposite behaviour in resonance central mass position and width can be observed for the p-wave $\Sigma(1385)$, which is attracted by 40 MeV at saturation density. To recapitulate our results do not support the strong interaction scenario of [16] and [17], where the existence of deeply bound and highly compressed strange nuclear systems is predicted.

We confirmed that the inclusion of a weak scalar mean-field only, whose strength corresponds to the difference of large scalar and vector mean-fields, does even qualitatively not reproduce our findings from incorporating both mean-fields. We conclude that a weak scalar mean-field, as it has been used in [14], is not sufficient for modeling implications from nuclear saturation.

The calculations at nuclear saturation density with and without mean-fields have been compared to results that rest on an angular average approximation, that in a similar manner is applied in [2] and [14]. It can be implemented within our covariant framework easily and is most advantageous from the point of view of numerical effort. The approximation turned out to be suitable for the computation of the antikaon spectral function and s-wave in-medium scattering amplitude, but it fails partly for describing the hyperon properties and particularly the $\Lambda(1520)$ d-wave resonance. For the latter resonance we obtain deviations up to 50 MeV in central mass position compared to the full calculation. The p- and d-wave phase-space cannot be reproduced accurately within an angular average approximation.

Kaonic atoms data provide a meaningful benchmark for any many-body approach to in-medium antikaon and hyperon properties. However, up to now the data could only be described by phenomenological optical potentials. Non-Local corrections to the optical potential have not been considered in a systematic way, as a simple momentum expansion of the antikaon self-energy is questionable because of the presence of subthreshold resonances. Our approach comprises non-local contributions to the self-energy that are caused by the momentum and density dependence of the $\bar{K}N$ in-medium scattering amplitudes and the finite size nucleus. In our approximation the non-local self-energy is computed from $\bar{K}N$ scattering amplitudes for infinite nuclear matter. The non-local optical potential that enters the Klein-Gordon equation for the calculation of atomic level shifts and widths can be evaluated from the non-local self-energy in a straight forward way. But for all that the treatment of non-local wave equations and the solution via an iteration process requires special care.

The non-local ansatz we have proposed is exact as long as free-space scattering is considered. Our approach has been approved by performing benchmark calculations in the local limit of a simplified semi-microscopic non-local model. This model allows to study the interplay of different partial waves, either by using free-space scattering amplitudes [4] exclusively or an appropriate density dependent interpolation of in-medium scattering amplitudes [5]. In the local limit the latter interpolation has been compared to existing density dependent effective scattering lengths successfully.

For the nuclei carbon, sulfur and chlorine considering free-space scattering amplitudes only fails. Both energy level shifts and widths are largely underestimated. With a density dependent semi-microscopic model we improve significantly on the agreement with experiment, but the non-local calculations including s-wave contributions only systematically lead to lower level widths than a local calculation with the corresponding effective scattering length. We observe that the in-medium properties of the s-wave $\Lambda(1405)$ resonance predominantly affect the calculation of kaonic atoms level shifts and widths. However, for our semi-microscopic model the inclusion of p-wave contributions has sizeable impact on the calculations, but it does not improve on the agreement with experiment.

For carbon a calculation with the full non-local self-energy has been done, based on the in-medium amplitudes of [5]. We have significant effects from a non-local treatment, but the results are still inconclusive and demand further investigation. The non-local approach is very sensitive to in-medium properties of the hyperon resonances in s- and p-waves. A simple local ansatz either using a constant or a density dependent scattering length seems to be inadequate for the description of kaonic atoms. Hence, we expect a better agreement with the experimental data from the application of our improved many-body approach including nuclear saturation effects within our non-local framework. A future issue will be to elaborate on the reliability of our assumptions made for finite size nuclei. An extended survey of non-local effects for a larger number of nuclei will also provide further insight to kaonic atoms and the underlying antikaon and hyperon in-medium properties.

Appendix A

Appendix: Antikaons and hyperons in nuclear matter

A.1 Projector algebra

The projectors P_{ij} and Q_{ij} introduced in (2.2.1) can be expressed in terms of appropriate building blocks $P_\pm$, $U_\pm$, V_μ and L_μ, R_μ:

$$\begin{aligned}
P_\pm(v) &= \frac{1}{2}\left(1 \pm \frac{\not{v}}{\sqrt{v^2}}\right), \\
U_\pm(v,u) &= P_\pm(v)\frac{-i\gamma\cdot u}{\sqrt{(v\cdot u)^2/v^2-1}}P_\mp(v), \\
V_\mu(v) &= \frac{1}{\sqrt{3}}\left(\gamma_\mu - \frac{\not{v}}{v^2}v_\mu\right), \\
X_\mu(v,u) &= \frac{(v\cdot u)v_\mu - v^2u_\mu}{v^2\sqrt{(v\cdot u)^2/v^2-1}}, \\
R_\mu(v,u) &= \frac{1}{\sqrt{2}}\left(U_+(v,u)+U_-(v,u)\right)V_\mu(v) - i\sqrt{\frac{3}{2}}X_\mu(v,u), \\
L_\mu(v,u) &= \frac{1}{\sqrt{2}}V_\mu(v)\left(U_+(v,u)+U_-(v,u)\right) - i\sqrt{\frac{3}{2}}X_\mu(v,u)
\end{aligned} \tag{A.1}$$

Note again that (A.1) is equivalent to the algebra used in [5] except for the argument v_μ instead of w_μ. The building blocks $P_\pm$, $U_\pm$, V_μ and L_μ, R_μ enjoy the following useful properties:

$$\begin{aligned}
&P_\pm \cdot P_\pm = P_\pm = U_\pm \cdot U_\mp, \quad P_\pm \cdot P_\mp = 0 = U_\pm \cdot U_\pm, \\
&V \cdot L = 0 = R \cdot V, \quad L \cdot V = -\frac{\sqrt{8}}{3}(U_+ + U_-) = V \cdot R, \\
&V \cdot V = L \cdot R = R \cdot L = 1, \quad R \cdot R = L \cdot L = \frac{1}{3}, \\
&P_\pm \cdot V_\mu = V_\mu \cdot P_\mp, \quad P_\pm \cdot L_\mu = L_\mu \cdot P_\pm, \quad P_\pm \cdot R_\mu = R_\mu \cdot P_\pm, \\
&U_\pm \cdot L_\mu = R_\mu \cdot U_\pm, \quad U_\pm \cdot R_\mu = L_\mu \cdot U_\pm, \\
&U_\pm \cdot V_\mu = -\frac{1}{3} V_\mu \cdot U_\mp - \frac{\sqrt{8}}{3} L_\mu \cdot P_\mp, \\
&V_\mu \cdot U_\pm = -\frac{1}{3} U_\mp \cdot V_\mu - \frac{\sqrt{8}}{3} R_\mu \cdot P_\mp.
\end{aligned} \tag{A.2}$$

With $\hat{v}_\mu = v_\mu / \sqrt{v^2}$ the Q-space projectors are

$$\begin{aligned}
Q_{11}^{\mu\nu} &= (g^{\mu\nu} - \hat{v}^\mu \hat{v}^\nu)\, P_+ - V^\mu \cdot P_- \cdot V^\nu - L^\mu \cdot P_+ \cdot R^\nu, \\
Q_{22}^{\mu\nu} &= (g^{\mu\nu} - \hat{v}^\mu \hat{v}^\nu)\, P_- - V^\mu \cdot P_+ \cdot V^\nu - L^\mu \cdot P_- \cdot R^\nu, \\
Q_{12}^{\mu\nu} &= (g^{\mu\nu} - \hat{v}^\mu \hat{v}^\nu)\, U_+ + \frac{1}{3} V^\mu \cdot U_- \cdot V^\nu \\
&\quad + \frac{\sqrt{8}}{3}\, (L^\mu \cdot P_+ \cdot V^\nu + V^\mu \cdot P_- \cdot R^\nu) - \frac{1}{3} L^\mu \cdot U_+ \cdot R^\nu, \\
Q_{21}^{\mu\nu} &= (g^{\mu\nu} - \hat{v}^\mu \hat{v}^\nu)\, U_- + \frac{1}{3} V^\mu \cdot U_+ \cdot V^\nu \\
&\quad + \frac{\sqrt{8}}{3}\, (L^\mu \cdot P_- \cdot V^\nu + V^\mu \cdot P_+ \cdot R^\nu) - \frac{1}{3} L^\mu \cdot U_- \cdot R^\nu.
\end{aligned} \tag{A.3}$$

Using the properties of the building blocks (A.2) reveals that the objects $Q_{[ij]}^{\mu\nu}$ indeed form a projector algebra. The P-space projectors have similar transparent representations, where the P-space algebra now includes objects without Lorentz index, one or two Lorentz indices:

$$\begin{array}{llll}
P_{11} = P_+, & P_{12} = U_+, & P_{21} = U_-, & P_{22} = P_-, \\
P_{31}^\mu = V^\mu P_+, & P_{32}^\mu = V^\mu U_+, & \bar{P}_{13}^\mu = P_+ V^\mu, & \bar{P}_{23}^\mu = U_- V^\mu, \\
P_{41}^\mu = V^\mu U_-, & P_{42}^\mu = V^\mu P_-, & \bar{P}_{14}^\mu = U_+ V^\mu, & \bar{P}_{24}^\mu = P_- V^\mu, \\
P_{51}^\mu = \hat{v}^\mu P_+, & P_{52}^\mu = \hat{v}^\mu U_+, & \bar{P}_{15}^\mu = P_+ \hat{v}^\mu, & \bar{P}_{25}^\mu = U_- \hat{v}^\mu, \\
P_{61}^\mu = \hat{v}^\mu U_-, & P_{62}^\mu = \hat{v}^\mu P_-, & \bar{P}_{16}^\mu = U_+ \hat{v}^\mu, & \bar{P}_{26}^\mu = P_- \hat{v}^\mu, \\
P_{71}^\mu = L^\mu P_+, & P_{72}^\mu = L^\mu U_+, & \bar{P}_{17}^\mu = P_+ R^\mu, & \bar{P}_{27}^\mu = U_- R^\mu, \\
P_{81}^\mu = L^\mu U_-, & P_{82}^\mu = L^\mu P_-, & \bar{P}_{18}^\mu = U_+ R^\mu, & \bar{P}_{28}^\mu = P_- R^\mu,
\end{array}$$

$$P_{ij}^{\mu\nu} = P_{i1}^\mu \bar{P}_{1j}^\nu = P_{i2}^\mu \bar{P}_{2j}^\nu. \tag{A.4}$$

A.2 Recoupling coefficients

We only state the nontrivial recoupling coefficients, the remaining ones are determined by the following symmetry relations:

$$\begin{aligned} C^{J^P}_{p,ij} &= C^{J^P}_{p,ji}, & C^{J^P}_{q,ij} &= C^{J^P}_{q,ji}, \\ C^{J^P}_{p,5i} &= -\sqrt{3}\, C^{J^P}_{p,3i}, & C^{J^P}_{p,6i} &= +\sqrt{3}\, C^{J^P}_{p,4i}. \end{aligned} \tag{A.5}$$

The coefficients are derived in the nuclear matter rest frame. The angular average approximation (2.3.2) does not affect the recoupling of the vacuum amplitudes, therefore the present form can also be used in the cm-frame.

In Q-space we have

$$\begin{aligned} C^{\frac{3}{2}\pm}_{q,11} &= -\frac{3}{2}\left[\frac{v_0 w_0 - \mathbf{w}^2}{\sqrt{v_0^2-\mathbf{w}^2}\,\sqrt{w_0^2-\mathbf{w}^2}} \pm 1\right], \\ C^{\frac{3}{2}\pm}_{q,12} &= \frac{3}{2}\,\frac{i\sqrt{\mathbf{w}^2}(v_0-w_0)}{\sqrt{v_0^2-\mathbf{w}^2}\,\sqrt{w_0^2-\mathbf{w}^2}}, \\ C^{\frac{3}{2}\pm}_{q,22} &= -C^{\frac{3}{2}\mp}_{q,11} \end{aligned} \tag{A.6}$$

and in P-space for $J=\frac{1}{2}$

$$\begin{aligned} C^{\frac{1}{2}\pm}_{p,11} &= \frac{1}{2}\left[\frac{v_0 w_0 - \mathbf{w}^2}{\sqrt{v_0^2-\mathbf{w}^2}\,\sqrt{w_0^2-\mathbf{w}^2}} \mp 1\right], \\ C^{\frac{1}{2}\pm}_{p,12} &= -\frac{1}{2}\,\frac{i\sqrt{\mathbf{w}^2}(v_0-w_0)}{\sqrt{v_0^2-\mathbf{w}^2}\,\sqrt{w_0^2-\mathbf{w}^2}}, \\ C^{\frac{1}{2}\pm}_{p,22} &= -C^{\frac{1}{2}\mp}_{p,11}. \end{aligned} \tag{A.7}$$

In P-space the diagonal elements for $J=\frac{3}{2}$ are

$$\begin{aligned} C^{\frac{3}{2}\pm}_{p,33} &= \frac{\mathbf{w}^2(v_0-w_0)^2}{3\sqrt{v_0^2-\mathbf{w}^2}^3\,\sqrt{w_0^2-\mathbf{w}^2}^3}\left[v_0 w_0 - \mathbf{w}^2 \pm \sqrt{v_0^2-\mathbf{w}^2}\,\sqrt{w_0^2-\mathbf{w}^2}\right], \\ C^{\frac{3}{2}\pm}_{p,44} &= -C^{\frac{3}{2}\mp}_{p,33}, \qquad C^{\frac{3}{2}\pm}_{p,55} = 3C^{\frac{3}{2}\pm}_{p,33}, \qquad C^{\frac{3}{2}\pm}_{p,66} = -3C^{\frac{3}{2}\mp}_{p,33}, \\ C^{\frac{3}{2}\pm}_{p,77} &= \frac{1}{6\sqrt{v_0^2-\mathbf{w}^2}^3\,\sqrt{w_0^2-\mathbf{w}^2}^3}\Big[-9\left(v_0^3 w_0^3 - \mathbf{w}^6\right) \\ &\quad +\mathbf{w}^2\left(v_0 w_0 - \mathbf{w}^2\right)\left(5\left(v_0^2+w_0^2\right)+17 v_0 w_0\right) \\ &\quad \pm\sqrt{v_0^2-\mathbf{w}^2}\,\sqrt{w_0^2-\mathbf{w}^2}\left(-9\left(v_0^2 w_0^2+\mathbf{w}^4\right)+\mathbf{w}^2\left(v_0^2+w_0^2+16 v_0 w_0\right)\right)\Big] \\ C^{\frac{3}{2}\pm}_{p,88} &= -C^{\frac{3}{2}\mp}_{p,77} \end{aligned} \tag{A.8}$$

and the off-diagonal elements

$$\begin{aligned}
C^{\frac{3}{2}\pm}_{p,34} &= \frac{i\mathbf{w}^3(v_0-w_0)^3}{3\sqrt{v_0^2-\mathbf{w}^2}^3\,\sqrt{w_0^2-\mathbf{w}^2}^3}\,,\\
C^{\frac{3}{2}\pm}_{p,37} &= -\frac{i\sqrt{\mathbf{w}^2}(v_0-w_0)}{3\sqrt{2}\sqrt{v_0^2-\mathbf{w}^2}^3\,\sqrt{w_0^2-\mathbf{w}^2}^3}\Big[3\left(v_0^2w_0^2+\mathbf{w}^4\right)-\mathbf{w}^2\left(v_0^2+w_0^2+4v_0w_0\right)\\
&\quad \pm 3\left(v_0w_0-\mathbf{w}^2\right)\sqrt{v_0^2-\mathbf{w}^2}\,\sqrt{w_0^2-\mathbf{w}^2}\Big]\,,\\
C^{\frac{3}{2}\pm}_{p,38} &= \frac{\mathbf{w}^2(v_0-w_0)^2}{3\sqrt{2}\sqrt{v_0^2-\mathbf{w}^2}^3\,\sqrt{w_0^2-\mathbf{w}^2}^3}\Big[\pm\sqrt{v_0^2-\mathbf{w}^2}\,\sqrt{w_0^2-\mathbf{w}^2}-2\left(v_0w_0-\mathbf{w}^2\right)\Big]\,,\\
C^{\frac{3}{2}\pm}_{p,47} &= -C^{\frac{3}{2}\mp}_{p,38}\,,\qquad C^{\frac{3}{2}\pm}_{p,48}=C^{\frac{3}{2}\mp}_{p,37}\,,\\
C^{\frac{3}{2}\pm}_{p,78} &= \frac{i\sqrt{\mathbf{w}^2}(v_0-w_0)}{6\sqrt{v_0^2-\mathbf{w}^2}^3\,\sqrt{w_0^2-\mathbf{w}^2}^3}\Big[3\left(v_0^2w_0^2+\mathbf{w}^4\right)+\mathbf{w}^2\left(v_0^2+w_0^2-8v_0w_0\right)\Big]\,.
\end{aligned}\tag{A.9}$$

A.3 Vacuum master loop functions

The free space loop matrix $J^{(p,q)}_{ij,V}(v,u)$ (2.41) is composed from thirteen vacuum master loop functions $J^H_i(v,u)$ in terms of the six non-vanishing $J^V_i(w)$ given by (2.52). Based on the definition (2.40) and the representation of the thirteen independent scalar loop function kernels for the imaginary part in terms of $(l\cdot\hat{w})$ and $(l\cdot X)$ (for notation see Appendix A.1),

$$\begin{aligned}
K_0 &= 1,\\
K_1 &= (l\cdot\hat{w}),\\
K_2 &= -(l\cdot X),\\
K_3 &= \frac{1}{2}\left(l^2-(l\cdot\hat{w})^2+(l\cdot X)^2\right),\\
K_4 &= (l\cdot\hat{w})^2,\\
K_5 &= (l\cdot X)^2,\\
K_6 &= -(l\cdot X)(l\cdot\hat{w}),\\
K_7 &= \frac{1}{2}\left(l^2-(l\cdot\hat{w})^2+(l\cdot X)^2\right)(l\cdot\hat{w}),\\
K_8 &= -\frac{1}{2}\left(l^2-(l\cdot\hat{w})^2+(l\cdot X)^2\right)(l\cdot X),\\
K_9 &= (l\cdot\hat{w})^3,\\
K_{10} &= -(l\cdot\hat{w})^2(l\cdot X),\\
K_{11} &= -(l\cdot X)^3,\\
K_{12} &= (l\cdot\hat{w})(l\cdot X)^2
\end{aligned}\tag{A.10}$$

we derive the vacuum master loop functions $J^H_i(v,u)$ by expanding the corresponding structures to (A.10) – $(\breve{l}\cdot\hat{v})$ and $(\breve{l}\cdot X(v,u))$ – from (2.40) with $\breve{l}_\mu = l_\mu - \Sigma_V u_\mu$ in terms of $(l\cdot\hat{v})$ and $l\cdot X(v,u)$. In order to identify the vacuum loops $J^V_i(w)$ in the latter expressions we use the following simple algebra identities:

$$\begin{array}{rcl}
l_\mu & \to & K_1 \hat{w}_\mu + K_2 X_\mu, \\
l_\mu l_\nu & \to & K_3 T_{\mu\nu} + K_4 \hat{w}_\mu \hat{w}_\nu + K_5 X_\mu X_\nu + K_6 \left(\hat{w}_\mu X_\nu + X_\mu \hat{w}_\nu \right), \\
l_\mu l_\alpha l_\nu & \to & K_7 \left(T_{\mu\nu} \hat{w}_\alpha + T_{\mu\alpha} \hat{w}_\nu + \hat{w}_\mu T_{\alpha\nu} \right) + K_8 \left(T_{\mu\nu} X_\alpha + T_{\mu\alpha} X_\nu + X_\mu T_{\alpha\nu} \right) \\
 & & + K_9 \hat{w}_\mu \hat{w}_\alpha \hat{w}_\nu + K_{10} \left(\hat{w}_\mu X_\alpha \hat{w}_\nu + X_\mu \hat{w}_\alpha \hat{w}_\nu + \hat{w}_\mu \hat{w}_\alpha X_\nu \right) \\
 & & K_{11} X_\nu X_\alpha X_\nu + K_{12} \left(X_\mu \hat{w}_\alpha X_\nu + \hat{w}_\mu X_\alpha X_\nu + X_\mu X_\alpha \hat{w}_\nu \right)
\end{array} \qquad \text{(A.11)}$$

with

$$T_{\mu\nu} = g_{\mu\nu} - \hat{w}_\mu \hat{w}_\nu + X_\mu X_\nu . \qquad \text{(A.12)}$$

Note that expressions (A.11) further simplify because of the vanishing $J_2 = J_6 = J_8 = J_{10} = J_{11} = 0$ in the vacuum. Finally we obtain

$$\begin{array}{rcl}
J_0^H(v,u) & = & J_0^V , \\
J_1^H(v,u) & = & -\Sigma_V \dfrac{(v \cdot u)}{\sqrt{v^2}} J_0^V + \dfrac{(v \cdot w)}{\sqrt{v^2}\sqrt{w^2}} J_1^V , \\
J_2^H(v,u) & = & \Sigma_V \sqrt{\dfrac{(v \cdot u)^2 - v^2}{v^2}} J_0^V - \dfrac{(X \cdot w)}{\sqrt{w^2}} J_1^V , \\
J_3^H(v,u) & = & J_3^V , \\
J_4^H(v,u) & = & \Sigma_V^2 \dfrac{(v \cdot u)^2}{v^2} J_0^V - 2\Sigma_V \dfrac{(v \cdot u)(v \cdot w)}{\sqrt{w^2} v^2} J_1^V \\
 & & + \dfrac{v^2 w^2 - (v \cdot w)^2}{v^2 w^2} J_3^V + \dfrac{(v \cdot w)^2}{v^2 w^2} J_4^V , \\
J_5^H(v,u) & = & \Sigma_V^2 \dfrac{(v \cdot u)^2 - v^2}{v^2} J_0^V - 2\Sigma_V \sqrt{\dfrac{(v \cdot u)^2 - v^2}{v^2}} \dfrac{(X \cdot w)}{\sqrt{w^2}} J_1^V \\
 & & - \left(1 + \dfrac{(X \cdot w)^2}{w^2} \right) J_3^V + \dfrac{(X \cdot w)^2}{w^2} J_4^V , \\
J_6^H(v,u) & = & -\Sigma_V^2 \dfrac{(v \cdot u)}{\sqrt{v^2}} \sqrt{\dfrac{(v \cdot u)^2 - v^2}{v^2}} J_0^V + \dfrac{(X \cdot w)(v \cdot w)}{\sqrt{v^2} w^2} \left(J_3^V - J_4^V \right) \\
 & & -\Sigma_V \dfrac{v^2 \left((v \cdot w) + (v \cdot u)(w \cdot u) \right) - 2(v \cdot u)^2 (v \cdot w)}{\sqrt{(v \cdot u)^2 - v^2} \sqrt{w^2} v^2} J_1^V , \\
J_7^H(v,u) & = & -\Sigma_V \dfrac{(v \cdot u)}{\sqrt{v^2}} J_3^V + \dfrac{(v \cdot w)}{\sqrt{v^2}\sqrt{w^2}} J_7^V , \\
J_8^H(v,u) & = & \Sigma_V \sqrt{\dfrac{(v \cdot u)^2 - v^2}{v^2}} J_3^V - \dfrac{(X \cdot w)}{\sqrt{w^2}} J_7^V ,
\end{array}$$

(A.13)

$$\begin{aligned}
J_9^H(v,u) &= -\Sigma_V^3 \frac{(v\cdot u)^3}{\sqrt{v^2}^3} J_0^V - 2\Sigma_V^2 \frac{(v\cdot u)^2}{v^2} J_1^H - 3\Sigma_V \frac{(v\cdot u)}{\sqrt{v^2}} J_4^H \\
&\quad -3 \frac{(v\cdot w)}{\sqrt{v^2}\sqrt{w^2}} \frac{(v\cdot w)^2 - v^2 w^2}{v^2 w^2} J_7^V + \frac{(v\cdot w)^3}{\sqrt{v^2}^3 \sqrt{w^2}^3} J_9^V\,, \\
J_{10}^H(v,u) &= -\Sigma_V^2 \frac{(v\cdot u)^2}{v^2} J_2^H - 2\Sigma_V \frac{(v\cdot u)}{\sqrt{v^2}} J_6^H \\
&\quad +\Sigma_V \sqrt{\frac{(v\cdot u)^2 - v^2}{v^2}} \left(\frac{v^2 w^2 - (v\cdot w)^2}{v^2 w^2} J_3^V + \frac{(v\cdot w)^2}{v^2 w^2} J_4^V \right) \\
&\quad + \frac{3(v\cdot w)^2 - v^2 w^2}{v^2 w^2} \frac{(X\cdot w)}{\sqrt{w^2}} J_7^V - \frac{(v\cdot w)^2}{v^2 w^2} \frac{(X\cdot w)}{\sqrt{w^2}} J_9^V\,, \\
J_{11}^H(v,u) &= \Sigma_V^3 \sqrt{\frac{(v\cdot u)^2 - v^2}{v^2}}^3 J_0^V - 3\Sigma_V^2 \frac{(v\cdot u)^2 - v^2}{v^2} J_2^H \\
&\quad +3\Sigma_V \sqrt{\frac{(v\cdot u)^2 - v^2}{v^2}} J_5^H + 3\left(1 + \frac{(X\cdot w)^2}{w^2}\right) \frac{(X\cdot w)}{\sqrt{w^2}} J_7^V \\
&\quad - \frac{(X\cdot w)^3}{\sqrt{w^2}^3} J_9^V\,, \\
J_{12}^H(v,u) &= 2\Sigma_V \sqrt{\frac{(v\cdot u)^2 - v^2}{v^2}} J_6^H - \Sigma_V^2 \frac{(v\cdot u)^2 - v^2}{v^2} J_1^H \\
&\quad +\Sigma_V \frac{(v\cdot u)}{\sqrt{v^2}} \left(\frac{w^2 + (X\cdot w)^2}{w^2} J_3^V - \frac{(X\cdot w)^2}{w^2} J_4^V \right) \\
&\quad + \frac{(v\cdot w)(X\cdot w)^2}{\sqrt{v^2}\sqrt{w^2}^3} J_9^V - \left(1 + 3\frac{(X\cdot w)^2}{w^2}\right) \frac{(v\cdot w)}{\sqrt{v^2}\sqrt{w^2}} J_7^V\,. \qquad \text{(A.14)}
\end{aligned}$$

and for $X_\mu = X_\mu(v,u)$ see (A.1). Note that the complete free-space loop matrix $J_{ij}^{(p,q),\mathrm{vac}}(v,u)$ in (2.41) can also be derived by applying the recoupling procedure described in Section 2.2.2 to the full vacuum loop matrix in the basis of $P_{ij}(w,u)$, etc. By construction the sums in (2.40) do not depend on Σ_V explicitly and there are no kinematical singularities at $v^2 = 0$.

A.4 Matrix elements vacuum loop functions

The vacuum loop functions $J_{ij,V}^{(p,q)}(v,u)$ are composed from the same algebra of the preceding Section A.5, but we have to substitute $J_i \to J_i^H$ and $m_N^* \to m_N$. The additional terms $\Delta J_{ij,V}^{(p,q)}$ arising from the definition (2.40) in the nuclear matter rest frame read

$$\Delta J_{11,V}^{(p)} = \frac{v_0}{\sqrt{v^2}} J_0^H\,, \qquad \Delta J_{12,V}^{(p)} = i\sqrt{\frac{v_0^2}{v^2} - 1}\, J_0^H\,,$$

$$\Delta J_{13,V}^{(p)} = \Delta J_{24,V}^{(p)} = -\frac{1}{\sqrt{3}}\sqrt{\frac{v_0^2}{v^2} - 1}\, J_2^H\,, \qquad \Delta J_{14,V}^{(p)} = \frac{i}{\sqrt{3}} \frac{v_0}{\sqrt{v^2}} J_2^H\,,$$

$$
\begin{aligned}
\Delta J^{(p)}_{15,V} &= \frac{v_0}{\sqrt{v^2}}\Big(\sqrt{w^2}J^H_0 - J^H_1\Big), &\qquad \Delta J^{(p)}_{16,V} &= \Delta J^{(p)}_{25,V} = i\sqrt{\frac{v_0^2}{v^2}-1}\Big(\sqrt{w^2}J^H_0 - J^H_1\Big),\\
\Delta J^{(p)}_{17,V} &= -i\sqrt{\frac{2}{3}}\frac{v_0}{\sqrt{v^2}}J^H_2, &\qquad \Delta J^{(p)}_{18,V} &= \Delta J^{(p)}_{27,V} = \sqrt{\frac{2}{3}}\sqrt{\frac{v_0^2}{v^2}-1}\,J^H_2,\\
\Delta J^{(p)}_{22,V} &= -\frac{v_0}{\sqrt{v^2}}J^H_0, &\qquad \Delta J^{(p)}_{23,V} &= -\frac{i}{\sqrt{3}}\frac{v_0}{\sqrt{v^2}}J^H_2,\\
\Delta J^{(p)}_{26,V} &= -\frac{v_0}{\sqrt{v^2}}\Big(\sqrt{w^2}J^H_0 - J^H_1\Big), &\qquad \Delta J^{(p)}_{28,V} &= i\sqrt{\frac{2}{3}}\frac{v_0}{\sqrt{v^2}}J^H_2,
\end{aligned}
\tag{A.15}
$$

$$
\begin{aligned}
\Delta J^{(p)}_{33,V} &= -\frac{1}{3}\frac{v_0}{\sqrt{v^2}}\Big(2J^H_3 - J^H_5\Big),\\
\Delta J^{(p)}_{34,V} &= -\frac{i}{3}\sqrt{\frac{v_0^2}{v^2}-1}\Big(2J^H_3 + J^H_5\Big),\\
\Delta J^{(p)}_{35,V} &= \Delta J^{(p),V}_{46} = -\frac{1}{\sqrt{3}}\sqrt{\frac{v_0^2}{v^2}-1}\Big(\sqrt{w^2}J^H_2 - J^H_6\Big),\\
\Delta J^{(p)}_{36,V} &= -\frac{i}{\sqrt{3}}\frac{v_0}{\sqrt{v^2}}\Big(\sqrt{w^2}J^H_2 - J^H_6\Big),\\
\Delta J^{(p)}_{37,V} &= \Delta J^{(p),V}_{48} = -i\frac{\sqrt{2}}{3}\sqrt{\frac{v_0^2}{v^2}-1}\,\Big(J^H_3 - J^H_5\Big),\\
\Delta J^{(p)}_{38,V} &= -\frac{\sqrt{2}}{3}\frac{v_0}{\sqrt{v^2}}\Big(J^H_3 + J^H_5\Big),\\
\Delta J^{(p)}_{44,V} &= \frac{1}{3}\frac{v_0}{\sqrt{v^2}}\Big(2J^H_3 - J^H_5\Big),\\
\Delta J^{(p)}_{45,V} &= \frac{i}{\sqrt{3}}\frac{v_0}{\sqrt{v^2}}\Big(\sqrt{w^2}J^H_2 - J^H_6\Big),\\
\Delta J^{(p)}_{47,V} &= \frac{\sqrt{2}}{3}\frac{v_0}{\sqrt{v^2}}\Big(J^H_3 + J^H_5\Big),\\
\Delta J^{(p)}_{55,V} &= \frac{v_0}{\sqrt{v^2}}\Big(v^2J^H_0 - 2\sqrt{w^2}J^H_1 + J^H_4\Big),\\
\Delta J^{(p)}_{56,V} &= i\sqrt{\frac{v_0^2}{v^2}-1}\Big(v^2J^H_0 - 2\sqrt{w^2}J^H_1 + J^H_4\Big),\\
\Delta J^{(p)}_{57,V} &= -i\sqrt{\frac{2}{3}}\frac{v_0}{\sqrt{v^2}}\Big(\sqrt{w^2}J^H_2 - J^H_6\Big),\\
\Delta J^{(p)}_{58,V} &= \Delta J^{(p)}_{67} = \sqrt{\frac{2}{3}}\sqrt{\frac{v_0^2}{v^2}-1}\Big(\sqrt{w^2}J^H_2 - J^H_6\Big),\\
\Delta J^{(p)}_{66,V} &= -\frac{v_0}{\sqrt{v^2}}\Big(v^2J^H_0 - 2\sqrt{w^2}J^H_1 + J^H_4\Big),\\
\Delta J^{(p)}_{68,V} &= i\sqrt{\frac{2}{3}}\frac{v_0}{\sqrt{v^2}}\Big(\sqrt{w^2}J^H_2 - J^H_6\Big),
\end{aligned}
$$

$$
\begin{aligned}
\Delta J^{(p)}_{77,V} &= \frac{1}{3}\frac{v_0}{\sqrt{v^2}}\Big(J_3^H - 2J_5^H\Big),\\
\Delta J^{(p)}_{78,V} &= -\frac{i}{3}\sqrt{\frac{v_0^2}{v^2}-1}\Big(J_3^H + 2J_5^H\Big),\\
\Delta J^{(p)}_{88,V} &= -\frac{1}{3}\frac{v_0}{\sqrt{v^2}}\Big(J_3^H - 2J_5^H\Big)
\end{aligned}
\tag{A.16}
$$

and

$$
\Delta J^{(q)}_{11,V} = \frac{v_0}{\sqrt{v^2}}J_3^H, \qquad \Delta J^{(q)}_{12,V} = i\sqrt{\frac{v_0^2}{v^2}-1}J_3^H, \qquad \Delta J^{(q)}_{22,V} = -\frac{v_0}{\sqrt{v^2}}J_3^H. \tag{A.17}
$$

A.5 Matrix elements loop functions

The loop matrix $J^{(p,q)}_{ij}(v,u)$ as introduced in (2.37) in terms of $v = w - \Sigma_0 u$ and with $m_N^* = m_N + \Sigma_S$ are listed below. They enjoy the symmetry relation $J^{(p,q)}_{ij}(v,u) = J^{(p,q)}_{ji}(v,u)$ and are determined by thirteen master loop functions $J_i(v,u)$ introduced in (2.45).

$$
\begin{aligned}
J^{(p)}_{11} &= m_N^* J_0 + J_1, & J^{(p)}_{12} &= -iJ_2,\\
J^{(p)}_{13} &= J^{(p)}_{24} = -\frac{1}{\sqrt{3}}\left(2J_3 - J_5\right), & J^{(p)}_{18} &= J^{(p)}_{27} = -\sqrt{\frac{2}{3}}\left(J_3 + J_5\right),\\
J^{(p)}_{14} &= \frac{i}{\sqrt{3}}\left(m_N^* J_2 + J_6\right), & J^{(p)}_{17} &= -i\sqrt{\frac{2}{3}}\left(m_N^* J_2 + J_6\right),\\
J^{(p)}_{15} &= -\Big[\Big(m_N^* - \sqrt{v^2}\Big)J_1 + J_4 - m_N^*\sqrt{v^2}J_0\Big], &&\\
J^{(p)}_{26} &= -\Big[\Big(m_N^* + \sqrt{v^2}\Big)J_1 - J_4 - m_N^*\sqrt{v^2}J_0\Big], &&\\
J^{(p)}_{16} &= J^{(p)}_{25} = i\left(J_6 - \sqrt{v^2}J_2\right), &&\\
J^{(p)}_{22} &= m_N^* J_0 - J_1, &&\\
J^{(p)}_{23} &= \frac{i}{\sqrt{3}}\left(m_N^* J_2 - J_6\right), &&\\
J^{(p)}_{28} &= -i\sqrt{\frac{2}{3}}\left(m_N^* J_2 - J_6\right), &&
\end{aligned}
\tag{A.18}
$$

$$
\begin{aligned}
J_{33}^{(p)} &= \frac{1}{3}\left(m_N^*\left(2J_3 - J_5\right) + J_{12} - 2J_7\right),\\
J_{34}^{(p)} &= -\frac{i}{3}\left(2J_8 - J_{11}\right),\\
J_{35}^{(p)} &= J_{46}^{(p)} = \frac{1}{\sqrt{3}}\left(2J_7 - J_{12} - \sqrt{v^2}\left(2J_3 - J_5\right)\right),\\
J_{36}^{(p)} &= -\frac{i}{\sqrt{3}}\left(\left(m_N^* + \sqrt{v^2}\right)J_6 - J_{10} - m_N^*\sqrt{v^2}J_2\right),\\
J_{37}^{(p)} &= J_{48}^{(p)} = \frac{i}{3}\sqrt{2}\left(2J_8 - J_{11}\right),\\
J_{38}^{(p)} &= \frac{\sqrt{2}}{3}\left(m_N^*\left(J_3 + J_5\right) - J_7 - J_{12}\right),\\
J_{44}^{(p)} &= \frac{1}{3}\left(m_N^*\left(2J_3 - J_5\right) - J_{12} + 2J_7\right),\\
J_{45}^{(p)} &= -\frac{i}{\sqrt{3}}\left(\left(m_N^* - \sqrt{v^2}\right)J_6 + J_{10} - m_N^*\sqrt{v^2}J_2\right),\\
J_{47}^{(p)} &= \frac{\sqrt{2}}{3}\left(m_N^*\left(J_3 + J_5\right) + J_7 + J_{12}\right),\\
J_{55}^{(p)} &= \left(m_N^* - 2\sqrt{v^2}\right)J_4 + J_9 + m_N^* v^2 J_0 + \left(v^2 - 2m_N^*\sqrt{v^2}\right)J_1,\\
J_{56}^{(p)} &= -i\left(J_{10} - 2\sqrt{v^2}J_6 + v^2 J_2\right),\\
J_{57}^{(p)} &= i\sqrt{\frac{2}{3}}\left(\left(m_N^* - \sqrt{v^2}\right)J_6 + J_{10} - m_N^*\sqrt{v^2}J_2\right),\\
J_{58}^{(p)} &= J_{67}^{(p)} = \sqrt{\frac{2}{3}}\left(J_7 + J_{12} - \sqrt{v^2}\left(J_3 + J_5\right)\right),\\
J_{66}^{(p)} &= \left(m_N^* + 2\sqrt{v^2}\right)J_4 - J_9 + m_N^* v^2 J_0 - \left(v^2 + 2m_N^*\sqrt{v^2}\right)J_1,\\
J_{68}^{(p)} &= i\sqrt{\frac{2}{3}}\left(\left(m_N^* + \sqrt{v^2}\right)J_6 - J_{10} - m_N^*\sqrt{v^2}J_2\right),\\
J_{77}^{(p)} &= \frac{1}{3}\left(m_N^*\left(J_3 - 2J_5\right) + J_7 - 2J_{12}\right),\\
J_{78}^{(p)} &= \frac{i}{3}\left(5J_8 + 2J_{11}\right),\\
J_{88}^{(p)} &= \frac{1}{3}\left(m_N^*\left(J_3 - 2J_5\right) - J_7 + 2J_{12}\right),
\end{aligned}
\tag{A.19}
$$

and

$$
J_{11}^{(q)} = m_N^* J_3 + J_7, \qquad J_{12}^{(q)} = -iJ_8, \qquad J_{22}^{(q)} = m_N^* J_3 - J_7. \tag{A.20}
$$

A.6 Renormalized scalar loop function kernels

The renormalized principal value in-medium loop function kernels $K_i^R(l, \bar{v}, v, u)$ in (2.55) are introduced as

$$
\begin{aligned}
K_0^R &= \frac{v^2}{\bar{v}^2}, \\
K_1^R &= \left(\frac{\sqrt{v^2}}{2} + \frac{(\bar{l}\cdot\bar{v})}{\sqrt{v^2}}\right)\frac{v^2}{\bar{v}^2}, \\
K_2^R &= -\frac{(v\cdot u)}{\sqrt{(v\cdot u)^2 - v^2}}\frac{(\bar{l}\cdot\bar{v})}{\sqrt{v^2}}\frac{v^2}{\bar{v}^2} + \frac{\sqrt{v^2}(\bar{l}\cdot u)}{\sqrt{(v\cdot u)^2 - v^2}}, \\
K_3^R &= \frac{1}{2}K_5^R - \frac{1}{2}\frac{v^2}{\bar{v}^2}\left(\frac{(\bar{l}\cdot\bar{v})^2}{v^2} - \bar{l}^2 - \frac{\bar{v}^2 - v^2}{4}\right), \\
K_4^R &= \left(\frac{\sqrt{v^2}}{2} + \frac{(\bar{l}\cdot\bar{v})}{\sqrt{v^2}}\right)^2\frac{v^2}{\bar{v}^2}, \\
K_5^R &= \frac{1}{(v\cdot u)^2 - v^2}\left[v^2(\bar{l}\cdot u)^2 - 2(v\cdot u)(\bar{l}\cdot\bar{v})(\bar{l}\cdot u) + (v\cdot u)^2\frac{(\bar{l}\cdot\bar{v})^2}{\bar{v}^2}\right] \\
&\quad -\frac{\bar{v}^2 - v^2}{12\bar{v}^2}v^2, \\
K_6^R &= \frac{\sqrt{v^2}}{2}K_2^R + \frac{(\bar{l}\cdot\bar{v})(\bar{l}\cdot u)}{\sqrt{(v\cdot u)^2 - v^2}} - \frac{(v\cdot u)}{\sqrt{(v\cdot u)^2 - v^2}}\frac{(\bar{l}\cdot\bar{v})^2}{\bar{v}^2}, \\
K_7^R &= \frac{1}{2}K_{12}^R + \frac{1}{2}\frac{v^2}{\bar{v}^2}\left(\bar{l}^2 + \frac{\bar{v}^2 - v^2}{4} - \frac{(\bar{l}\cdot\bar{v})^2}{v^2}\right)\left(\frac{\sqrt{v^2}}{2} + \frac{(\bar{l}\cdot\bar{v})}{\sqrt{v^2}}\right), \\
K_8^R &= \frac{1}{2}K_{11}^R + \left(\bar{l}^2 + \frac{\bar{v}^2 - v^2}{4} - \frac{(\bar{l}\cdot\bar{v})^2}{v^2}\right) \\
&\quad \times\left(-\frac{(v\cdot u)}{\sqrt{(v\cdot u)^2 - v^2}}\frac{(\bar{l}\cdot\bar{v})}{\sqrt{v^2}}\frac{v^2}{\bar{v}^2} + \frac{\sqrt{v^2}(\bar{l}\cdot u)}{\sqrt{(v\cdot u)^2 - v^2}}\right), \\
K_9^R &= \left(\frac{\sqrt{v^2}}{2} + \frac{(\bar{l}\cdot\bar{v})}{\sqrt{v^2}}\right)^3\frac{v^2}{\bar{v}^2}, \\
K_{10}^R &= -\frac{v^2}{4}\frac{v^2}{\bar{v}^2}\left(1 + 2\frac{(\bar{l}\cdot\bar{v})}{v^2} + 4\frac{(\bar{l}\cdot\bar{v})^2}{v^2 v^2}\right)\frac{(v\cdot u)}{\sqrt{(v\cdot u)^2 - v^2}}\frac{(\bar{l}\cdot\bar{v})}{\sqrt{v^2}} \\
&\quad +\frac{v^2}{4}\left(1 + 2\frac{(\bar{l}\cdot\bar{v})}{v^2} + 4\frac{(\bar{l}\cdot\bar{v})^2}{v^2 v^2}\right)\frac{\sqrt{v^2}(\bar{l}\cdot u)}{\sqrt{(v\cdot u)^2 - v^2}} \\
&\quad \frac{1}{2}\frac{\sqrt{v^2}(v\cdot u)}{\sqrt{(v\cdot u)^2 - v^2}}\left(\frac{(\bar{l}\cdot u)}{(v\cdot u)} - \frac{(\bar{l}\cdot\bar{v})}{\bar{v}^2}\right)(\bar{l}\cdot\bar{v}),
\end{aligned}
$$

$$\begin{aligned}
K^R_{11} &= \frac{\sqrt{v^2}}{\sqrt{(v\cdot u)^2 - v^2}^3}\Bigg[v^2(\bar{l}\cdot u)^3 - 3(v\cdot u)(\bar{l}\cdot u)^2(\bar{l}\cdot\bar{v})\frac{v^2}{\bar{v}^2} \\
&\quad +3(v\cdot u)^2(\bar{l}\cdot u)\frac{(\bar{l}\cdot\bar{v})^2}{v^2} - \frac{(v\cdot u)^3}{v^2}\frac{(\bar{l}\cdot\bar{v})^3}{\bar{v}^2}\Bigg], \\
K^R_{12} &= \frac{1}{(v\cdot u)^2 - v^2}\Bigg[\left(\frac{\sqrt{v^2}}{2} + \frac{(\bar{l}\cdot\bar{v})}{\sqrt{v^2}}\right)\frac{v^2}{\bar{v}^2}v^2(\bar{l}\cdot u)^2 \\
&\quad -2\left(\frac{\sqrt{v^2}}{2} + \sqrt{v^2}\frac{(\bar{l}\cdot\bar{v})}{v^2}\right)(v\cdot u)(\bar{l}\cdot u)(\bar{l}\cdot\bar{v}) \\
&\quad \left(\frac{\sqrt{v^2}}{2} + \frac{(\bar{l}\cdot\bar{v})}{\sqrt{v^2}}\right)(v\cdot u)^2\frac{(\bar{l}\cdot\bar{v})^2}{\bar{v}^2}\Bigg]
\end{aligned} \tag{A.21}$$

with the new variable

$$\bar{l}_\mu = l_\mu - \frac{\bar{v}_\mu}{2} \qquad \text{and} \qquad \bar{v}^2 = (\bar{v}\cdot u)^2 - (v\cdot u)^2 + v^2. \tag{A.22}$$

A.7 Subtraction terms

The subtraction terms J^C_i in (2.54) are decomposed with respect to internal and external variables $\bar{v}$ and v, while the dependence on $\bar{v}$ is shifted to the coefficients $C^{ijk}_{a,n}(\mathbf{w})$ defined by (2.57) and (2.61). They depend on three-momentum $\mathbf{w}$ exclusively after integrating over the internal energy $\bar{v}_0$ and thus the energy dependence of J^C_i is trivially given by v_0. In detail we derive

$$\begin{aligned}
J^C_0 &= (v\cdot u)C^{000}_{0,1}, \\
J^C_1 &= \frac{(v\cdot u)}{2\sqrt{v^2}}\left(v^2 C^{000}_{0,1} + 2C^{100}_{0,1}\right), \\
J^C_2 &= -\frac{(v\cdot u)^2}{\sqrt{v^2}\sqrt{(v\cdot u)^2 - v^2}}C^{100}_{0,1}, \\
J^C_3 &= \frac{1}{2}J^C_5 + 2\left((v\cdot u)C^{200}_{0,2} + C^{200}_{+1,2}\right), \\
J^C_4 &= \frac{(v\cdot u)}{4}\left(v^2 C^{000}_{0,1} + 4C^{100}_{0,1}\right), \\
J^C_5 &= \frac{2(v\cdot u)}{(v\cdot u)^2 - v^2}C^{110}_{-1,0},
\end{aligned}$$

$$
\begin{aligned}
J_6^C &= \frac{\sqrt{v^2}}{2} J_2^C - \frac{1}{\sqrt{(v\cdot u)^2 - v^2}} C^{110}_{-1,0}, \\
J_7^C &= \frac{1}{2} J_{12}^C - \frac{1}{16\sqrt{v^2}} \Big[-8C^{300}_{+1,2} + v^2 \Big(v^2 \Big(C^{000}_{+1,1} + 4C^{001}_{+1,2} - 16C^{200}_{+1,3} \Big) \\
&\quad + (v\cdot u) \Big(v^2 C^{000}_{0,1} + 2\Big(C^{100}_{0,1} - 2C^{200}_{0,2} + 8C^{300}_{0,3} \Big)\Big) \\
&\quad + 2\Big(C^{100}_{+1,1} + 4\Big(C^{101}_{+1,2} - 2\Big(C^{200}_{+1,2} + C^{300}_{+1,3} \Big)\Big)\Big)\Big)\Big], \\
J_8^C &= \frac{1}{2} J_{11}^C - \frac{1}{24\sqrt{v^2}\sqrt{(v\cdot u)^2 - v^2}} \Big[v^2 \Big(3C^{010}_{+1,0} + 12C^{011}_{+1,1} + 8C^{210}_{+1,2} \Big) \\
&\quad - 12C^{210}_{+1,1} - (v\cdot u)^2 \Big(3v^2 C^{100}_{0,1} + 8C^{300}_{0,2} \Big) \\
&\quad + (v\cdot u) \Big(12\Big(-C^{210}_{0,1} + C^{300}_{+1,2} \Big) + v^2 \Big(3C^{010}_{0,0} + 12C^{011}_{0,1} \\
&\quad - 3C^{100}_{+1,1} - 12C^{101}_{+1,2} + 8C^{210}_{0,2} - 8C^{300}_{+1,3} \Big)\Big)\Big], \\
J_9^C &= -\frac{1}{8\sqrt{v^2}} \Big[-(v\cdot u) v^2 \left(v^2 C^{000}_{0,1} + 6C^{100}_{0,1} \right) + 16(v\cdot u) C^{300}_{0,2} + 8C^{300}_{+1,2} \Big], \\
J_{10}^C &= -\frac{1}{12\sqrt{v^2}\sqrt{(v\cdot u)^2 - v^2}} \Bigg[6v^2 \Big(C^{110}_{-1,0} + C^{110}_{+1,1} \Big) + 12C^{210}_{+1,1} \\
&\quad + 16v^2 C^{210}_{+1,2} + (v\cdot u)^2 \Big(3v^2 C^{100}_{0,1} - 16C^{300}_{0,2} \Big) + 2(v\cdot u) \Big(6\Big(C^{210}_{0,1} - C^{300}_{+1,2} \Big) \\
&\quad + v^2 \Big(3C^{110}_{0,1} - 3C^{200}_{+1,2} + 8C^{210}_{0,2} - 8C^{300}_{+1,3} \Big)\Big) \Bigg], \\
J_{11}^C &= -\frac{1}{\sqrt{v^2}\sqrt{(v\cdot u)^2 - v^2}^{\,3}} \Big[-2(v\cdot u)(v^2)^2 C^{210}_{0,2} + 2(v^2)^2 C^{210}_{+1,2} \\
&\quad + (v\cdot u)^2 \Big(3v^2 C^{120}_{0,1} + 3C^{210}_{+1,1} - 2v^2 C^{210}_{+1,2} \Big) \\
&\quad + (v\cdot u)^3 \Big(3C^{210}_{0,1} + 2v^2 C^{210}_{0,2} - C^{300}_{+1,2} \Big)\Big], \\
J_{12}^C &= \frac{1}{6\sqrt{v^2}((v\cdot u)^2 - v^2)} \Bigg[(v\cdot u) \Bigg(12C^{210}_{+1,1} + v^2 \Bigg(3v^2 \Big(C^{020}_{0,1} - C^{110}_{-1,1} \Big) \\
&\quad + 6\Big(C^{110}_{-1,0} + C^{120}_{0,1} \Big) + 4C^{210}_{+1,2} \Bigg)\Bigg) + (v\cdot u)^3 \Bigg(3v^2 C^{-1,1}_{110} - 4C^{300}_{0,2} \Bigg) \\
&\quad + (v\cdot u)^2 \Big(12C^{210}_{0,1} - 6C^{300}_{+1,2} + v^2 \Big(3C^{110}_{0,1} - 3C^{200}_{+1,2} + 12C^{210}_{0,2} - 8C^{300}_{+1,3} \Big)\Big) \\
&\quad + (v^2)^2 \Big(-3C^{110}_{0,1} + 6C^{200}_{+1,2} - 8C^{210}_{0,2} + 4C^{300}_{+1,3} \Big) \Bigg]. \qquad \text{(A.23)}
\end{aligned}
$$

A.8 Renormalized scalar loop function kernels for low three-momenta w

For sufficiently low three-momenta $\mathbf{w}$ the loop functions $J_i^M(v_0, \mathbf{w})$ are defined by

$$J_i^M(v_0, \mathbf{w}) = \int_{-\infty}^{+\infty} \frac{d\bar{v}_0}{\pi} \frac{\mathrm{sign}(\bar{v}_0 - \mu)\, \mathfrak{Im} J_i^M(v_0, \bar{v}_0, \mathbf{w})}{\bar{v}_0 - v_0 - i\varepsilon(\bar{v}_0 - \mu)} \tag{A.24}$$

with the imaginary part analogous to (2.55)

$$\begin{aligned}
\mathfrak{Im} J_i^M(v_0, \bar{v}_0, \mathbf{w}) &= \int \frac{d^3 l}{2(2\pi)^3} \frac{1}{E_N^*} \\
&\quad \times \Big\{ K_i^M(l_+, v_0, \bar{v}_0, \mathbf{w}) \rho_K(\bar{v}_+, \mathbf{w} - \mathbf{l}) \left[\Theta(+\bar{v}_+) - \Theta(k_F - |\mathbf{l}|)\right] \\
&\quad + K_i^M(l_-, v_0, \bar{v}_0, \mathbf{w}) \rho_K(\bar{v}_-, \mathbf{w} - \mathbf{l}) \Theta(-\bar{v}_-) \Big\}, \\
l_\pm^\mu &= (\pm E_N^*, \mathbf{l}), \\
\bar{v}_\pm &= \bar{v}_0 \mp E_N^*.
\end{aligned} \tag{A.25}$$

The thirteen renormalized in-medium loop function kernels $K_i^M(l_\pm, v_0, \bar{v}_0, \mathbf{w})$ can be summarized from (A.21) and (A.23) and read:

$$\begin{aligned}
K_0^M &= 1 - \frac{(\bar{v} \cdot u)}{\bar{v}^2} \left[(\bar{v} \cdot u) - (v \cdot u)\right], \\
K_1^M &= \left(\frac{\sqrt{v^2}}{2} + \frac{(\bar{l} \cdot \bar{v})}{\sqrt{v^2}} \right) \left(1 - \frac{(\bar{v} \cdot u)}{\bar{v}^2} \left[(\bar{v} \cdot u) - (v \cdot u)\right] \right), \\
K_2^M &= -\frac{(v \cdot u)}{\sqrt{(v \cdot u)^2 - v^2}} \frac{(\bar{l} \cdot \bar{v})}{\sqrt{v^2}} \left(1 - \frac{(\bar{v} \cdot u)}{\bar{v}^2} \left[(\bar{v} \cdot u) - (v \cdot u)\right] \right) \\
&\quad + \frac{\sqrt{v^2}(\bar{l} \cdot u)}{\sqrt{(v \cdot u)^2 - v^2}}, \\
K_3^M &= \frac{1}{2} K_5^M - \frac{1}{2} \frac{v^2}{\bar{v}^2} \left(\frac{(\bar{l} \cdot \bar{v})^2}{v^2} - \bar{l}^2 - \frac{\bar{v}^2 - v^2}{4} \right) + 2 \frac{\bar{v}^2 - v^2}{\bar{v}^2} \frac{(\bar{l} \cdot \bar{v})^2}{\bar{v}^2}, \\
K_4^M &= \left(\frac{\sqrt{v^2}}{2} + \frac{(\bar{l} \cdot \bar{v})}{\sqrt{v^2}} \right) K_1^M - \frac{(\bar{l} \cdot \bar{v})^2}{\bar{v}^2} \frac{(v \cdot u)}{v^2} \left[(\bar{v} \cdot u) - (v \cdot u)\right],
\end{aligned}$$

$$
\begin{aligned}
K_5^M &= \frac{1}{(v\cdot u)^2 - v^2}\left[v^2(\bar{l}\cdot u)^2 - 2\frac{(v\cdot u)^2}{(\bar{v}\cdot u)}(\bar{l}\cdot\bar{v})(\bar{l}\cdot u) + (v\cdot u)^2\frac{(\bar{l}\cdot\bar{v})^2}{\bar{v}^2}\right] \\
&\quad -\frac{\bar{v}^2 - v^2}{12\bar{v}^2}v^2, \\
K_6^M &= \frac{\sqrt{v^2}}{2}K_2^M + \frac{(\bar{l}\cdot\bar{v})(\bar{l}\cdot u)}{\sqrt{(v\cdot u)^2 - v^2}}\frac{(v\cdot u)}{(\bar{v}\cdot u)} - \frac{(v\cdot u)}{\sqrt{(v\cdot u)^2 - v^2}}\frac{(\bar{l}\cdot\bar{v})^2}{\bar{v}^2}, \\
K_7^M &= \frac{1}{2}K_{12}^M + \frac{1}{2}\frac{v^2}{\bar{v}^2}\left(\bar{l}^2 - \frac{(\bar{l}\cdot\bar{v})^2}{\bar{v}^2}\right)K_1^M + \frac{3}{4}\sqrt{v^2}\left(1 - K_0^M\right)\frac{\bar{v}^2 + v^2}{\bar{v}^2}\frac{(\bar{l}\cdot\bar{v})^2}{\bar{v}^2} \\
&\quad +\frac{1}{2}\sqrt{v^2}\frac{\bar{v}^2 - v^2}{\bar{v}^2}\frac{(\bar{l}\cdot\bar{v})^3}{\bar{v}^2\bar{v}^2} - \frac{1}{2}\frac{(v\cdot u)}{\sqrt{v^2}}\frac{(\bar{v}\cdot u) - (v\cdot u)}{\bar{v}^2}\left(1 + 3\frac{v^2}{\bar{v}^2}\right)\frac{(\bar{l}\cdot\bar{v})^3}{\bar{v}^2}, \\
K_8^M &= \frac{1}{2}K_{11}^M + \frac{1}{2}\frac{v^2}{\bar{v}^2}\left(\bar{l}^2 - \frac{(\bar{l}\cdot\bar{v})^2}{v^2}\right)K_2^M - \frac{1}{3}\frac{\bar{v}^2 - v^2}{\bar{v}^2}\frac{(\bar{l}\cdot\bar{v})^2}{\bar{v}^2}K_2^M, \\
K_9^M &= \left(\frac{\sqrt{v^2}}{2} + \frac{(\bar{l}\cdot\bar{v})}{\sqrt{v^2}}\right)^2 K_1^M - \frac{3}{2}\frac{(v\cdot u)}{\sqrt{v^2}}\left[(\bar{v}\cdot u) - (v\cdot u)\right]\frac{(\bar{l}\cdot\bar{v})^2}{\bar{v}^2} \\
&\quad +\frac{1}{\sqrt{v^2}}\left(\frac{v^2 - \bar{v}^2}{v^2}K_0^M - 2(v\cdot u)\frac{(\bar{v}\cdot u) - (v\cdot u)}{\bar{v}^2}\right)\frac{(\bar{l}\cdot\bar{v})^3}{\bar{v}^2}, \\
K_{10}^M &= \frac{v^2}{4}\left(1 + 2\frac{(\bar{l}\cdot\bar{v})}{\bar{v}^2} + 4\frac{(\bar{l}\cdot\bar{v})^2}{\bar{v}^2\bar{v}^2}\right)K_2^M + \frac{1}{3}\frac{v^2 - \bar{v}^2}{\bar{v}^2}\frac{(\bar{l}\cdot\bar{v})^2}{\bar{v}^2}K_2^M \\
&\quad +\frac{1}{2}\frac{\sqrt{v^2}(v\cdot u)}{\sqrt{(v\cdot u)^2 - v^2}}\left(\frac{(\bar{l}\cdot u)}{(\bar{v}\cdot u)} - \frac{(\bar{l}\cdot\bar{v})}{\bar{v}^2}\right)(\bar{l}\cdot\bar{v}), \\
K_{11}^M &= \frac{\sqrt{v^2}}{\sqrt{(v\cdot u)^2 - v^2}^3}\left[v^2(\bar{l}\cdot u)^3 - 3(v\cdot u)(\bar{l}\cdot u)^2(\bar{l}\cdot\bar{v})K_0^M\right. \\
&\quad \left. +3(v\cdot u)^2(\bar{l}\cdot u)\frac{(\bar{l}\cdot\bar{v})^2}{\bar{v}^2} - \frac{(v\cdot u)^3}{v^2}\frac{(\bar{l}\cdot\bar{v})^3}{\bar{v}^2}K_0^M\right] \\
&\quad +2\frac{\sqrt{v^2}}{\sqrt{(v\cdot u)^2 - v^2}}\frac{\left[(\bar{v}\cdot u) - (v\cdot u)\right]^2}{\bar{v}^2}(\bar{l}\cdot u)\frac{(\bar{l}\cdot\bar{v})^2}{\bar{v}^2}, \\
K_{12}^M &= \frac{1}{(v\cdot u)^2 - v^2}\left[\left(\frac{\sqrt{v^2}}{2} + \frac{(\bar{l}\cdot\bar{v})}{\sqrt{v^2}}\right)K_0^M v^2(\bar{l}\cdot u)^2\right. \\
&\quad -2\left(\frac{\sqrt{v^2}}{2}\frac{(v\cdot u)}{(\bar{v}\cdot u)} - \sqrt{v^2}\left(1 - \frac{1}{3}\frac{\bar{v}^2 - v^2}{\bar{v}^2}\right)\frac{(\bar{l}\cdot\bar{v})}{\bar{v}^2}\right)(v\cdot u)(\bar{l}\cdot u)(\bar{l}\cdot\bar{v}) \\
&\quad \left. +\left(\frac{\sqrt{v^2}}{2}\left(2 - K_0^M\right) + \frac{(\bar{l}\cdot\bar{v})}{\sqrt{v^2}}\left(1 - \frac{2}{3}\frac{\bar{v}^2 - v^2}{\bar{v}^2}\right)K_0^M\right)(v\cdot u)^2\frac{(\bar{l}\cdot\bar{v})^2}{\bar{v}^2}\right] \\
&\quad -\sqrt{v^2}\left(1 - K_0^M\right)\left(1 + \frac{2}{3}\frac{(\bar{l}\cdot\bar{v})}{\bar{v}^2} - \frac{4}{3}\frac{(\bar{l}\cdot u)}{(\bar{v}\cdot u)}\right)\frac{(\bar{l}\cdot\bar{v})^2}{\bar{v}^2} \\
&\quad +\frac{\sqrt{v^2}}{2}\frac{\bar{v}^2 - v^2}{(\bar{v}\cdot u)}(\bar{l}\cdot u)\frac{(\bar{l}\cdot\bar{v})}{\bar{v}^2}
\end{aligned}
\tag{A.26}
$$

The free-space limit of expressions (A.26) can be obtained by applying the following vacuum replacement rules:

$$\begin{aligned}
(\bar{l}\cdot\bar{v}) &= \frac{m_N^2 - m_K^2}{2}, \\
(\bar{l}\cdot u) &= \frac{(\bar{v}\cdot u)}{\bar{v}^2}(\bar{l}\cdot\bar{v}), \\
(\bar{l}\cdot u)^2 &= \frac{(\bar{v}\cdot u)^2}{(\bar{v}^2)^2}(\bar{l}\cdot\bar{v})^2 + \frac{1}{3}\left(\bar{l}^2 - \frac{(\bar{l}\cdot\bar{v})}{\bar{v}^2}\right)\left(1 - \frac{(\bar{v}\cdot u)^2}{\bar{v}^2}\right), \\
(\bar{l}\cdot u)^3 &= \frac{(\bar{v}\cdot u)^3}{(\bar{v}^2)^3}(\bar{l}\cdot\bar{v})^3 + \frac{(\bar{v}\cdot u)}{\bar{v}^2}(\bar{l}\cdot\bar{v})\left(\bar{l}^2 - \frac{(\bar{l}\cdot\bar{v})}{\bar{v}^2}\right)\left(1 - \frac{(\bar{v}\cdot u)^2}{\bar{v}^2}\right)
\end{aligned} \tag{A.27}$$

and

$$\bar{l}^2 = \frac{m_N^2 + m_K^2}{2} - \frac{\bar{v}^2}{4}. \tag{A.28}$$

A.9 Self-energy

We recall the form of the invariant functions $c_{ij}^{(p,q)}(q,w,u)$:

$$\begin{aligned}
& c_{11}^{(q)} = \tfrac{1}{2}\,E_+\left(E_+\,E_- + (X\cdot q)^2\right), \quad c_{11}^{(p)} = E_+\,, \\
& c_{12}^{(q)} = -\tfrac{i}{2}\,(X\cdot q)\left(E_+\,E_- + (X\cdot q)^2\right), \quad c_{12}^{(p)} = -i\,(X\cdot q)\,, \\
& c_{22}^{(q)} = \tfrac{1}{2}\,E_-\left(E_+\,E_- + (X\cdot q)^2\right), \quad c_{22}^{(p)} = E_-\,, \\
& c_{13}^{(p)} = c_{24}^{(p)} = -\tfrac{1}{\sqrt{3}}\,E_+\,E_-\,, \quad c_{25}^{(p)} = c_{16}^{(p)} = -i\,(\hat{w}\cdot q)\,(X\cdot q)\,, \\
& c_{17}^{(p)} = -i\,\sqrt{\tfrac{2}{3}}\,E_+\,(X\cdot q)\,, \quad c_{15}^{(p)} = (\hat{w}\cdot q)\,E_+\,, \quad c_{14}^{(p)} = \tfrac{i}{\sqrt{3}}\,E_+\,(X\cdot q)\,, \\
& c_{28}^{(p)} = -i\,\sqrt{\tfrac{2}{3}}\,E_-\,(X\cdot q)\,, \quad c_{26}^{(p)} = (\hat{w}\cdot q)\,E_-\,, \quad c_{23}^{(p)} = \tfrac{i}{\sqrt{3}}\,E_-\,(X\cdot q)\,, \\
& c_{27}^{(p)} = c_{18}^{(p)} = -\sqrt{\tfrac{3}{2}}\left(\tfrac{1}{3}\,E_+\,E_- + (X\cdot q)^2\right),
\end{aligned} \tag{A.29}$$

and

$$
\begin{aligned}
& c^{(p)}_{33} = \tfrac{1}{3}\,E_-^2\,E_+\,, \quad c^{(p)}_{44} = \tfrac{1}{3}\,E_+^2\,E_-\,, \\
& c^{(p)}_{55} = E_+\,(\hat{w}\cdot q)^2\,, \quad c^{(p)}_{77} = \tfrac{1}{2}\,E_+\left(\tfrac{1}{3}\,E_+\,E_- - \big(X\cdot q\big)^2\right)\,, \\
& c^{(p)}_{66} = E_-\,(\hat{w}\cdot q)^2\,, \quad c^{(p)}_{88} = \tfrac{1}{2}\,E_-\left(\tfrac{1}{3}\,E_+\,E_- - \big(X\cdot q\big)^2\right), \\
& c^{(p)}_{35} = c^{(p)}_{46} = -\tfrac{1}{\sqrt{3}}\,(\hat{w}\cdot q)\,E_+\,E_-\,, \quad c^{(p)}_{57} = -i\,\sqrt{\tfrac{2}{3}}\,(X\cdot q)\,(\hat{w}\cdot q)\,E_+\,, \\
& c^{(p)}_{37} = c^{(p)}_{48} = i\,\frac{\sqrt{2}}{3}\,(X\cdot q)\,E_+\,E_-\,, \quad c^{(p)}_{68} = -i\,\sqrt{\tfrac{2}{3}}\,(X\cdot q)\,(\hat{w}\cdot q)\,E_-\,, \\
& c^{(p)}_{34} = -\tfrac{i}{3}\,(X\cdot q)\,E_+\,E_-\,, \quad c^{(p)}_{56} = -i\,(\hat{w}\cdot q)^2\,(X\cdot q)\,, \\
& c^{(p)}_{78} = i\,\big(X\cdot q\big)\left(\tfrac{3}{2}\,\big(X\cdot q\big)^2 + \tfrac{5}{6}\,E_+\,E_-\right)\,, \\
& c^{(p)}_{36} = \tfrac{i}{\sqrt{3}}\,(\hat{w}\cdot q)\,E_-\,(X\cdot q)\,, \quad c^{(p)}_{38} = \tfrac{1}{\sqrt{2}}\,E_-\left(\tfrac{1}{3}\,E_+\,E_- + (X\cdot q)^2\right)\,, \\
& c^{(p)}_{45} = \tfrac{i}{\sqrt{3}}\,(\hat{w}\cdot q)\,E_+\,(X\cdot q)\,, \quad c^{(p)}_{47} = \tfrac{1}{\sqrt{2}}\,E_+\left(\tfrac{1}{3}\,E_+\,E_- + (X\cdot q)^2\right)\,, \\
& c^{(p)}_{58} = c^{(p)}_{67} = -\sqrt{\tfrac{3}{2}}\,(\hat{w}\cdot q)\left(\tfrac{1}{3}\,E_+\,E_- + (X\cdot q)^2\right),
\end{aligned}
\tag{A.30}
$$

where $X_\mu = X_\mu(w,u)$ and

$$
E_\pm \equiv m_N^* \pm \big(\sqrt{w_0^2 - \mathbf{w}^{\,2}} - q\cdot\hat{w}\big)\,, \qquad E_+\,E_- = q^2 - (q\cdot\hat{w})^2\,. \tag{A.31}
$$

Appendix **B**

Appendix: Non-Local approach for kaonic atoms

B.1 Asymptotic and analytic solutions of the Klein-Gordon equation

For a spin-0 particle interacting with the electromagnetic field of the nucleus we can derive analytic solutions of the Klein-Gordon equation, constraining the boundary conditions with simple asymptotic solutions for $r \to 0$ and $r \to \infty$. For a point-like nucleus of charge Z the Coulomb potential $V_C = -\frac{Z\alpha}{r}$ enters the Klein-Gordon equation

$$\left[\nabla^2 + \left(\omega + \frac{Z\alpha}{r}\right)^2 - m_0^2\right]\phi(\mathbf{r}) = 0. \tag{B.1}$$

Here α is the fine structure constant and we use $r = |\mathbf{r}|$. It leads to an equation for the radial part $u_l(r)$ of the wave function $\phi(\mathbf{r})$

$$\left[\frac{d^2}{dr^2} - \frac{l(l+1)}{r^2} + \frac{Z^2\alpha^2}{r^2} + \frac{2\omega Z\alpha}{r} - m_0^2 + \omega^2\right] u_l(r) = 0. \tag{B.2}$$

by applying the standard angular momentum decomposition

$$\phi(\mathbf{r}) = \frac{1}{r} u_l(r) Y_{lm}(\vartheta, \varphi), \quad l = 0, 1, 2, \dots \tag{B.3}$$

for separation of variables in (B.1). The substitutions $\beta = 2\sqrt{m_0^2 - \omega^2}$ and $\rho = \beta r$ lead to

$$\left[\frac{d^2}{d\rho^2} + \frac{\lambda}{\rho} - \frac{l(l+1)}{\rho^2} + \frac{Z^2\alpha^2}{\rho^2} - \frac{1}{4}\right] u_l = 0 \tag{B.4}$$

with

$$\lambda = \frac{2\omega Z\alpha}{\beta} > 0. \tag{B.5}$$

The asymptotic solutions of the differential equation (3.4) follow from certain limiting cases of (B.4). For large radii $r \to \infty$ terms proportional to ρ^{-1} and ρ^{-2} can be neglected and the differential equation reduces to

$$\left[\frac{d^2}{d\rho^2} - \frac{1}{4}\right] u_l(\rho) = 0. \tag{B.6}$$

This equation is solved by

$$u_l(\rho) \xrightarrow{\rho\to\infty} a\, e^{-\rho/2} + b\, e^{\rho/2} \tag{B.7}$$

and because of normalizability of the wave function we require $b = 0$.

For small radii $\rho \to 0$ the $1/\rho^2$-terms dominate in (B.4) and the remaining equation

$$\left[\frac{d^2}{d\rho^2} - \frac{l(l+1)}{\rho^2} + \frac{Z^2\alpha^2}{\rho^2}\right] u_l = 0. \tag{B.8}$$

can be solved with the ansatz $u_l = a\rho^\nu$, where ν is determined by the equation

$$a\nu(\nu-1)\rho^{\nu-2} - a\left[l(l+1) - Z^2\alpha^2\right]\rho^{\nu-2} = 0 \tag{B.9}$$

as

$$\nu_\pm = \frac{1}{2} \pm \sqrt{\frac{1}{4} + l(l+1) - Z^2\alpha^2}. \tag{B.10}$$

The regular solutions are given by ν_+. In the case of kaonic atoms involving an optical potential and additional vacuum polarization corrections we have to modify the asymptotic behaviour $u_l \propto \rho^\nu$ with (B.10) for small radii. If we assume that none of the potentials is more singular than $\frac{1}{\rho^2}$ then (B.8) simplifies to

$$\left[\frac{d^2}{d\rho^2} - \frac{l(l+1)}{\rho^2}\right] u_l = 0 \tag{B.11}$$

and ν is determined by

$$\nu = \frac{1}{2} + \sqrt{\frac{1}{4} + l(l+1)} = l + 1. \tag{B.12}$$

Expression (B.12) reflects the well known asymptotic behaviour $u_l(r) \propto r^{l+1}$ and will be used as a boundary condition for $r \to 0$. Accordingly for the derivative we have $u'_l(r) \propto (l+1)r^l$. We observed that the solution of the Klein-Gordon equation (3.4) is rather insensitive to the actual form of the boundary condition for small radii. We obtain both a correct eigenvalue and – up to an arbitrary normalization constant of the wave function – a correct wave function solution even for any constant boundary value of the wave function and its derivative. Hence the solution is strongly determined by the applied potentials.

For completeness we will also give the analytic expressions for the complete solution and eigenvalues of the Klein-Gordon equation involving a point-like nucleus with pure Coulomb potential. It can be used as a benchmark for the numerical solution of the Klein-Gordon equation. A detailed discussion can be found in [62]. With the definition

$$\mu = \sqrt{\frac{1}{4} + l(l+1) - Z^2\alpha^2} \tag{B.13}$$

the solution of (B.4) reads

$$u_l(\rho) = N\rho^{\frac{1}{2}+\mu} e^{-\frac{\rho}{2}} f(\rho), \tag{B.14}$$

including a normalization constant N and $f(\rho)$ that guarantees normalizability of $u_l(\rho)$. Furthermore $f(\rho)$ should be constant for $\rho \to 0$. The function $f(\rho)$ will be constrained by plugging ansatz (B.14) into (B.4):

$$\frac{d^2}{d\rho^2} f(\rho) + \left(\frac{2\mu + 1}{\rho} - 1 \right) \frac{d}{d\rho} f(\rho) - \frac{\mu + 1/2 - \lambda}{\rho} f(\rho) = 0. \tag{B.15}$$

Equation (B.15) is solved by the confluent hypergeometric series ${}_1F_1\,(a, c; \rho)$ with $a \equiv \mu + \frac{1}{2} - \lambda$ and $c \equiv 2\mu + 1$. Using the definition

$${}_pF_q(\mathbf{a}, \mathbf{b}, x) = \sum_{k=0}^{\infty} \frac{(a_1)_k \cdot \ldots \cdot (a_p)_k}{(b_1)_k \cdot \ldots \cdot (b_q)_k} \frac{x^k}{k!}. \tag{B.16}$$

and $\mathbf{a} = (a_1, \ldots, a_p)$, $\mathbf{b} = (b_1, \ldots, b_q)$ we have

$$\begin{aligned} f(\rho) =& 1 + \frac{a}{c}\rho + \frac{a(a+1)}{c(c+1)} \frac{\rho}{2} + \ldots \\ &+ \frac{a(a+1)\ldots(a+n')}{c(c+1)\ldots(c+n')} \frac{\rho^{n'+1}}{(n'+1)!} + \ldots \end{aligned} \tag{B.17}$$

The hypergeometric series ${}_1F_1\,(a, c; \rho)$ diverges for $\rho \to \infty$:

$${}_1F_1\,(a, c; \rho \to \infty) = \frac{\Gamma(c)}{\Gamma(a)} \rho^{a-c} e^{\rho} \tag{B.18}$$

with the Euler gamma function

$$\Gamma(x) = \int_0^{\infty} dt\, e^{-t} t^{x-1}, \qquad \Gamma(x) \quad \text{convergent for} \quad x > 0. \tag{B.19}$$

So that u_l vanishes for $\rho \to \infty$ the hypergeometric series has to be truncated at a finite power n'. For $a = -n'$ all terms in (B.17) with power $m > n'$ are identically zero, hence a has to be a negative integer. Now the energy eigenvalue can be calculated. Starting from

$$\lambda = \mu + \frac{1}{2} + n' = \frac{Z\alpha\omega}{\sqrt{m_0^2 - \omega^2}} \tag{B.20}$$

and by making use of $\beta = 2\sqrt{m_0^2 - \omega^2}$, $\rho = \beta r$, (B.5) and (B.13) it follows that

$$\omega = \frac{m_0}{\sqrt{1 + Z^2\alpha^2\lambda^{-2}}} = m_0 \left[1 + \frac{Z^2\alpha^2}{\left(n' + \frac{1}{2} + \sqrt{\left(l + \frac{1}{2}\right)^2 - Z^2\alpha^2} \right)^2} \right]^{-\frac{1}{2}}. \tag{B.21}$$

As the product $Z\alpha$ is small compared to 1 except for heavy nuclei we can expand (B.21) in powers of Z. We define the main quantum number $n = n' + l + 1$ and obtain

$$\omega = m_0 \left[1 - \frac{Z^2\alpha^2}{2n^2} - \frac{Z^4\alpha^4}{2n^4} \left(\frac{n}{l + \frac{1}{2}} - \frac{3}{4} \right) + \mathcal{O}(Z^6\alpha^6) \right]. \tag{B.22}$$

It is instructive to have a closer look at the different contributions of ω. The first summand is nothing else but the rest energy of a particle with mass m_0, the second one is the kinetic energy of the particle subjected to a Coulomb field in the nonrelativistic approximation. The third summand is the first relativistic energy correction, depending on the quantum number l and reflecting a removed degeneracy.

B.2 Numerical solution of the Klein-Gordon equation

The method of [45] is utilising a pure starting value problem, thus explicitly making use of the pathologic behaviour of the wave function at large radii due to instabilities of the numerical solution. The integration of the differential equation is done in direction of the instabilities of the solution and the eigenvalue is iterated in order to minimize the absolute square of the wave function at a fixed large radius, pushing the exponential growth of the wave function due to the instabilities of the solution far away from the origin. The differential equation is of the form

$$\frac{d^2u(r)}{dr^2} + (\lambda_0^2 + V(r))u(r) = 0 \tag{B.23}$$

with a complex eigenvalue λ_0. The interaction $V(r)$ includes the centrifugal potential and vanishes for $r \to \infty$. Suppose for arbitrary λ and large radii we have two solutions, a regular one $u_\lambda^{(1)}(r)$ and an irregular one $u_\lambda^{(2)}(r)$ that behave like

$$u_\lambda^{(1)}(r) \to e^{-\lambda r} \quad \text{and} \quad u_\lambda^{(2)}(r) \to e^{+\lambda r}. \tag{B.24}$$

The bound state solution with $\lambda = \lambda_0$ behaves like r^{l+1} at the origin and diminishes exponentially for $r \to \infty$. The method of [45] imposes $u_\lambda(r) \propto r^{l+1}$ at the origin and the differential equation is integrated out to large radii. Now the wave function can be written as

$$\begin{aligned} u_\lambda(r) \quad &= \quad B(\lambda)\left[u_\lambda^{(1)}(r) + \left(\frac{\lambda-\lambda_0}{\lambda_0}\right)C(\lambda)u_\lambda^{(2)}(r)\right] \\ &\xrightarrow{r\to\infty} \quad B(\lambda)\left[e^{-\lambda r} + \left(\frac{\lambda-\lambda_0}{\lambda_0}\right)C(\lambda)e^{+\lambda r}\right]. \end{aligned} \tag{B.25}$$

The function $C(\lambda)$ vanishes for any λ except for the eigenvalue λ_0, in the region of which $B(\lambda)$ as well as $C(\lambda)$ can be regarded as constant. From now on we will treat these functions as constant. If λ is not an eigenvalue, the irregular component of $u_\lambda(r)$ will dominate the solution. For this reason minimizing $u_\lambda(r)$ with respect to λ at a fixed and large $r = r_0$ is an obvious choice. Because of the complex wave function and eigenvalue we have to minimize the absolute square $|u_k(r_0)|^2$, that looks like

$$|u_\lambda(r_0)|^2 \approx |B|^2 \left\{ e^{-2\mathfrak{Re}(\lambda r_0)} + \mathcal{O}\left[\frac{\lambda-\lambda_0}{\lambda_0}C\right] + |C|^2 \left|\frac{\lambda-\lambda_0}{\lambda_0}\right|^2 e^{2\mathfrak{Re}(\lambda r_0)} \right\}. \tag{B.26}$$

As the irregular component depends on $\mathfrak{Re}(\lambda r_0)$ exponentially the minimum converges on a very small region and a minimization of $|u_k(r_0)|^2$ would be inefficient. Thus we define a new function $v(\lambda)$, the fraction of the absolute square and the irregular component:

$$v(\lambda) = \frac{|u_\lambda(r_0)|^2}{|u_\lambda^{(2)}(r_0)|^2} \approx \frac{|u_\lambda(r_0)|^2}{e^{2\mathfrak{Re}(\lambda r_0)}}. \tag{B.27}$$

A Minimization of $v(\lambda)$ is much more efficient, typical values for r_0 are $200 - 300$ fm. Also r_0 should not be chosen too large because of growing numerical error. The method of [45] proved to be capable of providing the most accurate solutions for light nuclei and bound states with small l. The formulation as a pure starting value problem is its most severe disadvantage, resulting in an inevitable propagation and accumulation of errors and instabilities of the solution at large radii. Starting with $u(r_{min}) = r_{min}^{l+1}$ at small $r_{min} \approx h$ with an integration step size h leads to a wave function of the same order as the typical error of the integration, $\mathcal{O}(h^5)$, for $l \geq 4$. Further discussion can be found in [63].

The second method known as shooting [64] avoids the disadvantages of [45] and delivers stable solutions for high quantum numbers l. The inner solution with the same starting boundary condition r_{min}^{l+1} is stabilized by matching with an outer solution integrated from large radii to a fixed matching point. So we are dealing with a two-point boundary value problem, that requires the knowledge of the outer solution and its derivative as a boundary condition at r_{max}. The asymptotic solution (B.7) proved to be sufficient. An implementation of the full solution (B.14) does not result in a significant improvement of the wave function and matching process. A typical value of r_{max} is about 200 fm. The matching of the inner $u_l^{in}(r, \lambda)$ and outer solution $u_l^{out}(r, \lambda)$ is done at a matching point r_m with $r_{min} < r_m < r_{max}$, typically we use $r_m \approx 20$ fm. For the determination of the eigenvalue matching the derivative of the wave function would be sufficient. However, we introduce another matching parameter κ both for real and imaginary part that is multiplied onto the outer boundary condition (B.7), because the inner and outer solution are not normalized and can differ by an unknown absolute value at the matching point r_m. Thus the matching condition for the correct eigenvalue λ_0 reads

$$u_l^{in}(r_m, \lambda_0, \kappa) = u_l^{out}(r_m, \lambda_0, \kappa), \qquad \frac{d}{dr} u_l^{in}(r_m, \lambda_0, \kappa) = \frac{d}{dr} u_l^{out}(r_m, \lambda_0, \kappa) \tag{B.28}$$

and the minimization of an $N = 4$ dimensional vector, measuring the differences of wave function and its derivative at r_m, is done with respect to the (complex) parameters λ and κ.

B.3 General covariant self-energy coefficient functions

Covariant coefficient functions $c_{ij}^{(p,q)}(q, w, u)$ in Q-space

$$\begin{aligned}
c_{11}^{(q)} &= \frac{m_N^* + (p \cdot \hat{w})}{2\left((u \cdot \hat{w})^2 - 1\right)} \Big((\bar{q} \cdot \hat{w}) \left((q \cdot \hat{w}) - (q \cdot u)(u \cdot \hat{w})\right) \\
&\quad + (\bar{q} \cdot u)\left((q \cdot u) - (q \cdot \hat{w})(u \cdot \hat{w})\right) + (\bar{q} \cdot q)\left((u \cdot \hat{w})^2 - 1\right) \Big), \\
c_{12}^{(q)} &= -i \frac{(p \cdot u) - (p \cdot \hat{w})(u \cdot \hat{w})}{2\left((u \cdot \hat{w})^2 - 1\right)^{\frac{3}{2}}} \Big((\bar{q} \cdot \hat{w}) \left((q \cdot \hat{w}) - (q \cdot u)(u \cdot \hat{w})\right) \\
&\quad + (\bar{q} \cdot u)\left((q \cdot u) - (q \cdot \hat{w})(u \cdot \hat{w})\right) + (\bar{q} \cdot q)\left((u \cdot \hat{w})^2 - 1\right) \Big), \\
c_{21}^{(q)} &= c_{12}^{(q)}, \\
c_{22}^{(q)} &= \frac{m_N^* - (p \cdot \hat{w})}{2\left((u \cdot \hat{w})^2 - 1\right)} \Big((\bar{q} \cdot \hat{w}) \left((q \cdot \hat{w}) - (q \cdot u)(u \cdot \hat{w})\right) \\
&\quad + (\bar{q} \cdot u)\left((q \cdot u) - (q \cdot \hat{w})(u \cdot \hat{w})\right) + (\bar{q} \cdot q)\left((u \cdot \hat{w})^2 - 1\right) \Big)
\end{aligned} \tag{B.29}$$

and in P-space:

$$
\begin{aligned}
c_{11}^{(p)} &= m_N^* + (p\cdot\hat{w}),\\
c_{12}^{(p)} &= -i\frac{(p\cdot u) - (p\cdot\hat{w})\,(u\cdot\hat{w})}{\sqrt{(u\cdot\hat{w})^2-1}},\\
c_{13}^{(p)} &= \frac{(p\cdot q) - (p\cdot\hat{w})\,(q\cdot\hat{w})}{\sqrt{3}},\\
c_{14}^{(p)} &= -i\frac{(m_N^* + (p\cdot\hat{w}))\,\left((q\cdot u) - (q\cdot\hat{w})\,(u\cdot\hat{w})\right)}{\sqrt{3}\,\sqrt{(u\cdot\hat{w})^2-1}},\\
c_{15}^{(p)} &= (q\cdot\hat{w})\,\left(m_N^* + (p\cdot\hat{w})\right),\\
c_{16}^{(p)} &= -i\frac{(q\cdot\hat{w})\,\left((p\cdot u) + (p\cdot\hat{w})\,(u\cdot\hat{w})\right)}{\sqrt{(u\cdot\hat{w})^2-1}},\\
c_{17}^{(p)} &= i\sqrt{\frac{2}{3}}\frac{(m_N^* + (p\cdot\hat{w}))\left((q\cdot u) - (q\cdot\hat{w})\,(u\cdot\hat{w})\right)}{\sqrt{(u\cdot\hat{w})^2-1}},\\
c_{18}^{(p)} &= \frac{1}{\sqrt{6}\,\left((u\cdot\hat{w})^2-1\right)}\Big[3(p\cdot u)\left((q\cdot u) - (q\cdot\hat{w})\,(u\cdot\hat{w})\right) + (p\cdot q)\left((u\cdot\hat{w})^2-1\right)\\
&\quad +(p\cdot\hat{w})\left((q\cdot\hat{w}) - 3(q\cdot u)\,(u\cdot\hat{w}) + 2(q\cdot\hat{w})\,(u\cdot\hat{w})^2\right)\Big],\\
c_{21}^{(p)} &= c_{12}^{(12)},\qquad c_{22}^{(p)} = m_N^* - (p\cdot\hat{w}),\\
c_{23}^{(p)} &= -i\frac{(m_N^* - (p\cdot\hat{w}))\,\left((q\cdot u) - (q\cdot\hat{w})\,(u\cdot\hat{w})\right)}{\sqrt{3}\,\sqrt{(u\cdot\hat{w})^2-1}},\\
c_{24}^{(p)} &= c_{13}^{(p)},\qquad c_{25}^{(p)} = c_{16}^{(p)},\\
c_{26}^{(p)} &= (q\cdot\hat{w})\,\left(m_N^* - (p\cdot\hat{w})\right),\qquad c_{27}^{(p)} = c_{18}^{(p)},\\
c_{28}^{(p)} &= i\sqrt{\frac{2}{3}}\frac{(m_N^* - (p\cdot\hat{w}))\left((q\cdot u) - (q\cdot\hat{w})\,(u\cdot\hat{w})\right)}{\sqrt{(u\cdot\hat{w})^2-1}},\\
c_{31}^{(p)} &= c_{13}^{(p)}(q\leftrightarrow\bar{q}),\qquad c_{32}^{(p)} = c_{23}^{(p)}(q\leftrightarrow\bar{q}),\\
c_{33}^{(p)} &= \frac{(m_N^* - (p\cdot\hat{w}))\left((\bar{q}\cdot q) - (\bar{q}\cdot\hat{w})\,(q\cdot\hat{w})\right)}{3},\\
c_{34}^{(p)} &= \frac{i}{3\sqrt{(u\cdot\hat{w})^2-1}}\Big[-(p\cdot q)\,(\bar{q}\cdot u) - (p\cdot\bar{q})\,(q\cdot u) + (p\cdot\hat{w})\,(\bar{q}\cdot\hat{w})\,(q\cdot u)\\
&\quad +(p\cdot\hat{w})\,(\bar{q}\cdot u)\,(q\cdot\hat{w}) + (p\cdot u)\left((\bar{q}\cdot q) - (\bar{q}\cdot\hat{w})\,(q\cdot\hat{w})\right) - (p\cdot\hat{w})\,(\bar{q}\cdot q)\,(u\cdot\hat{w})\\
&\quad +(p\cdot q)\,(\bar{q}\cdot\hat{w})\,(u\cdot\hat{w}) + (p\cdot\bar{q})\,(q\cdot\hat{w})\,(u\cdot\hat{w}) - (p\cdot\hat{w})\,(\bar{q}\cdot\hat{w})\,(q\cdot\hat{w})\,(u\cdot\hat{w})\Big],\\
c_{35}^{(p)} &= \frac{(q\cdot\hat{w})\left((p\cdot\bar{q}) - (p\cdot\hat{w})\,(\bar{q}\cdot\hat{w})\right)}{\sqrt{3}},\\
c_{36}^{(p)} &= -i\frac{(q\cdot\hat{w})\,\left(m_N^* - (p\cdot\hat{w})\right)\left((\bar{q}\cdot u) - (\bar{q}\cdot\hat{w})\,(u\cdot\hat{w})\right)}{\sqrt{3}\,\sqrt{(u\cdot\hat{w})^2-1}},
\end{aligned}
$$

$$
\begin{aligned}
c_{37}^{(p)} &= \frac{i}{3\sqrt{2}\sqrt{(u\cdot\hat{w})^2-1}}\Big[-(p\cdot q)\,(\bar{q}\cdot u)+2(p\cdot\bar{q})\,(q\cdot u)-2(p\cdot\hat{w})\,(\bar{q}\cdot\hat{w})\,(q\cdot u) \\
&\quad +(p\cdot\hat{w})\,(\bar{q}\cdot u)\,(q\cdot\hat{w})+(p\cdot u)\,((\bar{q}\cdot q)-(\bar{q}\cdot\hat{w})\,(q\cdot\hat{w}))-(p\cdot\hat{w})\,(\bar{q}\cdot q)\,(u\cdot\hat{w}) \\
&\quad +(p\cdot q)\,(\bar{q}\cdot\hat{w})\,(u\cdot\hat{w})-2(p\cdot\bar{q})\,(q\cdot\hat{w})\,(u\cdot\hat{w})+2(p\cdot\hat{w})\,(\bar{q}\cdot\hat{w})\,(q\cdot\hat{w})\,(u\cdot\hat{w})\Big], \\
c_{38}^{(p)} &= \frac{m_N^*-(p\cdot\hat{w})}{3\sqrt{2}\left((u\cdot\hat{w})^2-1\right)}\Big[3(\bar{q}\cdot u)\,((q\cdot u)-(q\cdot\hat{w})\,(u\cdot\hat{w}))+(\bar{q}\cdot q)\left((u\cdot\hat{w})^2-1\right) \\
&\quad +(\bar{q}\cdot\hat{w})\left((q\cdot\hat{w})-3(q\cdot u)\,(u\cdot\hat{w})+2(q\cdot\hat{w})\,(u\cdot\hat{w})^2\right)\Big], \\
c_{41}^{(p)} &= c_{14}^{(p)}(q\leftrightarrow\bar{q}), \qquad c_{42}^{(p)}=c_{24}^{(p)}(q\leftrightarrow\bar{q}), \qquad c_{43}^{(p)}=c_{34}^{(p)}, \\
c_{44}^{(p)} &= \frac{(m_N^*+(p\cdot\hat{w}))\,((\bar{q}\cdot q)-(\bar{q}\cdot\hat{w})\,(q\cdot\hat{w}))}{3}, \\
c_{45}^{(p)} &= -i\frac{(q\cdot\hat{w})\;(m_N^*+(p\cdot\hat{w}))\,((\bar{q}\cdot u)-(\bar{q}\cdot\hat{w})\,(u\cdot\hat{w}))}{\sqrt{3}\,\sqrt{(u\cdot\hat{w})^2-1}}, \\
c_{46}^{(p)} &= c_{35}^{(p)}, \\
c_{47}^{(p)} &= \frac{m_N^*+(p\cdot\hat{w})}{3\sqrt{2}\left((u\cdot\hat{w})^2-1\right)}\Big[3(\bar{q}\cdot u)\,((q\cdot u)-(q\cdot\hat{w})\,(u\cdot\hat{w}))+(\bar{q}\cdot q)\left((u\cdot\hat{w})^2-1\right) \\
&\quad +(\bar{q}\cdot\hat{w})\left((q\cdot\hat{w})-3(q\cdot u)\,(u\cdot\hat{w})+2(q\cdot\hat{w})\,(u\cdot\hat{w})^2\right)\Big], \\
c_{48}^{(p)} &= c_{37}^{(p)}, \\
c_{51}^{(p)} &= c_{15}^{(p)}(q\leftrightarrow\bar{q}), \qquad c_{52}^{(p)}=c_{25}^{(p)}(q\leftrightarrow\bar{q}), \\
c_{53}^{(p)} &= c_{35}^{(p)}(q\leftrightarrow\bar{q}), \qquad c_{54}^{(p)}=c_{45}^{(p)}(q\leftrightarrow\bar{q}), \\
c_{55}^{(p)} &= (m_N^*+(p\cdot\hat{w}))\,(\bar{q}\cdot\hat{w})\,(q\cdot\hat{w}), \\
c_{56}^{(p)} &= -i\frac{(\bar{q}\cdot\hat{w})\,(q\cdot\hat{w})\,((p\cdot u)-(p\cdot\hat{w})\,(u\cdot\hat{w}))}{\sqrt{(u\cdot\hat{w})^2-1}}, \\
c_{57}^{(p)} &= -\sqrt{2}c_{54}^{(p)}, \\
c_{58}^{(p)} &= \frac{(\bar{q}\cdot\hat{w})}{\sqrt{6}\left((u\cdot\hat{w})^2-1\right)}\Big[3(p\cdot u)\,((q\cdot u)-(q\cdot\hat{w})\,(u\cdot\hat{w}))+(p\cdot q)\left((u\cdot\hat{w})^2-1\right) \\
&\quad +(p\cdot\hat{w})\left((q\cdot\hat{w})-3(q\cdot u)\,(u\cdot\hat{w})+2(q\cdot\hat{w})\,(u\cdot\hat{w})^2\right)\Big], \\
c_{61}^{(p)} &= c_{16}^{(p)}(q\leftrightarrow\bar{q}), \qquad c_{62}^{(p)}=c_{26}^{(p)}(q\leftrightarrow\bar{q}), \\
c_{63}^{(p)} &= c_{36}^{(p)}(q\leftrightarrow\bar{q}), \qquad c_{64}^{(p)}=c_{46}^{(p)}(q\leftrightarrow\bar{q}), \\
c_{65}^{(p)} &= c_{56}^{(p)}(q\leftrightarrow\bar{q}), \qquad c_{66}^{(p)}=(m_N^*-(p\cdot\hat{w}))\,(\bar{q}\cdot\hat{w})\,(q\cdot\hat{w}), \\
c_{67}^{(p)} &= c_{58}^{(p)}, \qquad c_{68}^{(p)}=-\sqrt{2}c_{63}^{(p)}, \\
c_{71}^{(p)} &= c_{17}^{(p)}(q\leftrightarrow\bar{q}), \qquad c_{72}^{(p)}=c_{27}^{(p)}(q\leftrightarrow\bar{q}), \\
c_{73}^{(p)} &= c_{37}^{(p)}(q\leftrightarrow\bar{q}), \qquad c_{74}^{(p)}=c_{47}^{(p)}, \\
c_{75}^{(p)} &= c_{57}^{(p)}(q\leftrightarrow\bar{q}), \qquad c_{76}^{(p)}=c_{67}^{(p)}(q\leftrightarrow\bar{q}),
\end{aligned}
$$

$$
\begin{aligned}
c_{77}^{(p)} &= \frac{m_N^* + (p\cdot\hat{w})}{6\Big((u\cdot\hat{w})^2-1\Big)}\Big[-3(\bar{q}\cdot u)\,((q\cdot u)-(q\cdot\hat{w})\,(u\cdot\hat{w}))+(\bar{q}\cdot q)\,\Big((u\cdot\hat{w})^2-1\Big)\\
&\quad+(\bar{q}\cdot\hat{w})\,\Big((q\cdot\hat{w})+3(q\cdot u)\,(u\cdot\hat{w})-4(q\cdot\hat{w})\,(u\cdot\hat{w})^2\Big)\Big],\\
c_{78}^{(p)} &= \frac{i}{6\Big((u\cdot\hat{w})^2-1\Big)^{\frac{3}{2}}}\Big[-2(p\cdot\bar{q})\,(q\cdot u)+2(p\cdot\hat{w})\,(\bar{q}\cdot\hat{w})\,(q\cdot u)+2(p\cdot\hat{w})\,(\bar{q}\cdot u)\,(q\cdot\hat{w})\\
&\quad+(p\cdot\hat{w})\,(\bar{q}\cdot q)\,(u\cdot\hat{w})-9(p\cdot\hat{w})\,(\bar{q}\cdot u)\,(q\cdot u)\,(u\cdot\hat{w})+2(p\cdot\bar{q})\,(q\cdot\hat{w})\,(u\cdot\hat{w})\\
&\quad-5(p\cdot\hat{w})\,(\bar{q}\cdot\hat{w})\,(q\cdot\hat{w})\,(u\cdot\hat{w})+2(p\cdot\bar{q})\,(q\cdot u)\,(u\cdot\hat{w})^2\\
&\quad+7(p\cdot\hat{w})\,(\bar{q}\cdot\hat{w})\,(q\cdot u)\,(u\cdot\hat{w})^2+7(p\cdot\hat{w})\,(\bar{q}\cdot u)\,(q\cdot\hat{w})\,(u\cdot\hat{w})^2\\
&\quad-(p\cdot\hat{w})\,(\bar{q}\cdot q)\,(u\cdot\hat{w})^3-2(p\cdot\bar{q})\,(q\cdot\hat{w})\,(u\cdot\hat{w})^3-4(p\cdot\hat{w})\,(\bar{q}\cdot\hat{w})\,(q\cdot\hat{w})\,(u\cdot\hat{w})^3\\
&\quad+2(p\cdot q)\,((\bar{q}\cdot u)-(\bar{q}\cdot\hat{w})\,(u\cdot\hat{w}))\,\Big((u\cdot\hat{w})^2-1\Big)\\
&\quad+(p\cdot u)\Big(9(\bar{q}\cdot u)\,((q\cdot u)-(q\cdot\hat{w})\,(u\cdot\hat{w}))+(\bar{q}\cdot q)\,\Big((u\cdot\hat{w})^2-1\Big)\\
&\quad+(\bar{q}\cdot\hat{w})\,\Big((q\cdot\hat{w})-9(q\cdot u)\,(u\cdot\hat{w})+8(q\cdot\hat{w})\,(u\cdot\hat{w})^2\Big)\Big)\Big],\\
c_{81}^{(p)} &= c_{18}^{(p)}(q\leftrightarrow\bar{q}),\qquad c_{82}^{(p)}=c_{28}^{(p)}(q\leftrightarrow\bar{q}),\\
c_{83}^{(p)} &= c_{38}^{(p)},\qquad c_{84}^{(p)}=c_{48}^{(p)}(q\leftrightarrow\bar{q}),\\
c_{85}^{(p)} &= c_{58}^{(p)}(q\leftrightarrow\bar{q}),\qquad c_{86}^{(p)}=c_{68}^{(p)}(q\leftrightarrow\bar{q}),\\
c_{87}^{(p)} &= c_{78}^{(p)},\\
c_{88}^{(p)} &= \frac{m_N^* - (p\cdot\hat{w})}{6\Big((u\cdot\hat{w})^2-1\Big)}\Big[-3(\bar{q}\cdot u)\,((q\cdot u)-(q\cdot\hat{w})\,(u\cdot\hat{w}))+(\bar{q}\cdot q)\,\Big((u\cdot\hat{w})^2-1\Big)\\
&\quad+(\bar{q}\cdot\hat{w})\,\Big((q\cdot\hat{w})+3(q\cdot u)\,(u\cdot\hat{w})-4(q\cdot\hat{w})\,(u\cdot\hat{w})^2\Big)\Big]. \qquad \text{(B.30)}
\end{aligned}
$$

B.4 Coefficient functions non-local self-energy

The coefficients in P- and Q-space read for $a = 1$, contribution $\propto \frac{1}{4}\nabla^2_{\mathbf{R}}$,

$$\begin{aligned}
c^{(p)}_{[33],1} &= -\frac{1}{3}\left(m^*_N - \frac{{m^*_N}^2 + \omega E^*_N - \mathbf{p}\cdot\mathbf{q}}{\sqrt{w_0^2 - \mathbf{w}^2}} \right), \\
c^{(p)}_{[34],1} &= \frac{i}{3\sqrt{w_0^2 - \mathbf{w}^2}\sqrt{(\omega + E^*_N)^2 - (w_0^2 - \mathbf{w}^2)}} \Big[\omega \left({m^*_N}^2 + {E^*_N}^2 - \mathbf{p}\cdot\mathbf{q} \right) \\
&\quad + E^*_N \left({m^*_N}^2 + \omega^2 - \mathbf{p}\cdot\mathbf{q} - \left(w_0^2 - \mathbf{w}^2 \right) \right) \Big], \\
c^{(p)}_{[37],1} &= \frac{1}{\sqrt{2}} c^{(p)}_{[34],1}, \qquad c^{(p)}_{[38],1} = \frac{1}{\sqrt{2}} c^{(p)}_{[33],1}, \\
c^{(p)}_{[44],1} &= -\frac{1}{3}\left(m^*_N + \frac{{m^*_N}^2 + \omega E^*_N - \mathbf{p}\cdot\mathbf{q}}{\sqrt{w_0^2 - \mathbf{w}^2}} \right), \\
c^{(p)}_{[47],1} &= \frac{1}{\sqrt{2}} c^{(p)}_{[44],1}, \qquad c^{(p)}_{[48],1} = c^{(p)}_{[37],1}, \\
c^{(p)}_{[77],1} &= \frac{1}{2} c^{(p)}_{[44],1}, \qquad c^{(p)}_{[78],1} = \frac{1}{2} c^{(p)}_{[34],1}, \\
c^{(p)}_{[88],1} &= \frac{1}{2} c^{(p)}_{[33],1}, \\
c^{(q)}_{[11],1} &= -\frac{1}{2}\left(m^*_N + \frac{{m^*_N}^2 + \omega E^*_N - \mathbf{p}\cdot\mathbf{q}}{\sqrt{w_0^2 - \mathbf{w}^2}} \right), \\
c^{(q)}_{[12],1} &= \frac{i}{2\sqrt{w_0^2 - \mathbf{w}^2}\sqrt{(\omega + E^*_N)^2 - (w_0^2 - \mathbf{w}^2)}} \Big[E^*_N (w_0^2 - \mathbf{w}^2) \\
&\quad - (\omega + E^*_N) \left({m^*_N}^2 + \omega E^*_N - \mathbf{p}\cdot\mathbf{q} \right) \Big], \\
c^{(q)}_{[22],1} &= -\frac{1}{2}\left(m^*_N - \frac{{m^*_N}^2 + \omega E^*_N - \mathbf{p}\cdot\mathbf{q}}{\sqrt{w_0^2 - \mathbf{w}^2}} \right),
\end{aligned} \tag{B.31}$$

for $a = 2$, contribution $\propto \frac{1}{4}\left(\mathbf{w}\cdot\nabla_{\mathbf{R}}\right)^2$,

$$\begin{aligned}
c^{(p)}_{[33],2} &= -\frac{1}{3(w_0^2 - \mathbf{w}^2)}\left(m^*_N - \frac{{m^*_N}^2 + \omega E^*_N - \mathbf{p}\cdot\mathbf{q}}{\sqrt{w_0^2 - \mathbf{w}^2}} \right), \\
c^{(p)}_{[34],2} &= -\frac{i}{3\sqrt{w_0^2 - \mathbf{w}^2}^3\sqrt{(\omega + E^*_N)^2 - (w_0^2 - \mathbf{w}^2)}} \Big[\omega \left({m^*_N}^2 + {E^*_N}^2 - \mathbf{p}\cdot\mathbf{q} \right) \\
&\quad + E^*_N \left({m^*_N}^2 + \omega^2 - \mathbf{p}\cdot\mathbf{q} + \left(w_0^2 - \mathbf{w}^2 \right) \right) \Big], \\
c^{(p)}_{[35],2} &= -\frac{1}{\sqrt{3}} \frac{{m^*_N}^2 + \omega E^*_N - \mathbf{p}\cdot\mathbf{q}}{\sqrt{w_0^2 - \mathbf{w}^2}^3},
\end{aligned}$$

$$
\begin{aligned}
c^{(p)}_{[36],2} &= \frac{i}{\sqrt{3}} \frac{\omega + E^*_N}{\left(w_0^2 - \mathbf{w}^2\right)\sqrt{(\omega + E^*_N)^2 - (w_0^2 - \mathbf{w}^2)}} \left(m^*_N - \frac{{m^*_N}^2 + \omega E^*_N - \mathbf{p}\cdot\mathbf{q}}{\sqrt{w_0^2 - \mathbf{w}^2}}\right), \\
c^{(p)}_{[37],2} &= \frac{\sqrt{2}\, i}{3\sqrt{w_0^2 - \mathbf{w}^2}^3 \sqrt{(\omega + E^*_N)^2 - (w_0^2 - \mathbf{w}^2)}} \Bigg[\omega\left({m^*_N}^2 + {E^*_N}^2 - \mathbf{p}\cdot\mathbf{q}\right) \\
&\quad + E^*_N\left({m^*_N}^2 + \omega^2 - \mathbf{p}\cdot\mathbf{q} - \frac{(w_0^2 - \mathbf{w}^2)}{2}\right)\Bigg], \\
c^{(p)}_{[38],2} &= \frac{1}{3\sqrt{2}(w_0^2 - \mathbf{w}^2)} \frac{2(\omega + E^*_N)^2 + (w_0^2 - \mathbf{w}^2)}{(\omega + E^*_N)^2 - (w_0^2 - \mathbf{w}^2)} \left(m^*_N - \frac{{m^*_N}^2 + \omega E^*_N - \mathbf{p}\cdot\mathbf{q}}{\sqrt{w_0^2 - \mathbf{w}^2}}\right), \\
c^{(p)}_{[44],2} &= -\frac{1}{3(w_0^2 - \mathbf{w}^2)} \left(m^*_N + \frac{{m^*_N}^2 + \omega E^*_N - \mathbf{p}\cdot\mathbf{q}}{\sqrt{w_0^2 - \mathbf{w}^2}}\right), \\
c^{(p)}_{[45],2} &= \frac{i}{\sqrt{3}} \frac{\omega + E^*_N}{\left(w_0^2 - \mathbf{w}^2\right)\sqrt{(\omega + E^*_N)^2 - (w_0^2 - \mathbf{w}^2)}} \left(m^*_N + \frac{{m^*_N}^2 + \omega E^*_N - \mathbf{p}\cdot\mathbf{q}}{\sqrt{w_0^2 - \mathbf{w}^2}}\right), \\
c^{(p)}_{[46],2} &= c^{(p)}_{[35],2}, \\
c^{(p)}_{[47],2} &= \frac{1}{3\sqrt{2}(w_0^2 - \mathbf{w}^2)} \frac{2(\omega + E^*_N)^2 + (w_0^2 - \mathbf{w}^2)}{(\omega + E^*_N)^2 - (w_0^2 - \mathbf{w}^2)} \left(m^*_N + \frac{{m^*_N}^2 + \omega E^*_N - \mathbf{p}\cdot\mathbf{q}}{\sqrt{w_0^2 - \mathbf{w}^2}}\right), \\
c^{(p)}_{[48],2} &= c^{(p)}_{[37],2}, \\
c^{(p)}_{[55],2} &= -3c^{(p)}_{[44],2}, \\
c^{(p)}_{[56],2} &= \frac{i}{\sqrt{w_0^2 - \mathbf{w}^2}^3 \sqrt{(\omega + E^*_N)^2 - (w_0^2 - \mathbf{w}^2)}} \Big[\omega\left({m^*_N}^2 + {E^*_N}^2 - \mathbf{p}\cdot\mathbf{q}\right) \\
&\quad + E^*_N\left({m^*_N}^2 + \omega^2 - \mathbf{p}\cdot\mathbf{q} - \left(w_0^2 - \mathbf{w}^2\right)\right)\Big], \\
c^{(p)}_{[57],2} &= -\sqrt{2}c^{(p)}_{[45],2}, \\
c^{(p)}_{[58],2} &= \frac{1}{\sqrt{6}\sqrt{w_0^2 - \mathbf{w}^2}^3 \left((\omega + E^*_N)^2 - \left(w_0^2 - \mathbf{w}^2\right)\right)} \\
&\quad \times \Bigg[2\left(\omega + E^*_N\right)^2 \left({m^*_N}^2 + \omega E^*_N - \mathbf{p}\cdot\mathbf{q}\right) \\
&\quad + \left(w_0^2 - \mathbf{w}^2\right)\left({m^*_N}^2 + \omega E^*_N - \mathbf{p}\cdot\mathbf{q} - 3E^*_N(\omega + E^*_N)\right)\Bigg], \\
c^{(p)}_{[66],2} &= -3c^{(p)}_{[33],2}, \qquad c^{(p)}_{[67],2} = c^{(p)}_{[58],2}, \qquad c^{(p)}_{[68],2} = -\sqrt{2}c^{(p)}_{[36],2}, \\
c^{(p)}_{[77],2} &= -\frac{1}{6\sqrt{w_0^2 - \mathbf{w}^2}^3} \frac{4(\omega + E^*_N)^2 - (w_0^2 - \mathbf{w}^2)}{\left((\omega + E^*_N)^2 - (w_0^2 - \mathbf{w}^2)\right)} \\
&\quad \times \left({m^*_N}^2 + \omega E^*_N - \mathbf{p}\cdot\mathbf{q} + m^*_N\sqrt{w_0^2 - \mathbf{w}^2}\right),
\end{aligned}
$$

$$
\begin{aligned}
c^{(p)}_{[78],2} &= \frac{i}{6\sqrt{w_0^2-\mathbf{w}^2}^3\sqrt{(\omega+E_N^*)^2-(w_0^2-\mathbf{w}^2)}^3} \\
&\quad \times \Bigg[E_N^*(w_0^2-\mathbf{w}^2)^2 + 8E_N^*(w_0^2-\mathbf{w}^2)(\omega+E_N^*)^2, \\
&\quad -(\omega+E_N^*)\left(4(\omega+E_N^*)^2+5(w_0^2-\mathbf{w}^2)\right)\left({m_N^*}^2+\omega E_N^*-\mathbf{p}\cdot\mathbf{q}\right)\Bigg], \\
c^{(p)}_{[88],2} &= \frac{1}{6\sqrt{w_0^2-\mathbf{w}^2}^3}\frac{4(\omega+E_N^*)^2-(w_0^2-\mathbf{w}^2)}{\left((\omega+E_N^*)^2-(w_0^2-\mathbf{w}^2)\right)} \\
&\quad \times \left({m_N^*}^2+\omega E_N^*-\mathbf{p}\cdot\mathbf{q}-m_N^*\sqrt{w_0^2-\mathbf{w}^2}\right), \\
c^{(q)}_{[11],2} &= \frac{1}{2\sqrt{w_0^2-\mathbf{w}^2}\left((\omega+E_N^*)^2-(w_0^2-\mathbf{w}^2)\right)}\left[{m_N^*}^2+\omega E_N^*-\mathbf{p}\cdot\mathbf{q}+m_N^*\sqrt{w_0^2-\mathbf{w}^2}\right], \\
c^{(q)}_{[12],2} &= -\frac{i}{2\sqrt{w_0^2-\mathbf{w}^2}\sqrt{(\omega+E_N^*)^2-(w_0^2-\mathbf{w}^2)}^3} \\
&\quad \times \left[E_N^*(w_0^2-\mathbf{w}^2)-(\omega+E_N^*)\left({m_N^*}^2+\omega E_N^*-\mathbf{p}\cdot\mathbf{q}\right)\right], \\
c^{(q)}_{[22],2} &= -\frac{1}{2\sqrt{w_0^2-\mathbf{w}^2}\left((\omega+E_N^*)^2-(w_0^2-\mathbf{w}^2)\right)}\left[{m_N^*}^2+\omega E_N^*-\mathbf{p}\cdot\mathbf{q}-m_N^*\sqrt{w_0^2-\mathbf{w}^2}\right],
\end{aligned}
\tag{B.32}
$$

and finally for $a=3$, contribution $\propto \frac{1}{4}\left(\mathbf{w}\cdot\nabla_{\mathbf{R}}\right)\left(\mathbf{p}\cdot\nabla_{\mathbf{R}}\right)$,

$$
\begin{aligned}
c^{(p)}_{[34],3} &= \frac{2i}{3\sqrt{w_0^2-\mathbf{w}^2}\sqrt{(\omega+E_N^*)^2-(w_0^2-\mathbf{w}^2)}}(\omega+E_N^*), \\
c^{(p)}_{[35],3} &= \frac{1}{\sqrt{3}\sqrt{w_0^2-\mathbf{w}^2}}, \\
c^{(p)}_{[37],3} &= -\frac{1}{2\sqrt{2}}c^{(p)}_{[34],3}, \\
c^{(p)}_{[46],3} &= c^{(p)}_{[35],3}, \qquad c^{(p)}_{[48],3} = c^{(p)}_{[37],3}, \\
c^{(p)}_{[58],3} &= \frac{1}{\sqrt{2}}c^{(p)}_{[35],3}, \\
c^{(p)}_{[67],3} &= c^{(p)}_{[58],3}, \\
c^{(p)}_{[78],3} &= -c^{(p)}_{[34],3}.
\end{aligned}
\tag{B.33}
$$

B.5 Implementing the pole structure for $J = \frac{1}{2}$ p-wave analytically

Each of the poles $\Lambda(1115)$ and $\Sigma(1195)$ can be approximated by

$$T = m_S \frac{-g^2}{s - m_P^2} \tag{B.34}$$

with a coupling constant g, a scaling mass m_S and the pole position at m_P. These yet unknown parameters will be determined by fitting (B.34) to the numerical data from the coupled channel calculation [4]. Writing (B.34) in terms of the kaon momentum $\mathbf{q}$ results in

$$T(|\mathbf{q}|) = m_S \frac{g^2}{\mathbf{q}^2 - m_{\tilde{P}}^2} \quad \text{with} \quad m_{\tilde{P}}^2 = (m_K + m_N)^2 - m_P^2. \tag{B.35}$$

In general for our semi-microscopic model the right hand side of the non-local Klein-Gordon equation takes the form

$$2\mu \int d^3r' U(\mathbf{r}', \mathbf{r}) \varphi(\mathbf{r}') = -\int d^3r' \mathcal{F}(\mathbf{r}', \mathbf{r}) \rho(\mathbf{r}', \mathbf{r}) \varphi(\mathbf{r}') \tag{B.36}$$

with

$$\mathcal{F} \equiv \mathcal{F}(\mathbf{r}', \mathbf{r}) = m_S\, g^2 \int \frac{d^3q}{(2\pi)^3} C^{\frac{1}{2}^+}(|\mathbf{q}|) \frac{e^{-i\mathbf{q}(\mathbf{r}'-\mathbf{r})}}{\mathbf{q}^2 - m_{\tilde{P}}^2}, \tag{B.37}$$

from the pole structure (B.35). In the following we will substitute $\mathbf{a} = \mathbf{r}' - \mathbf{r}$ and $a = |\mathbf{r}' - \mathbf{r}|$, $q = |\mathbf{q}|$, whereas $C^{\frac{1}{2}^+}(|\mathbf{q}|)$ is the coefficient from the trace evaluation in (B.52). Performing the angular integration in the latter expression yields

$$\mathcal{F} = m_S\, g^2 \int_0^\infty \frac{dq}{4\pi^2} \int_{-1}^{1} dz\, C^{\frac{1}{2}^+}(q) \frac{e^{-iqaz}}{q^2 - m_{\tilde{P}}^2} q^2 = m_S \frac{g^2}{a} \int_0^\infty \frac{dq}{2\pi^2} C^{\frac{1}{2}^+}(q) \frac{\sin(qa)}{q^2 - m_{\tilde{P}}^2} q. \tag{B.38}$$

This real integral can also be written as a complex one through

$$\int_{-R}^{+R} dq \frac{e^{iqa}}{q^2 - m_{\tilde{P}}^2} q = i \int_{-R}^{+R} dq \frac{\sin(qa)}{q^2 - m_{\tilde{P}}^2} q + \int_{-R}^{+R} dq \frac{\cos(qa)}{q^2 - m_{\tilde{P}}^2} q, \tag{B.39}$$

with the left hand side of (B.39) being part of a closed contour integral

$$\oint_C dq \frac{e^{iqa}}{q^2 - m_{\tilde{P}}^2} q \tag{B.40}$$

in the complex plane. Hence, we will solve (B.40), take the imaginary part and add a factor $\frac{1}{2i}$. According to Jordan's lemma the integral part along the infinite semicircle vanishes if the contour C is closed in the upper half plane for $a > 0$. Considering the coefficient $C^{\frac{1}{2}^+}$ we can split the integral

$$\mathcal{F} = m_S \frac{g^2}{a} \int_{-\infty}^{\infty} \frac{dq}{2\pi^2} C^{\frac{1}{2}^+}(q) \frac{e^{iqa}}{q^2 - m_{\tilde{P}}^2} q \tag{B.41}$$

into a sum of two contributions,

$$-\frac{1}{2}\frac{e^{iqa}}{q^2-m_{\tilde{P}}^2}q \qquad \text{and} \qquad \frac{1}{2}\frac{m_K+m_N}{\sqrt{(m_K+m_N)^2-q^2}}\frac{e^{iqa}}{q^2-m_{\tilde{P}}^2}q. \tag{B.42}$$

For each contribution there is a pole at $q = \pm m_{\tilde{P}}\sqrt{1 \pm \frac{i\varepsilon}{m_{\tilde{P}}^2}} \approx \pm m_{\tilde{P}} \pm i\varepsilon'$ and the poles are shifted in the complex plane according to

$$T = m_S\frac{-g^2}{s-m_P^2+i\varepsilon} \quad \Longrightarrow \quad T = m_S\frac{-g^2}{q^2-m_{\tilde{P}}^2-i\varepsilon}. \tag{B.43}$$

We pick up two residues for the two contributions (B.42), namely

$$\begin{aligned}
\mathcal{R}_1 &= -\frac{1}{4}e^{iam_{\tilde{P}}} \quad \text{and} \\
\mathcal{R}_2 &= \frac{1}{4}\frac{(m_K+m_N)}{\sqrt{(m_K+m_N)^2-m_{\tilde{P}}^2}}e^{iam_{\tilde{P}}}
\end{aligned} \tag{B.44}$$

in the upper half of the complex plane for $\varepsilon \to 0$. Collecting all terms and taking the imaginary part of the integral we obtain

$$\begin{aligned}
\mathcal{F} &= \mathfrak{Im}\left[m_S\frac{g^2}{8\pi a}\left(\frac{m_K+m_N}{m_P}-1\right)e^{iam_{\tilde{P}}}\right] \\
&= m_S\frac{ig^2}{8\pi a}\left(\frac{m_K+m_N}{m_P}-1\right)\sin\left(a\sqrt{(m_K+m_N)^2-m_P^2}\right)
\end{aligned} \tag{B.45}$$

The coupling g and scaling mass m_S remain to be determined by fitting the ansatz (B.34) to the numerical results of the coupled channel calculations for each of the two poles. The scaling mass turns out to be the pole mass m_P. The obtained fit is depicted in Figure B.1 for the isospin averaged amplitude.

Finally the pole structure will be modeled by the parameter set

$$\begin{aligned}
g_1 &= 10, \qquad m_P^{(1)} = 1115.5\,\text{MeV}, \\
g_2 &= 9.2, \qquad m_P^{(2)} = 1195\,\text{MeV}.
\end{aligned} \tag{B.46}$$

The real part of the $J = \frac{1}{2}$ p-wave contribution to the vacuum scattering amplitude (4.49) reads

$$\mathfrak{Re}\left[\bar{T}(q)\right] = C^{\frac{1}{2}^+}\mathfrak{Re}\left[\bar{M}_{\frac{1}{2}^+}(q)\right] - m_P^{(1)}\frac{g_1^2}{q^2-m_{\tilde{P}^{(1)}}^2} - m_P^{(2)}\frac{g_2^2}{q^2-m_{\tilde{P}^{(2)}}^2}. \tag{B.47}$$

The analytic imaginary part (B.45) is directly added to the non-local potential in coordinate space (B.36) for each of the poles.

B.6 Non-Local self-energy in the semi-microscopic model

We define the antikaon self-energy in the context of the approximation $\Pi(\omega = m_K, |\mathbf{q}|) = -\rho\bar{T}(|\mathbf{q}|)$. Note that here we are dealing with four-vectors, that is we have $x \neq |\mathbf{x}|$. We make use of the vacuum projector algebra introduced in Section 2.2.1.

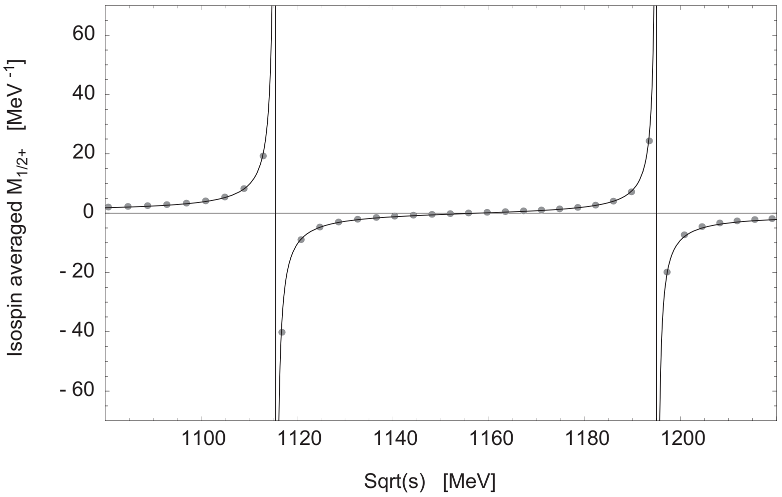

Figure B.1: Fit of the reduced amplitudes $J = \frac{3}{2}$ for $I = 0$ and $I = 1$ as described in the text to the numerical results of the coupled channel calculation of [4] (dots).

The self-energy is given by

$$\Pi(\omega = m_K, |\mathbf{q}|) = 2 \cdot \mathrm{Tr} \int \frac{d^4p}{(2\pi)^4} i\, \Delta S_N(p) \bar{T}(|\mathbf{q}|) \tag{B.48}$$

with an in-medium nucleon propagator analogous to (4.10), but neglecting the nucleon mean-fields Σ_S and Σ_V:

$$\Delta S_N = 2\pi i \cdot \Theta(p_0) \delta(p^2 - m_N^2) \Theta(k_F - |\mathbf{p}|)(\not{p} + m_N). \tag{B.49}$$

The projector decomposition of the vacuum scattering amplitude $\bar{T}(\mathbf{q})$ follows (2.22) and (2.23). In our approximation $\omega = m_K$ and $\bar{T}(|\mathbf{q}|)$ does not depend on the nucleon three-momentum $\mathbf{p}$. Using $p_0^2 = \mathbf{p}^2 + m_N^2 = E_N^2$ and $\delta(p_0^2 - E_N^2) = \frac{1}{|2E_N|} [\delta(p_0 - E_N) + \delta(p_0 + E_N)]$ the integration over p_0 can be carried out in (B.48) and we obtain

$$\begin{aligned} \Pi(\omega = m_K, q) &= -2 \sum_J \sum_{\pm} \int_0^{k_F} \frac{d^3p}{(2\pi)^3} C^{J^\pm}(q) \bar{M}_{J^\pm}(q) \\ &= -\sum_J \sum_{\pm} \frac{2}{3\pi^2} k_F^3 C^{J^\pm}(q) \bar{M}_{J^\pm}(q) \\ &\equiv -\rho \bar{T}(q). \end{aligned} \tag{B.50}$$

The coefficients $C^{J^\pm}$ are determined by evaluating the trace in (B.48), using the decomposition (2.22). In general the coefficients read

$$C^{J^\pm} = \frac{1}{2E_N} \mathrm{Tr} \left[\frac{1}{2} (\not{p} + m_N) P^{J^\pm} \right] \tag{B.51}$$

and in detail we have

$$
\begin{aligned}
\mathrm{Tr}\left[\frac{1}{2}(\not{p}+m_N)P^{\frac{1}{2}^-}\right] &= m_N + p\cdot\hat{w}, \\
\Rightarrow \quad C^{\frac{1}{2}^-} &= \frac{1}{2}\left(1+\frac{m_K+m_N}{\sqrt{s}}\right), \\
\mathrm{Tr}\left[\frac{1}{2}(\not{p}+m_N)P^{\frac{1}{2}^+}\right] &= -m_N + p\cdot\hat{w}, \\
\Rightarrow \quad C^{\frac{1}{2}^+} &= \frac{1}{2}\left(-1+\frac{m_K+m_N}{\sqrt{s}}\right), \\
\mathrm{Tr}\left[\frac{1}{2}(\not{p}+m_N)\bar{q}^{\mu}P^{\frac{3}{2}^+}_{\mu\nu}\,q^{\nu}\right] &= -2(m_N+p\cdot\hat{w})\left(q\cdot\bar{q}-(q\cdot\hat{w})(\bar{q}\cdot\hat{w})\right), \\
\Rightarrow \quad C^{\frac{3}{2}^+} &= \frac{m_N^2\mathbf{q}^2\left((m_K+m_N+\sqrt{s})\right)}{\sqrt{s}^3} \\
&\quad +\mathbf{q}^2\left(1+\frac{m_K+m_N}{\sqrt{s}}\right)\left(\frac{\mathbf{q}^2}{s}-1\right) \qquad \text{(B.52)}
\end{aligned}
$$

with $\hat{w}=\frac{w}{\sqrt{w^2}}$, $\mathbf{p}=0$, $\omega=m_K$ and $E_N=m_N$. In terms of antikaon momentum it is $s=(m_K+m_N)^2-\mathbf{q}^2$.

B.7 Density dependent semi-microscopic model

Both the vacuum $M_{J^P}(q)$ and in-medium reduced amplitudes $M_{ij}^{(p,q)}(q)$ are stated as functions of q. Note that $\sqrt{s}=\sqrt{(m_K+m_N)^2-q^2}$ in our schematic model. We define isospin-averaged reduced amplitudes

$$
\begin{aligned}
\overline{M}_0^{\frac{1}{2}^-}(q) &= \frac{1}{4}\left(M_{\frac{1}{2}^-}^{(I=0)}(q)+3M_{\frac{1}{2}^-}^{(I=1)}(q)\right), \qquad \mathrm{s-wave}, \\
\overline{M}_0^{\frac{3}{2}^+}(q) &= \frac{1}{4}\left(M_{\frac{3}{2}^+}^{(I=0)}(q)+3M_{\frac{3}{2}^+}^{(I=1)}(q)\right), \qquad \mathrm{p-wave} \qquad \text{(B.53)}
\end{aligned}
$$

for the vacuum case ($k_F=0$). The in-medium amplitudes take the same form

$$
\begin{aligned}
\overline{M}_{k_F}^{\frac{1}{2}^-}(q) &= \frac{1}{4}\left(M_{11}^{(p,I=0)}(q)+3M_{11}^{(p,I=1)}(q)\right), \qquad \mathrm{s-wave}, \\
\overline{M}_{k_F}^{\frac{3}{2}^+}(q) &= \frac{1}{4}\left(M_{11}^{(q,I=0)}(q)+3M_{11}^{(q,I=1)}(q)\right), \qquad \mathrm{p-wave} \qquad \text{(B.54)}
\end{aligned}
$$

at the desired Fermi momentum k_F in terms of the in-medium amplitudes $M_{ij}^{(p,q)}$ defined in Section 2.2.1. By 'p-wave' we denote the $J=\frac{3}{2}$ p-wave, the $J=\frac{1}{2}$ p-wave as well as the d-wave contribution will be neglected. Ad we take the in-medium $M_{ij}^{(p,q)}$ at vanishing three-momentum $\mathbf{w}$ in (B.54) the p-wave is degenerate in P- and Q-space and we can use both $M_{11}^{(q)}$ or $M_{77}^{(p)}$. We introduce the following notation:

$$\begin{aligned}
\rho_{(0)} &\equiv k_F^{(0)} \quad \text{at} \quad k_F = 0\,\text{MeV} \quad \approx \quad \rho = 0, \\
\rho_{(175)} &\equiv k_F^{(175)} \quad \text{at} \quad k_F = 175\,\text{MeV} \quad \approx \quad \rho = \frac{1}{4}\rho_0, \\
\rho_{(215)} &\equiv k_F^{(215)} \quad \text{at} \quad k_F = 215\,\text{MeV} \quad \approx \quad \rho = \frac{1}{2}\rho_0, \\
\rho_{(270)} &\equiv k_F^{(270)} \quad \text{at} \quad k_F = 270\,\text{MeV} \quad \approx \quad \rho = \rho_0.
\end{aligned} \tag{B.55}$$

Our final interpolation scheme between the the isospin-averaged amplitudes (B.53) and (B.54) reads

$$\begin{aligned}
\left[\overline{M}_{\text{int}}^{\frac{1}{2}^-,\frac{3}{2}^+}(k_F,q)\right]^{-1} &= \left[\overline{M}_{0}^{\frac{1}{2}^-,\frac{3}{2}^+}(q)\right]^{-1} \\
&+ 2\,k_1 \frac{{k_F}^2\left({k_F^{(270)}}^3 - {k_F}^3\right)\left({k_F^{(215)}}^3 - {k_F}^3\right)}{{k_F^{(175)}}^8\left(1+\frac{k_F}{k_F^{(175)}}\right)}\left(\left[\overline{M}_{175}^{\frac{1}{2}^-,\frac{3}{2}^+}(q)\right]^{-1} - \left[\overline{M}_{0}^{\frac{1}{2}^-,\frac{3}{2}^+}(q)\right]^{-1}\right) \\
&- 2\,k_2 \frac{{k_F}^2\left({k_F^{(270)}}^3 - {k_F}^3\right)\left({k_F^{(175)}}^3 - {k_F}^3\right)}{{k_F^{(215)}}^8\left(1+\frac{k_F}{k_F^{(215)}}\right)}\left(\left[\overline{M}_{215}^{\frac{1}{2}^-,\frac{3}{2}^+}(q)\right]^{-1} - \left[\overline{M}_{0}^{\frac{1}{2}^-,\frac{3}{2}^+}(q)\right]^{-1}\right) \\
&+ 2\,k_3 \frac{{k_F}^2\left({k_F^{(215)}}^3 - {k_F}^3\right)\left({k_F^{(175)}}^3 - {k_F}^3\right)}{{k_F^{(270)}}^8\left(1+\frac{k_F}{k_F^{(270)}}\right)}\left(\left[\overline{M}_{270}^{\frac{1}{2}^-,\frac{3}{2}^+}(q)\right]^{-1} - \left[\overline{M}_{0}^{\frac{1}{2}^-,\frac{3}{2}^+}(q)\right]^{-1}\right).
\end{aligned} \tag{B.56}$$

The coefficients k_i are determined numerically and guarantee that

$$\begin{aligned}
\left[\overline{M}_{\text{int}}^{\frac{1}{2}^-,\frac{3}{2}^+}(k_F=175,q)\right]^{-1} &= \left[\overline{M}_{175}^{\frac{1}{2}^-,\frac{3}{2}^+}(q)\right]^{-1}, \\
\left[\overline{M}_{\text{int}}^{\frac{1}{2}^-,\frac{3}{2}^+}(k_F=215,q)\right]^{-1} &= \left[\overline{M}_{215}^{\frac{1}{2}^-,\frac{3}{2}^+}(q)\right]^{-1}, \\
\left[\overline{M}_{\text{int}}^{\frac{1}{2}^-,\frac{3}{2}^+}(k_F=270,q)\right]^{-1} &= \left[\overline{M}_{270}^{\frac{1}{2}^-,\frac{3}{2}^+}(q)\right]^{-1}.
\end{aligned} \tag{B.57}$$

The interpolated density dependent amplitude $T_{\text{int}}^{\frac{1}{2}^-,\frac{3}{2}^+}$ involving s- and p-wave contributions can be obtained by multiplication with the phase-space coefficient $C^{\frac{1}{2}^-,\frac{3}{2}^+}(q)$ from (B.52),

$$T_{\text{int}}^{\frac{1}{2}^-,\frac{3}{2}^+}(k_F,q) = C^{\frac{1}{2}^-,\frac{3}{2}^+}(q)\left[\left[\overline{M}_{\text{int}}^{\frac{1}{2}^-,\frac{3}{2}^+}(k_F,q)\right]^{-1}\right]^{-1}, \tag{B.58}$$

where we kept all the arguments k_F and q for transparency.

Bibliography

[1] M.F.M. Lutz, "Dynamics of Kaons in Nuclear Matter", *Phys. Lett.*, **B426** (1998) 12.

[2] A. Ramos and E. Oset, "The properties of $\bar{K}$ in the nuclear medium", *Nucl. Phys.*, **A671** (2000) 481.

[3] M. Lutz and W. Florkowski, "Gradient terms in the microscopic description of K-atoms", *Acta Phys. Pol.*, **B32** (2001) 2081.

[4] M.F.M. Lutz and E.E. Kolomeitsev, "Relativistic chiral SU(3) symmetry, large N_C sum rules and meson-baryon scattering", *Nucl. Phys.*, **A700** (2002) 193.

[5] M.F.M. Lutz and C.L. Korpa, "Self consistent propagation of hyperons and antikaons in nuclear matter based on relativistic chiral SU(3) dynamics", *Nucl. Phys.*, **A700** (2002) 309.

[6] DEAR collaboration, *Int. J. Mod. Phys.*, **A20** (2005) 341.

[7] B. Borasoy, R. Nissler and W. Weise, "Chiral dynamics of kaon-nucleon interactions, revisited", *Eur. Phys. J.*, **A25** (2005) 79.

[8] T. Waas, N. Kaiser and W. Weise, "Low energy $\bar{K}N$ interaction in nuclear matter", *Phys. Lett.*, **B365** (1996) 12.

[9] T. Waas, M. Rho and W. Weise, "Effective kaon mass in dense baryonic matter: role of correlations", *Nucl. Phys.*, **A617** (1997) 449.

[10] V. Koch, "K^--proton scattering and the $\Lambda(1405)$ in dense matter", *Phys. Lett.*, **B337** (1994) 7.

[11] E.E. Kolomeitsev, D.N. Voskresensky and B. Kämpfer, "Kaon polarization in nuclear matter", *Nucl. Phys.*, **A588** (1995) 889.

[12] M.F.M. Lutz and E.E. Kolomeitsev, "Effective chiral theory of kaon-nucleon scattering", *nucl-th/0004021*.

[13] L. Tolos, A. Ramos, A. Polls and T.S. Kuo, "Partial wave contributions to the antikaon potential at finite momentum", *Nucl.Phys.*, **A690** (2001) 547.

[14] L. Tolos, E. Oset and A. Ramos, "Chiral approach to antikaon s- and p-wave interactions in dense nuclear matter", *Phys. Rev.*, **C74** (2006) 015203.

[15] A. Cieply, E. Friedman, A. Gal and J. Mares, "Study of chirally motivated low energy K^- optical potentials", *Nucl. Phys.*, **A696** (2001) 173.

[16] Y. Akaishi and T. Yamazaki, "Nuclear $\bar{K}$ bound states in light nuclei", *Phys. Rev.*, **C65** (2002) 044005.

[17] Y. Akaishi, A. Dote and T. Yamazaki, "Strange tribaryons as $\bar{K}$-mediated dense nuclear systems", *Phys. Lett.*, **B613** (2005) 140.

[18] M.F.M. Lutz, C.L. Korpa and M. Möller, "Antikaons and hyperons in nuclear matter with saturation", *nucl-th/07071283*, (2007).

[19] S. Weinberg, "Pion Scattering Lengths", *Phys. Rev. Lett.*, **17** (1966) 616.

[20] M. Lutz, "Nuclear kaon dynamics", *Phys. Lett.*, **B426** (1998) 12.

[21] E. Friedman, A. Gal and C.J. Batty, "Density-dependent K^- nuclear optical potentials from kaonic atoms", *Nucl. Phys.*, **A579** (1994) 518.

[22] M. Möller, *Diplomarbeit*, Master's thesis, Technische Universität Darmstadt (2003).

[23] B.D. Serot and J.D. Walecka, "The Relativistic Nuclear Many-Body Problem", *Adv. Nucl. Phys.*, **16** (1986) 1.

[24] R. Brockmann and R. Machleidt, "Relativistic Nuclear Structure", *Phys. Rev.*, **C42** (1990) 1965.

[25] E.G. Drukarev and E.M. Levin, "Structure of Nuclear Matter and QCD Sum Rules", *Prog. Part. Nucl. Phys.*, **27** (1991) 77.

[26] P. Finelli, N. Kaiser, D. Vrenetar and W. Weise, "Relativistic nuclear model with point-couplings constrained by QCD and chiral symmetry", *Nucl. Phys.*, **A735** (2004) 449.

[27] C. Fuchs, "The Relativistic Dirac-Brueckner Approach to Nuclear Matter", *Lect. Notes Phys.*, **641** (2004) 119.

[28] O. Plohl and C. Fuchs, "The relativistic self-energy in nuclear dynamics", *nucl-th/0607053*.

[29] G. Passarino and M. Veltman, "One-loop corrections for e^+e^- annihilation into $\mu^+\mu^-$ in the Weinberg model", *Nucl. Phys.*, **B160** (1979) 151.

[30] T. Hasegawa *et al.*, "Spectroscopic study of ${}^{10}_{\Lambda}B$, ${}^{12}_{\Lambda}C$, ${}^{28}_{\Lambda}Si$, ${}^{89}_{\Lambda}Y$, ${}^{139}_{\Lambda}La$, and ${}^{208}_{\Lambda}Pb$ by the (π^+, K^+) reaction", *Phys. Rev.*, (1996) 1210.

[31] S. Typel, *private communication*.

[32] C.J. Batty, S.F. Biagi, M. Blecher, R.A.J. Riddle, B.L. Roberts, J.D. Davis, G.J. Pyle, G.T.A. Squier and D.M. Asbury, "Measurement of Kaonic X-Rays from Li, LiH and Be", *Nucl. Phys.*, **A282** (1977) 487.

[33] G. Backenstoss, A. Bamberger, I. Bergstrom, B. Bounin, T. Bunaciu, J. Egger, S. Hultberg, H. Koch, M. Krell, U. Lynen, H.G. Ritter, A. Schwitter and R. Stearns, "Strong Interaction Shifts and Widths in Light Kaonic Atoms", *Phys. Lett.*, **B38** (1972) 181.

[34] G. Backenstoss, J. Egger, H. Koch, H.P. Povel, A. Schwitter and L. Tauscher, "Intensities and Strong Interaction Attenuation of Kaonic X-Rays", *Nucl. Phys.*, **B73** (1974) 189.

[35] C.J. Batty, S.F. Biagi, M. Blecher, S.D. Hoath, R.A.J. Riddle, B.L. Roberts, J.D. Davies, G.J. Pyle, G.T.A. Squier, D.M. Asbury and A.S. Clough, "Measurement of Strong Interaction Effects in Kaonic Atoms", *Nucl. Phys.*, **A329** (1979) 407.

[36] P.D. Barnes, R.A. Eisenstein, W.C. Lam, J. Miller, R.B. Sutton, M. Eckhause, J.R. Kane, R.E. Welsh, D.A. Jenkins, R.J. Powers, A.R. Kunselman, R.P. Redwine and R.E. Segel, "Measurement of Kaonic X-Rays from Al, Si, Ni and Cu", *Nucl. Phys.*, **A231** (1974) 477.

[37] C.E. Wiegand and G.L. Godfrey, "Measurement of x rays and γ rays from stopped kaons", *Phys. Rev.*, **A9** (1974) 2282.

[38] R. Kunselman, "Kaon Mass Measurement from Kaonic Atom X-Ray Energies; The 4f-3d Kaonic Transition in Chlorine", *Phys. Lett.*, **B34** (1971) 485.

[39] R. Kunselman, "Negative-kaon mass", *Phys. Rev.*, **C9** (1974) 2469.

[40] C.J. Batty, S.F. Biagi, R.A.J. Riddle, B.L. Roberts, G.J. Pyle, G.T.A. Squier, D.M. Asbury and A.S. Clough, "Nuclear Quadrupole Deformation Effects on Pionic and Kaonic X-Rays", *Nucl. Phys.*, **A355** (1981) 383.

[41] S.C. Cheng, Y. Asano, M.Y. Chen, G. Dugan, E. Hu, L. Lidofsky, W. Patton, C.S. Wu, V. Hughes and D. Lu, "K^- Mass from Kaonic Atoms", *Nucl. Phys.*, **A254** (1975) 381.

[42] J.P. Miller, Ph.D. thesis, Carnegie-Mellon University, Pittsburgh (1975).

[43] H. de Vries, C.W. de Jager and C. de Vries, "Nuclear Charge-Density-Distribution Parameters from Elastic Electron Scattering", *Atomic Data and Nuclear Data Tables*, **36** (1987) 495.

[44] G. Audi and A.H. Wapstra, "The 1995 update to the atomic mass evaluation", *Nucl. Phys.*, **A595** (1995) 409.

[45] M. Krell and T.E.O. Ericson, "The Bound-State Solution of Wave Equations for Real or Complex Eigenvalues", *Jour. Comp. Phys.*, **3** (1968) 202.

[46] E.A. Uehling, "Polarization Effects in the Positron Theory", *Phys. Rev.*, **48** (1935) 55.

[47] E.H. Wichmann and N.M. Kroll, "Vacuum Polarization in a Strong Coulomb Field", *Phys. Rev.*, **101** (1956)(2) 843.

[48] G. Källén and A. Sabry, *Dan. Mat. Fys. Medd.*, **29** (1955) 17.

[49] L.W. Fullerton and G.A. Rinker, "Accurate and efficient methods for the evaluation of vacuum-polarization potentials of order $Z\alpha$ and $Z\alpha^2$", *Phys. Rev.*, **A13** (1976)(3) 1283.

[50] J. Blomqvist, “Vacuum Polarization in Exotic Atoms”, *Nucl. Phys.*, **B48** (1972) 95.

[51] W.H. Furry, “On Bound States and Scattering in Positron Theory”, *Phys. Rev.*, **81** (1951) 115.

[52] M. Gyulassy, “Higher Order Vacuum Polarization for Finite Radius Nuclei”, *Nucl. Phys.*, **A244** (1975) 497.

[53] G. Soff and P.J. Mohr, “Vacuum polarization in a strong external field”, *Phys. Rev.*, **A38** (1988)(10) 5066.

[54] C.B. Dover and G.E. Walker, “The Interaction of Kaons with Nucleons and Nuclei”, *Phys. Rep.*, **89** (1982)(1) 1.

[55] M. Lutz, A. Steiner and W. Weise, “Kaons in baryonic matter”, *Nucl. Phys.*, **A574** (1994) 755.

[56] C.J. Batty, E. Friedman and A. Gal, “Strong interaction physics from hadronic atoms”, *Phys. Rep.*, **287** (1997) 385.

[57] R. Brockmann, W. Weise and L. Tauscher, “Y* Resonances and Kaonic Atoms”, *Nucl. Phys.*, **A308** (1978) 365.

[58] M. Mizoguchi, S. Hirenzaki and H. Toki, “Microscopic kaonic-atom optical potential in finite nuclei with $\Lambda(1405)$ and $\Sigma(1385)$ resonances”, *Nucl. Phys.*, **A567** (1994) 893.

[59] E. Oset and A. Ramos, “Non-perturbative chiral approach to s-wave $\bar{K}N$ interactions”, *Nucl. Phys.*, **A635** (1998) 99.

[60] A. Baca, C. García-Recio and J. Nieves, “Deeply bound levels in kaonic atoms”, *Nucl. Phys.*, **A673** (2000) 335.

[61] J. Knoll, Yu.B. Ivanov and D.N. Voskresensky, “Exact Conservation Laws of the Gradient Expanded Kadanoff-Baym Equations”, *Ann. Phys.*, **293** (2001) 126.

[62] A.S. Dawydow, *Quantenmechanik*, VEB Deutscher Verlag der Wissenschaften (1974).

[63] E. Oset and L.L. Salcedo, “Error Sources in the Standard Numerical Integration of the Schrödinger Equation: An Improved Method”, *Jour. Comp. Phys.*, **57** (1985) 361.

[64] W.H. Press, B.P. Flannery, S.A. Teukolsky and W.T. Vetterling, *Numerical Recipes*, Cambridge University Press (1986).

Lebenslauf

Name	Matthias Möller
Geburtsdatum	23. Juli 1977
Geburtsort	Hanau
Staatsangehörigkeit	deutsch
Familienstand	ledig

September 1984 bis Juli 1988	Besuch der Johannes-Gutenberg-Grundschule in Hainburg
September 1988 bis Juni 1997	Besuch des Franziskanergymnasiums Kreuzburg in Großkrotzenburg
Juni 1997	Abitur
Oktober 1997 bis April 2003	Studium der Physik and der Technischen Universität Darmstadt
Januar 2002 bis April 2003	Anfertigung der Diplomarbeit bei der Gesellschaft für Schwerionenforschung mbH in Darmstadt mit dem Thema *'Kaonische Atome'*
Seit Mai 2003	Wissenschaftlicher Mitarbeiter bei der Gesellschaft für Schwerionenforschung mbH in Darmstadt und Anfertigung der Dissertation